The Influence of Design and Operational Parameters on Micronizer Performance

by

AHMAD NA'IM KHAYYAT

A thesis submitted to the University of Aston in Birmingham for the Degree of Doctor of Philosophy.

DEPARTMENT OF CHEMICAL ENGINEERING
THE UNIVERSITY OF ASTON IN BIRMINGHAM
DECEMBER 1978

Thesis to be submitted for the Degree of Ph.D.

The Influence of Design and Operational Parameters on Micronizer Performance

by

A.N. Khayyat

SUMMARY

The design of the micronizer fluid energy mill has developed since its introduction in 1932. The literature tracing this development is reviewed and earlier work by several researchers concerning the influence of the various operational features is reported upon.

The research programme described in this thesis sought to establish the optimum features for maximum comminution efficiency. Using the optimum design the main operational parameters were studied. Fluid injection velocity and pressure of the fluid medium were varied and the influence of these and of the solids to fluid ratio on the comminution process are described. Conclusions are drawn as to the optimum and operational parameters.

These parameters have been correlated by dimensional analysis and the analysis is compared with that of other workers in different designs of fluid energy mill. Recommendations for future work are made based on these analyses and on the investigation of design features.

Keywords

Comminution
Micronizer
Fluid-Energy Mill
Fine particle
Sub-micron

To my Mother

and

The memory of my Father

ACKNOWLEDGEMENTS

The author wishes to express his sincere thanks and gratitude to:

Professor G V Jeffreys,
for providing the facilities for this research.

Dr R G Temple,
for his helpful guidance, encouragement and personal interest in the supervision of this project.

Airfilco Process Plant Ltd (Newbury - UK),
for providing the financial support for this research and for their helpful discussions.

Mr R Skelton,
the acting liaison industrial supervisor for his encouragement and for arranging contacts with industry.

The University of Aston in Birmingham,
for awarding me a studentship to pursue this research

Dr D E Creasy,
for his constant advice and interest throughout each phase of this study.

The members of the Technical Staff and Photographic section of the Department of Chemical Engineering.

Special thanks are extended to Miss A B Vose for her invaluable assistance in checking the manuscript and Mrs A Long for her endless patience in typing the thesis.

CONTENTS

Chapter 4

Chapter 5

Chapter 6

Chapter 9

1. Introduction

The microniser is essentially employed for comminuting powders to a superfine state and is, in many cases, capable of producing materials with mean particle diameter of less than 5 microns of narrow and controlled particle size distribution. Comminution is achieved in a flat cylindrical grinding chamber by the action of compressible fluid jets (usually air or steam) emerging from nozzles located around the periphery of the chamber. It is a type of fluid energy mill and classified as an impact mill and serves the two functions of comminution and classification.

The uses of the microniser are diversified and a large variety of materials are now processed - metallic/non-metallic minerals, pigments, dyes, insecticides, fungicides, cosmetics, pharmaceutical products and other organic and inorganic materials. In addition to comminution, this type of mill is also able to perform other functions, simultaneous drying and comminution using a heated fluid being a distinct advantage.

The microniser operating principle involves several physical phenomena such as gas-solid suspension properties, interparticle collision, comminution, compressible fluid jets, acceleration of particles and classification action. There are gaps in the knowledge of estimating the significance and effects of these properties. Comminution fundamentals concerning particle breakage, and modes of breakage processes

are presented in Chapter 2. The properties of gas-solid suspensions, and particle behaviour in these suspensions are discussed in Chapter 4.

In the past 40 years, since the microniser was used on an industrial scale, a number of papers have been published on fluid energy mills generally. The information available is scattered in a variety of journals, and although mainly qualitative, has contributed to the understanding of the fluid energy mill principles generally. Chapter 5 presents the most fundamental of these.

Limited information is available on the performance of the microniser and there has been little systematic study of its design and operation.

This research was undertaken to study the effect of important constructional features of a 0.2m diameter microniser (the Airfilco "Micronizer") and the main operational variables involved. Because of the overlapping effect of some of the constructional features and the operational parameters, it was necessary as far as possible to identify and assess the significance of each of the variables separately. Furthermore, the study was aimed at investigating feed materials which are in the fine to superfine region.

The microniser is specifically employed for comminuting materials down to superfine state and is much more costly than other means in terms of running cost. Hence its uses are

limited to industrial application where the economics and conditions of the final product are justifiable.

Chapter 2: Comminution Fundamentals

CHAPTER 2 : COMMINUTION FUNDAMENTALS

2.1 Introduction

Comminution has been discussed extensively in the literature. For example, Marshall(Ref 48) and Lowrison (Ref 42) presented a comprehensive study of comminution principles, machinery and energy consumptions and their relative importance in the processing industry. Bickle (Ref 11) presents a near complete bibliography of the subject and Perry and Chilton (Ref 83) give brief details of comminution laws and equipment. Up-to-date research and development of the subject are found in Snow's Annual Reviews of size reduction (Refs. 51 -54).

The fundamentals of comminution are complex and precise universal laws do not exist, because the subject is concerned with the solid state, which exhibits different properties depending on the pattern in which atoms or molecules of the solids are arranged, the inter-atomic and inter-molecular bonds and their strength and also on the degree of perfection and fault in the structure. Many relevant papers and textbooks which discuss the solid state and properties of materials have been published (Ref 48).

The principal conclusions and findings of those working in the field of comminution are presented below, with particular reference to superfine grinding (below 50 microns) in fluid energy mills and will be confined to the crushing of brittle materials.

2.2 Fracture Mechanics

2.1.1 General

Theories of fracture mechanics, crack growth and models for crack nucleation have been developed according to continuum, "atomistic" and energy theories. These are reviewed by Pugh (Ref 112).

The behaviour of solids under stress is related to their form. There are two general categories of solids: crystalline and amorphous (Ref 48). Some solids exhibiting intermediate properties are called "composite".

The knowledge of the breaking action within mills to a large extent depends on the knowledge of single particle fracture and the properties of solids. Comminution theories to date are based on propagation of cracks that already exist within the solid.

2.2.2 Breakage of Single Particles

Comminution consists of a process of propagating cracks within a solid mass. Cracks represent planes of rupture of molecular bonds and when a crack has reached the surface at all points of its perimeter, then, it has broken the material.

Before breakage of a material under stress occurs, it absorbs a given amount of energy called "strain energy". This is a function of the area below the stress/strain curve shown in Figure 2.1.

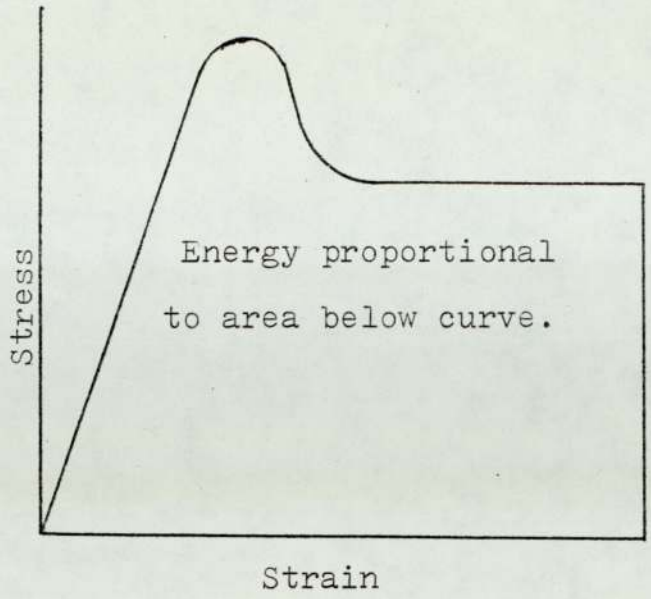

Figure 2.1: Typical stress/strain curve

Rupture occurs, when the strain energy exceeds a limiting value (the binding energy, or "surface energy") which is a characteristic of the material. Joffe (Ref 120) recognised that the strain energy is not uniformly distributed throughout the solid mass and is usually concentrated around holes and at corners.

2.2.3 Crack Propagation

Comminution processes usually take effect through the propagation of existing cracks. Griffith (Ref 113) pointed out that there ought to be a critical crack depth for any stress applied; below that depth the stress is too low to raise the stress at the tip to a level at which propagation occurs; above it the crack propagates.

The speed of propagation of cracks in material can approach the speed of sound. Practice confirms (Ref 48) that crack front velocity reaches a limiting value of about 40% of the speed of sound in the material. The propagation of cracks is related to the ability of the materials to propagate strain which in turn depends on its form - whether crystalline or amorphous.

Once cracks are formed, they can be self-propagating provided there is enough strain energy in the material. The law of conservation of energy holds, and breaking can only continue so long as there is energy remaining.

Strain energy required for crack propagation increases as particle size decreases because there is insufficient volume in small particles to provide sufficient strain energy to produce high stress concentration on the edge of the crack to initiate crack propagation. Hence the mean stress in smaller particles has to be higher in order to propagate the cracks.

Wasley (Ref 114) has reviewed the mathematical models of stress wave propagation.

2.3 The Rate of Application of Force and Modes of Impact

In Section 2.2.2. it was deduced that to effect breakage of a particle, a definite energy increment must be imparted to it sufficient to start fracture.

The amount of energy increment necessary to cause fracture within the solid's mass depends upon the material's strength, properties, particle dimensions, and the rate at which force is applied.

Marshall(Ref 48) listed some of the ways used to cause fracture in comminution processes, these are

(1) Compression
(2) Impact
(3) Attrition
(4) Cutting

A distinction is commonly drawn between compression and impact as modes of applying forces. But no rigid distinction can be drawn between them; they differ from each other essentially in the rate at which force is applied. Rumpf (Ref 10) has classified modes of applying force to cause comminution as follows:

I. Particles are loaded between two surfaces; energy is imparted to them and the magnitude of the force applied depends upon the movement of the surfaces. This is analogous to compression.

II. The particles are loaded against only one surface either against a grinding element or against another particle. The applied force is an inertia force deriving its effect from acceleration or deceleration of the particles. The energy available for size reduction is the kinetic energy of the relative motion of particle and wall, or particle and particle. This mode is

generally known as impact crushing.

III. Ambient liquid or gaseous media exert shear forces on the particle and under suitable conditions they can be large enough to cause breakage or at least disintegration of agglomerates.

Subdivision of size reduction methods into loading mechanisms I and II is equivalent to differentiation according to the loading velocity: loading velocities of up to 15m/s have been cited for mechanism I, while above this value for mechanism II (impact crushing).

Mechanisms I and III are outside the scope of this chapter, and discussion therefore is limited to impact crushing in relation to fine grinding, and fluid energy mills.

2.4. Energy Utilisation During Comminution Processes

There are two basic models concerned with energy consumption in comminution. In the first the theoretical energy required to cause fracture in a particle has been calculated based on the theoretical strength of the material. The energy so calculated was found to be greater than the experimental value (Ref 48). The second model is based on the "surface energy" of solids and gives values well below those found in practice. The actual energy requirements were found to lie between the value predicted by the two models.

The reason for this lies in the mechanism by which cracks are propagated (Section 2.2.3).

Attempts at using models to predict energy consumption are well known and are the basis of the Laws of Rittinger, Kick, Bond and Holmes (Refs 48, 83, 42). These have been based on linear regression analysis of experimental results. Although these general laws are much criticised in literature and various researchers have supported one or the other, they provide the only means of assessing many of the types of comminution equipment. The Laws incorporate one common assumption: namely that size reduction continues indefinitely so long as energy is supplied. They are found to be inapplicable to super fine grinding; as explained in Section 2.2, the minimum strain energy required to initiate fracture increases as particle size decreases. Also Marshall(Ref 48) argues that comminution equipment may be unable to promote further fracture, since any system will eventually reach an equilibrium state, so that $\frac{ds}{dE} = 0$ where $\frac{ds}{dE}$ is rate of change of surface area with power input.

2.4.1 Energy Utilisation in Impact Mills

Energy utilisation in high velocity impact mills has been discussed by Marshall (Ref 48). It was shown that in pin mills more than 80% of the energy is consumed by the mill under no-load conditions. In fluid energy mills the power consumption bears little or no relationship to the load on the mill. This will be discussed further in

Chapter 5.

Rumpf (Ref 10) discusses energy utilisation in impact mills in relation to the following:

1. Types of impact - eccentric or oblique. In practice oblique impact is much more frequent than eccentric impact. Oblique impact results in friction and thus in an energy wasting process.

2. Frequency of Impact between mill element and the particle or between particle and particle. This is a function of the concentration of particles in the mill, particle diameter and particle velocity. An examination of the particle collision frequency was illustrated in the study of Marble (Ref 110) which concerned collisions between particles of two sizes only.

3. Maximum stress. Fracture inception depends upon the magnitude of stresses and their distribution (Section 2.2.2). Since particle shapes encountered in comminution processes are often irregular exact stresses cannot be estimated. Rumpf (Ref 10) has shown that in the region of validity of Hook's Law, dimensional analysis shows, for example, that in the impact of a body of arbitrary shape and varied mass against a rigid surface

$$\sigma_{max} = \text{const.}\ m^{n}\ v_i^{2n}\ r^{-3n}\ E^{1-n} \qquad \text{Eq. 2.1}$$

where σ_{max} is maximum stress caused on impact

m is the body mass

v_i is the impact velocity

r is the length characterizing the body's shape at point of impact.

E is the modulus of elasticity.

n is simple power.

According to Rumpf (Ref 9), with two impacting masses and spherical point of impact the relationship is

$$\sigma_{max} = (0.098)^{\frac{1}{5}} \left(\frac{m1 \times m2}{m1+m2}\right)^{\frac{1}{5}} \left(\frac{1}{r_1} + \frac{1}{r_2}\right)^{\frac{3}{5}} \cdot v^{\frac{2}{5}} \cdot \left[\frac{1-\gamma_1}{E_1} + \frac{1-\gamma_2}{E_2}\right]^{-\frac{4}{5}} \quad \text{Eq 2.2}$$

where γ is Poisson Ratio, other symbols as given above, and subscripts refer to the two colliding bodies of mass m1 and m2 respectively.

A broad impact spectrum is disadvantageous; it includes many types of impacts which consume energy without substantial contribution to fracture inception and there are many high intensity impacts producing much fines. Thus for more efficient grinding the impact spectrum should be kept as narrow as possible.

Impact velocity is the principal factor governing control of impact stress, and should be adjusted to suit particle strength and size. Fine grinding requires higher impact velocities than coarse grinding and the magnitude of the velocities required can only be determined by experiments. Available data are very limited and observations of size reduction machinery usually record the grinding machine element velocity and not the actual impact velocity. Also, in fine grinding, air friction and frequency of interparticle impact considerably change impact velocity; this will be

discussed in Section 5.3.

2.4.2 Comminution Efficiency

Energy consumption in comminution processes has been discussed by several authors e.g. Greenwood (Ref 115). Methods of expressing efficiency of a comminution process were based on the net energy consumption, by simply relating it to the new surface energy and have more recently been replaced by definitions such as

$$\text{Efficiency} = \frac{\text{Energy effective in producing a given extent of fracture}}{\text{Gross Energy Input}}$$

The concept of free crushing was used by Stairmand (Ref 116) to assess comminution machinery efficiency. Free crushing refers to the crushing of monodisperse particles without recrushing of "daughter" particles. The energy consumed, "Associated Energy", represents the lowest practicable energy input for a given degree of comminution and the efficiency of a machine was based on this concept. Efficiencies calculated on this basis are shown in Figure 2.2. It is shown that values for efficiencies of industrial comminution machines are found to vary from 80% in the case of roller crushers down to 2% for fluid energy mills.

The loss of efficiency in comminution equipment has been attributed to many factors. Some of these are,

1) heat dissipation

2) deformation of particles

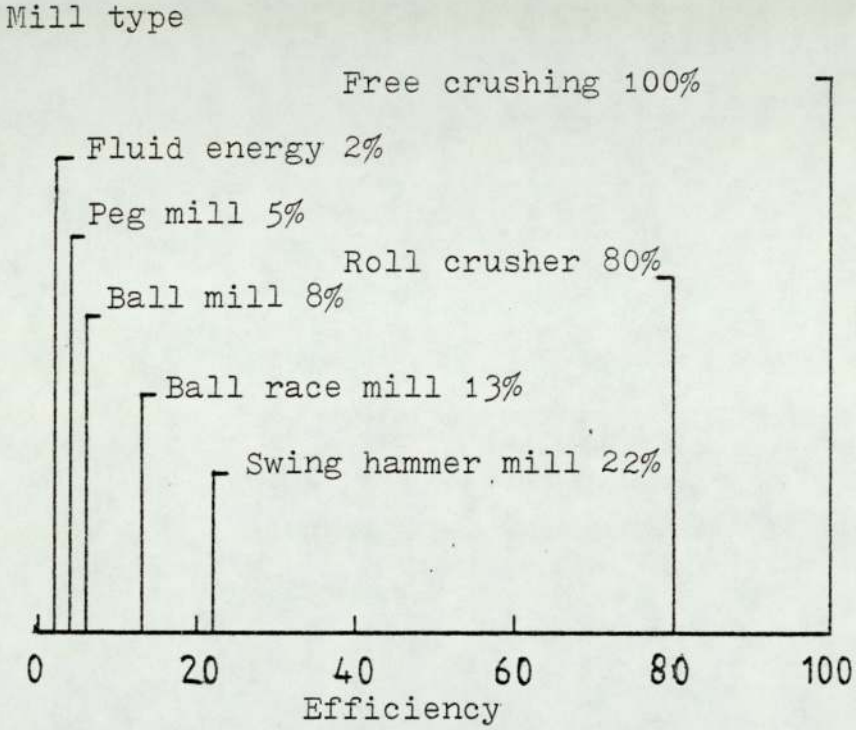

Figure 2.2 - Net grinding efficiency (based on free crushing) for selected comminution machinery.

(Ref 48, p10)

3) deformation of crushing element or machinery

4) frictional losses between surfaces.

For example, in vibration mills, Rose has estimated that only 0.25% of the energy input goes to creating new surface area, 37% is lost in transmission and 47% is lost as heat.

In fluid energy mills, frictional losses are considerable. Also, Menyhart (Ref 117) has shown that considerable energy is transformed to affect the crystalline structure of the material being ground, producing a mechanochemically activated state. These findings will be discussed in Chapter 5.

2.5. Simulation of Comminution Processes

The modelling themes of comminution processes are generally limited to either:-

(a) The prediction of energy requirement (Section 2.4)

(b) The prediction of size distribution of product.

Both modelling themes (a) and (b) are regarded by many authors as unrelated, though the operational parameters for energy models are evaluated by reference to size reduction parameters.

Recent efforts have been spent in the development of particle size distribution models (PSD) which are based on

empirical models of breakage phenomena and attempt to relate particle size distribution with process conditions.

The PSD models have mostly been based on a description of comminution processes attributed to Epstein (Ref 137). Such models have been developed from mass balance considerations, and are phrased in terms of discrete size ranges. Both kinetic and mechanistic "Probalistic" approaches have been used by Broadbent et al (Ref 65), Gardner (Ref 64), Austin and Klimpel (Ref 69). These models basically involve the use of two functions; the breakage function and the selection function. The breakage function is a statement of the size distribution of particles produced on breakage of a single representative feed particle. The selection function is a statement of probability of breakage of a specific particle during a specific time interval. Both functions may be represented in a form of matrix. Some attempts have been made to relate the matrix element with ore type and operating conditions, but these efforts have met with little success.

More recent forms of PSD models have been developed on a basis of the population balance of Randolph (Ref 70), but its use is limited, and involves considerable number of assumptions and detailed computation.

The above PSD models have been applied in some comminution processes in both closed circuit and open circuit grinding.

The development of theoretical models that are capable of practical application necessitates a thorough understanding of the fundamentals of the process, identification

of all variables involved and a combination of mathematical analyses and process comprehension.

2.6 Representation of Particle Size Distribution

Representations of particle size distribution of comminuted products in a mathematical form have been made by a number of researchers. Equations of particle size distribution are presented, reviewed and criticised in the literature by Bleke (119), Allen (74) Cadle (78) Irani and Callis (81), Marshall (48) and Randolf (118).

Cumulative distribution whether based on number, length, surface area, volume or mass, provides a convenient way of representing particle size distribution. In many instances, it can be represented graphically: the abscissa is particle size and the ordinate the percentage smaller than or larger than the stated size. This has the advantage that properties of the distributions such as means are readily read or derived, also particle population in a given size range is directly read.

Several empirical forms and functions exist for expressing a distribution. The most widely known are the normal, log-normal and Rosin-Rammler distributions.

The normal distribution is expressed by

$$y = \frac{1}{\delta\sqrt{2\pi}} \exp \left[\frac{-(x - \bar{x})^2}{2\delta^2}\right] \qquad \text{Eq. 2.3}$$

$$= \delta\sqrt{\frac{\Sigma(x - \bar{x})^2}{N - 1}} \qquad \text{Eq. 2.4}$$

where y is mass fraction oversize

x is particle diameter

$\bar{x}$ arithmetic mean of value x

δ arithmetic standard deviation

and N is the number of observations.

$\delta$and $\bar{x}$ are both adjustable parameters: they are a measure of the uniformity and absolute size of the population of particles. A powder whose size distribution fits the above equation gives a straight line, when the distribution is plotted on normal probability axes.

Allen (74) and Randolph(118) stated that this type of distribution has a limited use in comminution processes.

The equation representing the log-normal distribution is

$$y = \frac{1}{\delta_g \sqrt{2\pi}} \exp\left[\frac{-(\ln x - \ln \bar{x}g)^2}{\delta_g^2}\right] \qquad \text{Eq. 2.5}$$

where $\bar{x}g$ is the geometric mean of size x

and δ_g is the geometric standard deviation.

When the powder distribution follows the log-normal equation, this gives a straight line when plotted on log-probability axes.

Conversion from one distribution property to another when the distribution is log-normal is easy using the

equations given by Allen (Ref 74), also calculation of specific surface area S can be made by applying

$$S = \frac{6}{X_{50}} \text{ Exp } \left[\frac{1}{2} (\ln \sigma_g)^2\right] \qquad \text{Eq. 2.6}$$

This is not the case for normal distributions. The log normal distribution is often used in characterising products from comminution equipment Marshall (Ref 48) and Randolph (Ref 118).

The Rosin-Rammler distribution is given by:

$$\text{Log-Log } \frac{100}{R_p} = \text{const} + n \log x \qquad \text{Eq. 2.7}$$

where R_p percentage retained on sieve of aperture x
n is a characteristic of the substance being analysed.

Specially prepared graph paper is obtainable on which this function yields a straight line.

Rosin-Rammler distribution function was developed for broken coal and found to apply to certain other materials. Also it was found useful for monitoring grinding operations of highly skewed distributions. Caution should be used when applying this function since the taking of logs twice reduces scatter and can obscure significant variations.

Chapter 3: Super-fine Comminution Machinery

3.0 SUPERFINE COMMINUTION MACHINERY

3.1 Introduction

The lack of standardization of the comminution machinery is due to: the variety of materials to be ground and product qualities demanded, the limited useful comminution theories available, and to the varying requirements of different industries of the economic balance between investment cost and operating cost.

A wide variety of comminution equipment is available and may be classified according to the method by which forces are applied; this has been discussed above in Section 2.3. Practical classification of comminution equipment has been made by e.g. Marshall(Ref 48), Lowrison (Ref 42) and Perry and Chilton (Ref 83). Figure 3.1 below sets out the particle size range of operation of machines encountered in the comminution of brittle materials. The description and characteristics of each machine may be found in the above references. The selection of a comminution machine for superfine grinding is based upon a number of factors such as: feed size, required product size, material hardness, grindability, shape, melting point, stickiness etc., also safety and contamination must be taken into account. Rink et al (Ref 14) discussed the factors affecting the selection of a mill with reference to the chemical industries; they concluded that the thermal effect of comminution on the product is the decisive

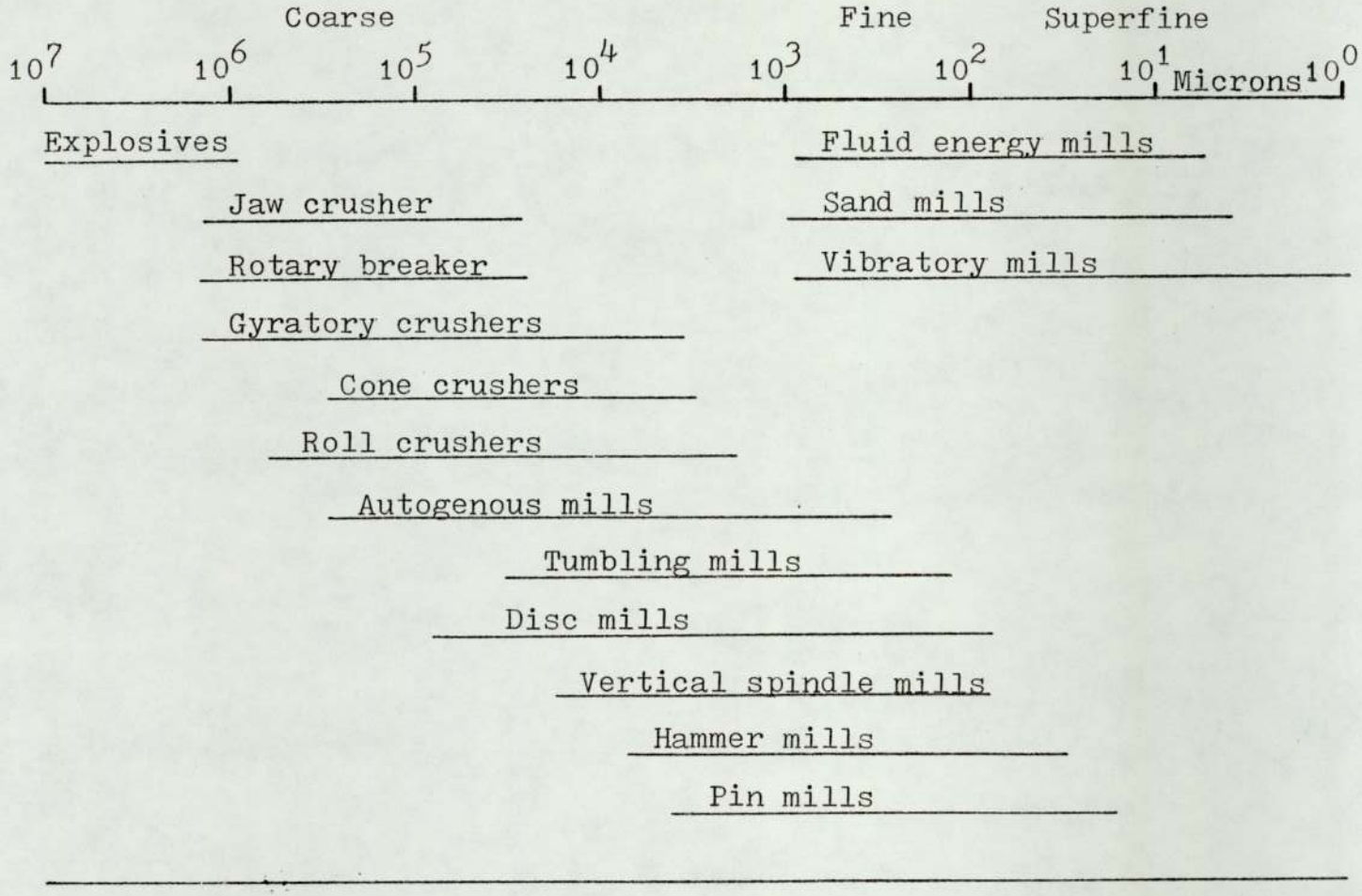

Figure 3.1 - Range of operation of comminution machines.

factor. Bond (Ref 34) has reviewed some fine grinding machines and the economics of selection. Also, Berry (Ref 41) compares various size reduction machines in the superfine range.

Superfine Comminution Equipment

3.2 Vibration Mills (Ref 121 and 122)

A typical vibration mill is shown in Figure 3.2. It consists of a container, two thirds filled with grinding medium such as steel balls, and is vibrated by means of an off-centre weighted motor. Other design approaches are also encountered (Ref 121), they may be operated batch-wise or continuously. In the latter, feed is introduced at the top and moves through the vibrating mass. The grinding action occurs mainly by impact between particles and the surface of the balls, and between particle and particle. They are capable of wet or dry grinding and can be operated either by the open or closed circuit principles. They are limited to a maximum feed size of 6×10^{-3}m and a product size down to 10^{-6}m.

They are found unsuitable for grinding heat sensitive materials because of the localised high temperature generated during impacts. Also, impurities are introduced from the grinding medium.

3.3 Peg or Pin Mills (Ref 115)

Figure 3.3 illustrates the main features of Peg or

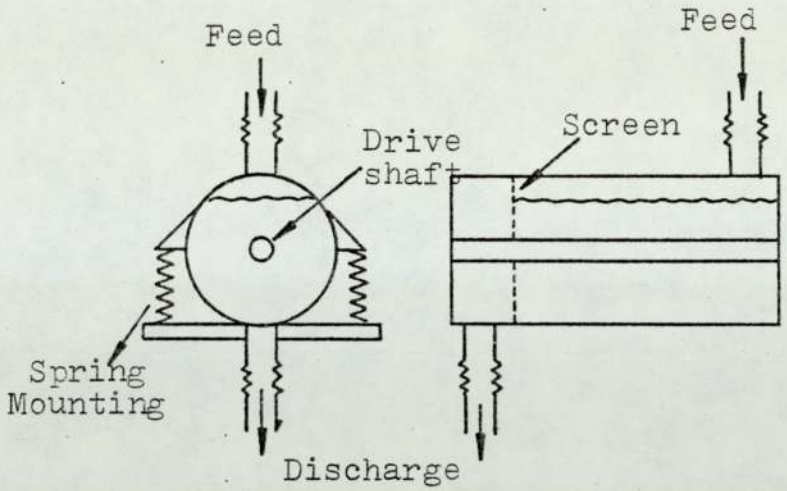

Figure 3.2: Vibrating Mill (End and Side Elevations)

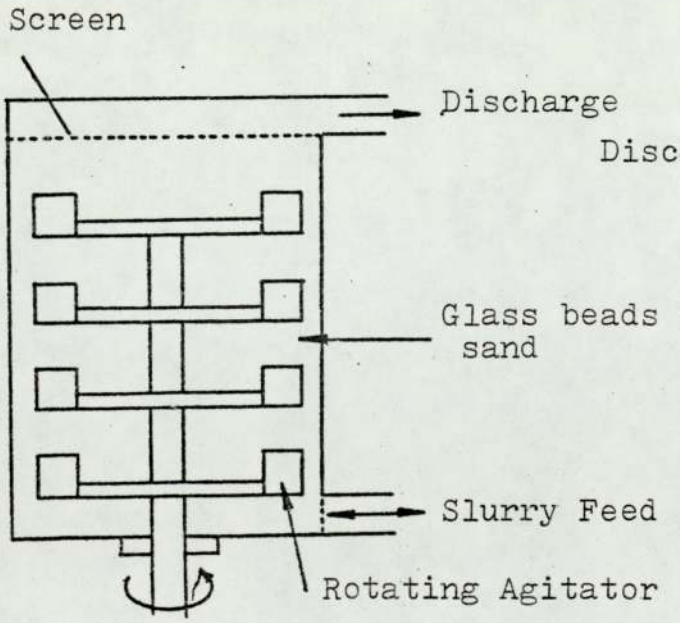

Figure 3.4: Pearl or Sand Mill

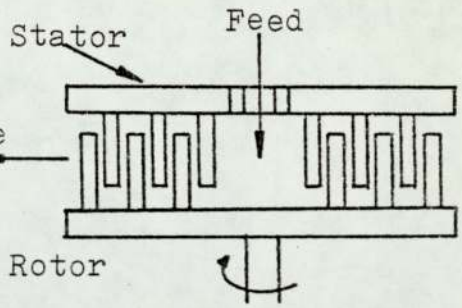

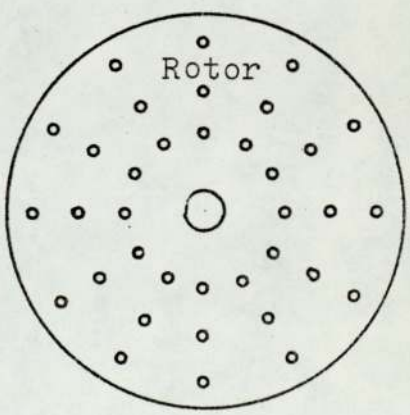

Figure 3.3: Pin or Peg Mill

Pin mills. It consists of two discs which rotate at high speed relative to each other. Each disc has a series of pegs so arranged at radii which allow them to pass close to each other. Feed is introduced either centrally or from the side by an air current. Particles are crushed by impact and by attrition when passing between adjacent pins as they are thrown outward by the centrifugal force generated by the rotating discs. Peripheral speeds lie in the range of 5 - 15 m/s.

They provide a large reduction ratio (ratio of feed size to product size) and product down to 2.0×10^{-5} m is obtainable with non-abrasive materials. They are suitable for heat sensitive materials, since induced air flow helps to cool the particles.

3.4 Sand or Pearl Mills (Ref 122)

The sand mill shown in Figure 3.4, consists of a cylinder containing sand or other fine media which is agitated by a revolving paddle. Continuous wet operation is usual in this type of mill which is mainly used for superfine grinding and/or dispersion in liquid medium, as encountered in the paint industry.

The grinding action takes place mainly by impact between the grinding media and particles. The momentum for impact is provided by the revolving paddles.

3.5 Fluid Energy Mills (Ref 48, 42 and 83)

Three classes of fluid energy mill are shown:

(i) The two-opposing jet Figure 3.5(a), also called the counter current fluid energy mill,

(ii) the jet-o-miser in Figure 3.5(b),

(iii) the micronizer in Figure 3.5(c).

The action of comminution is basically the same for the three classes. Compressible fluid is introduced into a container - the Grinding Chamber - through a number of nozzles forming high velocity jets and particles are entrained into the jet stream where kinetic energy is imparted to them and they are accelerated. On collision with particles emerging from opposing jet or nearby particle stream fracture occurs. The detailed mechanism will be discussed in more detail in the following Chapter 5.

Fluid energy mills are classified as impact mills (Ref 48), but reference has been made to them as attrition mills. Comparison of these mills with others of moving parts was discussed by Temperley and Blyth (Ref 38). Also, Dotson (Ref 32) compared various types of FEM with the ball mill and fluidised bed.

Operating cost of fluid energy mills was briefly discussed by Spiers (Ref 31) in relation to milling of ceramic materials, by Duff et al (Ref 26) and (Ref 34).

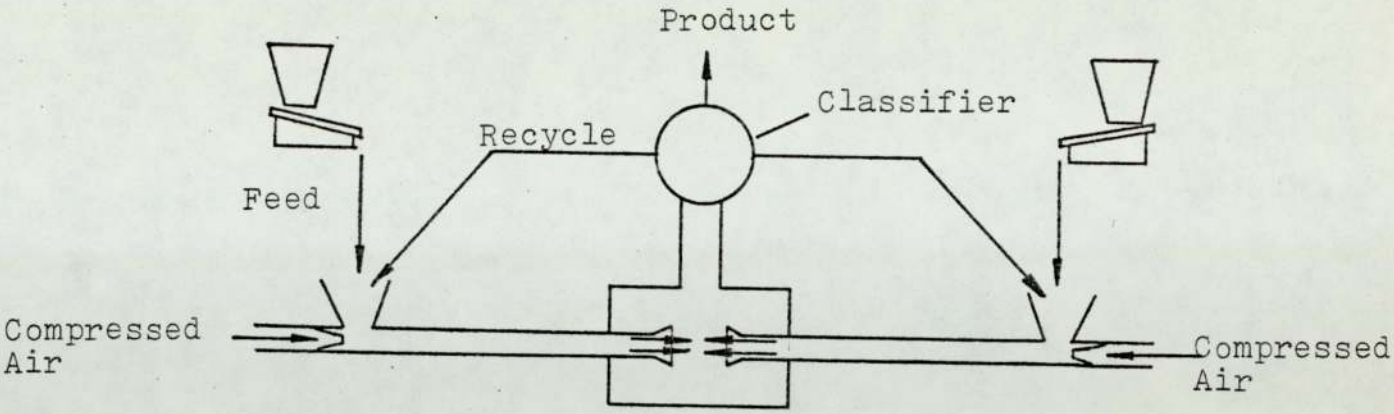

Figure 3.5(a): Two-Opposing Jet

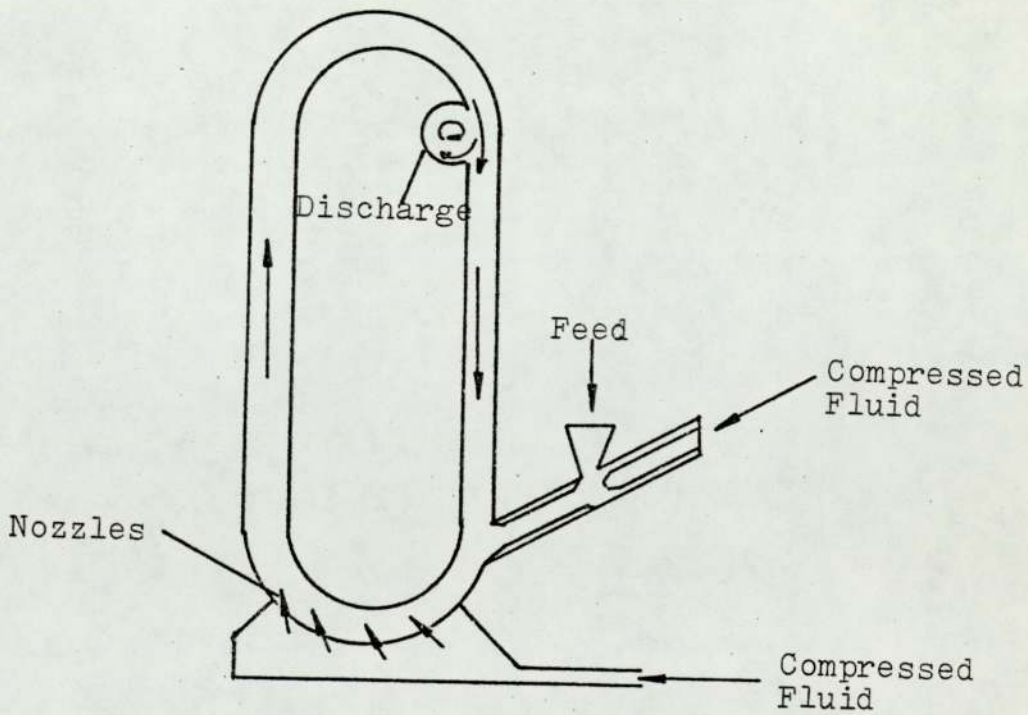

Figure 3.5(b): The Jet-O-Miser Fluid Energy Mill

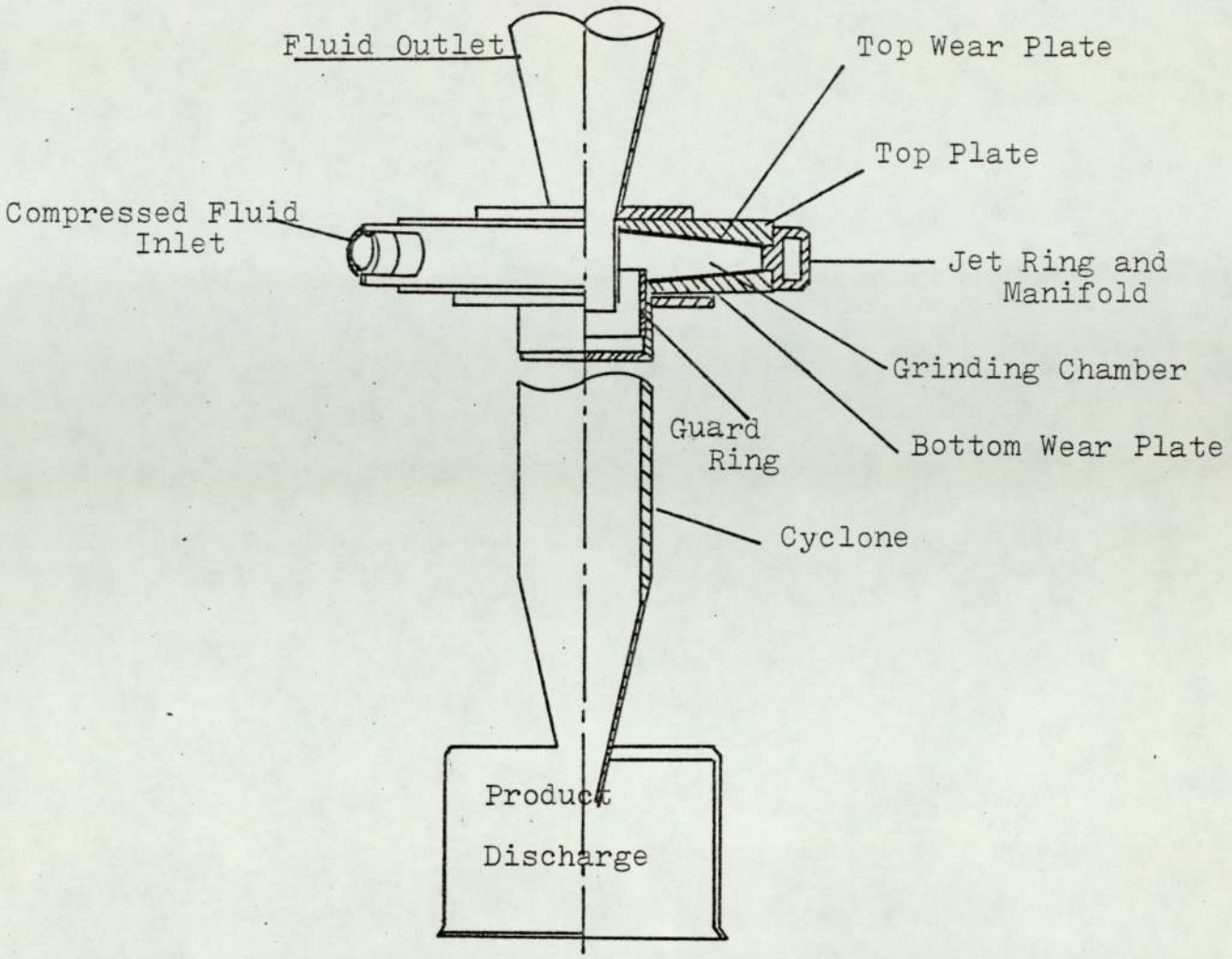

Figure 3.5(c): The Micronizer Fluid Energy Mill (Airfilco Micronizer)

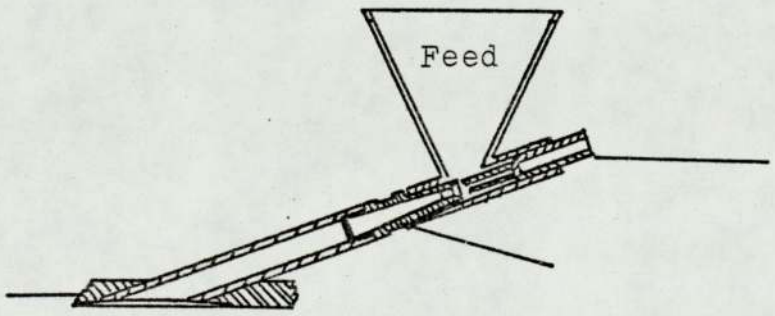

Figure 3.6: Typical Venturi Feeder incorporated with the micronizer.

Factors influencing the choice of fluid energy mills, their applications, plant layout and explosion protection were given by Baines (Ref 24).

Most fluid energy mills users argue that, in spite of high energy cost of running the mill, the cost was not higher than that anticipated in other machines if classification costs are included since the fluid energy mill fulfils the two functions of classification and comminution. Generally, the high cost of FEM is an acceptable state of affairs since no other mill operated in the same size range can offer the same advantages to those discussed in Section 3.53., and with the same throughput.

3.5.1 History and Types of Fluid Energy Mills

The first reported work on jet grinding was by Taggart in 1880, when trials were conducted using two horizontally-opposed air streams. Comminution did occur to a limited extent.

The major, and so far the most important, development on jet-pulverising principles came in 1931 when Andrews (Ref 37) investigated the effect of angling the jets in a cylindrical grinding chamber. This resulted in the air stream and entrained particles rotating at high speed and classification occurred due to centrifugal action. A mill, which later became known as the "Microniser" or "Spiral Mill" was patented (Ref 37) in the U.S.A., in 1936 under

the name of N.H. Andrews and the International Pulverising Corporation of New Jersey. The main initial use was for milling sulphur.

Alternative designs of fluid energy mill emerged after the micronizer, such as the 'Wheller-Stepnoff Mill', 'Oval Mill', 'Jet-O-Miser' or 'Reductioniser'. These designs will be discussed below. Such units have been operating successfully in many plants, but it is the often asserted view that the simpler designs based on the Andrews' micronizer are advantageous due to low initial cost and the ease of replacing parts.

3.5.1.1 The Opposing Jet Mills

This mill is also known as the Majac jet pulveriser, and is illustrated in Figure 3.5(a). It consists of two or four jets opposing each other in pairs. Powder is introduced into the nozzle where it is entrained by the compressible fluid and is accelerated by the opposing high velocity fluid streams so that particles are impacted against each other.

For closed circuit operation a mechanical classifier is usually incorporated in such a mill which is available in various sizes and operated on quantities of compressed air ranging from 20 - 4500 free c.f.m.

The two opposing jets (counter-current) type has been

investigated by Haese (Ref 11) and Rink et al (Ref 1, 2).

3.5.1.2 The Jet-o-Miser

This mill is also known as the Reductioniser, the oval mill, or the jet pulveriser. It consists of a double U-shaped tunnel as shown in Figure 3.5(b). Fluid energy is introduced in the form of super heated steam at $2 \times 10^6 N/m^2$, or compressed air at $6.9 \times 10^5 N/m^2$, via a number of nozzles mounted tangentially around the periphery of one of the curved portions. The jet-o-miser operates on a closed circuit grinding principle and size reduction and classification take place in the same unit.

Solid materials introduced into the jet-o-miser are entrained in and conveyed by the fluid, interparticle collision causes the size reduction, and classification takes place in the tube bend, due to the centrifugal force on the particles travelling in the stream undergoing stratification. Fine particles and fluid leaving at the exit are fed into a cyclone to retain the product.

Jet-o-misers having a tube diameter of 25 to 200mm are in industrial use. Their capacities and sizes have been reported by Dotson (Ref 32), Gillingham (Ref 36) and Berry (Ref 41).

3.5.1.3. The Micronizer

The micronizer, also known as the Spiral Mill, is shown diagramatically in Figure 3.5c and incorporates a flat cylindrical chamber. Comminution of particles which may be free particles or agglomerated results from the action of jets of compressible fluid emerging from the nozzles located around the periphery of the chamber. Basic principles of the micronizer operation will be presented in Chapter 5.

3.5.1.3.1. The Component Parts of the Micronizer

The Jet Ring and the Manifold

A typical arrangement of the jet ring with the fluid manifold is shown in Figure 3.5c Top and bottom plates are clamped to either side of the jet ring to form the grinding chamber. There are two basic designs of the manifold. In small sizes, say up to 200mm in diameter, micronisers have two concentric rings clamped between top and bottom plates, the manifold being formed by the gap between the rings, with jets drilled in the inner ring. In larger micronisers, the manifold forms an integral part with the jet ring, as shown in Figure 6·2. The nozzles are drilled into the inner wall of the jet ring at an angle. The nozzles' axes are in the same direction and are tangential to a hypothetical circle of a diameter less than that of the jet ring.

The Venturi Feeder

The feed material enters the micronizer through an inclined tube leading from the venturi feeder. The venturi section, illustrated in Figure 3.6, consists of a convergent-divergent nozzle, which is positioned close to the base of the feed funnel and leads to the grinding chamber. The end of the venturi jet is set at the entrance to the convergent part of the venturi nozzle and has an adjustable position. The feed tube of the venturi system normally leads to the top plate. In some micronisers the tube drops down from the venturi and then turns to lead up to the bottom plate of the unit. The layout of venturi feeder has been reported by Rink et al. (Ref 14), and Rumpf (Ref 1). A twin-feed system has also been used on some micronisers (Ref 26). This employs similar feed arrangement as described above.

Some micronisers have employed a screw feed system instead of the venturi feeder. The barrel of the screw conveyor connects directly to one plate of the mill. However, the material being fed must form a plug in the conveyor barrel to hold seal on the chamber pressure & the applicability of this device is limited to material (of difficult flow-ability) which will not pack in the feed screw.

Product Discharge and Removal

Product classification is effected in the grinding chamber. It occurs because of the combination of the

centrifugal action of the rotating mass of gas and sweeping action of the gas flow from the periphery to the centre; this will be discussed below in Section 5.

During the comminution action of the micronizer and once the particles have reached a definite size, depending on the operating conditions (Section 5.3), they are swept away in direction of the bulk gas flow towards the central concentric outlets, and leave from one of the plates, either top or bottom or both. In smaller air micronisers - up to 200mm in diameter and all steam micronisers, the fine product passes first into a cyclone attached to the bottom plate (Figure 3.5) where the bulk of the product is removed. In larger air micronisers, over 0·20m in diameter, it is customary to carry out the solid removal from the carrying air in a separate collection system, a cyclone, the bulk of solid and gas leaving via the top plate. In all micronisers filter bags are used to strip the waste gases from the remaining particles.

To prevent random larger particles penetrating to the centre outlet at the bottom plate, two over-lapping concentric rings are fitted at the outlet point (Figure 3.5c). The outer ring - the weir or guard ring - is attached to the bottom plate, and the inner ring is attached to the top plate. The overlap is varied in operation to achieve optimum product size specification. This, and the effect of configuration of the jet ring, will be discussed in Chapter 5.

3.5.2 Fluid Energy Source

The fluids commonly used are air or steam depending on the characteristics of the material to be ground and the required quality of the product.

Air is the fluid most commonly used in the FEM, since it required less auxiliary equipment. Pressures of about 6.9×10^5 N/m^2 abs., have often been reported. Air consumption varies with size, capacity and structural features of the FEM and approximate reported values of air consumption are shown in Table 3.1. These are the results of experience during a range of operations in each case due to the absence of more specific studies. The associated compressor power requirement has also been reported. Mori and Jimbo (Ref 43), and Tanaka (Ref 21) have drawn the following relationship for the jet-o-miser and the micro-niser,

$$G \propto P^n$$

where G is the mill capacity

P is the compressor power

n = 2.2 - 3.3 (Ref 43)

n = 2.0 (Ref 21)

Superheated steam at pressures up to 2×10^6 N/m^2, and a temperature of about 100°C of superheat, is used when substantial air consumption is involved, ie, for micronizer type mills of 0.5m diameter and upwards. However, two factors should be considered when the utilisation of steam is considered -

Table 3.1: Approximate Air Consumption in the Micronizer

Micronizer Diameter mm	Air Consumption m^3/s			
	Refs (43 & 28)	Ref 32	Ref 26	Ref 24
50	0.010			
75	-			0.014
100	0.02	0.03		
200	0.047			0.071
300	0.105			
400	0.167			0.170
500	0.260		0.47	0.190
600	0.470			
800	0.700			

1. the material must withstand high temperature, and
2. economically, the use of steam involves severe heat losses.

Other compressible fluids have been used; for specialised applications argon was used to micronise lithium hydride; nitrogen can be used cryogenically and also, where an inert atmosphere is desirable as reported by Chopey (Ref 35). Fekete (Refs 108 and 109), Fekete used carbon dioxide as a part of a research project aimed at the utilisation of high pressure natural CO_2, to comminute a number of materials. It was found that CO_2 causes considerable structural changes in the material and it was also found that the use of air was far more efficient.

It can be seen that the use of fluids other than air or steam becomes uneconomical unless such factors as safety make it absolutely necessary or the product value can justify it.

3.5.3 Applications of Fluid Energy Mills

Comminuting solids to sub-sieve range is becoming increasingly important, because of the advantages resulting from the increased surface area of small particle sizes. The applications of fluid energy mills have been frequently reported, (Refs 15, 24, 31, 32, 35, 35, 36, 38, 39 and 41). The widest applications of fluid energy mills can be summarised as follows:-

1. where narrow particle size distribution and an upper size limit are required, as in abrasives for polishing lenses, in insecticides, in chemicals to be sprayed through fine orifices and in the paint industry,

2. for increased product purity: due to the absence of moving parts there is no contamination (- of greatest importance in the pharmaceutical and drug industries),

3. to avoid attritional heat: the Joule-Thomson effect, or the cooling effect of the grinding fluid as it expands at the jets, compensates for the heat generated during grinding (useful in the comminution of heat sensitive materials and explosives),

4. combination operations: in addition to grinding in the FEM, one can combine other operations such as mixing or coating small particles with oil, waxes or any other chemicals, and

5. dehydration: FEM using hot air or steam can be used at the same time as grinding and for complete dehydration.

Chapter 4: Two-Phase Flow

4.1. Introduction

The fluid energy mills are a specialised application of the gas-solid suspension systems, where the particulate material is continuously suspended in a vortex-type flow, and also accelerated in the fluid jet intersecting the rotating suspension. The system involves several physical phenomena such as turbulence, interparticle collision, momentum transfer, breakage of single particles, etc.

The literature in the field of gas-solid suspensions is extensive, and is found e.g., in the book of Soo (Ref 124) and Zenz and Othmer (Ref 125), together with the more recent text of Boothroyd (Ref 71), in which most phenomena involved in the subject are presented. These include, particle dynamics, momentum and heat transfer, compressible flow suspension, turbulence generation, effect of electrostatic charge and many related topics. However many important gaps remain in the knowledge of the fundamentals of gas-solid suspensions, and in many cases the difficulties of clarifying turbulent flow behaviour are found to be considerable (Ref 71). Hence experimental studies are often the only source of the basic knowledge.

High speed compressible flow of suspensions has been largely neglected in literature, except with regard to the behaviour of solid-propellant rockets as in references 95 - 107; these will be reviewed later in the chapter. Sound attenuation in gas-solid suspensions has been investigated by Rumpf (Ref 62).

4.2 Particle Behaviour in a Fluid Vortex

The generalised motion equations for a particle moving in a rotating fluid are complex (Ref 131, 132). For a particle moving radially at velocity v_r and tangential velocity v_t the equation of radial motion is:

$$\frac{dv_r}{dt} - \frac{v_t^2}{r} = \frac{(F_{e,r} - F_r)}{m_p} \qquad \text{Eq. 4.1}$$

and tangentially

$$\frac{dv_t}{dt} + \frac{2v_r\, v_t}{r} = \frac{(F_{e,t} - F_t)}{m_p} \qquad \text{Eq. 4.2}$$

where $\sqrt{(F_r^2 + F_t^2)} = \frac{C_D \rho_f A_p}{2} \left[(U_r - v_r)^2 + (U_t - v_t)^2 \right]$

F_r and F_t are radial and tangential friction factors

C_D particle drag coefficient

A_p particle projected area

ρ_f fluid density

U_r gas radial velocity

U_t gas tangential velocity

m_p particle's mass

and $F_{e,r}$ and $F_{e,t}$ are any external forces acting on the particle.

In a centrifuge, for example, the radial pressure gradient may become significant (Ref 71), equation 4.1 becomes:

$$\frac{dv_r}{dt} = \frac{v_t^2}{r} \left[1 - \frac{\rho_f\, U_t^2}{\rho_p\, V_t^2} \right] - \frac{F_r}{m_p} \qquad \text{Eq. 4.4}$$

However, where Stoke s' law is justified and slip velocity between the particle and gas is low, this equation may be simplified to:-

$$v_r = \frac{U_t^2 (\rho_p - \rho_f) d_p^2}{18 \mu r} \qquad \text{Eq. 4.5}$$

where μ is fluid viscosity and dp is particle diameter

4.3 Unsteady Motion of Particles

When a particle is accelerating in a fluid, it experiences drag forces which are additional to that given by Stoke s law. For particle Reynolds Number $Re_p \ll 1$, the equation of motion remains linear (Ref 71); for the case when the fluid motion is also unsteady as in the case of particles travelling in a jet stream, the equation is given by:

$$\underbrace{\frac{\pi d^3 \rho_p}{6} \frac{dU_p}{dt}}_{\text{I}} = \underbrace{3\pi \mu d (U_f - U_p)}_{\text{II}} + \underbrace{\frac{\pi d^3 \rho_f}{6} \frac{dU_f}{dt}}_{\text{III}}$$

$$+ \underbrace{\frac{\pi d^3 \rho_f}{12} \left(\frac{dU_f}{dt} - \frac{dU_p}{dt} \right)}_{\text{IV}}$$

$$+ \underbrace{\frac{3}{2} d^2 (\pi \rho_f \mu)^{\frac{1}{2}} \int_{t_o}^{t} \frac{\frac{dU_f}{dt'} - \frac{dU_p}{dt'}}{(t - t')^{\frac{1}{2}}}}_{\text{V}} \qquad \text{Eq. 4.6}$$

Term I is the force required to accelerate the particle, term II is due to Stoke's law, term III is considered to be due to pressure gradient in the fluid. IV is an account of the extra force due to relative acceleration of the fluid around the particle and V describes the additional force on the particle due to the deviation of the flow pattern around the particle for steady state conditions. Terms III to V are found (Ref 71) to be negligible compared with I and II for large values of $\frac{\rho_p}{\rho_f}$.

4.4 Particle Rotation

The Stoke's law idealisation of a particle moving without angular velocity in a fluid in which there is no other form of shear cannot be realised in practice.

The rotation of a particle can arise through:

1) impact of a particle with a surface such as the micronizer liner plates surfaces.

2) shearing of the fluid eddy in which it is present, and

3) by impact with another particle. This is likely to be significant for relatively large particles.

When spinning particles move through a fluid there is net Magnus' force (F_L) acting on spinning object of large size.

This lift force on a particle is of the form

$$\rho_f U_p d_p^3 \frac{dU_f}{dy} \qquad \text{Eq. 4.7}$$

where y is the distance from the wall.

U_f and U_p are fluid and particle mean velocities.

and was shown to be significant by Serge and Silberg (Ref 127).

The effect of nearby wall (Ref 128) interfering with the fluid flow pattern around individual particles is not of great concern in flowing-multiparticle systems. Interference effects between particles are of more direct importance as they extend throughout the fluid.

4.5 Inter-particle Collision

In turbulent flow, particle collisions inevitably occur, and the frequency of collision is greater when there are particles of different sizes. This follows because differently sized particles follow different trajectories in an accelerating fluid. Frequency of collision also increases approximately as the square of the particle numerical concentration.

The consequences of collision are discussed by Boothroyd

(Ref 71), and are agglomeration or breakage, also both may take place simultaneously. Because of velocities encountered in the fluid energy mill, the breakage of particles would be the predominant phenomenon.

An examination of the particle collision frequency is illustrated in the study of Marble (Ref 110) who considered collisions between particles of two sizes only in an accelerating gas. Thus assuming maximum impaction rate a particle of diameter d_1, will collide with those of diameter d_2 with an average frequency of

$$\frac{n\, d_2\, \pi\, (d_1 + d_2)^2}{4} \left| \bar{U}_p(d_2) - \bar{U}_p(d_1) \right| \qquad \text{Eq. 4.9}$$

where n is the numerical concentration of the particles. It has been argued that if a particle obeys Stoke's law it will tend to regain the velocity it would have in the absence of collision in an interval of the same order as its relaxation time $t_v = \rho_p\, d_1^2/18\mu$ therefore if t_c is the average time interval between successive particle collision, for $\frac{t_v}{t_c} << 1$ particles of size d_1 will tend to return to the velocity they would have in the absence of collision, before they suffer any further collision.

The situation in the microniser is far more complex than this, because of the presence of wide size spectrum, and high turbulence.

4.6 Momentum Transfer

The equivalent of the Navier-Stokes equations for momentum conservation of the suspension flowing in pipe was considered by Hinze (Ref 136), by obtaining fluid phase and particle continuum phase momentum conservation equations. Turbulent suspension flow equations were also considered by Boothroyd (Ref 71).

The fall in pressure of a suspension as it flows along a pipe can be due to friction, acceleration of fluid, or gravitational effect. Boothroyd, by assuming a one dimensional flow and ignoring variation of properties across the pipe stated that if the measured pressure drop across a length of the pipe is ΔP_m, only part of ΔP_t is due to friction, and that in fact,

$$\Delta P_t = \Delta P_m - \Delta P_{as} - \Delta P_{ag} - \Delta P_{\rho s} - \Delta P_{\rho f}. \qquad \text{Eq. 4.9}$$

where ΔP_{as} and ΔP_{ag} are caused by acceleration of the solid and gas respectively. Hydrostatic pressure of the gas and solids also produce pressure differentials $\Delta P_{\rho g}$ and $\Delta P_{\rho s}$. The fall in pressure due to solid acceleration may be evaluated from

$$\Delta P_{as} = 2\pi \left[\left\{ \int_0^{D/2} r \, \rho_{ds} \, U_p^{\,2} \, dr \right\}_{out} - \left\{ \int_0^{D/2} r \, \rho_{ds} \, U_p^{\,2} \, dr \right\}_{in} \right] \qquad \text{Eq. 4.10}$$

this requires the knowledge of ρ_{ds} the dispersed phase density, and Us.

Also for a gas

$$\Delta P_{ag} \approx R \left(\frac{W_g}{A}\right)^2 \left[\frac{T_o}{P_o} - \frac{T_1}{P_1}\right] \qquad \text{Eq. 4.11}$$

And, if the slip velocity is fairly small then

$$\Delta P_{as} = \frac{W_s}{W_g} \Delta P_{ag}. \qquad \text{Eq. 4.12}$$

where W_s is solids rate of flow

W_g is Gas rate of flow

A is cross-sectional Area of flow.

The relative magnitude of the various contributions to ΔP_m can vary considerably, Boothroyd (Ref 71) found that for a flow of 30 m/s in 1" pipe ΔP_t, ΔP_{ag} and ΔP_{as} can have large values, whereas by comparison $\Delta P_{\rho s}$ and $\Delta P_{\rho g}$ are negligible. Conversely $\Delta P_m \approx \Delta P_{\rho s}$ in a 6" bore riser conveying catalyst in an oil refinery.

The slip velocity $(\bar{U}_f - \bar{U}_p)$ is hard to estimate. Boothroyd (Ref 130), by assuming a simplified gas-solid suspension system argues that the slip velocity will increase strongly with increase of particle size: large particles will receive considerable momentum from impact with smaller particles travelling in the same direction, this is illustrated schematically in Fig 4.1. The momentum sharing

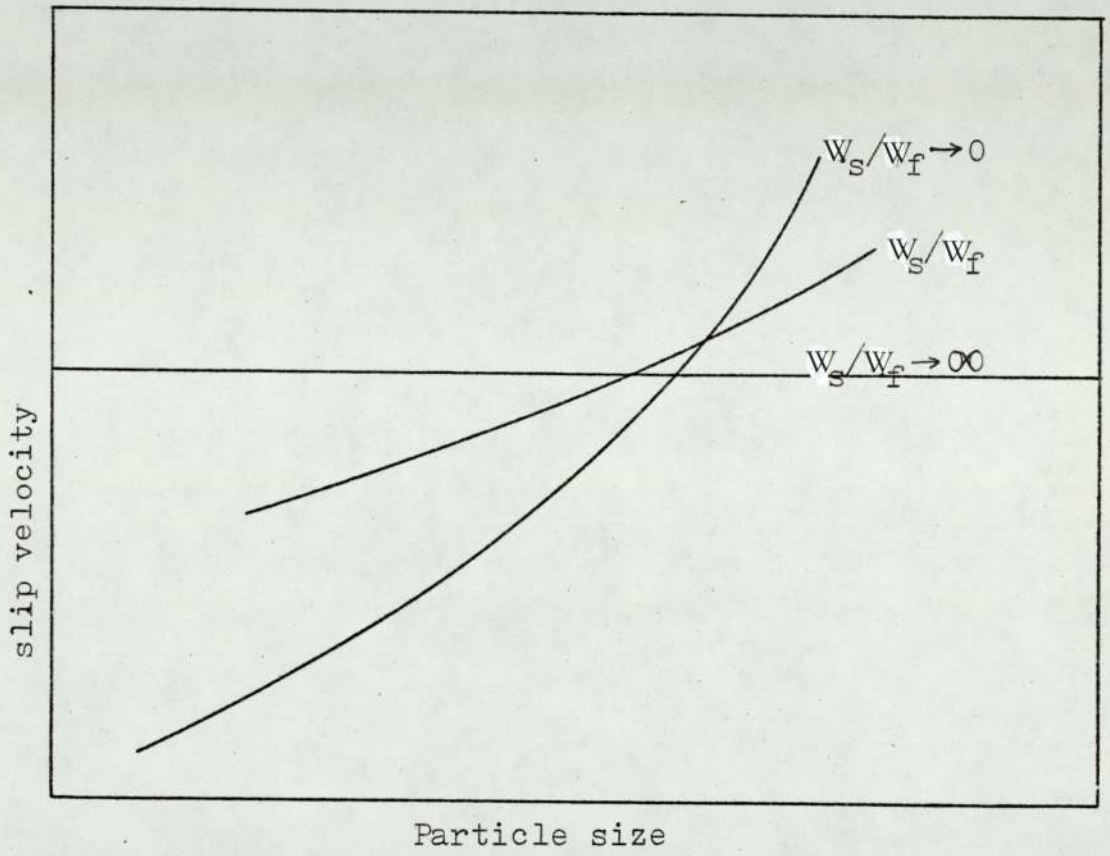

Figure 4.1 - Schematic illustration of tendency of particles to acquire the same slip velocity at higher solids loadings due to the particle collisions. (Ref 71, p 139)

will increase with loading ratio W_s/W_f, so that all particles tend to acquire the same slip velocity at high loading ratio. This hypothesis needs backing from experimental data however.

Particle velocity U_p, relaxation time $t_v = \frac{\rho_p d^2}{18\mu}$ and L the mean free path between particle collisions (Ref 110) are thought to have considerable effect. For example for large values of $U_p t_v/L$, momentum transfer between particles is likely to be primarily by collision with each other, whereas at low values of $U_p t_v/L$ momentum transfer by viscous interaction with the gas is more significant.

The physical significance of L can be considered with reference to the jet length L', so for $U_p t_v/L' \ll 1$ then particles tend to follow changes in velocity and temperature quite closely and be in equilibrium with the gas. However if $U_p t_v \ll L'$ then the particle is almost completely unaffected by this change.

Unfortunately relatively little attention has been given to suspensions containing particles of different sizes. A small size range of particles may define different regimes since the relaxation time is related to the square of particle diameter.

4.7 Influence of Particles on Field of Fluid Turbulence

A high degree of turbulence is thought to exist within

fluid energy mills, particularly in the vicinity of the jets. The evidence is generally that solids reduce the gas eddy diffusivity (133, 134). However, an increase has also been reported (Ref 135). Few experimental studies have been made to investigate the turbulence of gas solid suspensions which are sufficiently dense for interference with the gas turbulence to be significant.

For very fine particles which have a relaxation time t_v, which is much less than the eddy life time t_e, the average rate of work done on the particle by unit volume of the eddy is given by Owen (Ref 137) to be

$$3\pi\mu \; d_p N U^2 \; t_v/t_e \qquad \text{Eq. 4.13}$$

where N is numerical concentration of particles
where U is the turbulent velocity fluctuation

of the gas. The particles may be expected to reduce turbulence according to

$$\frac{\text{Turbulence Intensity with Solids}}{\text{Turbulence Intensity in absence of solids}} = \frac{1}{\left(1 + \alpha \frac{\rho_{ds}}{\rho_f}\right)^{0.5}} \qquad \text{Eq. 4.14}$$

For fine particles (where $t_v << t_e$), $\alpha = 1$ and for large particles $\alpha = t_e/t_v$.

4.8 Re-entrainment of coarse Particles

The occasional instantaneous occurrence of a strong eddy near the wall, is thought to contribute markedly to the

increased entrainment of solids into a stream, and these eddies may account for much of the entrainment which actually occurs.

In Owen's analysis (Ref 137), the state of re-entrainment is shown from momentum considerations to be self adjusting: when particles are accelerated down stream, this will cause a reduction in the shear stresses of the fluid on the particles within the flow. When there is a large concentration of entrained particles, this will reduce the shear stress below the minimum necessary - given by:

$$\lambda o \geq \frac{2}{3\sqrt{3}} \, d \, \rho_p \, g \qquad \text{Eq. 4.15}$$

where λo is the fluid shear stress near the particles.

Thus entrainment is reduced to an equibrium value. This phenomenon is clearly automatically self adjusting either way. Also interparticle collision must be taken into account as this aids solid re-entrainment.

Chapter 5: The Microniser Literature

5.1 Introduction

To date much of the literature available on fluid energy mills has been concerned with their description and emphasising their uses and potential. Some research aimed at investigating the mechanisms of comminution and classification in the microniser have succeeded in qualitatively describing both mechanisms. But the literature is deficient in papers dealing with the extent and significance of other features of the microniser operation. The gas-solid suspension aspects were discussed in Chapter 4. Other literature concerning the microniser is presented below.

5.2 Grinding Mechanism

Fluid energy mills are classified as impact mills (Ref 48) where comminution occurs mainly by interparticle collision. There have been various theories as to what mechanism plays the major part in jet grinding. Whether it is:

(1) the high velocity jets (Ref 9, 10 and 43)

(2) high velocity air currents and turbulence effects (Ref 48 and 83)

(3) collision between suspended particles and microniser wall, or

(4) the creation of high momentary internal pressure within the particle (Ref 33) (although this action is unlikely to take place except to a

very limited extent in cases where the material is porous and binding forces extremely weak).

The comminution mechanism, based on the investigation of flow patterns in the microniser (Section 5.4), was explained and investigated by Rumpf and Kurten (Ref 4): their theory was that within the microniser chamber two zones exist. As shown in Figure 5.1 the outer zone nearer to the jet ring wall is the comminution zone, while the remainder is the classification zone. This was also assumed by Hendry (Ref 23) and Tanak (Ref 21). In the comminution zone the fluid jets entrain some of the streaming particles from the rotating suspension. The mixing effect caused by the eddies formed near the jets and reduced pressure in that region create favourable conditions for the entrainment of particles into the jet. The particles largely follow the flow and penetrate the jet (Figure 5.2) at a velocity which varies according to the distance from the nozzle exit, and the particle size (Section 5.5). In this way relative differences of the particles penetrating the jet and those being accelerated in the direction of the jet are obtained causing interparticle collision. The probability and frequency of collision increases with increased numerical concentration of the particles and particle diameter (Section 4.6). The comminution mechanism II introduced in Section 2.3 is taking place, in which both oblique and eccentric impacts occur.

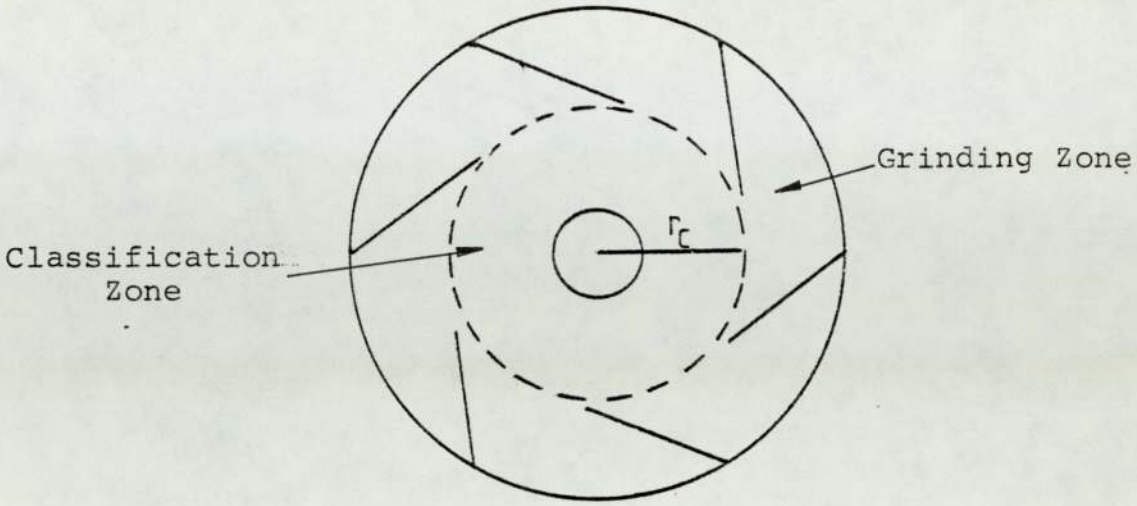

Figure 5.1 - Illustration of Grinding and Classification Zones in the Micronizer Chamber

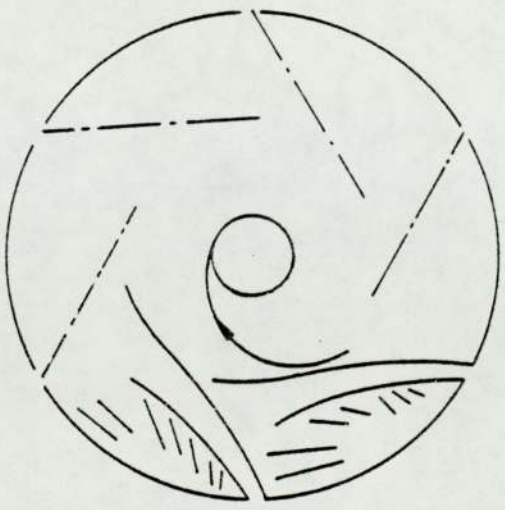

Figure 5.2 - Illustration of Jet Flow and Particles Penetration into the Jet Stream

Rumpf and Kurten (Ref 4) and Muschelknautz et al (Ref 1, 2) studied the comminution mechanism in a 50mm diam (10mm high) micronizer using triboluminescent photographs produced by the fluorescence emitted on crushing sugar crystals. They showed qualitively that comminution takes place largely through the collision of the suspended particles in the boundary zones of the jets, and in the front and back of the jet.

Mori and Jimbo (Ref 43), classified the comminution mechanism in the jet-o-miser, into two distinct categories:

(1) "Bulk shattering" grinding, which results in the disintegration and collapse of particles, and
(2) "Surface grinding", which results in tearing off small fragments from the particle surface.

In the above hypothesis it is thought that bulk shattering or body crushing results in medium-sized particles while surface grinding results in fines. The grinding rate in fluid energy mills is believed to be "bulk shattering" controlled. However it was discussed in Section 2.3 that both mechanisms are variations of the same "Particle - Particle impact", bulk shattering occurs by eccentric impact while surface grinding occurs by oblique impact, the extent of either being dependent on the solid concentration in the grinding zone (hold-up). At low concentrations of solids, the collision rate would be low and increasing with concentration; the grinding rate would be "bulk shattering"-controlled. At high concentration the jets would be swamped

so that too many particles would have too low an energy level to shatter on impact; thus fines will result only from surface grinding. An extreme example of the latter case is the grinding obtained in a fluidised bed (6, 32). Also it was observed that "surface grinding" - controlled operation occured for comparatively hard materials (Ref 7), while rather brittle materials were crushed by impact stress in which particles were split into fine and intermediate sizes.

It has been suggested by Muschelknautz et al (Ref 2) that the point at which the number of interparticle collisions producing fracture drops considerably is when the volumetric solids concentration fraction exceeds 0.1. The influence of solids concentration in the mill chamber is further discussed in Chapter 7.

5.3 Classification Mechanism

In micronisers, comminution and classification take place in the same unit. Rumpf and Kurten (Ref 4) and Muschelknautz et al (Ref 1, 2) found that the zone of comminution and zone of classification are clearly recognisable, as illustrated in Figure 5.1. The circle denoted by diameter r_c, has been assumed the boundary between both zones.

The flow pattern in the classification zone of the microniser is similar to the flat vortex cyclone which

Beverlow et al (Ref 56) have investigated. Three differing patterns for vortex-type flow are described mathematically; these are:

(a) constant angular momentum flow,

(b) constant tangential velocity flow,

and (c) solid-disc type flow.

The most favourable flow pattern for classification of particles, is that of constant tangential velocity - Archimedes spiraled flow -, and was the basis for the design of vortex classifiers discussed by Lukens (Ref 60), in which particle size, shape and weight effects upon cut size were investigated, also by Gedridge et al.(Ref 57), Payne (Ref 58) and Goets (Ref 59). This flow pattern was also assumed by Tanaka (Ref 21). In a study of scaling-up of micronisers, it was concluded that a uniform velocity distribution over the total height H_j of the mill chamber cannot be expected, due to the two-dimensional flow that occurs near the upper and lower surfaces of the mill chamber. The effective height of the classifying zone was defined by H_j, which is presumably a function of the nozzle diameter. The tangential velocity was assumed uniform, and to follow the Archimedes spiraled flow.

For particle size classification, the cut off particle size (d_p^*) can be calculated assuming Stoke's Law (for Reynold's Number < 0.1) thus

$$d_p^* = \left[\frac{18\ U_r\ r_i \mu}{v_t^2}\right]^{0.5} \qquad \text{Eq. 5.1}$$

where U_r is the radial velocity

r_i the radius at point of interest

v_t tangential velocity

μ viscosity of fluid

In the microniser determination of U_r and v_t become difficult, due to the presence of solid suspension and lack of satisfactory measurement techniques. However, Tanaka (Ref 22), calculated U_r from

$$U_r = (V_n + V_s)/2\pi r_o H_j \qquad \text{Eq. 5.2}$$

where V_n is volume of fluid introduced at the jets

V_s is volume of fluid introduced at the venturi feeder.

r_o is the outlet radius

H_j effective height of the classification zone.

The limiting particle size calculated in equation 5.1 by references (2) and (40), in the case of true size reduction, is generally smaller than the average particle size of comminuted material from the mill. It seems that these differences are due to the fact that the tangential velocity of the particles in the classifying zone is considerably lower than that of the fluid stream, and that this velocity is greatly reduced due to the presence of particles in suspension.

5.4 Flow Pattern in the Micronizer Chamber

Flow in the micronizer can be characterised by a basic stream which follows a spiral path. This basic stream is disturbed by the jets, and the streaming medium is taken up from the basic stream by the jets because of pressure gradients in the field. A wedge-shaped area is formed between two successive jets and the jet-ring section. Counter current eddies are thought to exist in this wedge.

Rumpf and Kurten (Ref 4) qualitatively studied the flow phenomena in a model micronizer operated with water, and using dye. It was shown, that the jet on leaving the nozzle retains its direction and shape, but soon is deflected in the direction of the basic stream, and widens. At the same time, a return flow towards the periphery of the chamber occurs above and below the jet nozzle plane as shown in Figure 5.3. In the vicinity of the top and bottom plate and in the inner radius of the micronizer the stream was observed to take a spiral course towards the outlet port (Figure 5.4). Using a six-nozzle jet-ring, Rumpf and Kurten (Ref 4) observed that a "hexagonal" ring was formed by the jets.

The experiments with water revealed some information on the qualitative flow phenomena in the micronizer, but since water is an incompressible medium, complete similarity does not exist between the mill operated with water and that operated with air, i.e. compressibility should not be

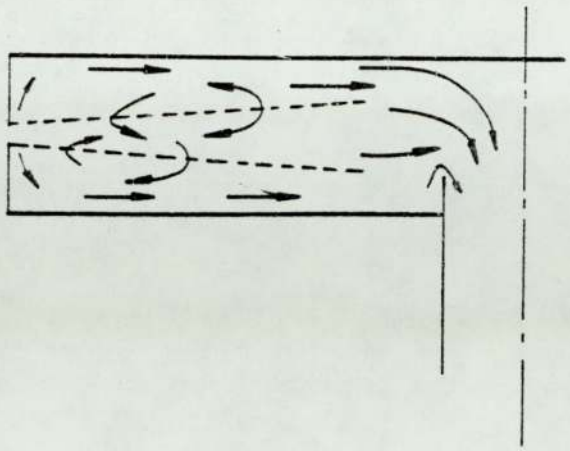

Figure 5.3 Cross Section of the Micronizer Chamber, Showing the Jet Flow and Return Flow Above and Below the Jet Plane

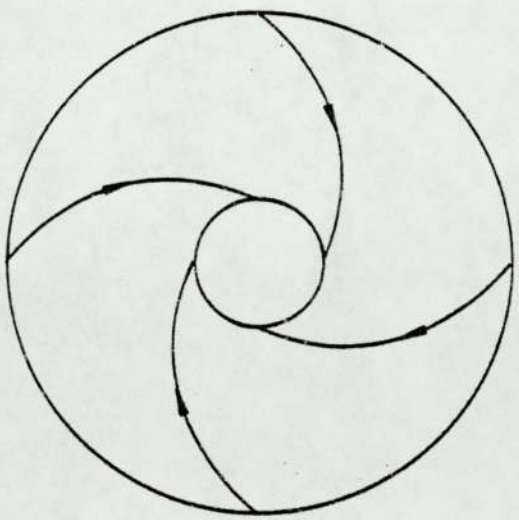

Figure 5.4 Flow Pattern in the Vicinity of Top and Bottom Plates

disregarded. As far as is known the field of velocity and flow pattern in and around a jet in the micronizer has not yet been investigated.

The momentum of the jets is always greater than that of the main stream, cross-current. According to Abramovich (Ref 91), when considered in the direction of flow of the parallel stream, the cross current is decelerated by the free jet, as illustrated in Figure 5.5. A velocity gradient exists between them, and the flanks of the jet are subject to shearing stresses, and a field of excess pressure.

The jet, which is round at the nozzle exit becomes deformed under the influence of field of pressure and shearing stresses (Figure 5.5). Hence, after a short distance its cross section becomes kidney-shaped and the jet itself is deflected in the direction of the parallel current. This is analogous to flow around a cylinder (Ref 91); eddies are formed in the cross stream behind the free jet which are carried away by the free jet since the momentum of the latter is stronger than that of the cross-stream. These eddies entrain the surrounding fluid and cause inner circulation in the jet, which, in turn causes a strong mixing effect. Hence, the velocity of flow in the jet is reduced more rapidly than in a free jet with stagnant surroundings.

5.5.1 Jet Characteristics

Theoretical analysis of the velocity distribution and fluid entrainment ratio has been discussed by Schlichting

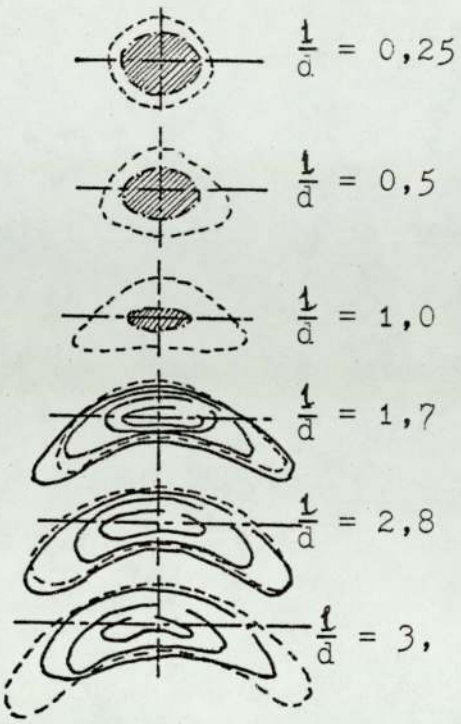

Figure 5.5a: The cross-sectional configurations of a jet in a lateral flow at various distances from the first section. (d = 20 mm., u_o = 77.6 m/sec, w = 35.6 m/sec.

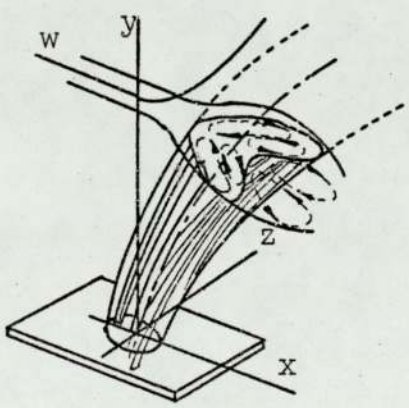

Figure 5.5b: Diagram of a jet in a lateral deflecting flow.

(Ref 90) and Abramovich (Ref 91). The latter, presents an extensive theoretical study of turbulent jets. In the case of turbulent round free jets, velocity profile is known to be a function of jet length x. As shown in Figure 5.6 three jet regions can be identified: region I up to $x = 4.44d_N$ corresponds to the jet core length, region III greater than $10d_N$ and less than $30d_N$, and transition region II lies between these two regions.

Region I is thought to be the determining section for particle acceleration. The knowledge of velocity distribution in this region is scarce, and few authors have investigated the effect of nozzle diameter and velocities encountered in fluid energy mills.

In region II, approximation data on the velocity distribution are given by Shih - I-Pai (Ref 92), Turve (Ref 86) and Albreston et al (Ref 87). The mean longitudinal velocity U_m along the jet centre is given by the equation

$$\frac{U_m}{U_o} = \frac{K\, d_N}{x_m} \qquad 5.3$$

$$K = 6.2 \quad \text{for} \quad 7 < \frac{x}{d_N} < 100 \quad \text{(Ref 86 and 87)}$$

$$K = 6.5 \quad \text{for} \quad 10 < \frac{x}{d_N} < 30 \quad \text{(Ref 92)}$$

where U_o is the jet velocity at the nozzle exit

d_N is nozzle diameter

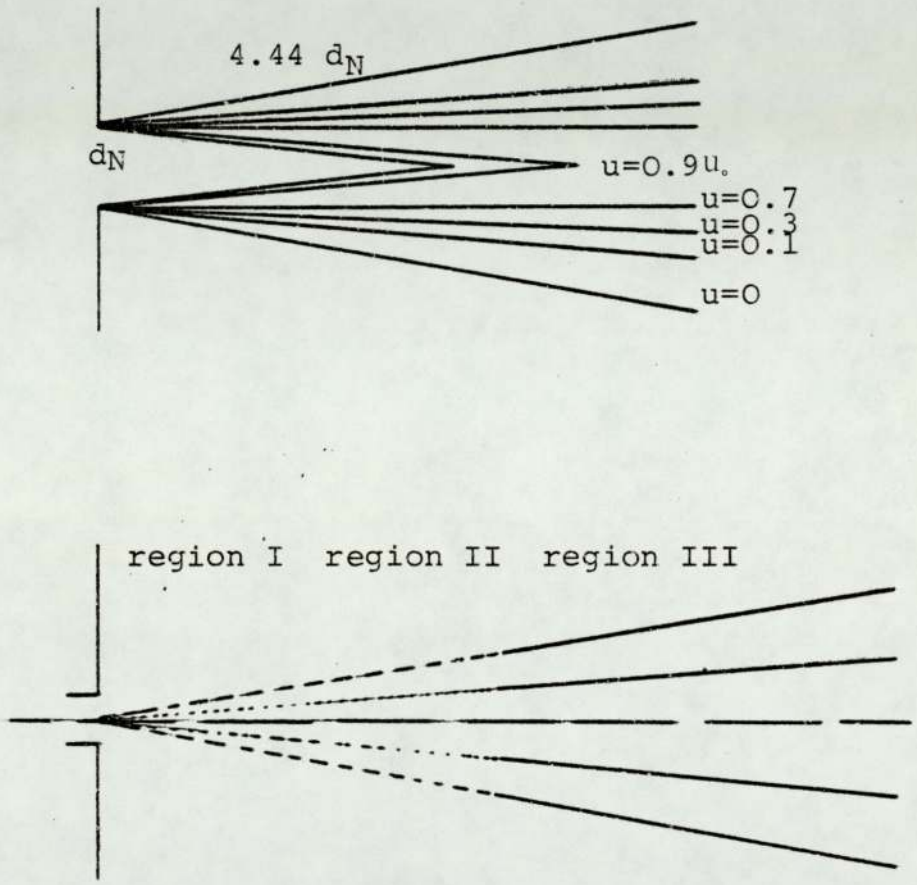

Figure 5.6 : Lines of equal Velocity u in Nozzle Vicinity for a Turbulent Round Free Jet (according to Shi-I-Pai). Also Showing the Three Regions of a Free Jet.

x_m is distance from exit along the nozzle axis.

Jet momentum dissipation in a fluidised bed was investigated by Behir et al (Ref 3) when the momentum was found to be dissipated within a cone angle of 36°. Alberston et al (87) determined the jet angle to be 20°. Density gradient affects the rate of spread of a single-phase free jet. This is discussed by Keegy and Weller (Ref 88) and Cleeves and Boelter (Ref 89).

Jet characteristics discussed above were confined to discharge of the jet into quiescent flow media or flow media moving at constant velocity in the jet direction, where as in the microniser and the jet-o-miser, there is significant movement of the flow medium around the jets.

5.5.2 Particle Behaviour

Particle movement and velocity in free jets was investigated by Rumpf (Ref 9). Closely-sized particles were fed into the periphery of the outlet of a single jet discharging into a supposedly, quiescent flow medium. The velocity of these spherical particles was measured using stroboscope and photography. Particle entry to the jet did not follow a uniform pattern. As observed by Rumpf (Ref 9); many particles penetrated a considerable distance into the jet and others only reached the jet boundary. This might be due to difference in the initial traverse particle velocity.

Particle velocity V_p as a function of jet length x_m is shown in Figure 5.7. This reaches a maximum value depending upon particle size (Figure 5.8 a and b) and jet initial velocity U_o.

Computed jet velocities from equation 5.3 did not agree with measured particle velocity, indicating that drag coefficient of the particle is appreciable. The known drag coefficient relationship (Ref 9) is a function of particle Reynolds Number, and the accuracy with which this is known, since different expressions are used for differing ranges, of Reynolds Number.

5.6 Preliminary Design of Microniser

Acceleration of particles to the impact velocity is a requirement to induce fracture. The maximum stress caused by the collision of two elastic spherical bodies was discussed in Section 2.3. It was shown that;
Maximum Stress caused (σ_{max}) and Particle Impact velocity V_i are related by $\sigma_{max} \alpha (V_i)^{2/5}$ (Eq. 2.2, p12)

The data for impact velocity necessary for size reduction is not as yet known.

A certain distance is necessary to accelerate the particles, entrained into a jet, from initial velocity V_o to an impact velocity V_i. Rumpf (Ref 9), using a simplified assumption of constant drag coefficient for

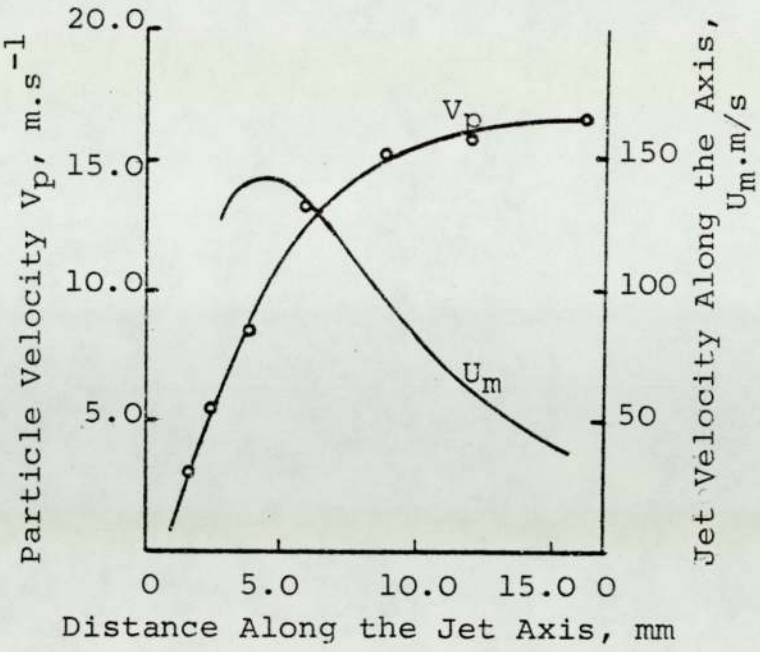

Figure 5.7 : Measured Particle Velocity V_p and Calculated Jet Velocity U_m on a Particle Path

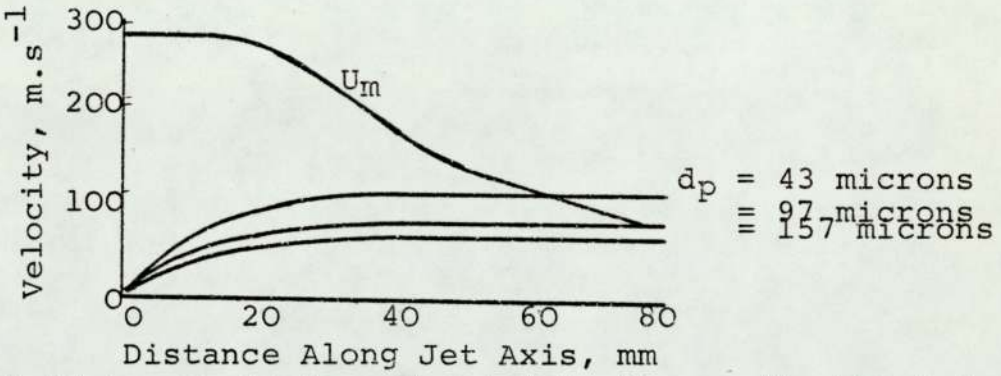

Figure 5.8(a) : Particle and Jet Velocity on the Jet Axis

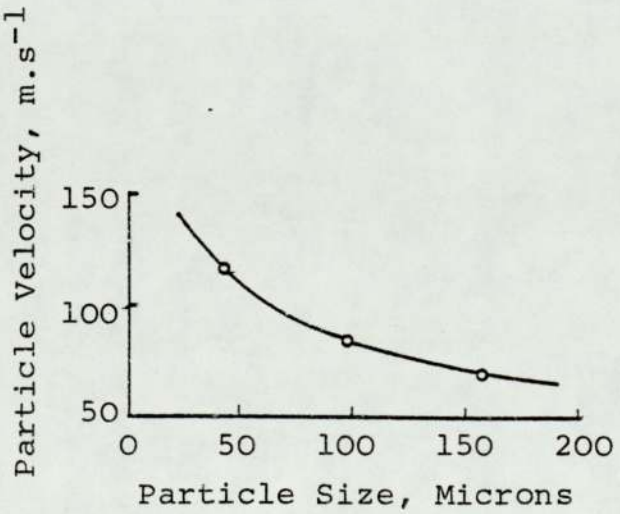

Figure 5.8(b) : Maximum Obtainable Particle Velocity for Jet Exit Velocity = 282 m.s^{-1}

particle Reynolds Numbers from 600 to 200,000, and from consideration of the motion of particles under conditions where the effect of gravity can be neglected, obtained the acceleration distances,

$$s = \frac{4}{3} d_p \cdot \frac{\rho_p}{\rho_f} - \left[\left(\frac{Vp}{V_p - V_i} - 1\right) - \ln \frac{Vp}{V_p - V_i}\right] \quad \text{Eq. 5.4}$$

d_p particle diameter (μm)

ρ_p particle density (gm/cm^3)

ρ_f fluid density (gm/cm^3)

V_p particle velocity m/s

V_i impact velocity m/s

Because acceleration distance increases with particle size, calculations must be considered for the largest particles present. The nozzle diameter (d_N) should be chosen so that the effective length of the jet X_{max} given by

$$X_{max} = 10 - 20\, d_N \quad \text{Eq. 5.5}$$

is comparible with s (Eq. 5.4). Also in the preliminary design of the microniser the chamber diameter D_m can be made so that

$$D_m = 20\, d_N \quad \text{Eq. 5.6}$$

The necessary impact velocity for larger particle diameter is probably less than for smaller diameters as strain energy required for fracture increases with decreasing

particle diameter (see Section 2.2).

5.7 Factors Influencing Micronizer Performance

5.7.1 Introduction

Micronizer performance may be evaluated in relation to some of the physical properties of the comminuted material, such as the particle size distribution, the specific surface area, the mean diameter etc. The specific property of interest in micronizer operation is chosen according to the eventual application of the finished product, as discussed above in Chapter 3.

The factors influencing these properties in the micronizer operation may be divided into three categories;

1 - feed Material properties

2 - operational parameters of the micronizer

3 - structural features.

Some of the factors considered are interrelated to each other. This, and the effect of various parameters, are discussed below.

5.7.2 Operational Parameters

5.7.2.1 Fluid Throughput and Jet Pressure

From considerations of mass and energy balance equations, the exit jet velocity, for non-ideal gas, and a negligible

down stream pressure is given by,

$$U = \sqrt{\gamma P v_f} \qquad \text{Eq. 5.7}$$

where U is the velocity at the exit

P is upstream pressure

v_f is specific fluid volume

$\gamma = C_p/C_v$

The pressure at the nozzle determines both fluid throughput and jet velocity which also determines the velocity of the particles travelling in the jet and their impact velocities. The classification is also influenced by the jet velocity and fluid throughput; thus as pressure increases so does the ratio of tangential velocity V_t to the radial velocity U_r.

The effect of pressure on the grinding rate, which was defined by Mori (Ref 7) by the percentage of comminuted material less than a given particle size, was studied by Mori and Jimbo (Ref 43) and Mori (Ref 7), in the jet-o-miser and fluidised bed types. It was shown experimentally (Ref 43) that the grinding rate g_r is directly proportional to the modified pressure at the jet, thus

$$g_r = k \cdot P_N \qquad \text{Eq. 5.8}$$

$$P_N = (P_J - P_{min}) \qquad \text{Eq. 5.9}$$

where P_{min} is the minimum pressure necessary to entrain particles into the jet stream.

This relationship was determined for materials of differing feed size between 20 and 40 mesh, which is well above sizes encountered in fluid energy mills. A realistic explanation of P_{min} would be to consider it as the minimum pressure required at the nozzle to induce high jet and particle velocity to incite fracture on impact. Typical results are shown in Figure 5.9 obtained by Mori (Ref 7). Also Menyhart and Miskiewicz (Ref 117) observed a linear relationship between pressure and change in specific surface area for various materials. Ramanujam and Venkateswarlu (Ref 24) studied the comminution of calcite of particle size range 0.15 - 1.7 mm in an experimental jet-o-miser of 20 mm diameter. A correlation for specific surface area, solid feed rate and air throughput was derived.

Limited information on the effect of pressure in the microniser has been published. The effect of pressure on product particle size is expected to be similar to that in the jet-o-miser.

5.7.2.2 Material Throughput

The effect of solid throughput on the product particle size is related to the rate at which particles are fractured at the jet, which in turn determines the quantity of particles held in the mill, i.e. hold-up. Increased hold-up, for a given fluid throughput, reduces the tangential velocity of the fluid in the classification zone (Section 5.3), the effect has not been investigated with relation to the microniser.

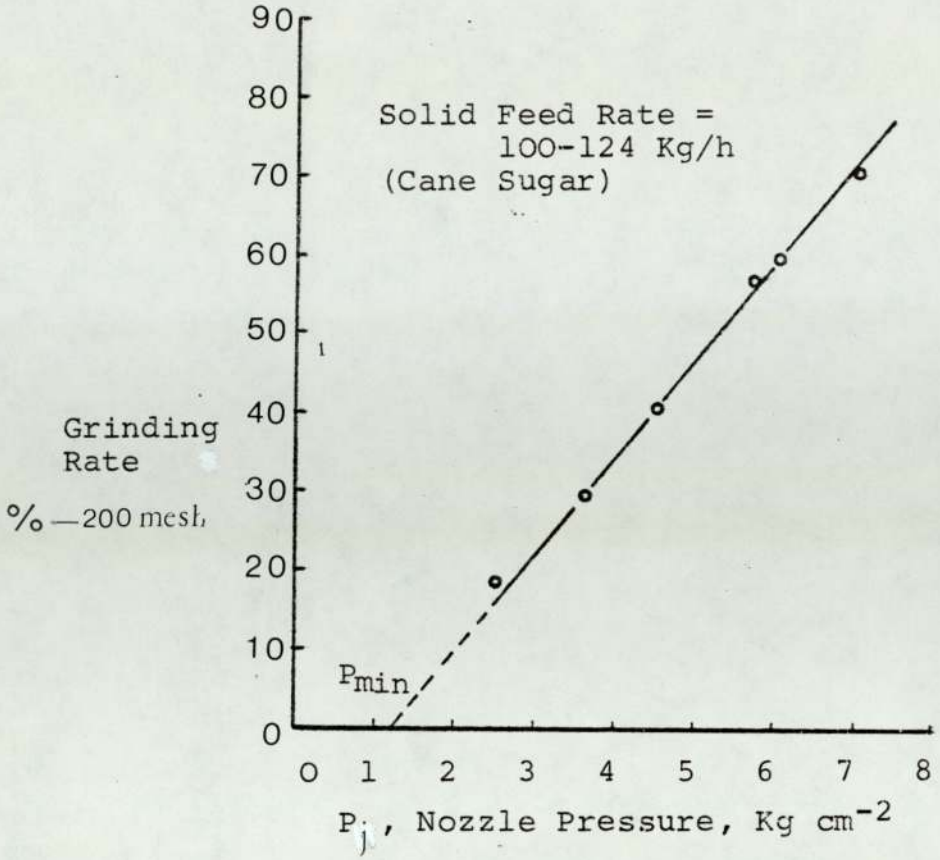

Figure 5.9 : Effect of Pressure on Product Fineness

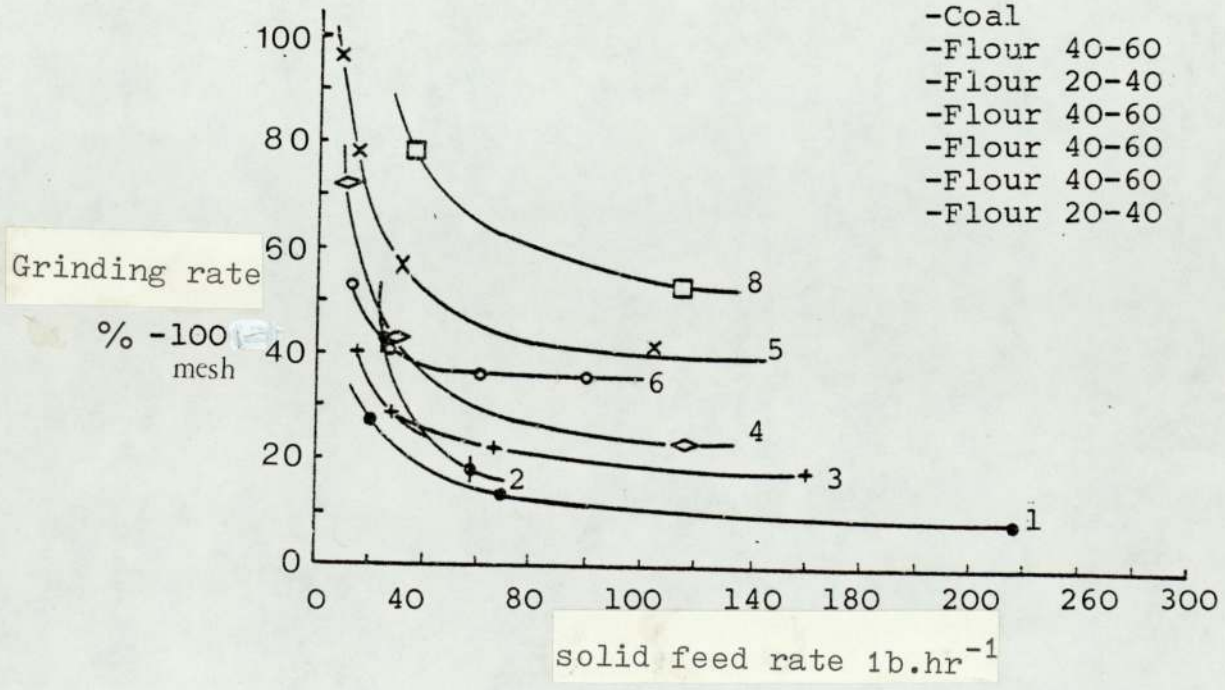

Figure 5.10 : Effect of Solid Feed Rate on Degree of Grinding, for Various Feed Sizes

Hendry (Ref 23), and Dobson and Rothwell (Ref 40) have experimentally shown that for a given pressure at the nozzles, the mean particle diameter of the product increases with increased feed rate. Ramanujam and Venkateswarlu (Ref 27), Mori (Ref 7), and Mori and Jimbo (Ref 43) achieved similar results in their studies of jet-o-miser mill, as shown in Figure 5.10. Furthermore, it was found that product mean particle diameter approaches the value of the feed mean diameter at high solid throughput. Ramanujam (Ref 27) observed that at high values of solid feed rate the jet-o-miser operation becomes unsteady and fluctuation in product size occurs. Hence, the feed rate must be kept below this value, which is a function of mill size, and fluid throughput.

5.7.3 Constructional Features

5.7.3.1 Jet Injection Angle

The axes of the nozzles in the jet ring are normally in a clockwise direction and tangential to a hypothetical circle of smaller diameter than that of the jet ring. This is illustrated in Figure 5.1, where the jet angle is also shown. The jet injection angle may influence the micronizer performance in two ways. Firstly, the jet penetration into the main stream and the bulk of the suspension is affected and, hence the change in the direction and velocity of the incoming particles and their effect on the degree of comminution. Secondly, the effect upon the tangential velocity of the rotating fluid, and the classification effect

within the chamber is directly related to the jet angle.

Radial pressure distribution within the micronizer chamber was measured by Muschelknautz et al (Ref 1) and as shown in Figure 5.11 for 30° to 75° injection angle, increases with the mill radius. It is also seen that in the presence of solids, the pressure drops markedly within the mill and decreases with increased solid to air ratio.

The tangential velocity at the micronizer outlet was calculated from pressure drop observation. Figure 5.12 shows the calculated tangential velocities versus jet injection angle, with feed rate as a parameter; the tangential velocity is highest at that point for jet injection angle between 65° and 75°.

5.7.3.2 Nozzle Diameter and Number of Nozzles

The quantity of fluid introduced into the micronizer is determined by the upstream pressure, nozzle diameter and number of nozzles. The upstream pressure, as discussed in Section 5.7.2.1 influences the jet momentum and momentum imparted to the suspended particles.

The number of nozzles used in the micronizer design was reported by Dufour and Chilton (Ref 26) and (Ref 2); it varies from 3 to 20. The effect of nozzle diameter, spacing and number of nozzles is not reported in the literature. Also the optimum conditions for fluid

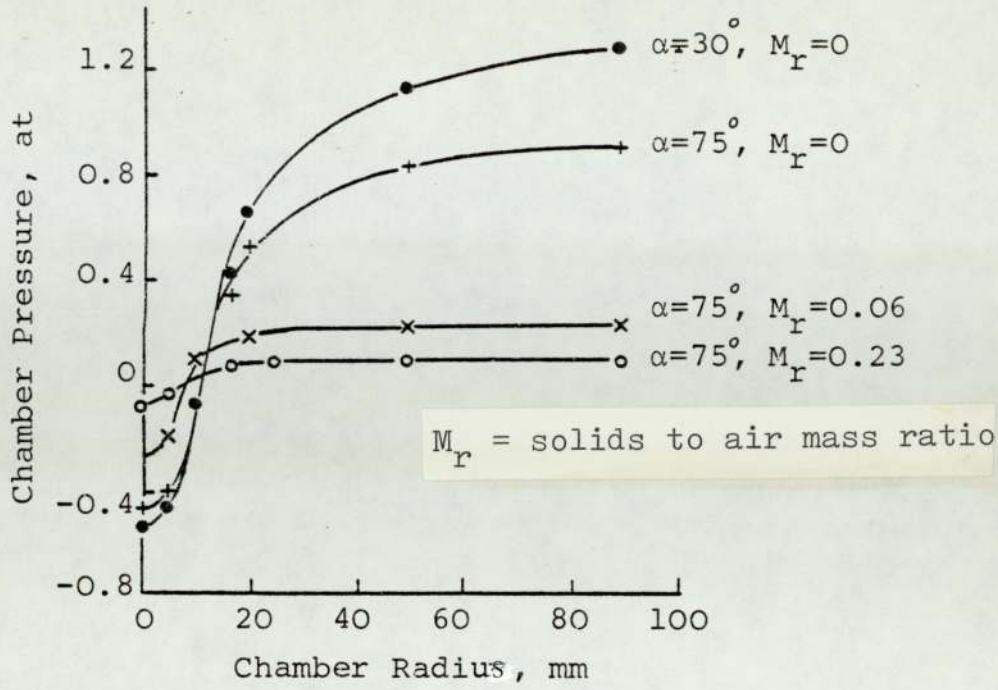

Figure 5.11 : Chamber Static Pressure at Various Points Along Chamber Radius and for differing Solid/Air Ratios.
Material : Sugar Crystals

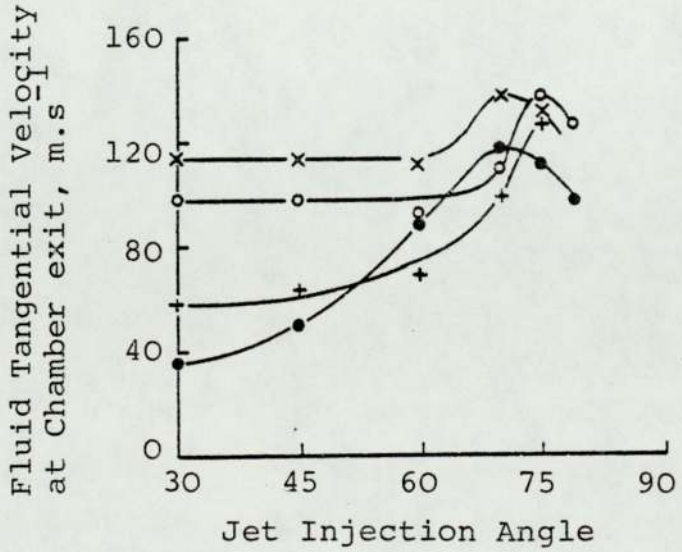

Figure 5·12 : Tangential Velocity for Various Jet Injection Angle and for a Variety of Materials.
- sugar, - softner, - filler, - insecticide

utilization with respect to both nozzle diameter and their number have not received consideration in literature. The effective length of the jet increases linearly with nozzle diameter (d_N); this should be accompanied by an increase in the rate of entrainment of solid particles into the jet stream, due to an increase of jet boundary area. From experiments of entrainment, (the effect of a jet stream injected into a pipe surrounded by particles,) Mori (Ref 7) found that the rate of entrainment W can be expressed as

$$W = 708 \ (\rho_s \ d_p^{\ 3})^{\frac{1}{6}} \ d_N \ (P - P_{min})^{\frac{1}{2}} \qquad \text{Eq. 5.10}$$

where ρ_s is Material specific gravity

d_p is Particle diameter

d_N is Nozzle diameter

P, P_{min} are Pressures at the nozzle as in equation 5.10 (see figure 5.10)

By designing the nozzle with an expansion section the air velocity may be increased. However, Creasy (Ref 47) argues that, since the mass throughput under sonic conditions is determined by the supply pressure the increased velocity is only achieved at a loss of pressure and hence density. Therefore the increase in momentum Δmu^2 is not as great as might be expected.

5.7.3.3 Grinding Chamber Contour

The cross section of the grinding chamber of the

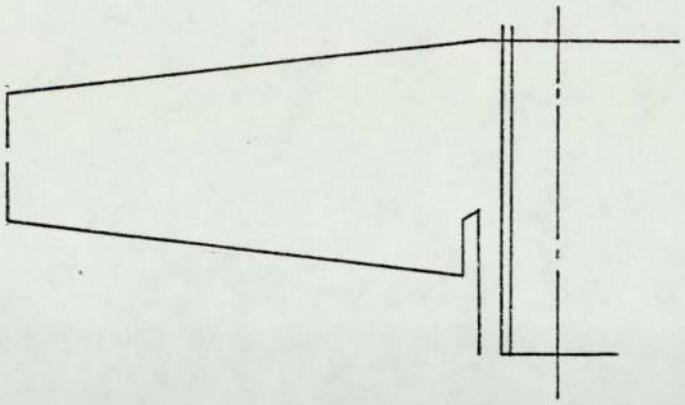

Figure 5·13(a): Divergent tapered cross section.

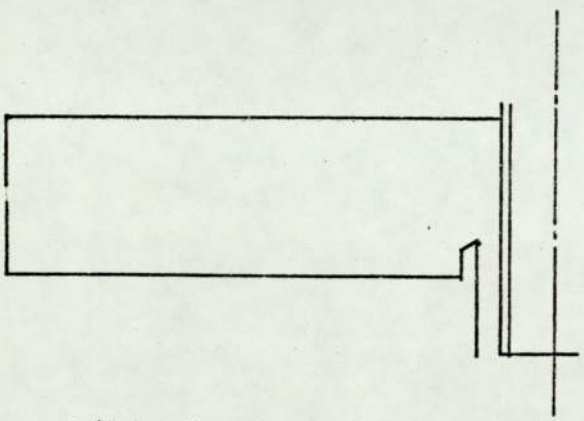

Figure 5·13(b): Rectangular cross section.

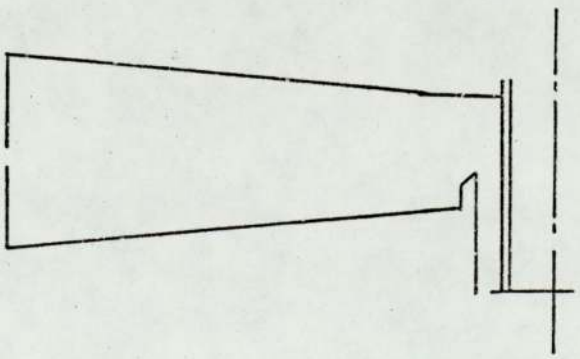

Figure 5·13(c): Convergent tapered cross section.

Microniser grinding chamber contour.

microniser takes one of the following shapes:-

1 - divergent, tapered cross section, shown diagrammatically in Figure 5.13(a). This is found in the smaller-sized microniser up to 250 mm in diameter.

2 - rectangular cross section in Figure 5.13(b). Due to the ease of forming, it is found in larger size micronisers, and

3 - convergent tapered cross Section 5.13(c).

The advantages and disadvantages of the three and other possible contours are not yet fully investigated. Hendry (Ref 23), has investigated the velocity distribution, obtained from pressure measurement of flow within a 4" model microniser. Figures 5.14(a) and (b) show the velocity distribution plotted in a dimensionless form of $\frac{v}{Vo} \cdot \frac{r}{R}$ versus $\frac{r}{R}$ for divergent tapered and rectangular mills respectively. Also Figure 5.15 illustrates the theoretical difference between the above three designs. It is shown that the tangential velocity is higher for all values of r in the divergent type.

5.4.7 Material Properties

Strength of materials and their form have been discussed in Chapter 1 with relation to single particle breaking, and comminution processes. Other materials and properties which influence behaviour under comminution and call for consideration are moisture content, hardness, abrasion, ductility, stickiness, grindability, brittleness,

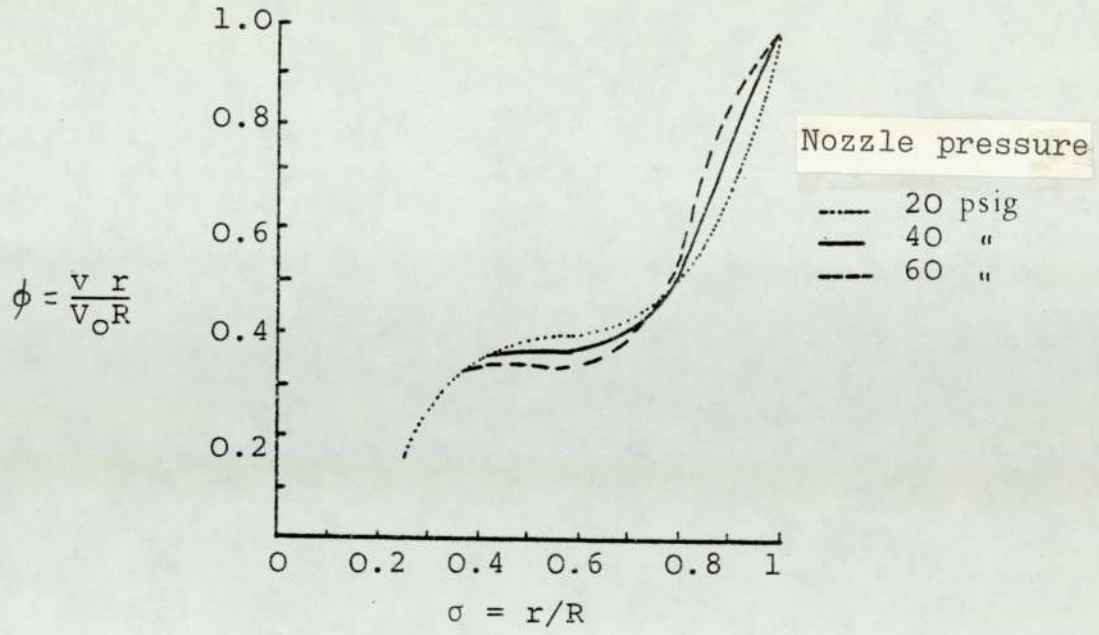

Figure 5.14(a) : Velocity Distribution for Divergent Cross Section.

v - Tangential Velocity at Radius, r

V_o - Tangential Velocity at Radius, R(the Chamber Radius)

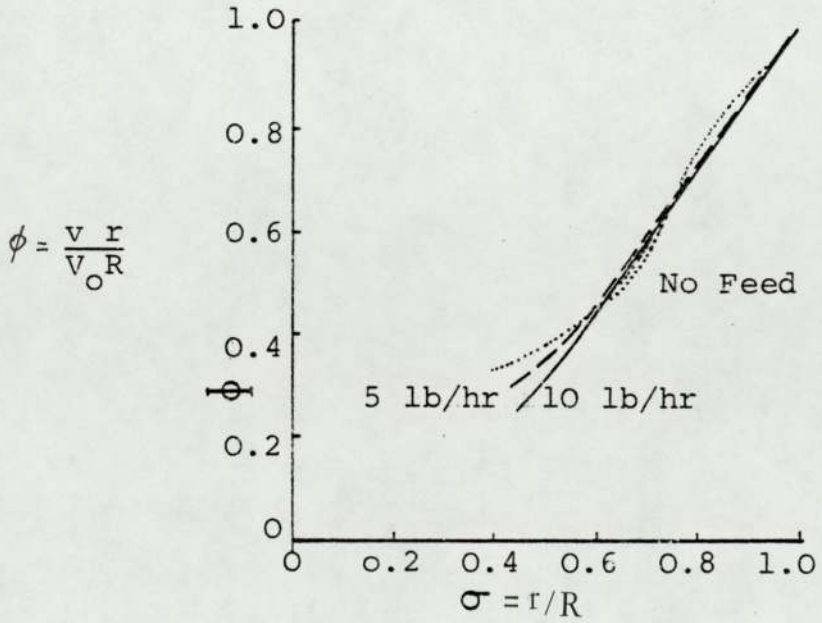

Figure 5.14(b) : Velocity Distribution for Rectangular Cross Section Mill

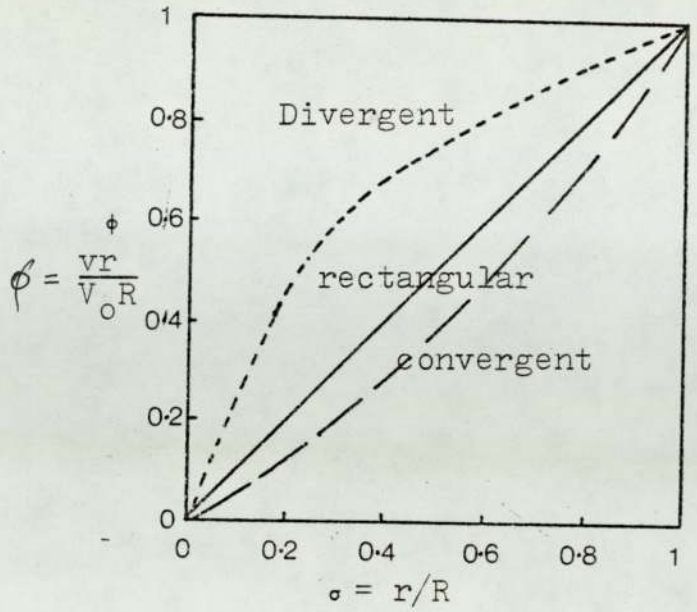

Figure 5.15: Ideal ϕ vs σ for various shapes of grinding chamber.

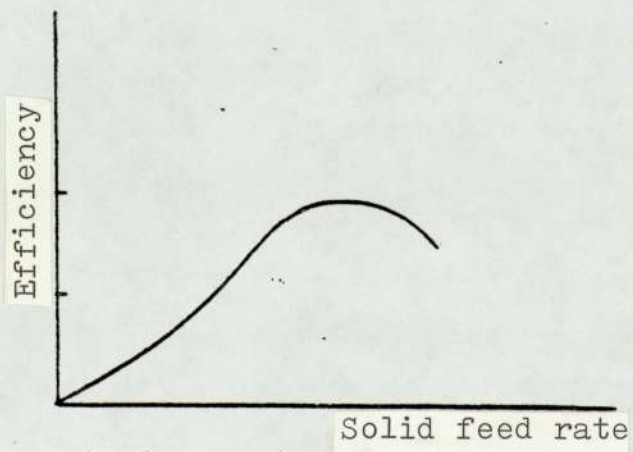

Figure 5.16: Typical fluid energy mill grinding efficiency curve.

toughness, stiffness and particle size. These properties are discussed in literature (Ref 42).

Effect of the feed particle size on the product size for a given feed flow rate was studied by Dobson and Rothwell (Ref 40) Closely-sieved fractions of powder were used in a 4" diameter micronizer; it was observed that as the size of the feed increased, the range in the product distribution increased although the 50 Wt% oversize occurs at the same point. Hendry (Ref 23) developed a mathematical model to predict particle size distribution of the product from knowledge of particle size analysis of feed, classifying function, breakage function and selection function. He determined theoretically that for an ideal classification, increasing of feed size to cut size increases the recycle and increases the mean particle size of the product, also that a finer product is obtained with closely-sieved feed, than with a feed covering a wide range of particle size, even when the size of the closely-sized material is two or three times the average size of the wider-sized material.

5.8 Energy Consumption

This, has already been discussed in section 2.4 with reference to fine grinding generally. It is acknowledged that energy consumption in fine grinding in general, and by fluid energy mills in particular, is high with low efficiency quoted to be around 0.4 - 2.0% for the latter.

Nevertheless this is an acceptable condition since fluid energy mills mainly operate in a product size range where no other mill is acceptable.

Researchers (Ref 48 and 42) have considered that the required energy is related to the new surface area produced and on this basis grinding to micron size can be expected to require enormous energy consumption. However, from data Holmes (Ref 29) it can be shown that the energy consumption is only proportional to the specific surface area produced raised to the power 0.8 and therefore fine grinding uses less energy than anticipated. The minimum particle size in this work was only 50μm, which is the common feed size for fluid energy mill.

Grinding efficiency of fluid energy mills has been defined as the ratio between energy output (increase in surface energy) and energy input. The latter has been considered on one of the following bases:-

(i) the flow energy, pressure x volume as in the work of Rumpf (Ref 10)

(ii) the adiabatic process considerations, Mori (Ref 45), or

(iii) the isothermal process considerations.

It has been shown (Ref 27) that efficiency obtained from experimental data and based on adiabatic or isothermal processes has correlated well, while that based on flow energy showed scatter of results. The efficiency for

grinding calcite (Ref 27) was found to be ranging from 0.4 to 2%.

Dotson (Ref 32), based on data obtained from manufacturers showed that for each fluid energy mill and gas throughput there is an optimum feed rate which gives maximum efficiency and this was verified by Ramanujam (Ref 27). A family of curves was obtained for solid to air mixing ratio, the general shape as shown in Figure 5.16.

The efficiency was found to be independent of feed size and grinding nozzle pressure. However, most researchers have established that the efficiency is strongly dependent on the jet velocity. The quoted efficiencies, can not be truly that of fluid energy mill, since the supplied energy is for all three following functions:

(1) classification of the powder,
(2) transport of the powder,
(3) comminution.

Dotson (Ref 32) found that the efficiencies of the jet-o-miser and the ball mill were the same, these efficiencies were based on the new surface area generated for unit power input. Also he found that the microniser efficiency was about 25% of that of the ball mill. The results obtained do not give conclusive evidence of the effect since experiments carried out were at differing operating conditions with respect to feed rate and particle feed size.

Chapter 6: Experimental and Data Acquisition

6.1 Introduction

Studies carried out on both the microniser and the jet-o-miser were discussed in Chapter 5. The studies concerning the microniser have been directed at investigating the flow pattern and comminution mechanism, while studies concerning the jet-o-miser were spent on investigating some of the operational parameters involved. The basis for the preliminary design of microniser were given in Section 5.6.

There is little data in literature concerning the effect and significance of the constructional features and operational parameters involved in the microniser operation. It was concluded that a study that will consider all the variables involved, carried out on a single microniser, would be greatly beneficial. The research programme was therefore planned to study the effects of the following parameters:

a) Constructional
   - (i) number of nozzles
   - (ii) diameter of nozzles
   - (iii) nozzle angle

b) Operational
   - (i) solid feed rate
   - (ii) air velocity at the grinding nozzles
   - (iii) air throughput

(iv) velocity at the venturi feeder nozzle

and (v) feed size.

6.2 Experimental Apparatus

6.2.1 The Micronizer

A flow diagram of the micronizer installation used for experimenting is shown in Figure 6.1, while Plate 6.1 shows the experimental rig.

The model chosen was the 8 inch Airfilco "Micronizer". This was modified to study and vary certain constructional features of the micronizer, as will be explained in 6.2.1. The max. design pressure was 15 bar, and pressure at the jet ring and the venturi feeder was variable from 1 bar to 10 bars.

The other features of the Micronizer are shown in Figure 3.5 (C) and are similar to that explained in Chapter 3. The chamber is concave in shape, with two linear plates. Most of the product was collected in the primary cyclone at the chamber base, and the remainder in the top filter bag. (The latter has a surface area of 4.5 m^2).

The air supply line consisted of 0.038 m diameter pipe, and reduced to 0.025m prior to splitting into two streams, one to the jet ring and the other to the venturi feeder. Hose connections were made by means of a quick

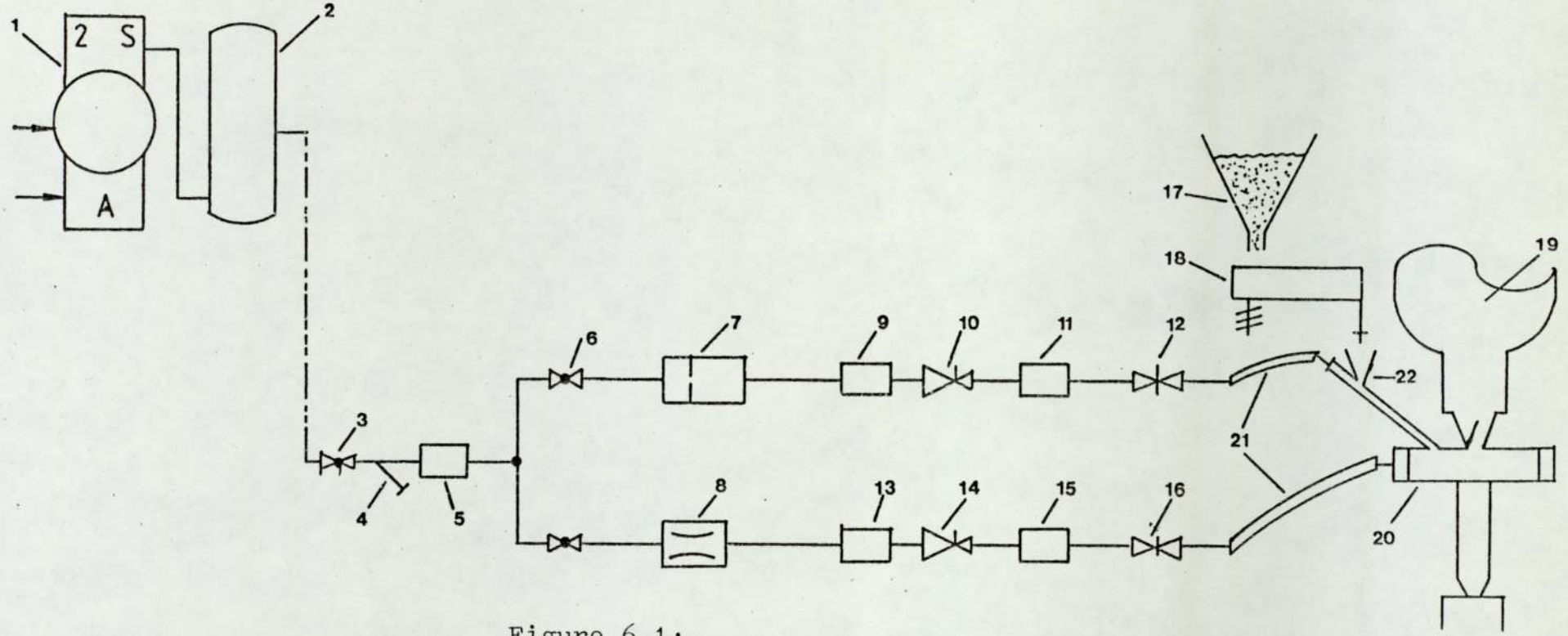

Figure 6.1:

1 - Compressor Two-Stage Air-cooled
2 - Air Reservoir
3 - Valve
4 - Water Strainer
5 - Pressure Gauge
6 - Valve
7 - Orifice
8 - Venturi tube
9 - Pressure Gauge
10 - Pressure Regulator
11 - Pressure Gauge
12 - Valve
13 - Pressure Gauge
14 - Pressure Regulator
15 - Pressure Gauge
16 - Valve
17 - Vibrating Hopper.
18 - Vibrating Trough
19 - Filter bag
20 - Micronizer
21 - Flexible Hose
22 - Venturi Feeder

Plate 6.1: The Microniser Experimental Rig

A - 0.2m Microniser

B - Top filter bag

C - Bottom filter bag and product discharge

D - Screw feeder

E - High pressure manometer

F - Venturi feeder (feed inlet)

G - Vibrating trough

H - Pressure regulator

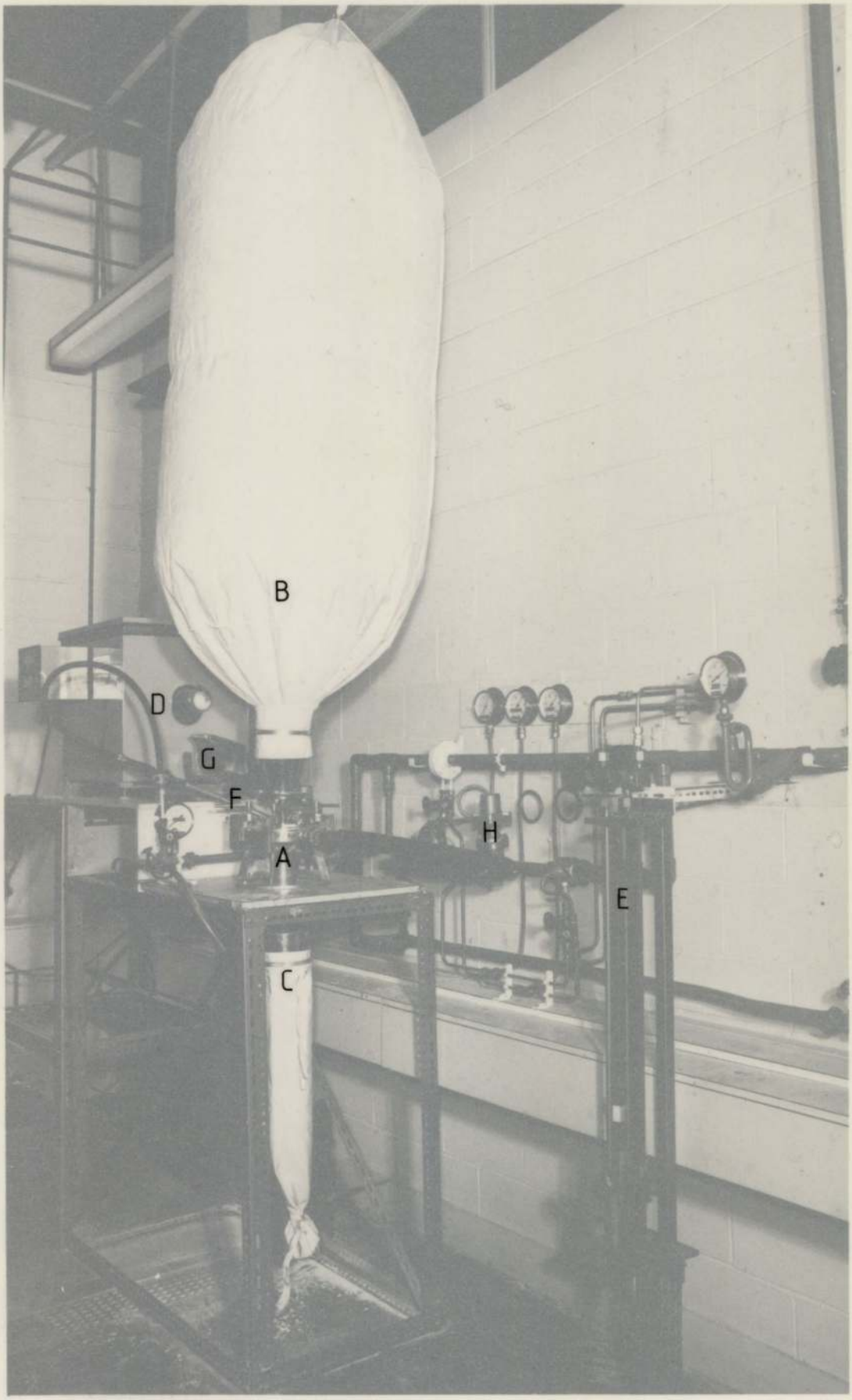
B
D
G
F
A
H
E
C

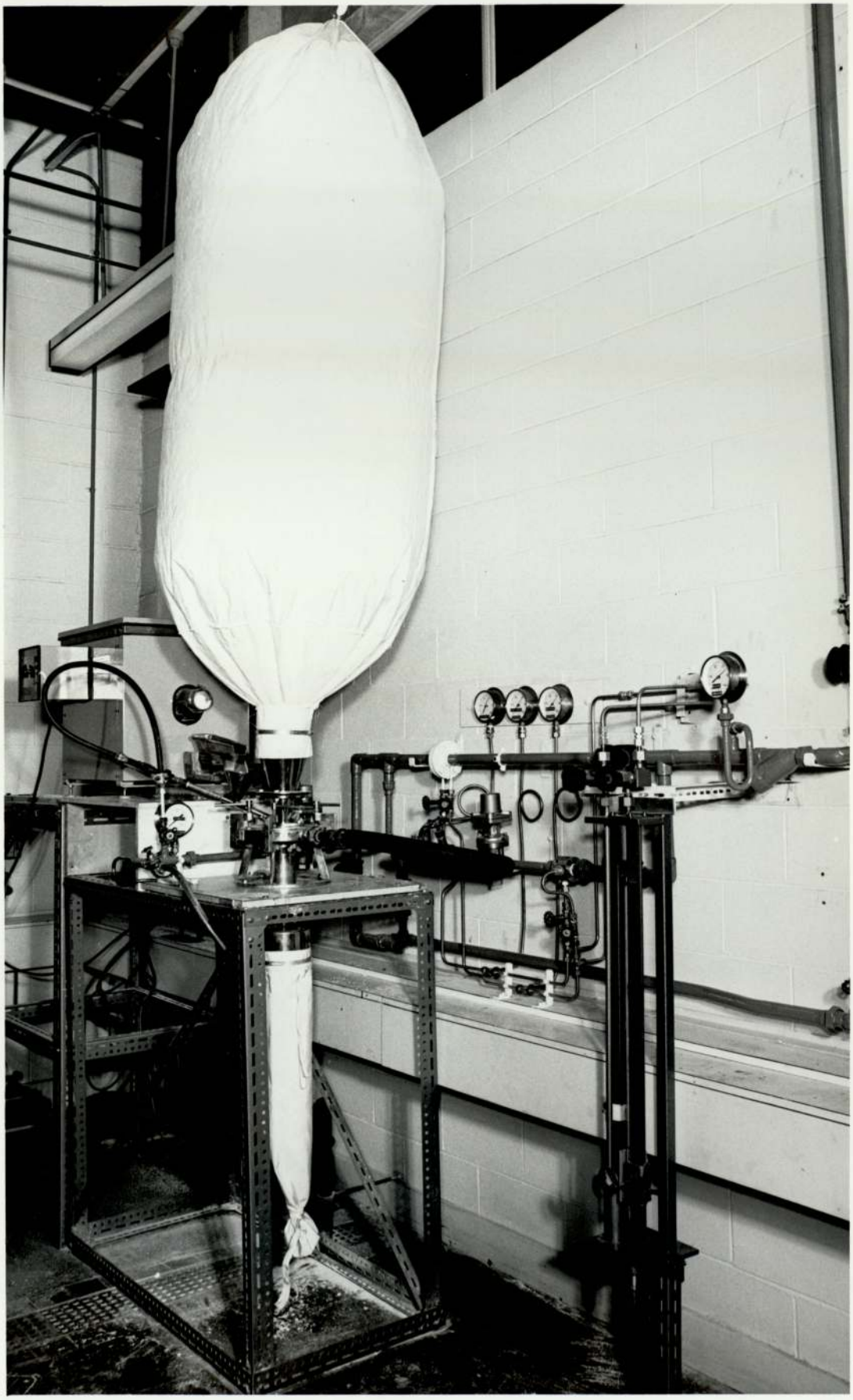

detachable coupling to simplify dismantling the equipment.

6.2.1.1 The Jet Ring

The jet ring whose dimensions are shown in Figures 6.2(a) and 6.2(b), is the most important feature of the microniser determining where and how the compressible fluid is discharged and distributed; it forms the circular part of the grinding chamber. Plate 6.2 shows the features of the ring. It was designed to allow study of the constructional variables - the number of nozzles N, nozzle diameter d_N, and angle α. Its inner diameter is 0.2m, around which twelve 'nozzle sockets' are drilled of 0.0127m diameter each. The axes of these are tangential to an imaginary circle 0.127m diameter.

The nozzle sockets accommodate the desired nozzle plugs (Figure 6.2(b)), which are held in position by means of an $\frac{1}{8}$ inch Allen screw fitted to the upper surface of the ring. The tight fit nozzle plugs are removed and adjusted in position by the aid of $\frac{1}{4}$ inch rod that can be inserted through the $\frac{1}{2}$ inch holes drilled directly behind each of the nozzle sockets. To these holes $\frac{1}{4}$ inch nipples are welded, and are sealed by plugs. They are also used for cleaning the manifold which extends all round the ring, and through which air is supplied to the nozzles. A $\frac{3}{4}$ inch diameter connection is made to the manifold for the air mains supply. The manifold forms an integral part of the jet ring.

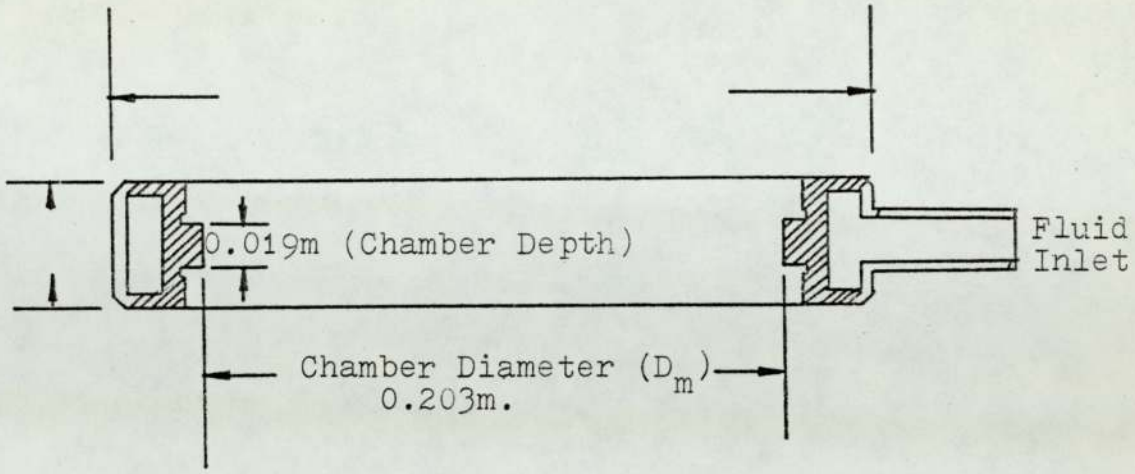

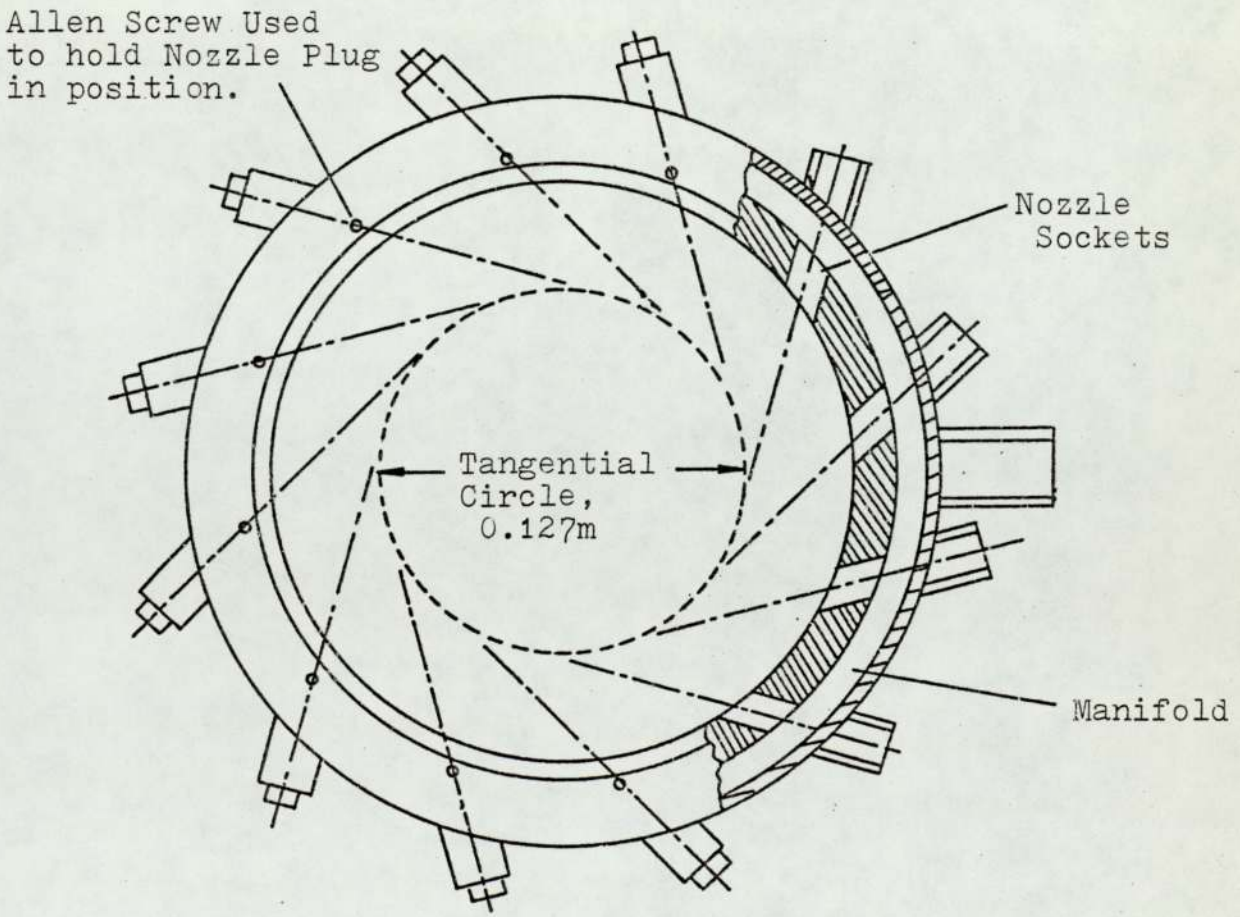

Figure 6.2: The Experimental Micronizer Jet Ring

Plate 6.2: The Experimental Jet Ring

A - The manifold

B - Air inlet

C - Nozzle plug in position

D - Nozzle plug off position

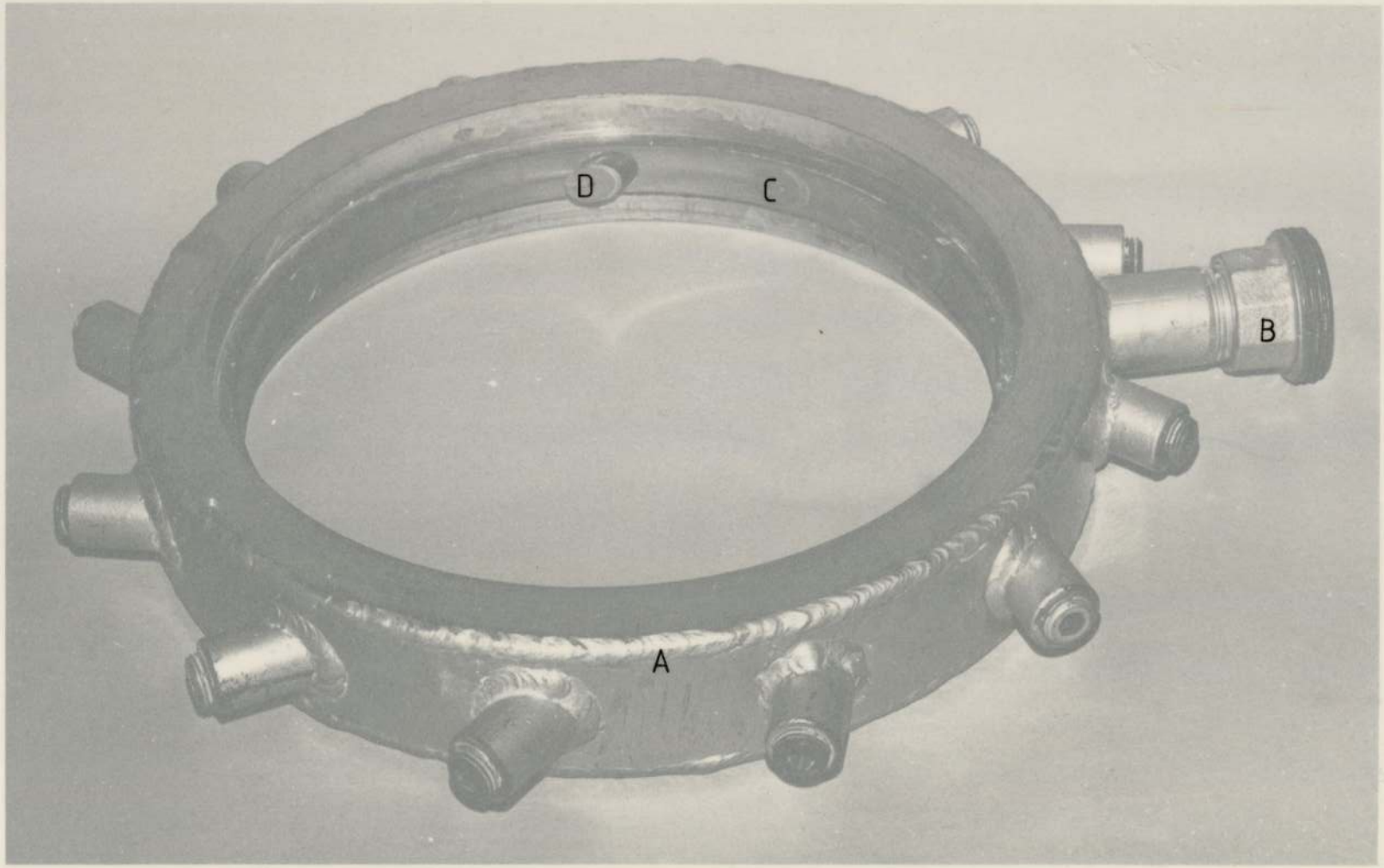
D
C
B
A

6.2.1.2 Nozzles

Nozzles were made into 'Nozzle Plugs', which constituted 0.0127m diameter rods of about 0.025m long. Straight holes of given size, and angle α (Figure 6.3) were drilled in the rods and machined and polished to give a tight fit when placed in the sockets. The inner face was smoothed with the inner diameter of the jet ring. Figures 6.3(a) and 6.3(b) illustrate the nozzle plug.

Allen screws were tightened to secure the plug in position. The nozzle surface was coated with sealant prior to fitting to prevent air leaking.

Eight sets of nozzle plugs were used ; nozzle diameter and angle are shown in Table 6.1.

6.2.1.3 Assembling The Microniser

The assembly of the microniser is illustrated in Figure 3.5(a). Proper consideration was given to the positioning of the wear plates and the cyclone. Gaskets were placed between the wear plates and the jet ring periphery to prevent air leaking. The jet ring was placed in position, with the jets' axes directed clockwise. The guard ring was inserted into position through the concentric holes of the bottom wear plate and the base, so that part of the ring rested inside

Table 6.1

MARK	NO MADE	DIAMETER mm	OTHER DIMEN X	Y	TANG. CIRCLE DIAM.	ANGLE	
BLANK°	12	BLANK					
A°	12	1.58	3.175	3.175		127	
B°	12	2.38	3.175	3.175		127	
C°	12	3.175	4.760	3.175		127	
D°	12	1.58	3.175			127	DIVERGE AT 8° AROUND AXIS.
E	12	3.175	4.760			127	
F°	12	1.58	3.175			152	
G	12	2.38	3.175			152	
H	12	3.175	4.760			152	
I°	12	1.588	3.175			178	
J	12	2.38	3.175			178	
K	12	3.175	4.760			178	
L°	12	1.588	3.175			102	
M	12	2.38	3.175			102	
N	12	3.175	3.175			102	

° Nozzle plugs used in this experimental work

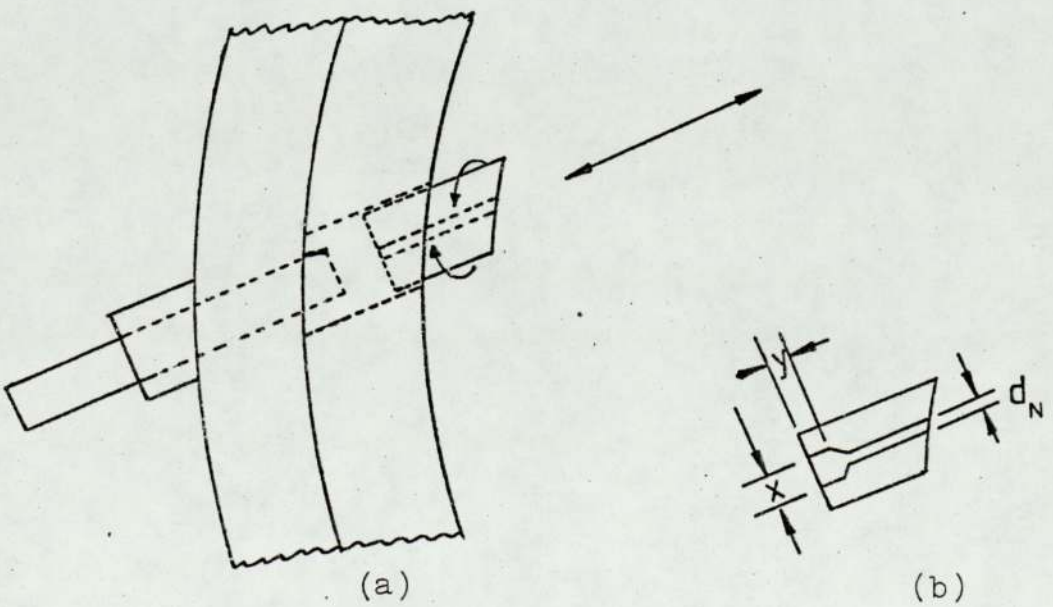

Figure 6.3: The Nozzle Plug

the cyclone collector, and was secured by a bolt fixed to the cyclone top end and used to fix the height of the guard ring protruding into the chamber after adjustment.

The top wear plate and the top plate were secured together, so that the two holes leading from the venturi coincide with each other, also the two concentric holes coincided with each other, then, both and a 1.5 mm thick gasket were placed in position on top of the jet ring before clamping together with the four G-clamps.

The venturi feeding system was assembled as shown in Figure 3.7. About 0.005m distance between the air nozzle outlet and the convergent divergent nozzle inlet was allowed.

6.2.2 Air Supply

The air was supplied at 10 bar pressure, and a delivery rate capacity of 0.11 m^3/s at compressor intake conditions. The compressor used was Broome Wade two-stage, air-cooled, powered with a 60 horse-power motor.

An air reservoir of a capacity of 2 m^3 at 11 bar was used in conjunction with the compressor, together with an in-line filter.

6.2.3 Material Feeding Method

Achievement of reproducible results from the microniser,

requires accurate and controllable continuous feeding system to deliver powder under test to the venturi of the microniser.

A vibrating hopper feeder, made by Riley, shown diagrammatically in Figure 6.1, was used for most of the experimental work. It consists of a feed hopper, with a vibrator fixed to its surface. The material falls from the hopper outlet onto one end of an inclined vibrating trough which delivers the material from the hopper to the microniser feed system. The feed rate is varied by changing the amplitude of vibration of the trough, and by varying the height of the outlet of the feeder hopper above the trough. The calibration method and calibration graphs of feed rate versus amplitude control setting for limestone of different particle size are given in Appendix A6. The maximum deviation of feed rate from the calibrated values was 5.3%.

The vibrator attached to the hopper was switched on to aid flow only when powder of the size range 0÷500μm was being fed, and little segregation occured, but it was switched off when larger particle size fractions were fed, as in the case of 300 - 600μm range, to avoid segregation. In this size range the material flowed under its own weight.

Certain materials when extremely fine cause blockage of the vibrating hopper, in these cases a variable speed

screw feeder was used.

6.2.4 Air Flow Measurements

Throughput of air at the jet ring manifold and the venturi feeder nozzle, were determined by means of pressure drop measurements using a venturi tube and an orifice plate respectively. Both elements were designed in accordance to BSS 3061 and were fitted upstream of the pressure regulators (Figure 6.1). High pressure manometer containing liquid paraffin was used to read the pressure drop across the elements. The pipe connections consisted of 6 mm diameter stainless steel pipes, provisions were made to read the pressure drop across one element while the other was isolated. Both elements were calibrated at normal conditions using a gas meter. Volumetric flow rate of air (Q_v) was calculated from

$$Q_v = K_m \sqrt{\Delta P} \quad m^3/s \quad (\pm 5\%)$$

K_m = 0.0026 (orifice plate)

= 0.0167 (venturi tube)

ΔP Pressure drop observed (inches)

6.3.1 Operating Procedure

1. Microniser Assembly

Prior to starting operation, the microniser assembly was checked to ensure that:

(a) the jet-ring was installed correctly with the the jets and the venturi feeder directed clockwise.

(b) the jets were correctly inserted and secured in position (Section 6.2.1.1 - 3)

(c) the air nozzle in the venturi feeder is correctly positioned with respect to the venturi itself (Section 6.2.1.3).

2. Air supply.

All lines leading to the micronizer were vented free from condensed water.

3. Solid Feed System.

The vibrating hopper feeder was switched on, and it was checked that material was flowing freely. Then the feeder was calibrated, as described in Appendix A1.

4. High Pressure Manometer.

The manometer valves were set so as to prevent manometer fluid being forced into the main airlines.

5. Micronizer Operation.

The main air line valve 3 (Figure 6.1) was opened fully, then valves 6 and 12 to the venturi feed line were also opened. Then the valves that were leading to the jet manifold 16 were adjusted until the pressure in the jet ring reached the desired value. The micronizer was then checked for leaks at the points between top and bottom plates and the jet ring. Air flow to the venturi feeder was reduced gradually by adjusting valve 12 until air was about to be forced back out of the feed funnel. The air feed was again slightly increased so that the funnel was under reduced pressure.

The trough amplitude controller was set at the selected feed rate, and then the feeder switched on to commence operation.

Initially, the micronised product was rejected and

allowed to pass through to the dust collector, until the chamber manometer (Figure 6.2) reading dropped to a steady value, thus indicating that a steady state has been reached, (the time taken for the operation to reach a steady state is given in Appendix A3 , and a typical graph of chamber pressure versus time is shown in Figure 8.9), the lower bag out-let was then closed and product collection proceeded and for duration given in Appendix A3.

The pressure drop across the venturi tube and the orifice plate were recorded.

6.3.2 Shut Down

Solid feeder and air supply to both the venturi feeder and the jet ring 12 and 16 were simultaneously turned off. The time lag between switching the solid feeder off and completely closing valve 12 and 16 was of the order of 3 to 5 seconds. This procedure required care to prevent high pressure forcing solids back through the venturi system.

The micronisermwas dismantled in order to collect the grinding chamber content.

6.4 Experimental Material

Powders that are commonly ground in the micronisermare many and varied in nature, physical properties and

dimensions. Their applications are diverse, and each may show specific features during micronisation. Hence it is not possible to select an entirely representative material powder to experiment on. However, the powder to be selected for this study must meet certain initial conditions. It should be:

1. non-toxic or hazardous,
2. readily available,
3. cheap,
4. homogeneous in structure and content,
5. of medium hardness (Moh's index) and
6. should flow readily.

Powders that meet all the above conditions are very few. Before the final selection was made, consideration was given to the size of the feed material.

It is noticable, through contacts with institutions operating micronisers, that the interest lies in micronisation of powders which are already fine (50-5μm).

Economically, it is preferable that the material undergoes pregrinding until reduced to a reasonable size prior to feeding into the micronizer, since overall this saves a considerable amount of energy spent in grinding the coarser material.

A variety of materials were tested in the micronizer, some of which presented practical and control difficulties.

Some experimentation was carried out on Italian talc powder grade '00000'. The talc presented difficulties during the particle size analysis of the samples obtained, because of its poor dispersion. A satisfactory method of dispersion was developed (see 6.6.2.1); however since talc:

(1) Is plate type particles, which is not truly representative of most materials micronised, and

(2) Is low in the Moh's hardness index,

it was thought that a different material should be sought.

Limestone was ultimately chosen as the test material used to study the various constructional and operational parameters of the micronizer.

6.4.1 Preparation of Limestone

The limestone used for experimentation was obtained from the I.C.I. quarries near Buxton in Derbyshire (U.K.) Two grades of limestone were obtained "Fine" - 100% below 120 μm, and "coarse" - 100% below 1500 μm

The size ranges used in the experimental work were 0 - 120 μm, 0 - 250 μm, 0 - 500 μm and

300 - 600 μm.

The fine limestone was prepared in batches of 50Kg each, spread on trays and "air-dried" at room temperature for 48 hours with occasional mixing. Samples were taken to check for moisture content, by further drying the samples in an oven at 60°C. The batch was then ready for micronising experiments.

A number of samples were taken for particle size analysis; a typical distribution of the feed material is given in Appendix A2.

6.4.2 Preparation of Various Feed Size Fractions

The coarse feed was also "air-dried" and then sieved to minus 250 μm, minus 500 μm or 300 - 600 μm fractions. On average the coarse limestone supplied, contained 25% below 250 μm, 45% below 500 μm or 30% of 300 - 600 μm. Sieving time was of the order of one hour per 24Kg sieved fraction.

Fractions of a given size were collected together and thoroughly mixed and sampled to ensure consistency of particle size within the batch. Particle size distributions were obtained as explained in Section 6.5 , and are given in Appendix A4.

6.5 Particle Size Analysis Methods

Methods which are commonly used for determining the average particles size, surface area and full size distribution are shown in Figure 6.6(Ref 42). The details, applicability and merits of each of the methods may be found in the literature e.g. Allen (Ref), Irani and Callis (Ref 81), Herdan (Ref 82) and Cadle (Ref 79).

Most of the methods listed in Figure 6.6 have been found (Ref 42) to give reasonably reproducible results provided an exact procedure is followed such as is set down in one of the standards.

Two methods were adopted in obtaining the full particle size distribution and specific surface area of the micronised product. These are

(1) Coulter Counter method, (Section 6.5.2), this technique is found eminently suitable for powders in the subsieve range down to about 1 μm in size.

(2) Sieve analysis is a well-established technique used for size ranges greater than 45 μm.

Optical and electron microscopy were also used to verify some of the analysis obtained by the above method, and to estimate the particle size range, particle shape and degree of dispersion of various samples.

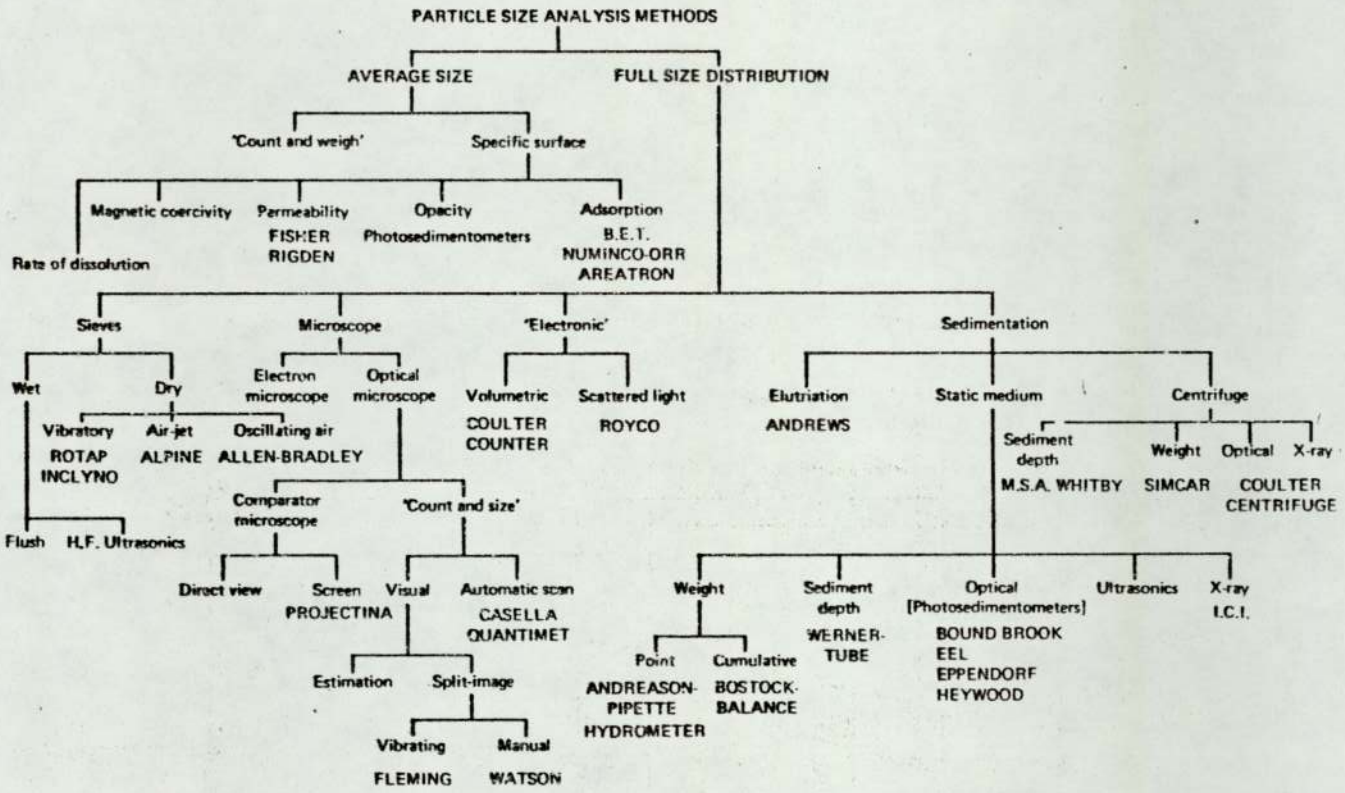

Figure 6.4: Classification of methods of particle size analysis

6.5.1 Sieve Analysis

In the course of particle size analysis, it was necessary to use sieve analysis either for complete determination of particle size distribution of the coarse fraction, or to sieve some samples to below 63μm for the Coulter Counter analysis.

British Standard 1796 methods were adopted, using 200mm sieves. Samples of 30 - 90 gms were prepared as described below, charged into the top sieve of a series of sieves having an aperture ratio of 1.414, and machine shaken. The mass of material retained on each sieve was periodically checked, until not more than 0.1% of the original sample has passed one sieve in 2min. Mass retained was recorded and was checked that it came to about 99% of the original sample. Three samples were taken from each test, and when deviation was greater than 2%, the analysis was repeated. Sieve Analysis of products from various runs are shown in Appendix A4.

6.5.2 Coulter Counter Techniques

The Coulter Counter model ZB was used to determine particle size distribution of product obtained from the microniser experiments. Particle size analysis over the range of 20 - 150μm for certain batches was carried out using a range of orifice tubes of 50 - 280μm diameter.

Dual threshold techniques were adopted to determine the number of particles (Δn) or the mass fraction in a small size range in the overall range being counted; This would provide a relatively more accurate estimate of specific surface area of the sample under study.

The Coulter Counter operation, based upon the electrical sensing zone principle (Ref 74), has received considerable attention by workers in powder technology, and a schematic diagram showing the Coulter principle is given in Appendix A5. Also theory, calibration procedure and analysis technique are given in Appendix A5.

Proper consideration was taken to ensure that the electrolyte was saturated with limestone to avoid the disolution of the sample being analysed, see Appendix A5 , also, the electolyte was filtered several times prior to analysis.

6.6.1 Sample Preparation

Since the analysis for particle size distribution can not be more accurate than the sampling procedure it is therefore necessary that the selected samples for measurement should be representative of the bulk in grain size distribution. Several methods of sampling prior to analysis are available, these are reviewed and discussed by Allen (Ref 74) and the theory of particulate sampling was developed by Gy (Ref 76).

It is generally accepted that

(1) The powder should be sampled when in motion.

(2) The whole of the powder should be taken for many short increments of time in preference to part of the stream being taken for the whole of the time.

The Table 6.2 below, shows comparison between various techniques of sampling powders.

Table 6.2 Comparison of various techniques of powder sampling. (Ref 74)

Techniques	STANDARD DEVIATION SUGAR/ SAND %	SAND/ SAND%	EST. MAX % ERROR SUGAR/ SAND %	SAND/ SAND%
Cone quartering	5.76	6.81	19.2	
Scoop sampling	6.31	5.14	21.0	17.1
Table sampling	2.11	2.09	7.0	7.0
Chute splitter	1.10	1.01	3.7	3.4
Spinning riffler	0.27	0.13	0.9	0.4

Therefore little confidence is placed in any of the first three techniques.

The technique adopted in obtaining a sample for analysis is described below. The weight of the sample required for the Coulter Counter analysis was approximately 15 - 30 mg, total product obtained was 0.5 - 3 Kg; once the micronised product was collected, it was then transfered into a vibrating hopper,

segregation was reduced by avoiding formation of heaps. The hopper discharged into a vibrating trough, which was set to a delivery rate of q Kg/s, the samples collected into two containers, and duration of each increment was θ_i sec. so that $\frac{\theta_T}{\theta_i} > 30$

where $\theta_T = \frac{x}{q}$ (sec) (Total collection time of the whole bulk).

x is mass charged to the hopper.

i.e. The bulk of the powder was divided into a minimum of 30 samples, half of which was alternately collected into each of the containers, mixed well, and division of one of the containers content was done in the same way, until a final sample of $10 - 15 \times 10^{-3}$ Kg is obtained.

To obtain a smaller sample of approximately 10^{-3} Kg, a chute splitter was used; it consists of a V-shaped trough along the bottom of which is a series of chutes alternately feeding two trays placed on either side of the trough. The $10 - 15 \times 10^{-3}$ Kg sample was poured into the chute and repeatedly halved until a sample of 10^{-3} Kg was obtained.

6.6.2 Sample Dispersion

The preparation of talc or limestone samples for Coulter Counter analysis or for optical microscopy was carried out:

1. To ensure that the sample taken is truly

representative of the bulk sample.

2. To disperse particles fully, i.e. break down light aggregation without fracturing particles.

Techniques developed for dispersion of talc and of limestone are described below. The techniques chosen were checked by observing the samples under optical microscope.

6.6.2.1 Dispersion of Talc

A lacquer consisting of 1.5% Nitrocellulose, 1.5% triethyl phosphate and 1.5% dibutyl phthalate in amyl-acetate was prepared. 10ml of the lacquer plus approximately 0.25×10^{-3}Kg of talc were placed in a 10ml beaker and agitated by an ultrasonic bath for 1 - 3 minutes until it appeared homogeneous, swirling constantly. Two to four 1ml samples were withdrawn from the agitated suspension for size analysis, smaller samples were taken for the optical microscopy.

6.6.2.2 Dispersion of Limestone

Sample obtained (Section 6.6.1) , was made into a thick paste using about 2ml of electrolyte, and diluted to 100cc. An ultrasonic probe for a period of 30 seconds was used to aid dispersion.

The suspension was stirred continuously, and 4 samples

of 1ml each were drawn by means of a thick needle syringe and diluted to about 200ml which was then analysed. Analysis procedure and data conversion is given in Appendix A5. The Coulter Counter data was converted to particle size distribution (Appendix A4) using Basic Computer Programme given in Appendix A2.

Chapter 7: Constructional Features: Results and Discussion

7.1 Air Flow Rate Dependence on the Nozzle Diameter, Number of Nozzles and Jet Ring Pressure

This study was undertaken for three reasons:

(i) to enable an estimate to be made of the rate of fluid introduction at the jet ring from the pressure gauge reading without using a flow-measuring device, and

(ii) either to determine the compressor capacity needed given the diameter, number of nozzles and supply pressure of an existing or designed micronizer, or

(iii) to determine the number and diameter of nozzles required once the pressure and fluid supply rate have been decided upon.

The rate of discharge of compressible fluid through an orifice or a nozzle may be derived theoretically (Ref 75) assuming that

(1) the air behaves as an ideal gas,

(2) the pressure ratio between nozzle pressure and chamber pressure does not fall below $P_n\ r_c$, where P_n is the nozzle pressure and r_c the ratio of Nozzle pressure to the critical pressure P_c.

(3) the maximum discharge rate occurs,

(4) there is negligible pressure in the chamber, and

(5) the process is reversible.

By applying energy and mass balance equation

$$\frac{\Delta U^2}{2\alpha} + g\,\Delta z + \int v dP + W + F = 0 \quad \text{Eq. 7.1}$$

$\alpha = 1$ for turbulent flow, $\alpha = 0.5$ for Laminar

and

$$\int v dP = \int_1^2 \left(\frac{P_1 V_1}{P}\right)^{\frac{1}{\gamma}} dP \quad \text{Eq. 7.2}$$

where ΔU^2 the kinetic energy term

Δz the potential energy term

v the specific volume

ΔP the pressure energy term

W work done

F frictional losses

terms Δz, W, F are assumed zero.

Using the above assumptions, the following relationship was derived for circular cross-section nozzle

$$Q = C_D \times N \times A_n^2 \sqrt{K \left(\frac{P_n}{v}\right)\left(\frac{2}{k+1}\right)^{k+1/k-2}} \quad \text{Eq. 7.3}$$

where Q = air throughput at 15°C and 1 atm.

N = number of nozzles

A_n = cross sectional area of the nozzle

P_n = Pressure at the jet ring

v = Specific volume at pressure P_N.

C_D = Equivalent to coefficient of discharge.

$k = \gamma$ for isothermal process

For the conditions listed in Table 7.1, namely pressure range, number and diameter of nozzles, the air throughput at the jet ring was determined from the pressure drop measurements across the pre-calibrated venturi tube (see Section 6).

Table 7.1: Conditions of Air Throughput Measurements

Nozzle Mark	Nozzle Diameter mm	No. of Nozzles.	Pressure at the Jet Ring $\times 10^5$ N/m^2
N-A	1.588	12	2.758 - 9.652
		6	"
N-B	2.245	12	"
		6	"
N-C	3.175	6	"
		3	"

Figures 7.1a, b and c show plots of the predicted and measured values of volumetric air flow rate through the nozzles versus jet ring pressure, for nozzles N-A, N-B and N-C respectively, with the number of nozzles as a parameter.

Experimentally determined throughput of air at the jet ring agrees (within 95%) with the theoretically predicted values for the three nozzle sizes N-A, N-B and N-C and for a maximum number of nozzles shown in Table 7.1. The coefficient of discharge C_D was obtained from literature (Ref 92).

For the 12-nozzle arrangement (N-B) and 6 nozzles (N-C) good agreement is shown at pressure up to 7-8 x 10^5 N/m^2 absolute. But for higher pressure deviation was apparent and particularly in the case of 12-nozzles (N-C) arrangement (Figure 7.1c). This deviation was due to the increase in the chamber pressure. The chamber pressure was measured for the

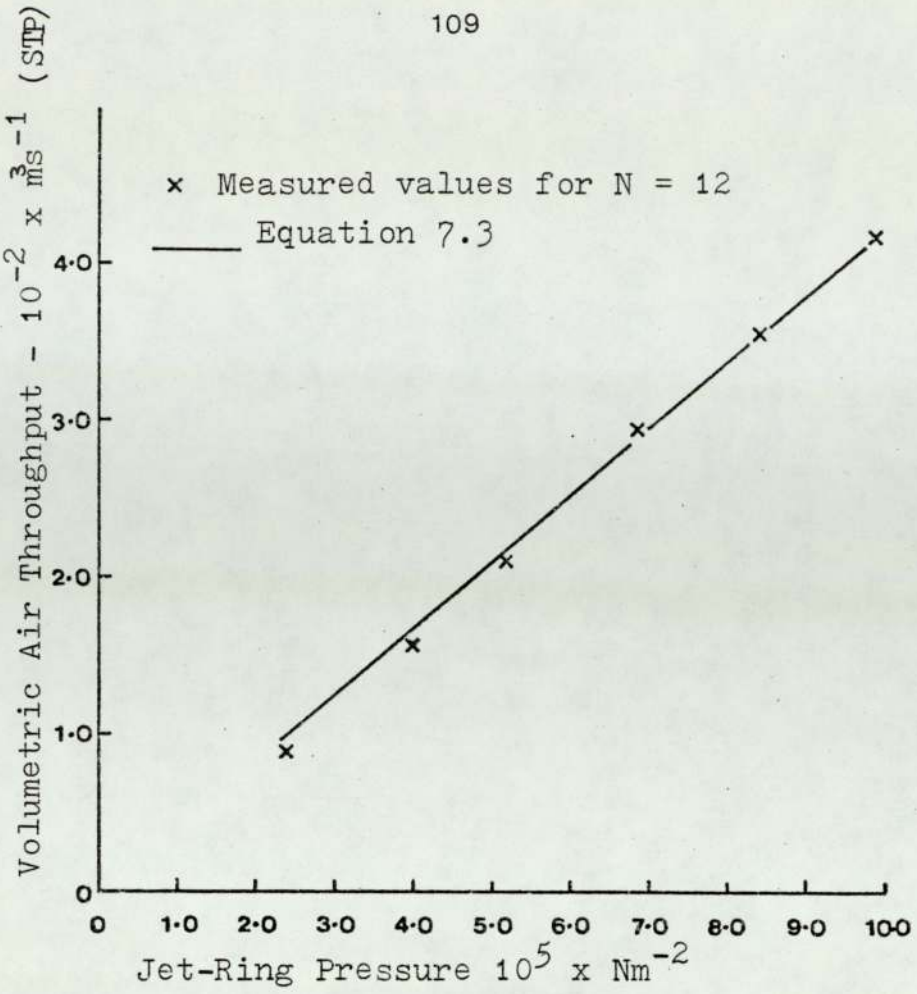

Figure 7.1a: Air throughput at nozzles (N-A)
d_N = 1.5875mm C_D = 0.57

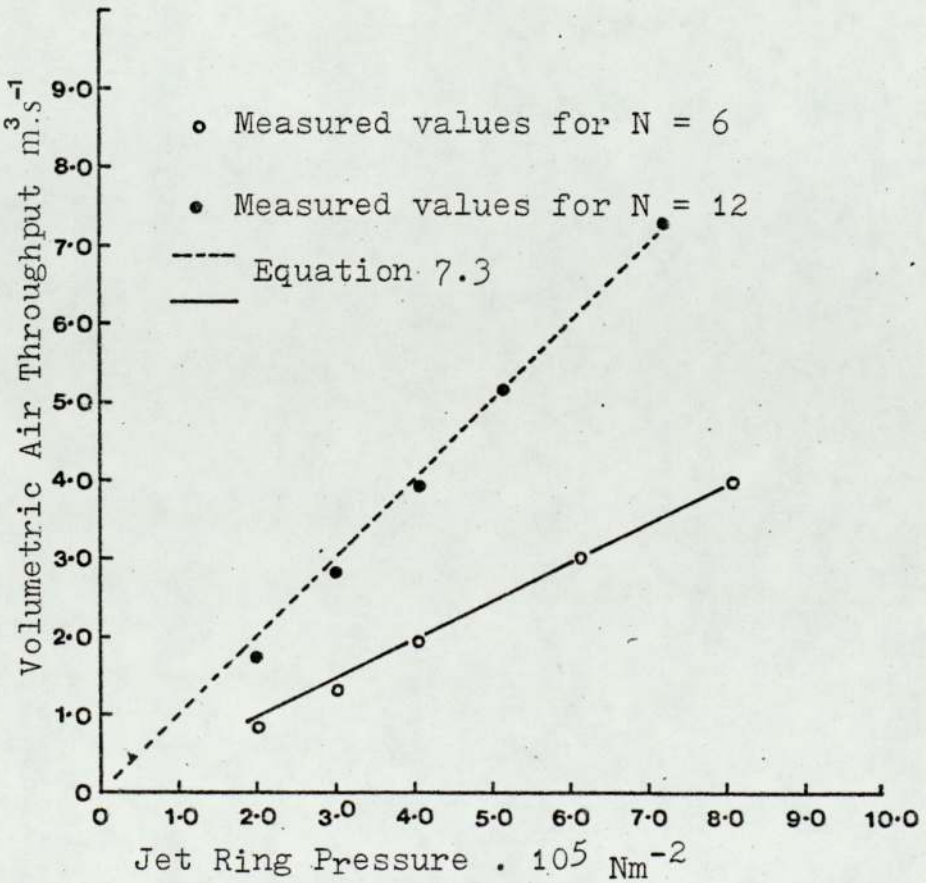

Figure 7.1b: Airthroughput at Nozzles (N-B) d_N = 2.245mm
C_D = 0.6

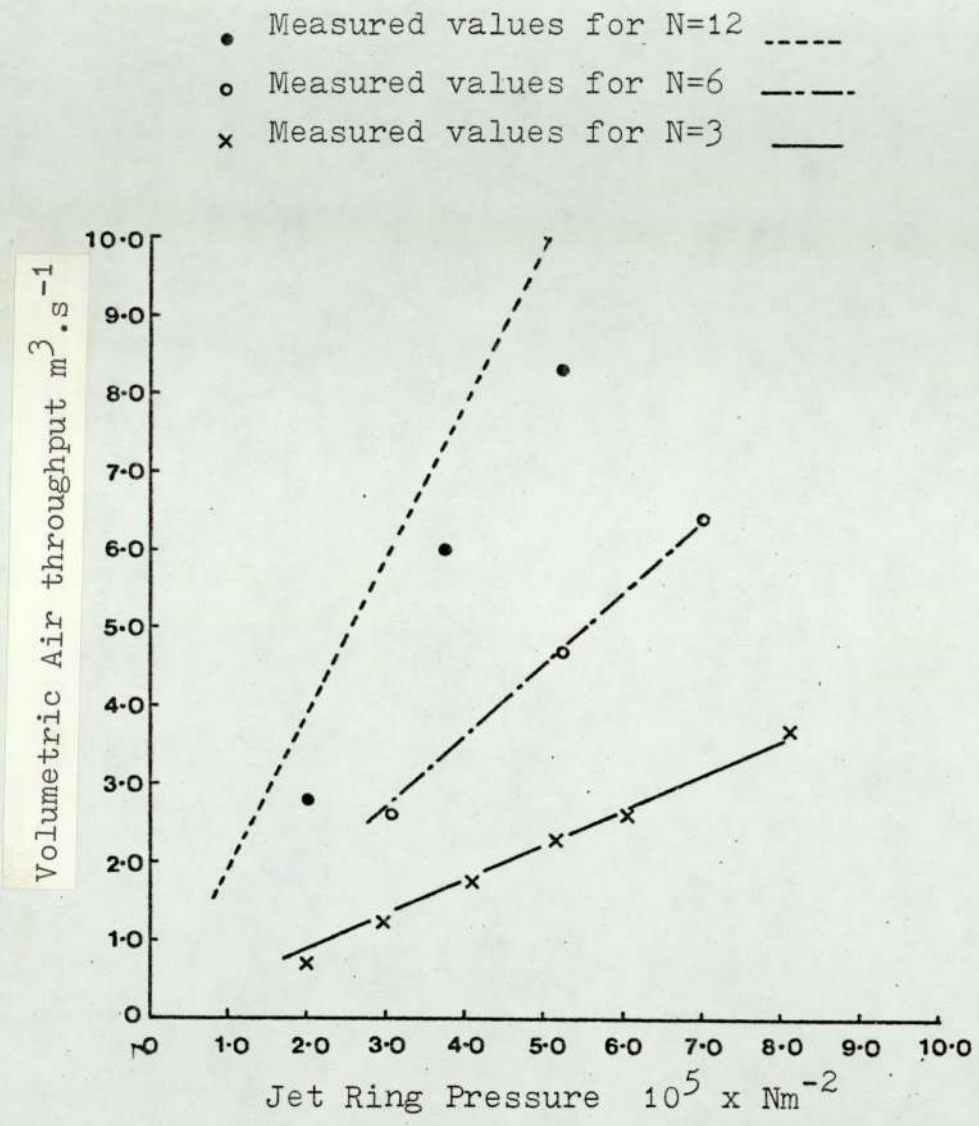

Figure 7.1c: Air throughput at Nozzles (N-C)

$d_N = 3.175$ $C_D = 0.59$

corresponding range of jet ring pressures. It was found for this number of nozzles that the chamber pressure, in the absence of solids was approaching that within the jet ring. Hence, the assumption made in deriving Equation 7.3 and concerning negligible pressure in the chamber was no longer valid. Increased chamber pressure was mainly due to the limitation imposed by the confined space into which the compressible fluid was discharged, i.e. the grinding chamber volume, also by the back pressure caused by the filter bags. The effect also indicates that the air discharged is not fully expanded within the chamber and thus energy available is not fully utilized. In these circumstances it becomes less advantageous to use a larger number and / or increased diameter of nozzles.

7.1.1 Discussion

The aim of investigating the constructional variables of the microniser was to establish the optimum constructional conditions for the utilisation of the compressible fluid in terms of energy supplied and mass of fluid provided. Ideally to eliminate operating variables one would maintain constant pressure and velocity at the nozzle throughout the investigation. However, maintaining both constant nozzle pressure and velocity is almost impracticable. As shown above, for a given fluid throughput the pressure variation in the study concerning the number and diameter of nozzles was within ± 4% This variation was found to have anegligible effect on the overall results.

7.2.1 The Effect of Diameter and Number of Nozzles

This study was undertaken,

(a) to determine the degree of comminution in terms of increase in specific surface area, and change in the mean diameter of the product while varying nozzle diameter, number of nozzles and solid feed rate, keeping air consumption constant,

(b) to detect the interaction, if any, between the variables stated in (a),

(c) to establish the optimum conditions, concerning the number and diameter of nozzles in terms of specific surface area produced per unit mass of air consumed and also mean diameter of product, from data obtained in (a).

Available data on the effect of nozzle diameter (Mori Ref 7, 43) is only concerned with a single nozzle, and was obtained in an apparatus similar to a fluidised bed. No data or information was found in the literature concerning the effect of nozzle diameter or number of nozzles on the performance of the micronizer, nor of the jet-o-miser. This was discussed in Chapter 5.

Evidence indicates that the jet momentum (the velocity at the jet, as discussed in 5.5) is the determining factor in the degree of comminution and extent of classification in fluid energy mills. The jet velocity is determined by the pressure at the nozzle, thus,

$$U_2 = \sqrt{U_1 P_1} \qquad \text{Eq. 7.4}$$

The mass of fluid discharged into the microniser chamber through the nozzles is a function of number and diameter of nozzles and upstream pressure as was shown in Section 7.1

Comparison between the product fineness achieved with varying number and diameter of nozzles was, therefore, based upon the following:

(1) keeping the velocity at the jet exit constant in each series of tests, and,

(2) having the same consumption of air, so that energy consumptions were kept constant.

It was, therefore, necessary to keep the total cross sectional area of the nozzles constant throughout this study.

The above variables (the diameter and number of nozzles) were investigated experimentally for a range of solid feed rates. It was decided to use 12 nozzles, each 1.5875mm in diameter, and operating pressure of 6.9×10^5 N/m^2 (100 PsIG) as the datum point and to arrange so that for 3- and 6- nozzle groups (N-B and N-C) the same total cross sectional area was maintained.

The pressure of 6.9×10^5 N/m^2 at the jet ring, was selected largely because many industrial and available air micronisers operate at this pressure.

TABLE: 7.2

The Condition of Experimental Study in 7.2 of 200mm Micronizer

Conditions: Volumetric Air Feed Rate — Appendix A3 — Tangential circle diameter = 0.127m.

Mass Air Feed Rate

Solid Feed Rate = $1.67 - 11.1 \times 10^{-3}$ Kg/s

Feed Size Range = $0 - 120\mu m$

Nozzle Mark	Nozzle Diameter $\times 10^{-3}$	Cross Sectional Area of a nozzle $* 10^{-6}$ sq. meter.	No. of Nozzles	Total x Sectional Area 10^{-6}	Operating Pressure	Runs No.
N-A	1.5875	1.979	12	23.7518	90	B3/1-9 & B4/1-2
N-B	2.2450	3.959	6	23.7518	85	B4/3-8
N-C	3.1750	7.917	3	23.7518	87	B4/9-11 & B5/1-6

The tangential circle diameter was selected to be two thirds of the microniser diameter, using a nozzle angle of 52^{o}, as shown in Figure 7.2.

The experimental variables investigated in this study and conditions of operation are listed in Table 7.2, and these were carried out in the equipment described in 6.1.

The nozzles were arranged symmetrically in each experiment, as shown in Figure 7.2a, b, and c.

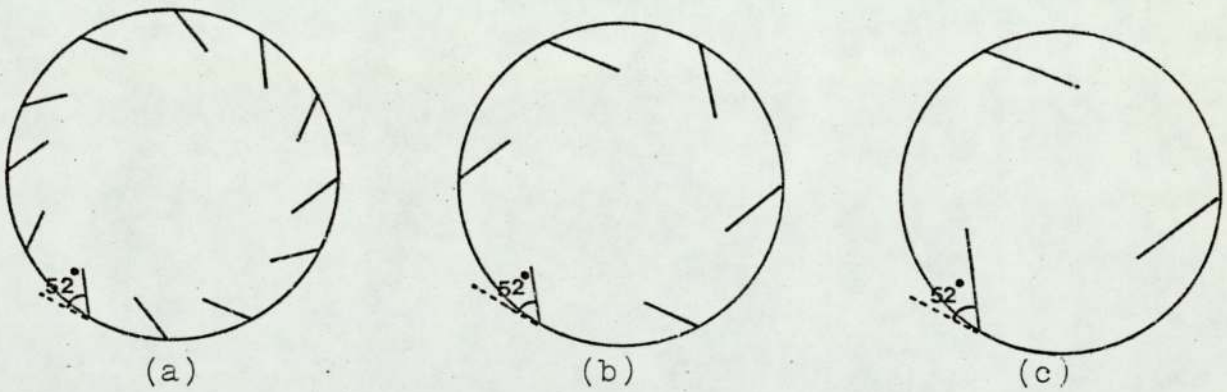

Figure 7.2: Nozzles arrangements for (a) 12 N-A (b) 6 N-B (c) 3 N-C

The quantity of air supplied to the jet ring was regulated and measured according to the pressure drop observed across the venturi tube. Because of the coefficient of discharge dependency on the nozzle diameter, as shown in part 7.1, the pressure at the jet ring varied slightly from one set of nozzles to another. This variation in pressure was $\pm$ 4%, while the corresponding change in velocity was about 2%.

Reproducibility of the particle mean diameter for a

given operating condition was found to be ± 5.38%, and that of the particle size analysis was within ± 3.3%, obtained by techniques described in part 6.3

The particle size distribution data obtained in the above study are shown in Appendix A4. The distributions were examined to see whether they followed one of the known distributions (see Section 2.6). It was found that the log-normal distribution law gave the best fit as shown in Figures 7.3 and 7.4. The visually best straight-line fit was drawn through the central region, the scatter is only observed at the limits of the distribution.

Figure 7.3 shows the distribution obtained at solid feed rate of .001986 Kg/s, for nozzles arrangement N-A, N-B and N-C and at conditions stated in Table 7.2. The comparison between the distribution can be made by directly reading the median diameter d and the geometric standard deviation. It was found that median diameter was almost equal for nozzles N-A and N-B within the experimental errors, while that for N-C was markedly higher. Similarly, the observations made when considering the plots in Figure 7.4, indicate that product obtained when using N-A is finer than N-B, and the latter is finer than N-C. The product size distribution is given in Appendix A4.

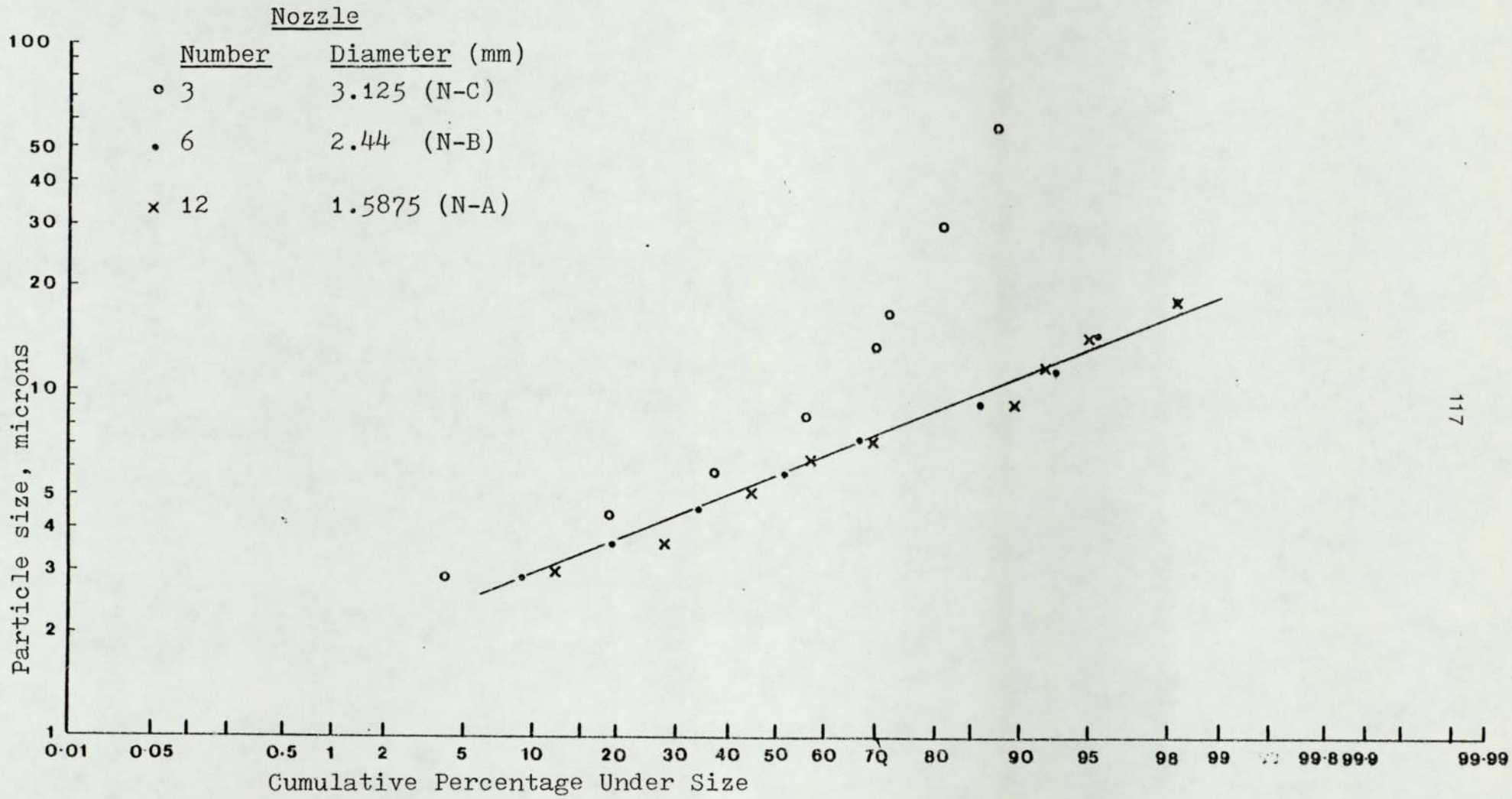

Figure 7.3: Particle size Distribution of product obtained using 3 sets of nozzles (above) and at low solid feed rate 0.019 Kg s^{-1}.

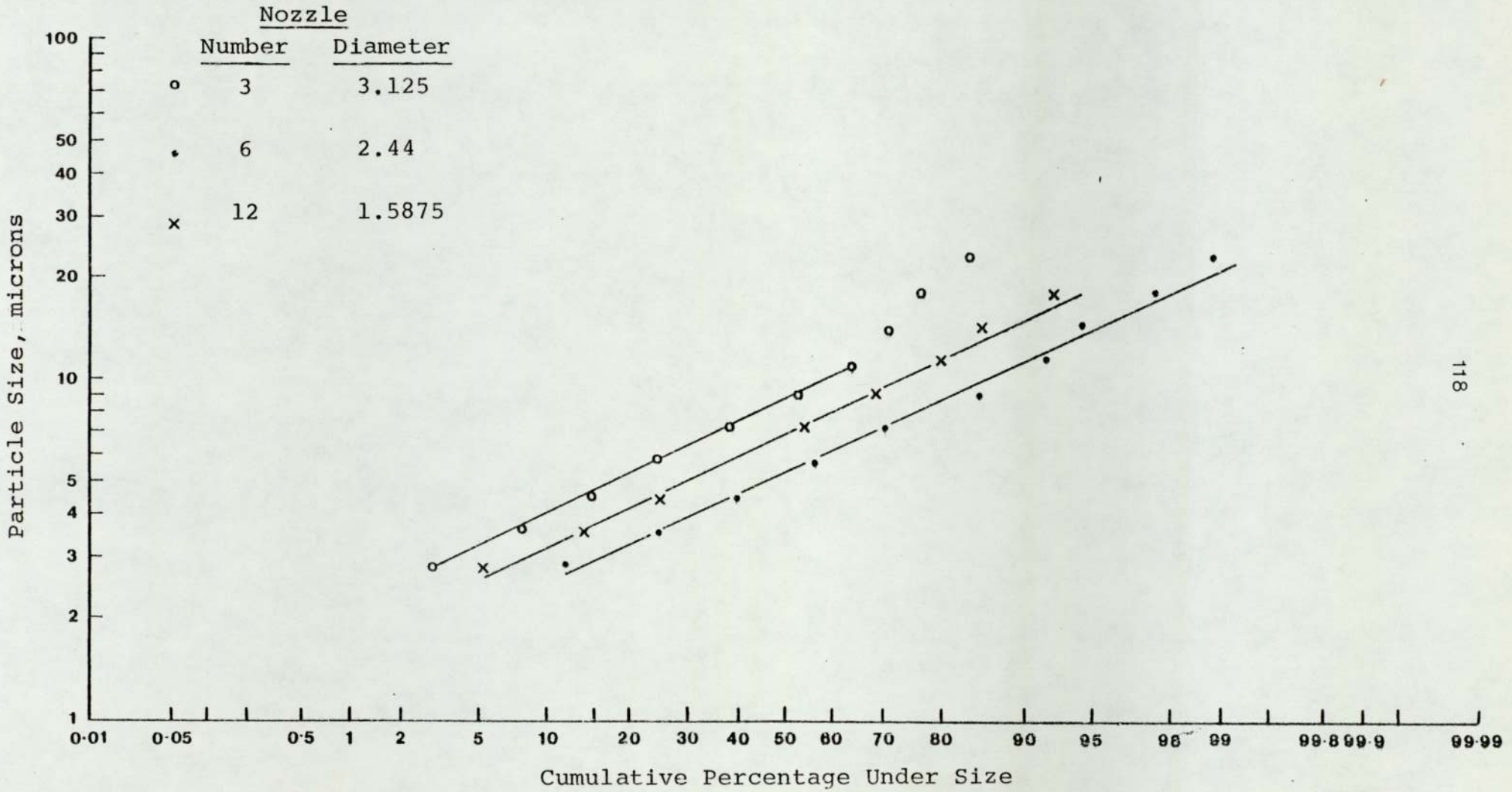

Figure 7·4 : A Typical Particle Size Distribution Obtained from the Micromiser. Also Showing the Distribution Obtained from Each Set of Nozzles at Solid Feed Rate 2.78 kg s^{-1}

Figure 7.5 is a plot of the product mean volume diameter against the solid feed rate, with the nozzle type and number as a parameter. The product obtained when using the 3 N-C nozzles was considerably coarser than that obtained when using either the N-A or N-B nozzles under the same conditions of operation and using feed material of same distribution throughout. At low solid feed rate (up to about 4.1 - 5.6 x 10^{-3} Kg/s) the mean diameters of product obtained using nozzles N-B were equal to those resulted when using nozzles N-A. At increased feed rate, the mean diameters obtained when using N-B were markedly higher than those obtained using N-A nozzles.

Figure 7.6 shows a plot of the specific surface area of product versus solid feed rate. The specific surface area was estimated in the expression given in part 5.5 from the particle size distribution data. The effect of varying nozzle number and diameter is illustrated (Figures 7.5 , 7.6) and it can be seen that higher surface area for same fluid consumption is obtained when using 12 nozzles of N-A.

7.2.2 Discussion of Results on Number and Diameter of Nozzles

The results obtained in this study are shown in Section 7.2. When comparing the specific surface area produced for

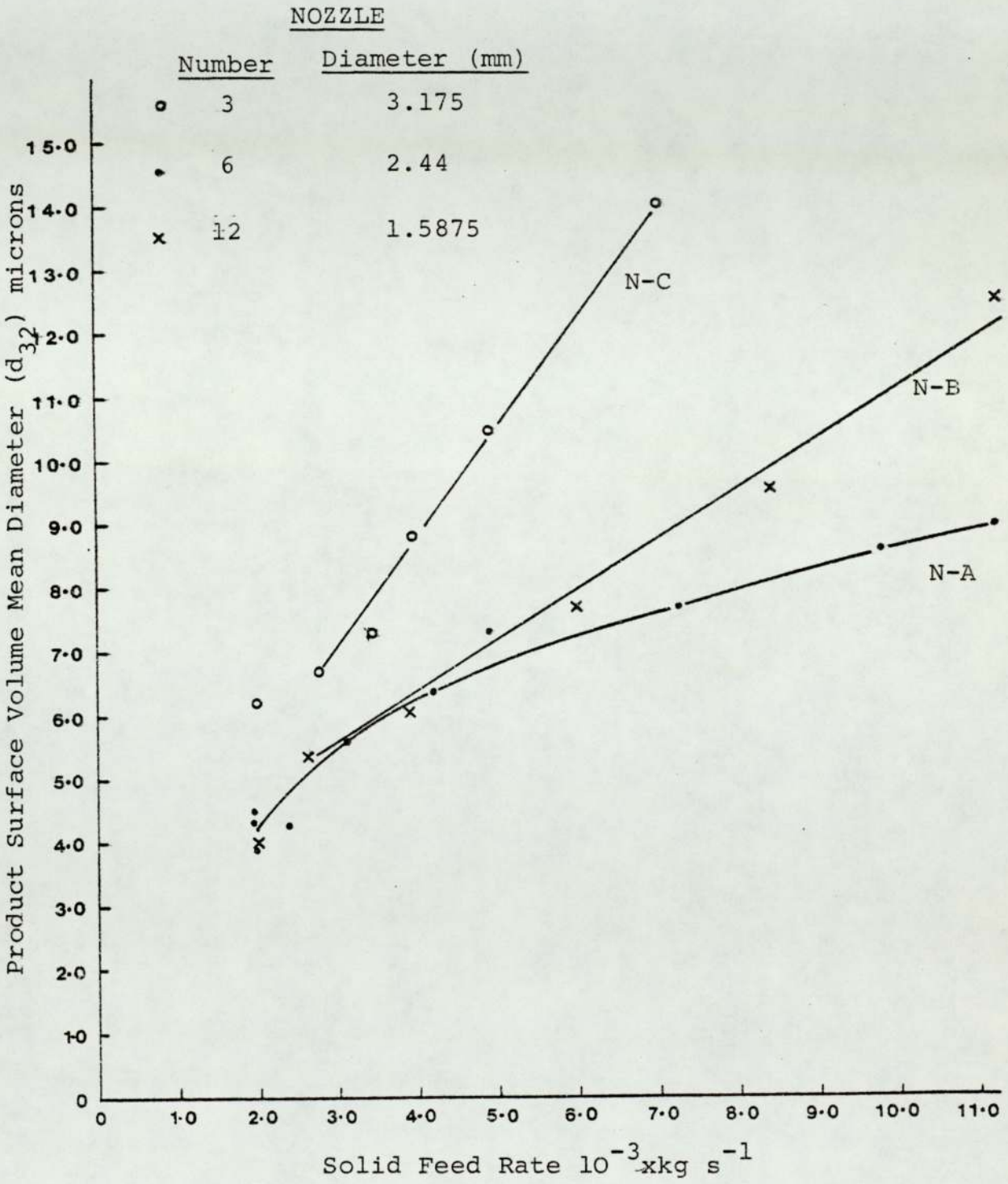

Figure 7·5 : Product Mean Diameter Versus Solid Feed Rate for Various Number and Diameter of Nozzles (Feed 0-120 μm)

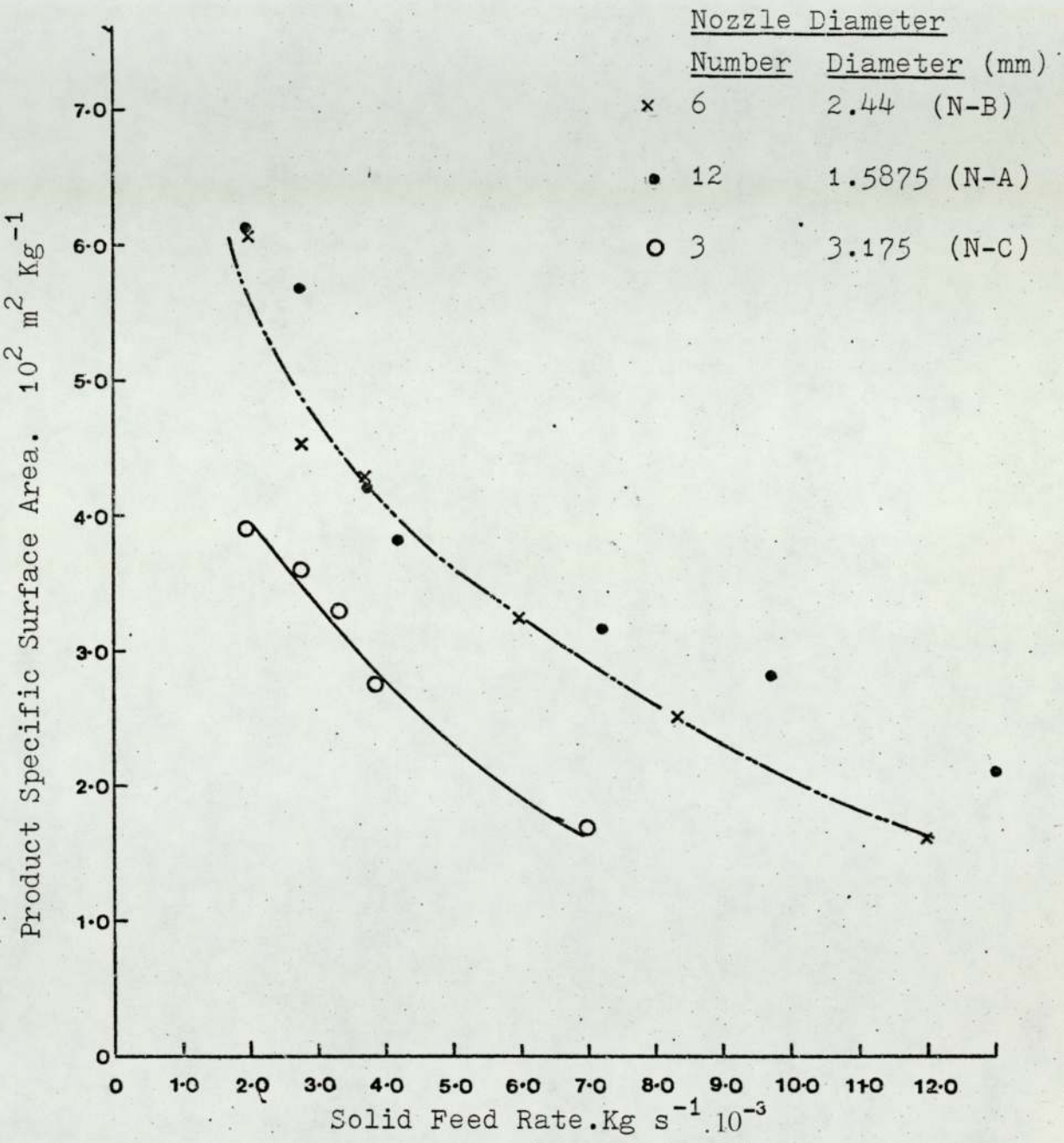

Figure 7.6: Effect of Number and Diameter of Nozzles on products specific surface Area.

each set of nozzles, at a given flow rate and solid feed rate and at approximately the same pressure. The difference is pronounced between the results obtained using three nozzles of 3.175mm each and using twelve nozzles 1.5875 each, both having equal cross-sectional area: the specific surface area produced when using the twelve nozzles was consistently higher than that obtained with the three nozzle, at all solid feed rates. For the six nozzles, the specific surface area produced at low solid feed rate and up to 0.0033Kg/s was comparable to that obtained from the twelve N-A nozzles. At higher solid feed rate, the twelve N-A nozzles resulted in higher specific surface area. Also investigating the graphs it can be seen that the capacity of the microniser, for a given product specific area, is markedly increased by the increased number of nozzles, e.g. for product specific surface area of 260 m^2/Kg, the solid feed rates were

12 nozzles (N-A): 0.0097 Kg/s

6 nozzles (N-B): 0.0069 Kg/s

3 nozzles (N-C): 0.0042 Kg/s

However, care should be taken when designing a microniser with increased number of nozzles of smaller diameter, or lesser number of larger diameter, since the ratio between nozzle diameter and chamber height could be significant, as it was observed during experimentation that the 6 and 3 nozzles caused noticible erosion on the liner plates within a relatively short time of operation. This is attributed to the high velocity jets and particles suspension. The nozzle diameter to chamber depth ratios were as follows:

Nozzles	d_N/H_m
N-A	0.083
N-B	0.125
N-C	0.167

The reasons for loss of grinding efficiency in the case of lesser number of nozzles with increased diameter can be attributed to a number of factors, these are:

I. The probability of entraining particles into the effective region of the jet.

The effective region is the zone where the particles are accelerated and given the momentum for breakage on collision; it is found to extend to a distance $10 \sim 20 d_N$ from the nozzle exit, as discussed in Section 5.3, and spreads at an angle of 10^o approximately to the plane of the nozzle exit, (see Figure 5). Hence as nozzle diameter increases, the jet stream penetrates further into the micronizer chamber, and also impinges on the micronizer liner plates from a distance closer to the nozzle exit, and extending to a distance proportional to d_N. In addition, the shear force of the rotating stream causes the jet to spread in the vertical direction and to be deflected. Therefore, particles that entrain into the jet are carried further away in the jet stream (away from the nozzle exit, and most probably join the next jet stream well away from the nozzle exit, hence undergo a lesser degree of acceleration, than if they were entrained at the nozzle exit. Also, because of increased width of the jet stream, and its impingement on the liner plates, the gas-solid suspension is only entrained on the

reverse side of the jet since the field of velocity would be too high to allow the suspension flow to entrain from other points in the jet boundary. Conversely, a smaller nozzle diameter in relation to the chamber height, should allow particles to be entrained over a greater part of the jet stream boundary, and particles would not be ejected so far from the grinding zone.

II. Degree of Turbulence and Formation of eddies in the jet vicinities

Studies of flow pattern in the micronizer were discussed in Section 5.3. These were conducted in a 0.2m diameter model micronizer having six nozzles. It was shown that a return flow occurs above and below the jet stream, and it was expected that eddies would form in the wedge between successive nozzles. The formation of eddies, and intensity of turbulence in the vicinity of the jets, is likely to have a significant effect on the degree of comminution and entrainment of particles into the jet stream. This would be influenced by the number of jet streams and the distance between successive nozzles, and also by the total particle concentration which will be discussed below. The likelihood of formation of eddies is greater in the case of closely-positioned jets. This would have the effect of increased inter-particle collision, and would aid entrainment of particles into the jet stream. As discussed in Section 5.1, eddies increase turbulence and contribute towards reducing the stream velocity, but this effect may not be significant in comparison with inter-particle collision effects.

Increased solid concentration was found to reduce fluid turbulence, (Section 4.5) thereby to a certain extent reducing the rate of inter-particle collision.

III. Classification Pattern

The flow pattern in the microniser chamber is similar to that obtained in flat vortex classifiers (Section 5.3.1 and 5.2) and the turbulence and wall friction have a powerful influence on the separation of particles. Turbulence counteracts the separation by scattering the particles already separated, while both turbulence and wall friction have the effect of decreasing the tangential velocities of the vortex motion which determines the centrifugal forces necessary to effect a separation.

Rietema and Krajenbrink (Ref 16) have found that a complete symmetry of revolution of fluid in flat cyclones can be best approached by using a series of vanes around the circumference of the cyclone and in this case the ratio of u/v is fairly high. (Where u and v are radial and tangential velocity respectively).

When considering the number of nozzles around the periphery of the chamber and the length of the jet which is a function of its diameter, it would be expected that a complete symmetry is approached by using an increased number of nozzles, although this would form an additional point of turbulence. However when the jet length is relatively short compared with chamber diameter, the turbulence would be

Plate 7.1: Top wear plate, also showing erosion caused by a six nozzles jet ring.

confined only in the periphery of the chamber. As the results in Figures 7.5 and 7.6 indicate an increased number of nozzles with shorter jet length was the more efficient.

Lesser number of nozzles with larger diameter may have two disadvantages in the classification action, the first being loss of symmetry of the rotating fluid. It was observed during experimentation that the three N-C nozzles left a triangular pattern on the wear plates which was caused by the high velocity gas-solid jets. Similarly for the six N-B nozzles a hexagonal ring was formed as shown in (Plate 7·1), and was close to the outlet port. The second disadvantage is that increased nozzle diameter results in an increase in the jet length (spreading from the exit). The jet stream thus causes a considerable turbulence in the classification zone at large nozzle diameter extending nearer to the discharge port. This has an adverse effect at high solid concentration within the chamber, as seen when comparing the particle size distribution shown in Figure 7.4. The twelve N-A nozzles shows a clear cut in the distribution while the six N-B and three N-C have exhibited an irregular distribution.

7.3.1 Jet Injection Angle Effects

This study was undertaken:

(a) to investigate the resulting effect on particle size distribution and specific surface area of the product,

(b) to detect any interaction between jet injection angle and solid feed rate,

(c) to determine the optimum jet injection angle, on the basis of product fineness and air consumption, and,

(d) to find the limiting fineness for each nozzle.

Tangential velocity at the chamber exit was investigated by Rink et al (Ref 1), with respect to the jet injection angle, as discussed above in part 5. It was found that for a given pressure at the jet ring, higher tangential velocity was achieved when the jets were directed at an angle between 65° and 75°.

Thus assuming that classification takes place at the exit, it would appear that the cut size (diameter at which all particles less than stated size will leave the chamber) is least for this angle. However no previous experimental data was available in support of this finding. Also the above investigation was confined to the classification effect only. The interaction between the jet streams and the basic stream have not been considered.

Four sets of nozzles, at different angles were investigated in this study. On the basis of the findings given in Section 7.2 concerning the effect of number and diameter of nozzles, twelve nozzles of 1.5875 mm diameter were selected for this study, the injection angle

of each is given in Table 7.3 below.

The average pressure at the jet ring for all experiments in this study was fixed at 7.9×10^5 N/m^2 ($\pm$ 5%) absolute. There was slight deviation in pressure required to give a fixed volumetric air flow from one set of nozzles to another. This deviation was found not to have a noticeable effect on the results.

Table 7.3: Specifications of Nozzles Used for Jet Injection Angle Experiments

Nozzle Mark	Injection Angle (o)	Tangential Circle Diameter (m)	Nozzle Diameter (10^{-3} m)
N-A	52	.127	1.5875
N-F	41	.152	1.5875
N-I	28	.172	1.5875
N-L	60	.102	1.5875

Table 7.4: Conditions of Experiments of Preliminary Study

Jet Injection Angle:	As shown in table 7.4	
Number of Nozzles	:	12
Pressure	:	7.9×10^5 N/m^2(A) $\pm$ 5%
Air throughput	:	35.5×10^{-3} Kg/s
Feed Size	:	'A'
Feed Rate	Low Level	: 1.96×10^{-3} Kg/s
	High	: 8.33×10^{-3} Kg/s

7.3.2 Preliminary Study

This was carried out to investigate the effect of nozzle injection angle on the product size, and to detect possible interaction between feed rate and the nozzle angle. Initially the experiment was carried out at two levels of material feed rate. The experimental conditions are listed in Table 7.4.

Figure 7.7 is a graphical representation of specific surface area of product versus jet injection angle with solid feed rate as a parameter. It was found that at a solid feed rate of 1.96×10^{-3} Kg/s, the volume mean diameter decreased, hence, specific surface area increased with decreasing nozzle angle α, while at 8.66×10^{-3} Kg/s feed rate, a maximum specific surface area resulted at an angle of 52°, for the same air consumption.

Further experimentation was planned and carried out to investigate the effect of nozzle angle over a range of solid feed rate.

7.3.3 Investigation of Jet Injection Angle Over a Range of Material Feed Rate

Table 7.5 is a listing of experimental conditions used for this set of experiments. Specific surface

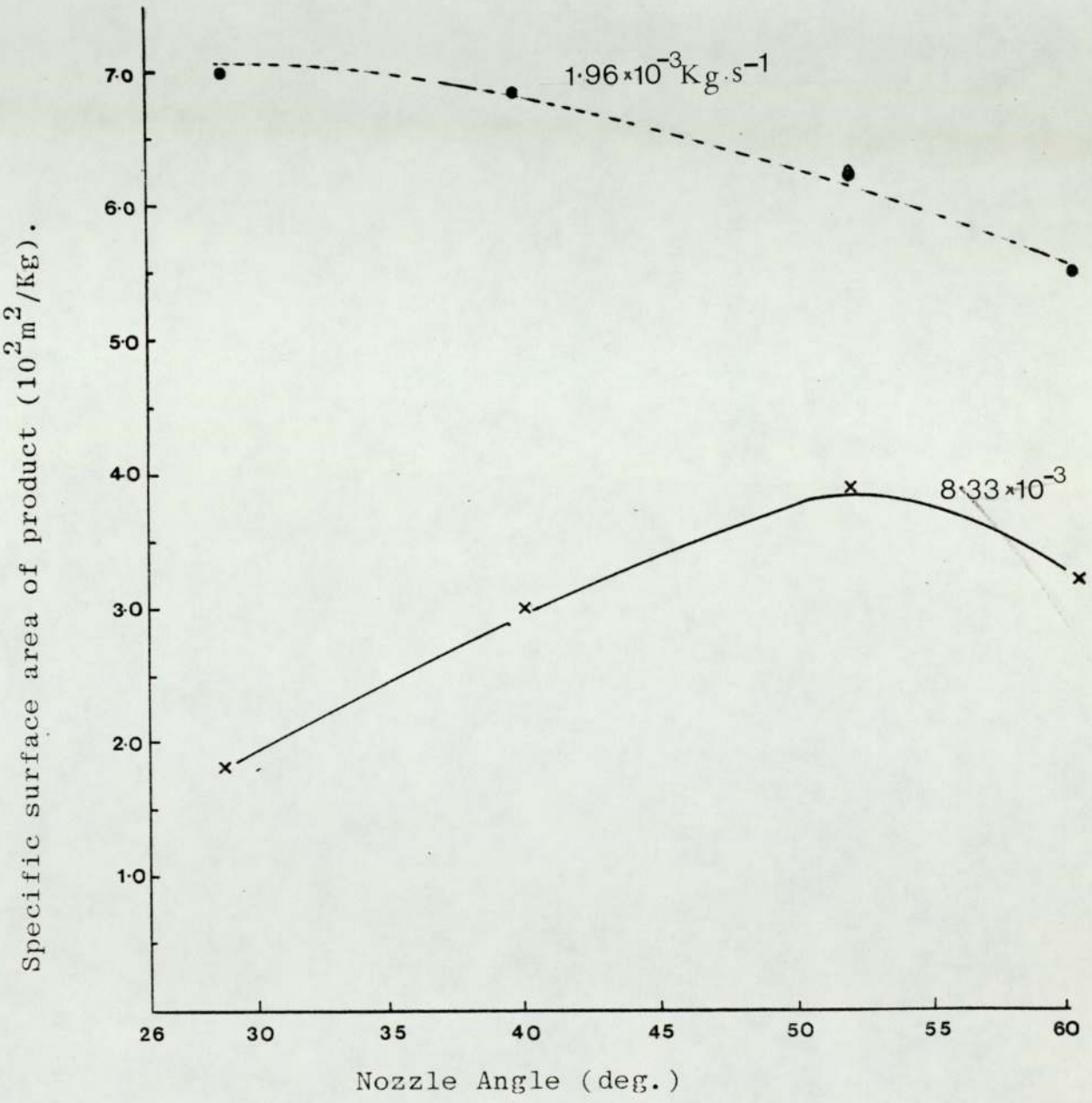

Figure 7.7 : Preliminary experiment results on jet injection angle (Nozzle Angle). Obtained at two solid feed rate

Table 7.5 Conditions of Experiment for Nozzle Injection Angle

(Experiments B10/1 - B12/12)	=
Number of Nozzles	= 12
Nozzle Diameter	= $1.5875 * 10^{-3}$ m
Feed Size	= Fraction 'A'
Solid Feed Rate	= 1.67 - 11.1 x 10^{-3} Kg/s. (Appendix A3)

Air pressure and air flow rate - see Appendix A3

area versus material feed rate, with the jet injection angle as a parameter, is shown in Figure 7.8
The results obtained in this study confirmed the earlier results given in 7.3.2, in that at low solid feed rates (up to 2.5×10^{-3} Kg/s) a higher degree of comminution was achieved when using nozzle N-I which has a jet injection angle of 28°. When inspecting the particle size distribution at material feed rate below 2.5×10^{-3} Kg/s, the N-1 arrangement resulted in the sharpest cut size product. The distribution is listed in Appendix A4.

As feed rate increases, the maximum surface area produced tended to move to the next smallest jet injection angle, this phenomena is noted when inspecting Figure 7.9 Thus for feed rate between $6 - 11.1 \times 10^{-3}$ Kg/s the highest surface area was produced at jet injection angle of 52°.

Figure 7.9 shows that for all nozzle injection angles considered, the surface area decreases and volume mean diameter increases with increasing feed rate.

The static pressure for each of the runs in this investigation was measured. The point of measurement was at the periphery of the chamber. The change in static pressure with material feed rate is illustrated in Figure 7.10. It was found that as feed rate increases the measured static pressure falls to give an assymptotic value. This pressure is an indication of the tangential velocity at point of observation, and a fall in its value,

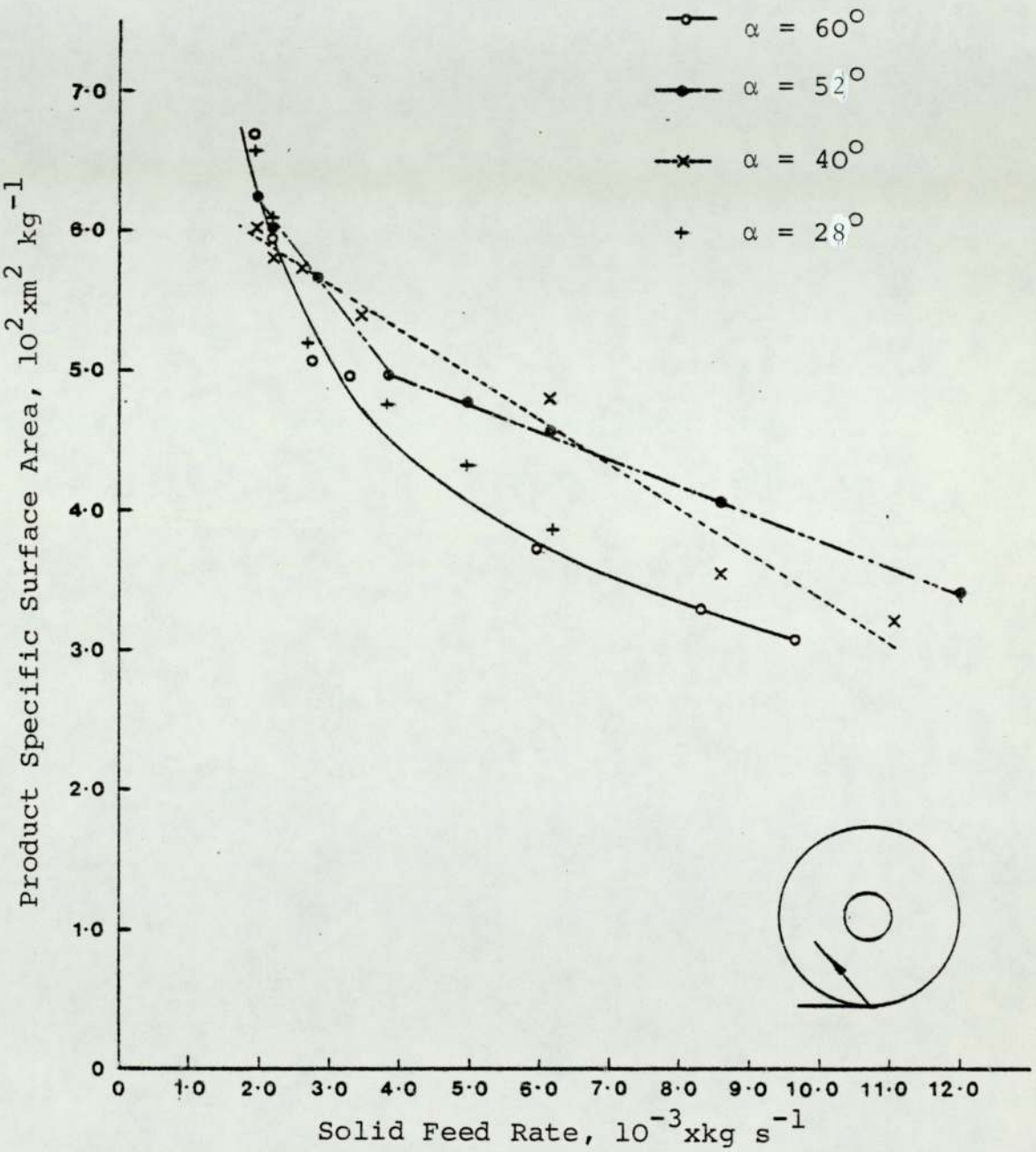

Figure 7·8 : Product Specific Surface Area Versus Feed Rate for Various Jet Injection ANgles α (Feed 0-120 μm)

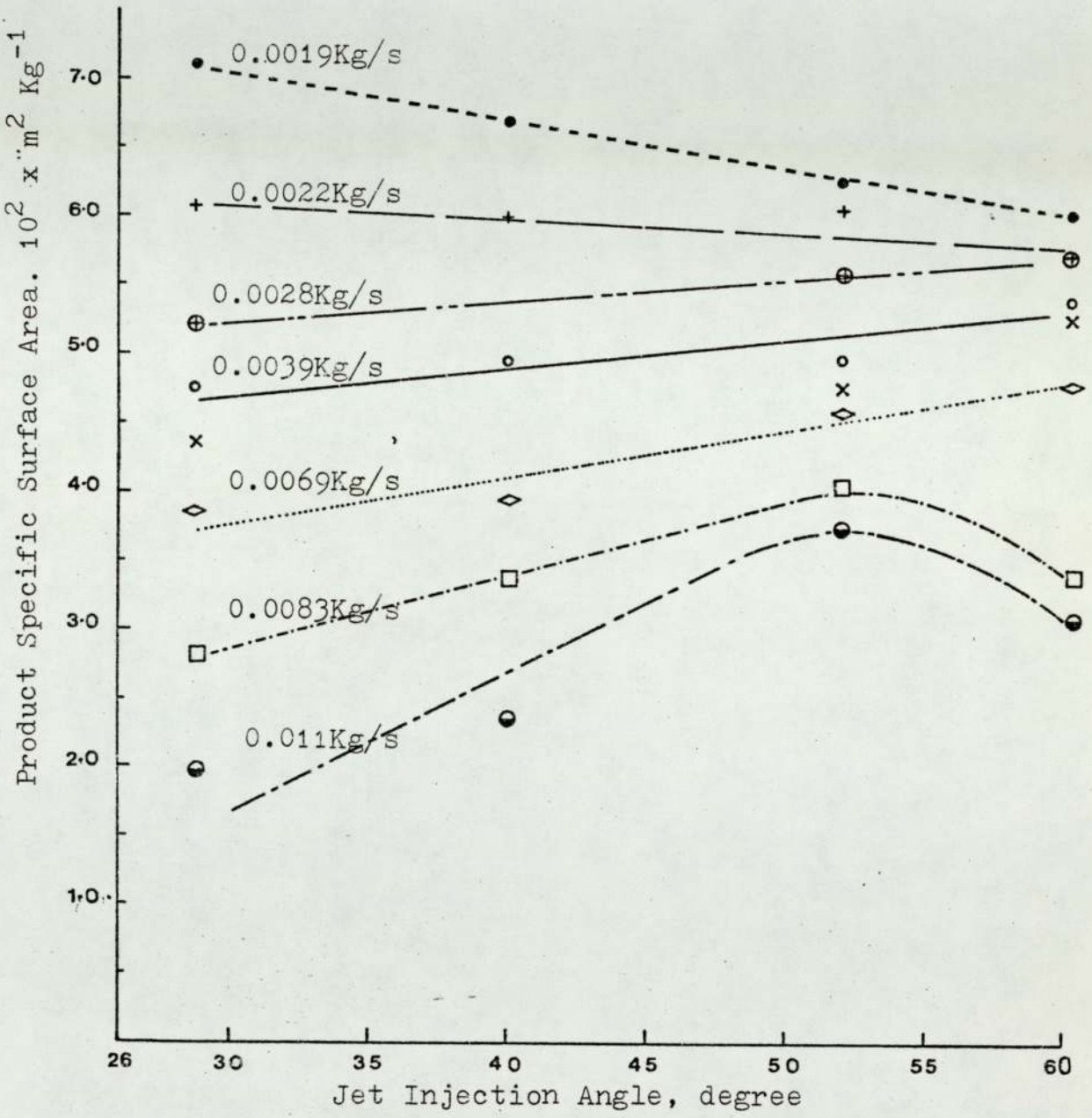

Figure 7.9: Product Specific Surface Area for Various jet injection angles and at Various solid feed rate.

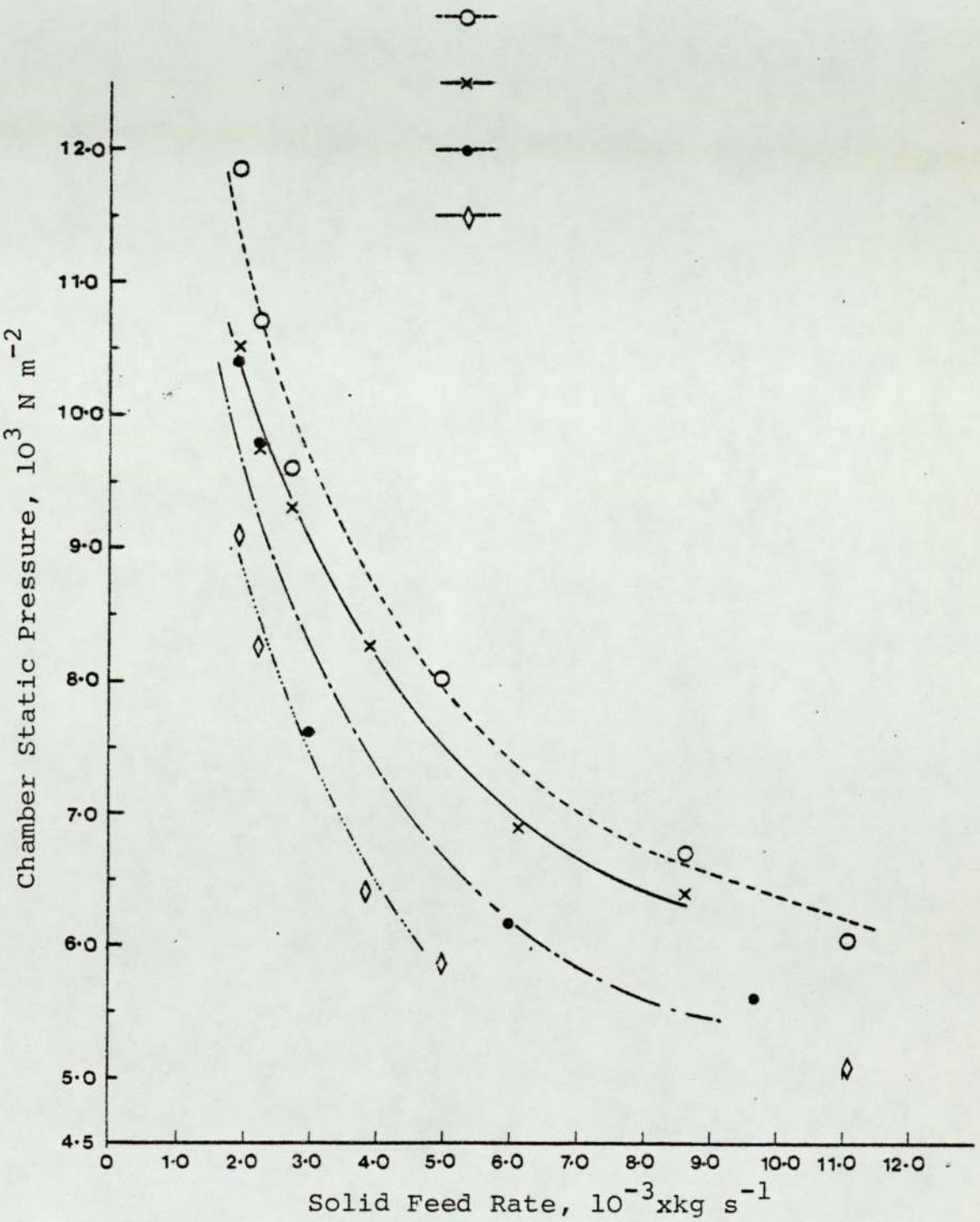

Figure 7.10 : Measured Chamber Static Pressure Versus Solid Feed Rate for Various Jet Injection ANgles

can be viewed as a drop in the tangential velocity at that point.

7.3.4 The Effect When Using a Combination of Jet Angles

It was decided to investigate the effect of using a combination of jet injection angles, i.e. with jets set at differing jet angles in two groups.

The experimental conditions and the results are listed in Table 7.6. The degree of comminution occuring was determined by sieve analysis, in which the product was sieved through 45 μm sieve as described in Chapter 6.

Inspecting the results shown in Table 7.6, the percentage of product retained on the sieve was an average of at least 3 samples. It was found that this percentage increased when various combinations were attempted. The comparison was based on the size of product produced when using 12 nozzles of N-A, at a given solid feed rate, and air throughput; both these parameters were kept the same for all combinations.

As seen in Table 7.6, using a combination of jet injection angles has no advantages, and in the case of using N-L it was disadvantagous.

7.3.5 Discussion of Results of the Jet Injection Angle

The influence of jet injection angle on the classifi-

Table 7.6: Results of Product Size Using a Combination of Jet Injection Angle

Nozzle Diameter = 1.5875mm

Total number of Nozzles = 12

Feed size = 0 - 120μm

Pressure at the jet ring = $6.894 * 10^5$ N/m^2

Run	Nozzle Mark	No.	Nozzle Mark	No.	Arrangement	Feed Rate	Average % Retained on 45 μm sieve	%age max. deviation.
B15/1	A	12	-	-	-	9.06	NIL	
B15/2	A	12	-	-	-	30.00	12.16	$\pm$1.23%
B15/3	A	9	L	3	One of I after	9.06	NIL	
B15/4	A	9	L	3	every 3 of A	30.00	16.7%	$\pm$1.52%
B16/1	A	12	-	-		30.00	11.67	$\pm$1.38%
B16/2	A	11	L	1		30.00	11.41	$\pm$1.70%
B16/3	A	9	L	3	One of L following 3 of 'A' alternately	30.00	15.13%	$\pm$1.15%
B16/4	A	6	L	6		30.00	15.76%	$\pm$1.02%
B16/5	A	6	I	6		30.00	12.04%	
B16/6	A	6	I	6		30.00	11.70%	

cation action within the micronizer chamber was discussed in Section 5.6.3.1. It was shown by Rink et al (Ref 1) that the tangential velocity component at the central discharge port increased with nozzle angle α (Figure 7.11 below). Theoretical studies of the flat vortex classifier by

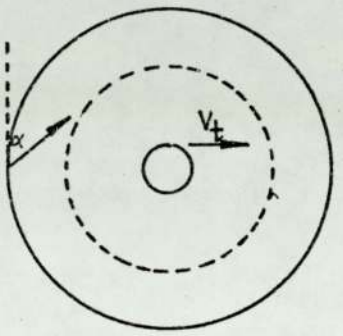

Figure 7.11

Rietema (Ref 12) confirm maximum velocity at the exit port.

The specific surface area of product and comparison of particle size distributions obtained for a range of solid feed rates and for four jet injection angles are presented in Section 8.3.2. The results indicate that at the lower material feed rates the increase in product specific surface area tends to be higher for smaller angle α which contradicts the above analysis. This is most probably due to the low hold-up in the mill at low material feed rates (Section 8.5) and to the particles mostly being concentrated nearer the periphery of the chamber. When the angle α is small the jets are directed closer to the chamber periphery and considerable number of particle-wall impacts are taking place. However, at higher solid feed rates the particle concentration in the chamber increases, and hence

inter-particle collisions predominate over wall collision. This can be seen when comparing the increase in specific surface area of the product obtained using injection angles $\alpha = 28^{\circ}$ and 40° with that for $\alpha = 52^{\circ}$ and 60°; the latter two angles gave an improvement over the former of the order of 20 - 30%.

Inspecting the results obtained for angles $\alpha = 52^{\circ}$ and 60°, it is seen from Figure 7.8 that an overlapping occurs; at material feed rate below 2.8×10^{-3} Kg/s higher increase of specific surface area was achieved for injection angle of 52°, at feed rates between $3.33 - 6.4 \times 10^{-3}$ Kg/s the increase was higher for injection angle of 60°, but above that feed rate, an injection angle of 52° gave a higher increase.

In addition to the influence of jet injection angle on the classification action (see Section 5.2) consideration should also be given to the variation of particles' impact velocities with jet angle, this is illustrated in Figure 7.12 below:

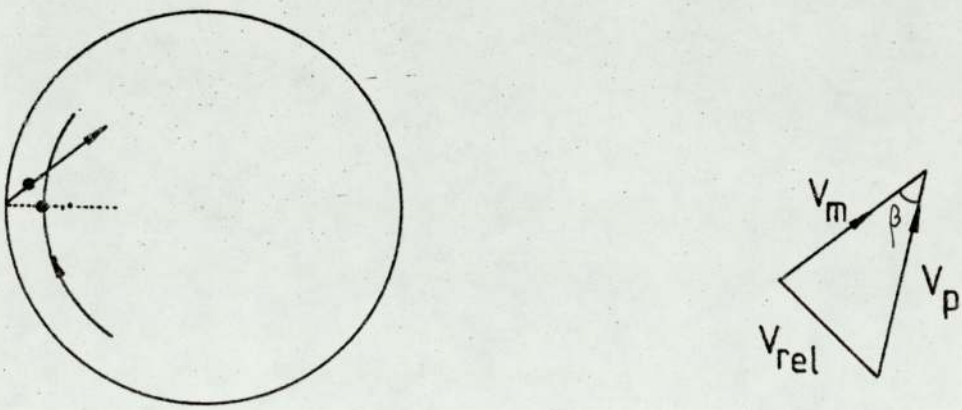

Figure 7.12 : Velocity diagram

Consider a particle moving at a velocity v_m in the jet stream (Figure 7.12) and another approaching it at velocity v_r moving in a circular path parallel to the jet ring; upon collision the relative velocity v_{rel} can be determined from the velocity diagram above. For a given nozzle diameter and upstream pressure, v_m is independent of nozzle angle The effect of nozzle angle on v_r can be considered negligible but angle β will influence v_{rel} which greatly influences the probability of fracture of a particle upon impact.

7.4 Experiment to Determine the Effect of Guard Ring Height and Configuration

Two types of guard rings are usually used in the microniser, the "slotted" guard ring shown in Figure 7.13 and the "straight pipe" guard ring.

Increasing the height of the guard ring protruding into the chamber, it is claimed, should result in a finer product. The height of the ring in the chamber does not have any significant effect on the actual comminution process but it may influence the ratio of tangential to radial velocity. The former is theoretically dependent upon nozzle angle, fluid throughput and solid concentration, while radial velocity at the outlet is dependent upon fluid throughput and also must depend on the area available for flow at that point. This area is determined by height of the ring, therefore, increased height results in increased radial velocity, while the tangential velocity should remain the same. This should result in a coarser product.

The presence of a guard ring is essential because it acts as a "weir" preventing larger particles at the lower inner surface of the micronizer from escaping from the chamber.

Tests carried out on various configurations of guard ring showed that no significant difference is observed - PSD shown in Appendix A4. Increased height of the guard ring resulted in a coarser product at high solid feed rates, but there was no real difference at low feed rates.

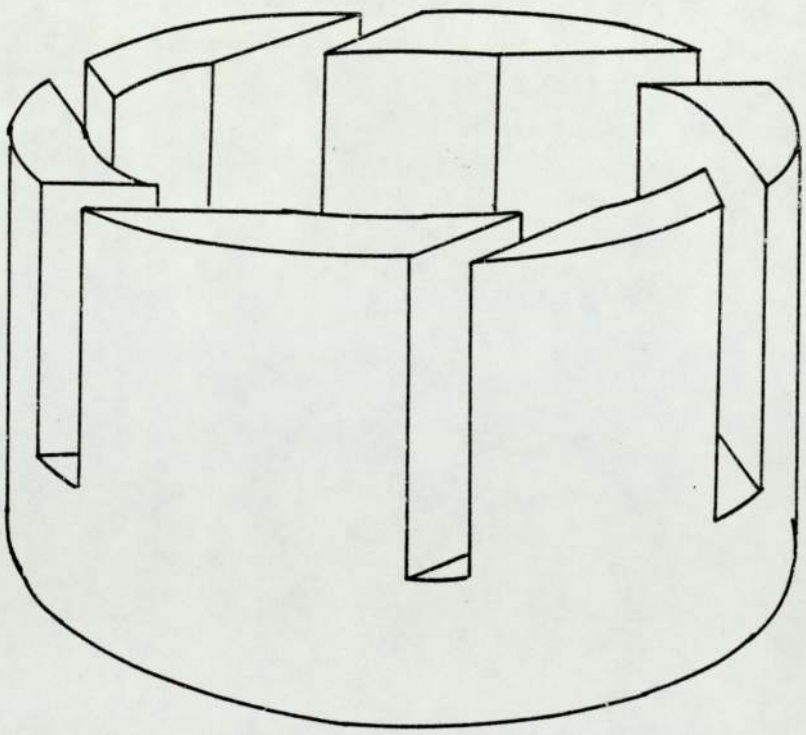

Figure 7.13: Slotted guard ring

Chapter 8: Operational Parameters: Results

8.0 STUDY OF OPERATIONAL PARAMETERS

8.1 Aim

This study was undertaken:

(a) to investigate the effect of air throughput on product fineness,

(b) to investiagate the effect of feed size on the degree of comminution and efficiency,

(c) to investigate the solid feed rate for (a) and (b), and

(d) to determine the material hold-up in the grinding chamber for (a), (b) and (c).

In Section 5.7.2 studies concerning the performance of fluid energy mills generally, in relation to the particle size of the feed and to the solid material throughput have been discussed. These were mainly concerned with the jet-o-miser. Few studies are published on the micronizer performance, the most notable of these were carried out on laboratory scale micronisers (50 - 100mm diameter). These papers contained no details regarding constructional features of the micronizer or magnitude of fluid quantities used. The particle size of the feed has been limited to a minimum of 250μm and in most cases the feed was closely-sized fractions. However, in practise the particle size of the feed to the micronizer is below 150μm and contains a range of sizes. The pressure noted in these studies was limited to a maximum of 6.5×10^5 N/m^2. It is thought that higher nozzle pressures

must be considered since it is agreed that increased pressure increases microniser capacity.

A number of experiments were carried out in a 200mm microniser to investigate the operational parameters involved. These are given in Table 8.1 where the nozzles details are also given.

Table 8.1 Variables and Conditions of Experiments on Operational Parameter Studies

Nozzle Diameter: = 1.5875mm

Number of Nozzles: = 12

Nozzle Mark: = N-A, (angle 52^{o})

Solid Feed Rate Range: = 1.667×10^{-3} Kg/s - 11.1×10^{-3} Kg/s.

Pressure-Range: = 4.1×10^{5} - 10×10^{5} N/m^2 (AIR)

Material: = Limestone

Feed Size: = See below

FRACTION	A	B	C	D	E
Feed Size Range μm *	0-120	0-250	0-500	300-600	600-1180
$d_{50\%}$	20	40	80	450	850

* Particle size distribution of these fractions is given in Appendix A2.

8.2 Presentation of Results

8.2.1 Solid Feed Rate

The effect of solid feed rate on the particle size of the product is terms of specific surface area of the product is presented in Figure 8.1.

It is found that for a given air throughput and for all feed sizes considered, the surface volume mean diameter increased and specific surface area decreased, as solid feed rate was increased. This behaviour is common in all cases of other feed sizes tested, as shown in Figure 8.1. These results were obtained at $6.9 \times 10^5 N/m^2$ pressure irrespective of solid feed rate.

8.2.2 Feed Size

As shown in Figure 8.1 at a given feed rate the product specific surface area decreases with increasing feed size, except, at very low feed rate when the specific surface area is the same within the experimental errors, and independent of the feed size.

The rate of change of product specific surface area with respect to the solid feed rate, decreases as the latter increases i.e. at higher solid feed rate the specific surface area of the product approaches that of the feed. Also as the feed size is increased the specific surface area of the

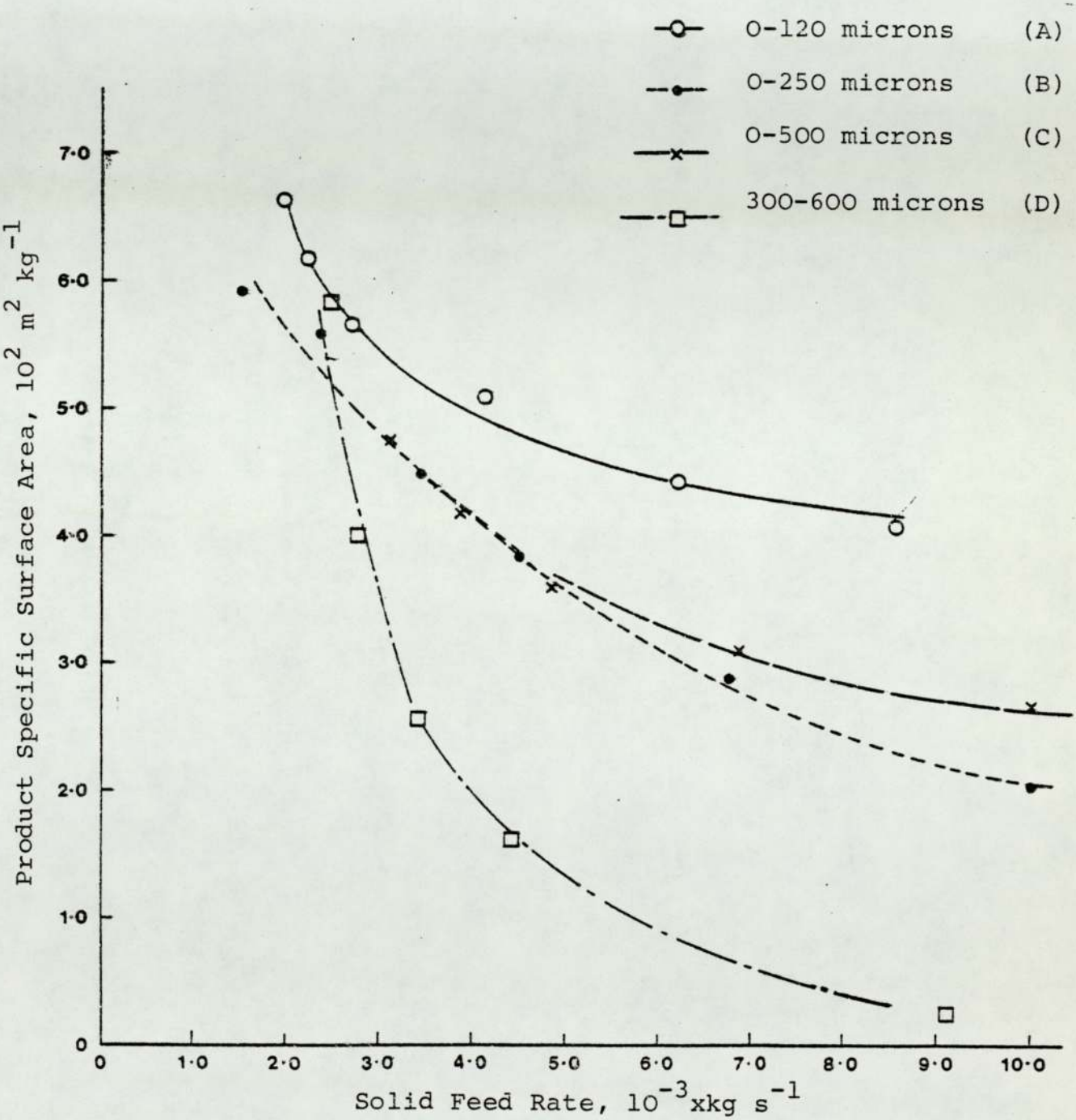

Figure 8·1 : Specific Surface Area of Product Versus Solid Feed Rate for Various Particle Feed Size

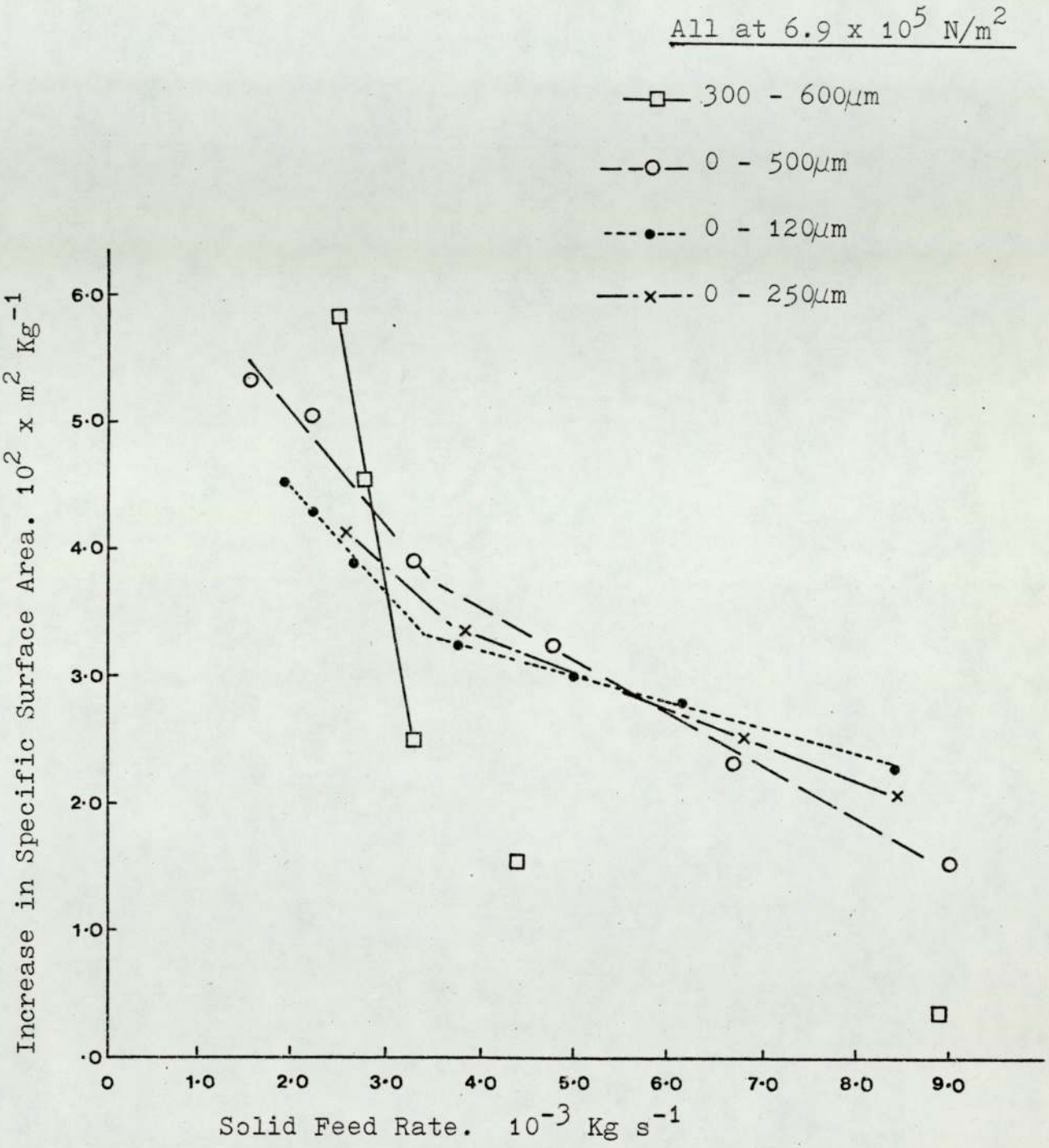

Figure 8.2: Effect of solid feed rate and feed size on increase in specific surface area Δs.

product and the feed approached each other at a lower feed rate; this was particularly noticable when feed 'D' was used. However, the more useful criterion is the increase in specific surface area (ΔS). This increase was plotted against solid feed rate, with the feed size as a parameter, as shown in Figure 8.2. It was observed that ΔS decreases in a linear manner with solid feed rate and is irrespective of feed size. The slope of the line, which is negative, is a measure of change of ΔS with feed rate. The slope changes and assumes a lower value at around 3.33×10^{-3} Kg/s feed rate, but for feed 'D' the linearity at higher solid feed rate was not evident.

Below feed rate of 3.33×10^{-3} Kg/s the slope of the line decreases with increased feed size thus ΔS increases with increasing feed size. At higher feed rate ΔS tends to decrease with increasing feed size, and approaches zero at high solid feed rate values. Similar results were also obtained at other pressures as will be shown in Section 8.2.3.

The rate of production of surface area S_R per unit time was calculated from:

$$S_R = \Delta S \times Q_S$$

where $S_R = S_P - S_F$

Q_S = Feed rate of solids.

A plot shown in Figure 8.3, of S_R versus Q_S, was obtained with feed size as a parameter. It is observed that for feed

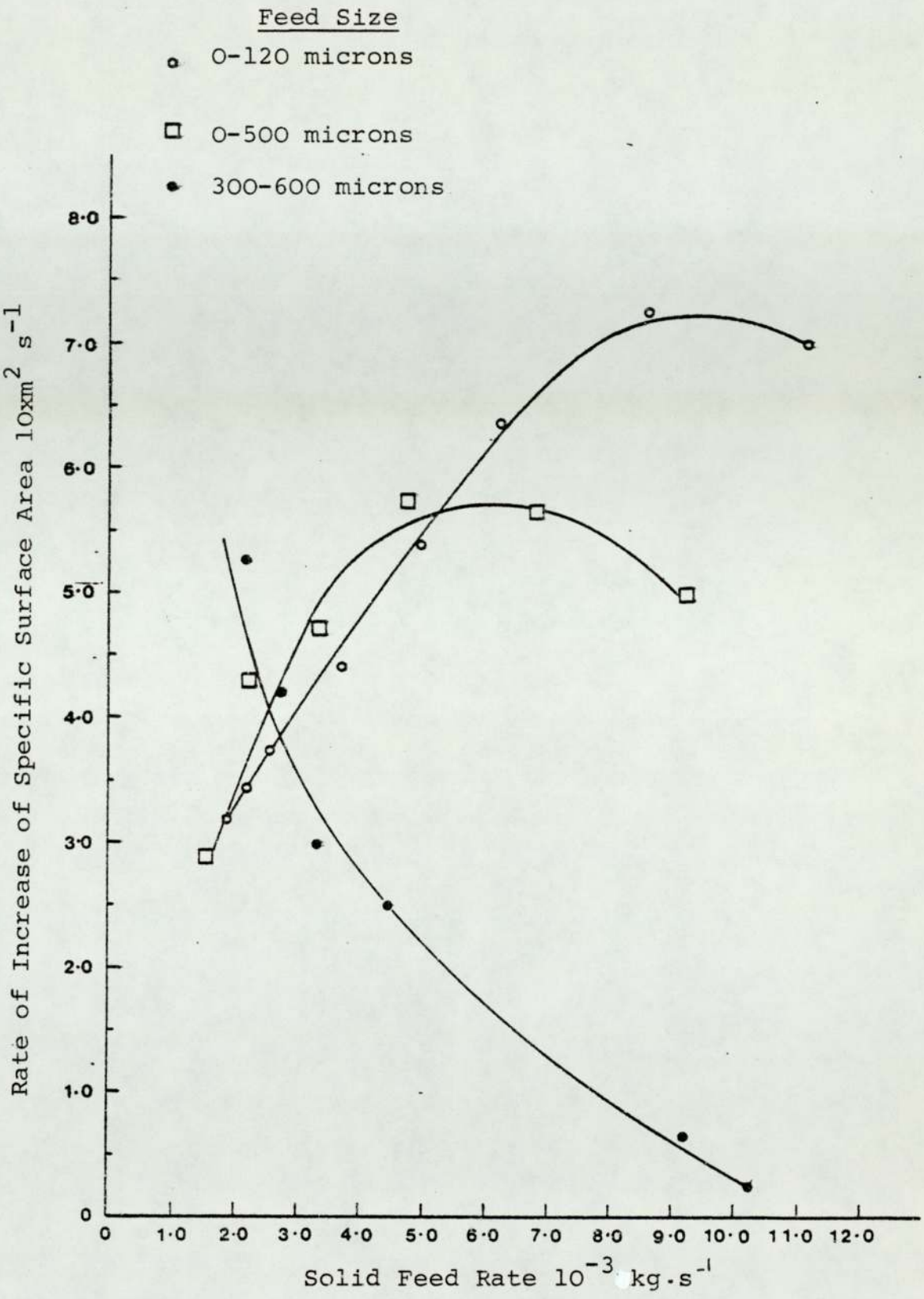

Figure 8.3 : The Rate of Production of Surface Area vs Solid Feed Rate for Various Feed Size Fractions (all at 6.9×10^5 N/m^2 Pressure)

fractions A, B, and C the surface produced per unit time increases with feed rate of solids until it reaches a maximum value Beyond this maximum value S_R decreases with increasing feed rate of solids. However the feed rate of solids at which the maximum S_R occurs, is a function of the feed size and of pressure at the jet ring of a given microniser. The effect of feed size on the maximum S_R is shown in Figure 8.3.

8.2.3 Air Throughput and Nozzle Pressure

The effect of the jet ring pressure, (i.e. air throughput) on the surface mean diameter and specific surface area are shown in Figure 8.4. It was found that increased pressure at the jet ring, for a given solid feed rate, resulted in a finer product. Several tests were carried out, by varying both the fluid throughput and solid feed rate, so that solid to air mass ratio was kept constant. The results are shown in Figure 8.5, where product specific surface area is plotted against material feed rate, with the loading ratio as a parameter. It was found that for a given loading ratio the product specific area increased linearly with solid feed rate, thus showing that the capacity of a given microniser may be increased considerably without loss in product specification simply by increasing pressure.

8.3 Hold Up In The Microniser Chamber

The hold-up, which is the mass of solids circulating

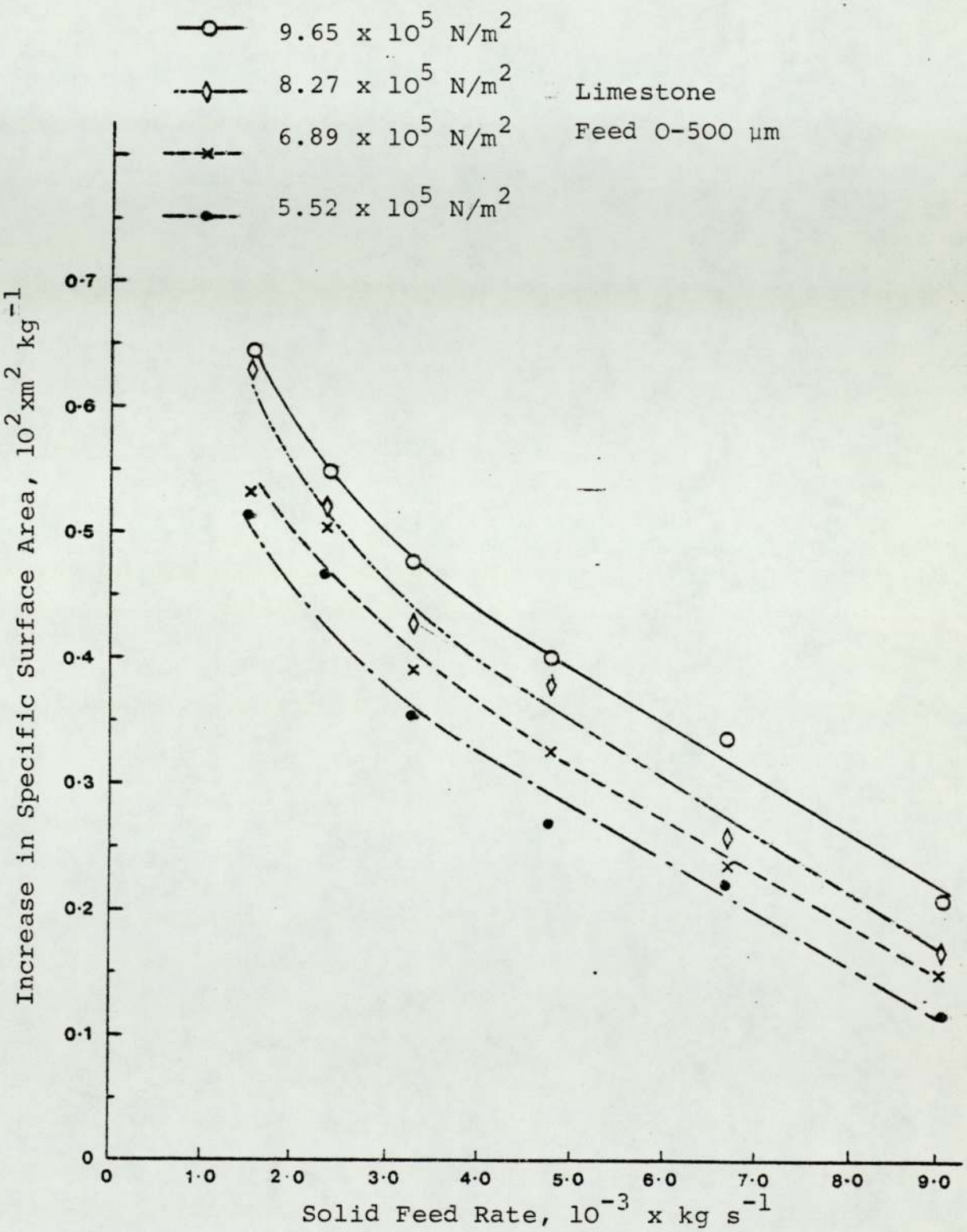

Figure 8·4 : Increase in Specific Surface Area Versus Solid Feed Rate for Various Pressure at the Jet Ring

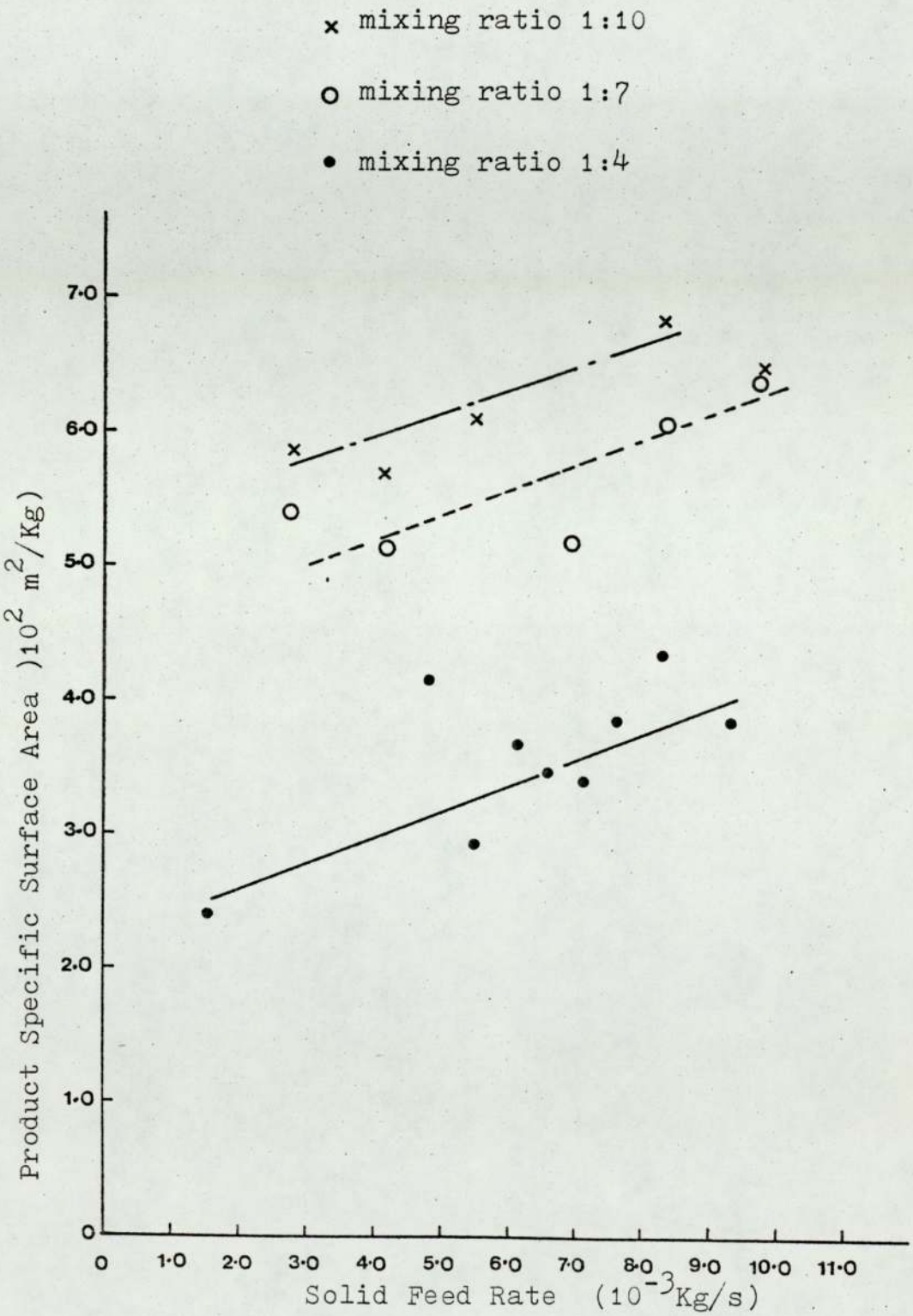

Figure 8.5: Specific surface area of product for various air to solid mixing ratios.

within the chamber at any time was determined experimentally by the method given in part 6.3.2 for a range of solid feed rates, air throughput and feed size.

Figure 8.6 shows typical hold-up results obtained for feeds over a range of solid feed rate(1.0 - 11.0 x 10^{-3}Kg/s), and for a number of jet injection angles. As shown, the hold-up increases with increasing feed rate, until it reaches a maximum value beyond which the change is negligible. This, also applies to other nozzle angles, and to a certain extent the hold-up was found to be independent of the jet injection angle.

The change of hold-up with air throughput is shown in Figure 8.7 for 0-500 μm feed size. The hold-up at a given feed rate, decreases with increasing air throughput at the jet ring. The curves obtained show similar behaviour to that shown in Figure 8.6, where the hold-up reaches maximum value at higher feed rates. The maximum value was found to be constant for a range of air throughput considered, and was about 0.513 Kg $\pm$ 5%.

The variation of hold-up with feed size is also shown in Figure 8.6, in which hold-up versus feed rate with feed size as a parameter was plotted. The behaviour is similar for all feed sizes; Furthermore as particle size of the feed increases the maximum hold-up, as expected, was reached at lower feed rate, and tends to increase with the feed size.

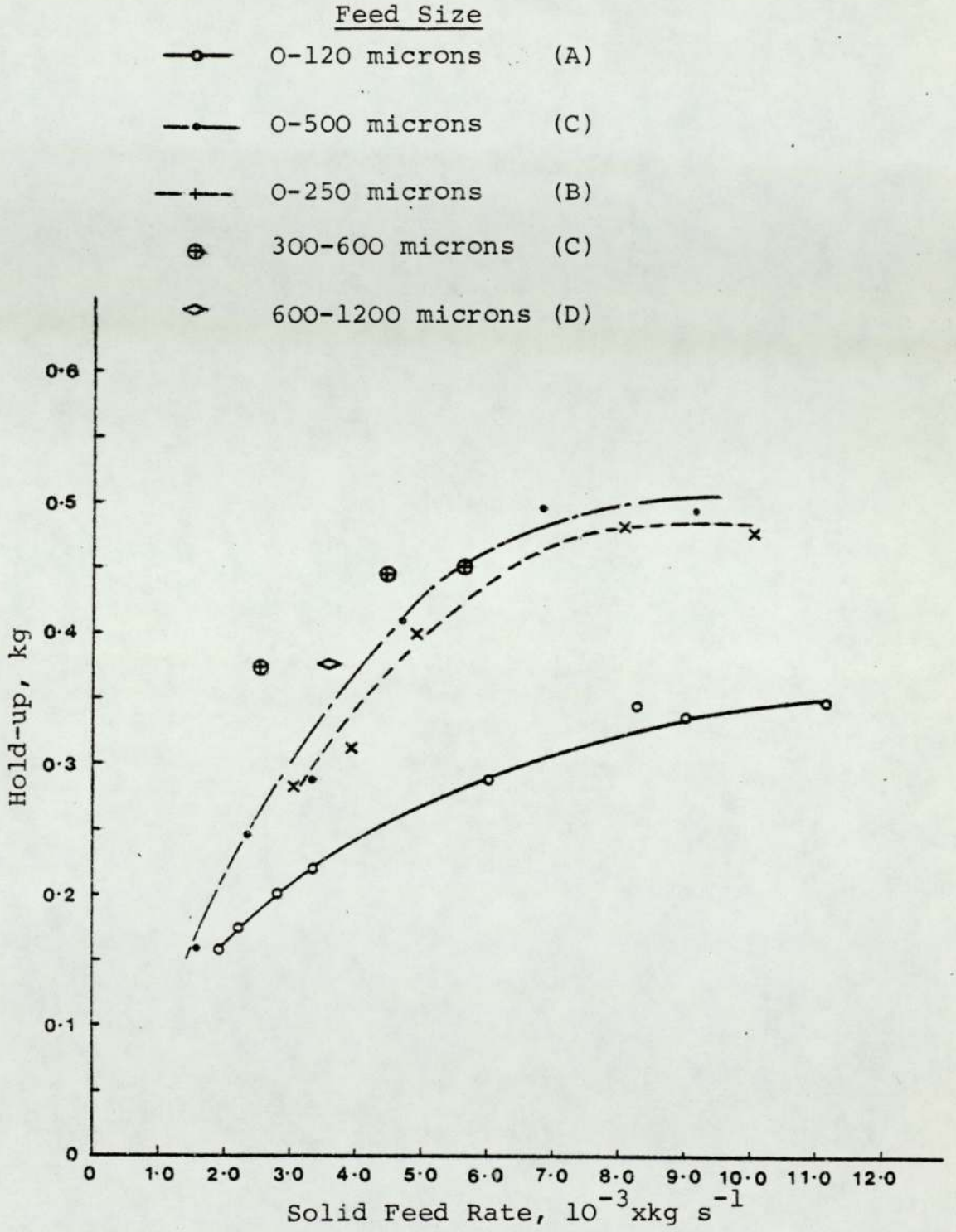

Figure 8.6 : Hold-up Versus Solid Feed Rate for Various Size Fractions (all at 6.9×10^5 N/m^2)

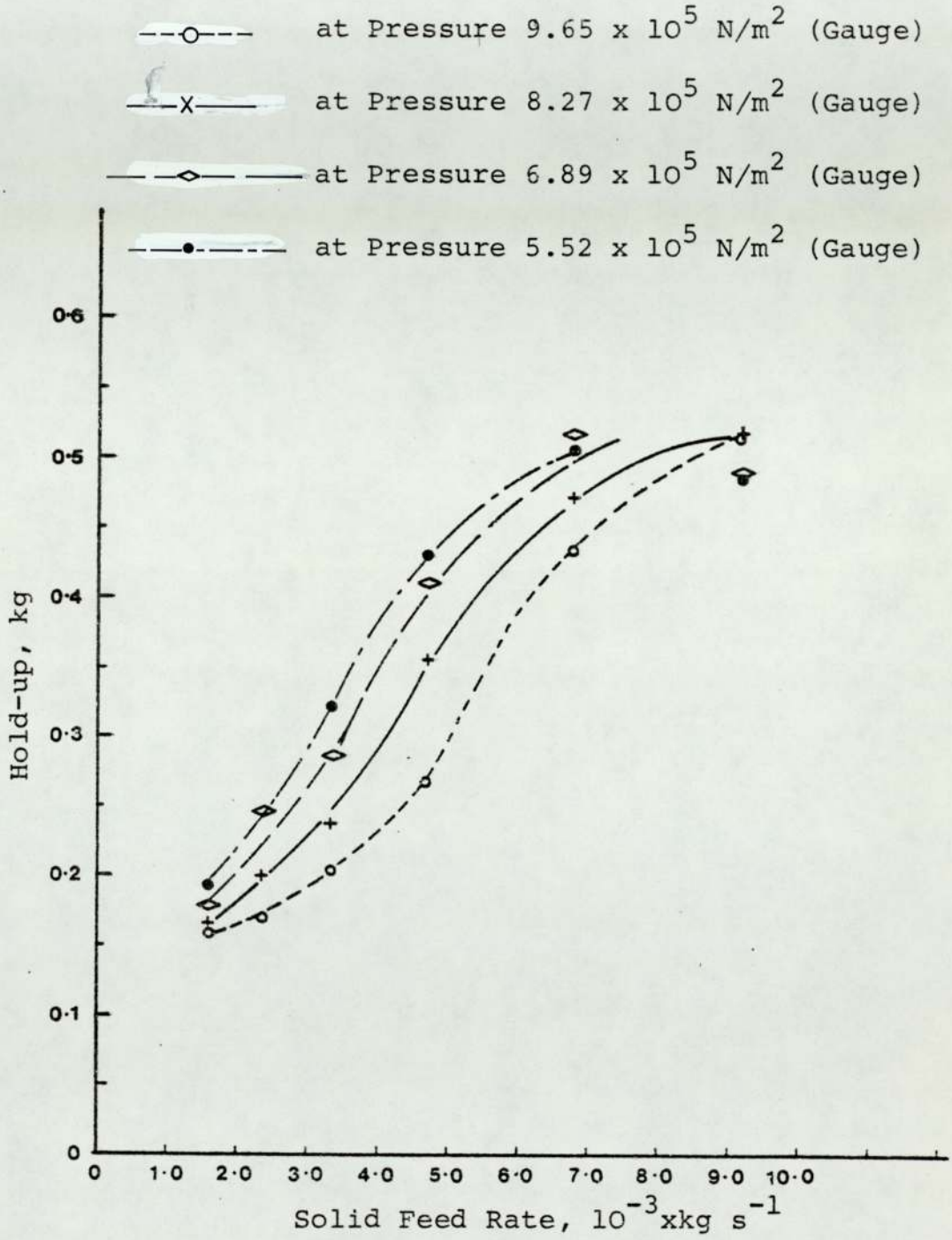

Figure 8·7 : Solids Hold-up in the Micronizer Chamber Versus Solid Feed Rate and for Varying Air Pressure (Feed 0-500 μm)

The fractional volume of the chamber occupied by the particles was plotted against solid feed rate, and a linear relationship was observed up to 8 x 10^{-3}Kg/s (the maximum hold-up value) as shown in Figure 8.8. However this does not imply that, where the hold-up is low, the particles suspension occupies the whole space within the chamber. It is likely as has been suggested that in general the higher concentration of particles is in the vicinity of the peripheral wall.

8.4 Effect of Air Throughput at The Venturi Feeder on Product Size

A minimum pressure is required in the pipe leading from the venturi feeder to the chamber, to overcome the chamber pressure. Below that minimum pressure, the content of the chamber would blow back through the venturi feeder. This pressure is related to the fluid throughput at the venturi feeder injector nozzle. Appendix A3 shows experimentally determined minimum air throughput required at the venturi nozzle versus jet ring pressure or air throughput at the jet ring.

It has been quoted (Ref 41), that the flow at the venturi varies from 25% to 75% of the total air consumption in the micronizer, but no published data was found on the effect of the air throughput at the venturi feeder on product size. Therefore an investigation was undertaken to determine

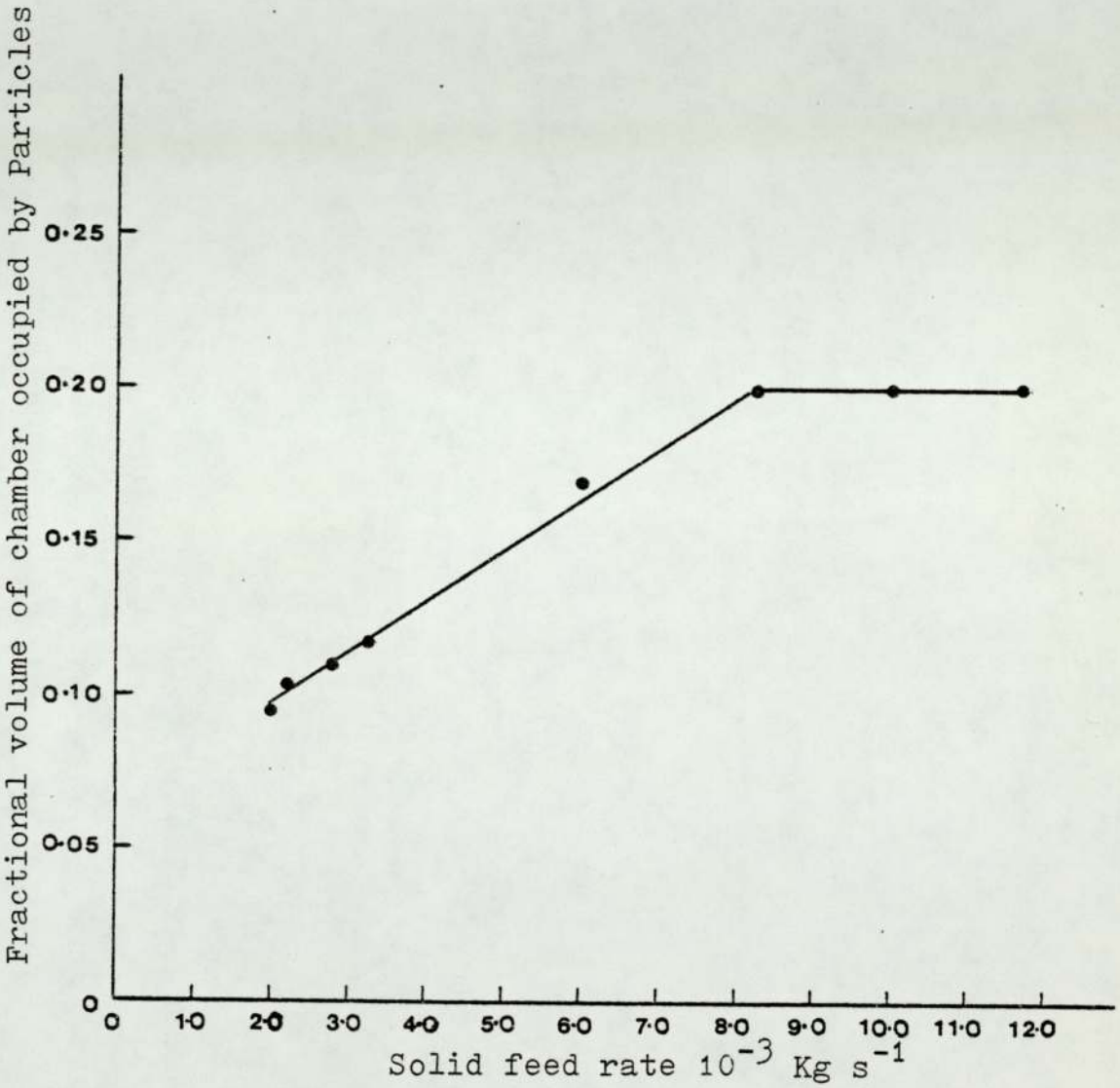

Figure 8.8: Fraction volume of chamber occupied by Particles versus solid feed rate.

(Feed fraction 0 - 120 m at 6.9×10^5 $N.m^{-2}$)

Table 8.3 Experiments to Determine the Effect of Air Throughput at the Venturi Feeder on Product Size.

Material : Limestone

No. of Nozzles : 12 Diameter : 1.5875 Angle :52

Feed Size : 0 - 120 μm

Jet Ring Pressure = 6.9×10^5 N·m^{-2} Volume Air Throughput =

Run	Air Throughput At The Venturi	Solid Feed Rate	$d_{32\mu m}$ Product
B17/4	21.0	30	6.96
B17/5	1.1	30	7.78
B17/6	10.2	30	7.15
B17/7	14.8	30	7.35
B17/8	21.0	30	7.08
B17/9	5.25	30	7.10
B17/10	3.5	30	6.78
B17/11	21.0	7.14	3.90
B10/1	3.5	7.14	3.95
B10/7	3.5	30	6.00

Average of d_{32} at 30 Kg/hr = 7.025μm

S.D = $\pm$ .509

this effect.

The conditions and results of the investigation are tabulated in table 8.3.

8.5 Discussion of Results

As discussed in Chapter 5, published studies on the operational variables of the micronizer are scarce. The jet-o-miser has received some attention in this respect but still there is much more scope for research and development of fluid energy mills.

In the previous chapter, the results and discussion on some constructional features of the micronizer are presented. Those are mainly concerned with the number and diameter of nozzles and the jet injection angle and it was found that over the range of operational and constructional parameters investigated, the degree of comminution in terms of increase in specific surface area and product mean diameter was optimum for the twelve nozzles of 1.5875×10^{-3}m diameter each and a jet injection angle between 52° and 60°.

In Chapter 7 it was suggested that consideration must be given to the nozzle diameter to chamber depth ratios, also nozzle diameter to chamber diameter.

The study of the operational variables was based on the findings disclosed in Chapter 7 and the jet ring used in this

experimental programme was constructed from a set of nozzles shown in table 8.1 and the materials used were talc and limestone.

The use of talc has presented major difficulty in the determination and analysis of particle size. The plate-shaped particles that talc is composed of present dispersion problems because of the tendency of the particles to stack upon each other. This was observed under the scanning electron microscope. However, a satisfactory dispersion technique was developed as described in section 5.3, and was adapted to obtain the particle size distribution using the Coulter Counter.

The data obtained from the Coulter Counter is based on the measurement of the volume of the particle and because of the considerable variation in the ratios of thickness to length and width to length of individual talc particles, the interpretation of the data obtained was of little practical value in this study.

8.5.1 Effect of Material Feed Rate on Product Size

The observations and results presented in this chapter were obtained from experiments using limestone; other products comminuted in the micronizer are likely to exhibit similar behaviour.

The change in the size of product, (expressed by the volume mean diameter and specific area), with the material

feed rate is shown in Figures 8.1 and 8.2; it was found that for a given feed size and fluid throughput the specific surface area decreases with increasing feed rate of solids. This agrees with previous studies conducted in fluid energy mills for a variety of materials, except that the rate of change of product size with feed rate differs with each material and depends on its grindability.

The decrease in product fineness with increased feed rate is due basically to the higher concentration of particles in the chamber as was shown in Section 7. Although this has the advantage of increased frequency of interparticle collisions (Section 4.) it also has the effect of reducing the tangential velocity and thus the ratio v_t/U_r. Hence the particle cut size is increased, and size of particles retained in the chamber is also increased.

Because of the increased hold-up and increased particle size retained in the mill chamber the jet stream becomes swamped with particles and thus the momentum supplied by the jet is shared among a greater number of particles of increased mass. In effect the particle will have too low a velocity to cause fracture on collision.

Increased particle concentration in the chamber results in a decrease of the mean free path of individual particles (Equation 4.6). This mean free path is necessary for particles to accelerate within and reach sufficiently high velocity to cause fracture on impact. Also at such a high

numerical concentration of particles, individual particles will receive momentum from collision with other particles, unfortunately the extent of this cannot be estimated.

8.5.2 Pressure Effect on Product Size

Increased pressure at the jet ring results in higher velocities of the jet stream and in effect increases the tangential and radial velocity components in the chamber. Higher velocity of the jet would inevitably cause higher impact velocities, hence probability of fracture is increased. As was shown in Section 8 for a given feed size and feed rate the rate of grinding (specific surface area produced per unit time) increased with increasing pressure.

The particle size distributions obtained at various pressures are shown in Appendix A.4; it was found that at higher pressures the product did not contain the larger particles which might otherwise escape at the exit. This was due to the higher centrifugal velocity obtained caused by the high velocity at the jets.

The capacity of a given micronizer can be increased, or product size altered by the variation of pressure and this effect will be examined mathematically in the next chapter.

8.5.3 The Feed Size and Product Size

Experiments were carried out over a range of feed

particle size, (see Table 8.1). In the literature, there have been conflicting statements on the effect of material feed size on the efficiency and rate of grinding.

For the range of sizes investigated in these experiments it was observed that for fraction 'E' (600-1200μm) considerable erosion of the jet ring and liner plates occured within an hour of operation. This is expected, since the centrifugal force tends to throw the larger particles towards the periphery and rotate them against the metal surface, and due to the high velocity encountered (of the order of 50 m/s) a rubbing and attrition action takes place between the individual particles and the metal surface.

At extremely low feed rate of feed 'E' (about 3 Kg/hr) the product obtained was fine and homogeneous; however at higher solid feed rate the product obtained contained particles of extreme fineness and most of the product was of the diameter of the feed. This was also observed for feed 'D' at high feed rate (9.12×10^{-3} Kg/s), but the erosion was considerably less.

Inspecting Figure 8.2, it was found that the increase in specific surface area was higher for the coarse feed only at low solid feed rate. At higher feed rates the increase and the efficiency were greater for smaller size feed.

Chapter 9: Data Analysis

9.1 Residence Time in the Micronizer

The measured hold-up values and particles concentration in the mill chamber are presented in Chapter 8. It was found experimentally that the hold-up (h_c) was a function of the following:

1. material's properties such as size and density.
2. material's grinding properties, strength and grindability.
3. air flow rate into the micronizer.
4. material feed rate.

The residence time (t_r of material within the chamber can be estimated from the hold-up (h_c) and material feed rate (Q_m), thus,

$$t_r = \frac{h_c}{Q_m} \quad \text{(seconds)} \qquad \text{Eq. 9.1}$$

It was also shown that the hold-up within the chamber reaches a maximum limiting value. This is thought to be determined by the chamber volume, the voidage necessary for the movement of individual particles, and particle size. Thus for feed size of 0 - 120 μm the maximum hold-up obtained was approximately 0.35Kg, and for -500 μm feed it was approximately 0.520Kg. As the feed rate of the material increased, so did the size of the material retained in the chamber. Figure 9.1 shows a typical plot of percentage of hold-up particles retained on a 45 micron sieve versus solid

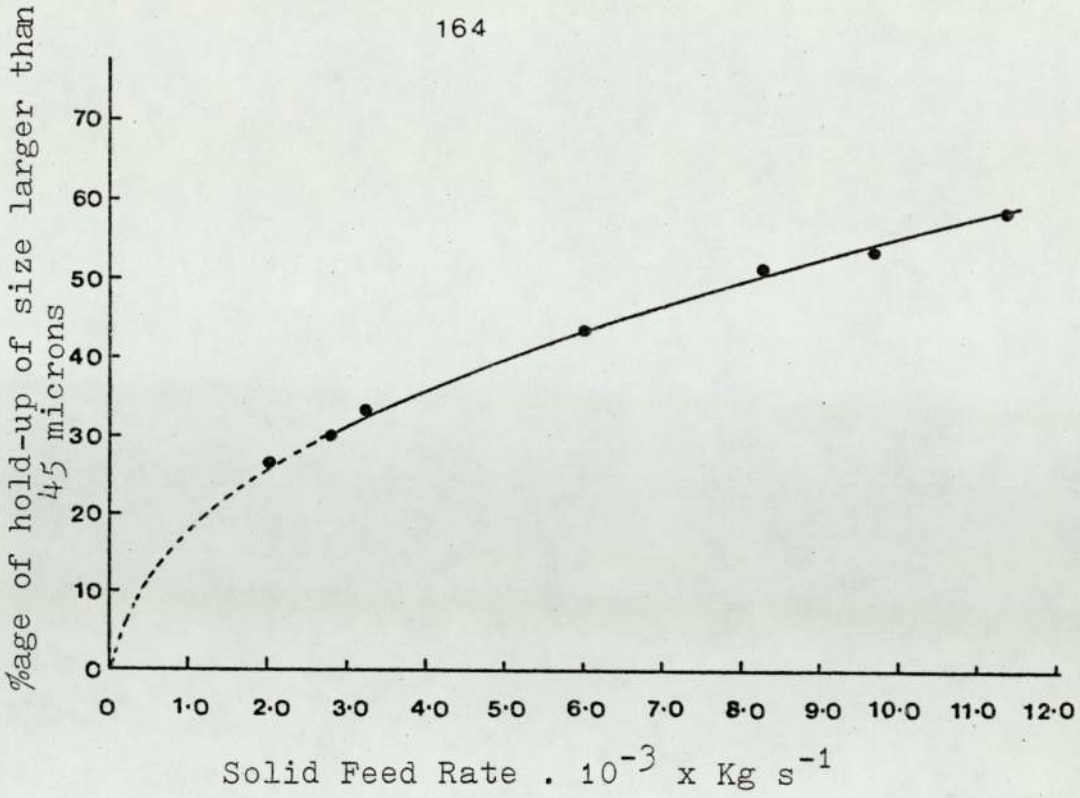

Figure 9.1: Effect on solid feed Rate on the hold-up particle size.

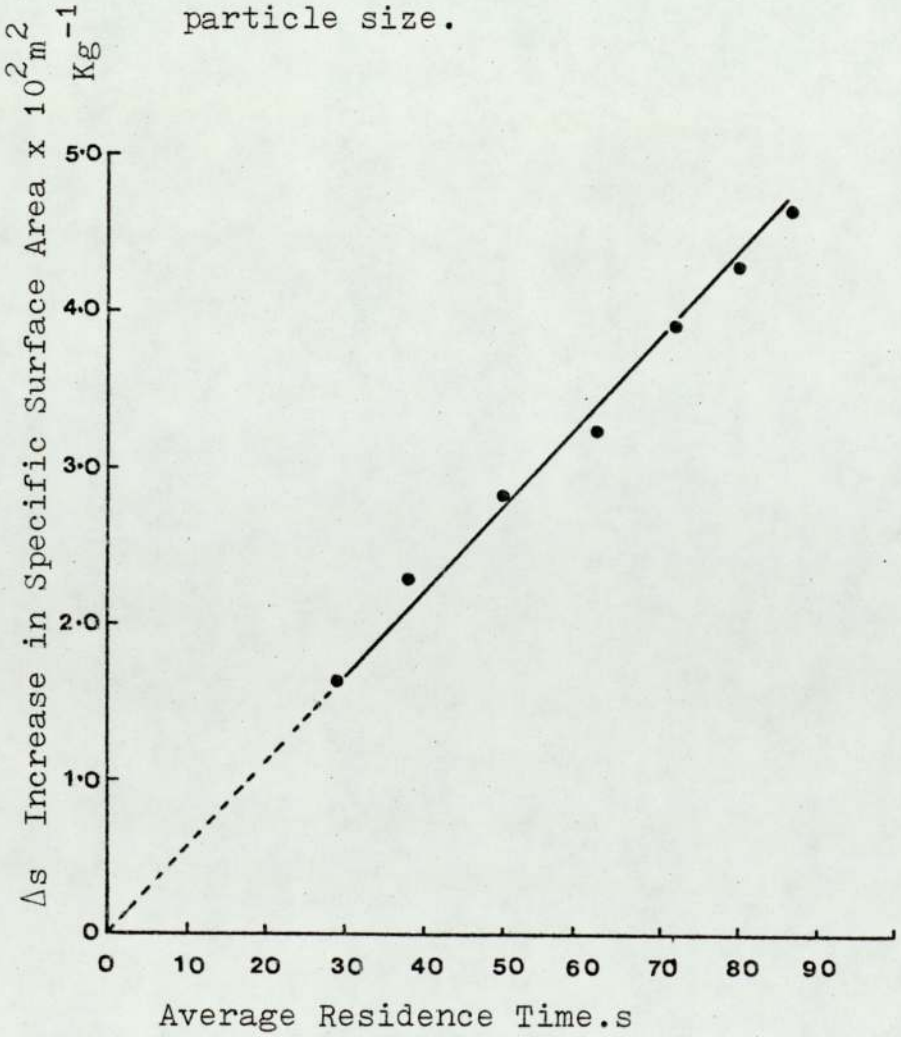

Figure 9.2: Variation of Increase in specific surface area with average residence time.

feed rate. One expects that the hold-up size will increase until it consists entirely of particles of the same size as the top fraction of the feed.

The residence time of solid material within the chamber was calculated using equation 9.1. The experimentally-estimated residence times are average values. Since the feed material in most cases spreads over a wide range, the residence time for the finest material approaches zero, and increases with particle size. However, these average values indicate the trend of mill performance with residence time and in terms of increase in specific surface area (Figure 9.2).

For a given pressure and air throughput to the micronizer (and thus energy input) it would be expected that the degree of comminution is a function of residence time of the material within the mill chamber. The increase in specific surface area will be assumed here as a measure of the degree of comminution of the material.

Figure 9.2 is a plot of residence time versus the resulting increase in specific surface area for feed fraction 'A' micronised by air at 7.908×10^5 N/m^2 absolute. The resulting relationship is linear and passes through the origin. However, this straight line has not been extra-polated beyond 90 seconds shown on the graph since it would be expected that the increase in specific surface area (ΔS) will reach a limiting asymptotic value, as t_r increases. A family of curves is obtained showing that the rate of increase in specific surface area with time also increases with pressure,

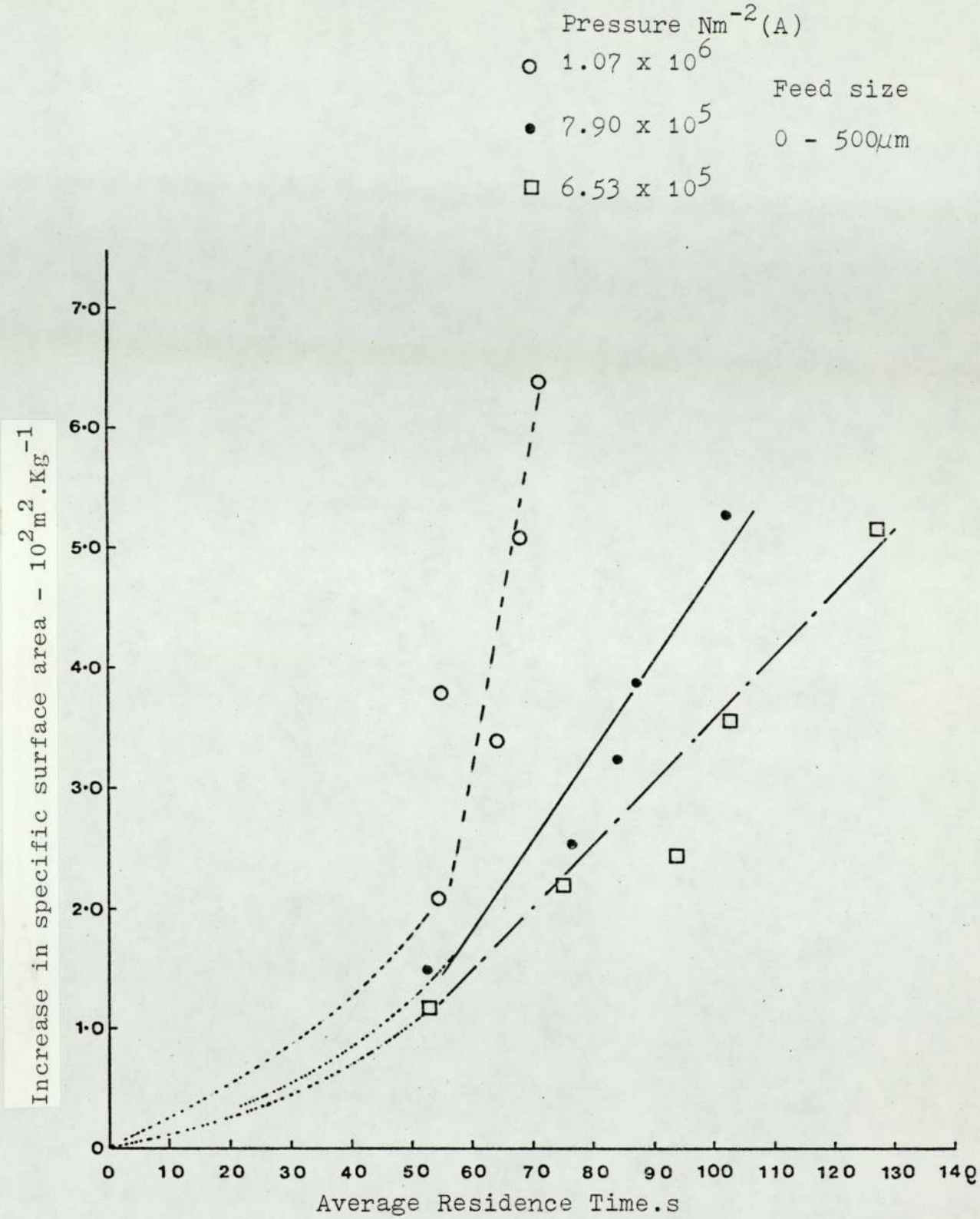

Figure 9.3: Change of Increase in specific surface Area with average Residence time at various pressures.

(Figure 9.3) and at residence time greater than 60 seconds (corresponding to solid feed rate less than 6.8×10^{-3} Kg/s) the relationship appears to be linear.

9.2 Energy Input

The energy utilized in the microniser operation and in the comminution action arises from the expansion of the fluid from the fluid jets. The energy expended by the compressible fluid per unit time was calculated from consideration of thermodynamics. Assuming the expansion of air to be an adiabatic reversible process, the following relationship is obtained

$$E = \frac{\gamma}{\gamma - 1} W \bar{R} T_i \left[\left(\frac{P_j}{P_c} \right)^{\frac{\gamma-1}{\gamma}} - 1 \right] \qquad \text{Eq. 9.2}$$

where γ ratio of specific heats of gas

W molal flow rate of gas Kmol/s

R gas constant = 8.314 KJ/Kmol K

T_i initial temperature of the gas K

P_j jet ring pressure N/m^2 (absolute)

P_c chamber pressure N/m^2 (absolute)

Energy input rate E, from Eq. 9.2, for a range of pressures at the jet ring was calculated and is shown in Figure 9.4.

9.3 Specific Energy Input

The specific energy input E_s was assumed here to be the ratio between total energy input E and solids feed rate Q_m

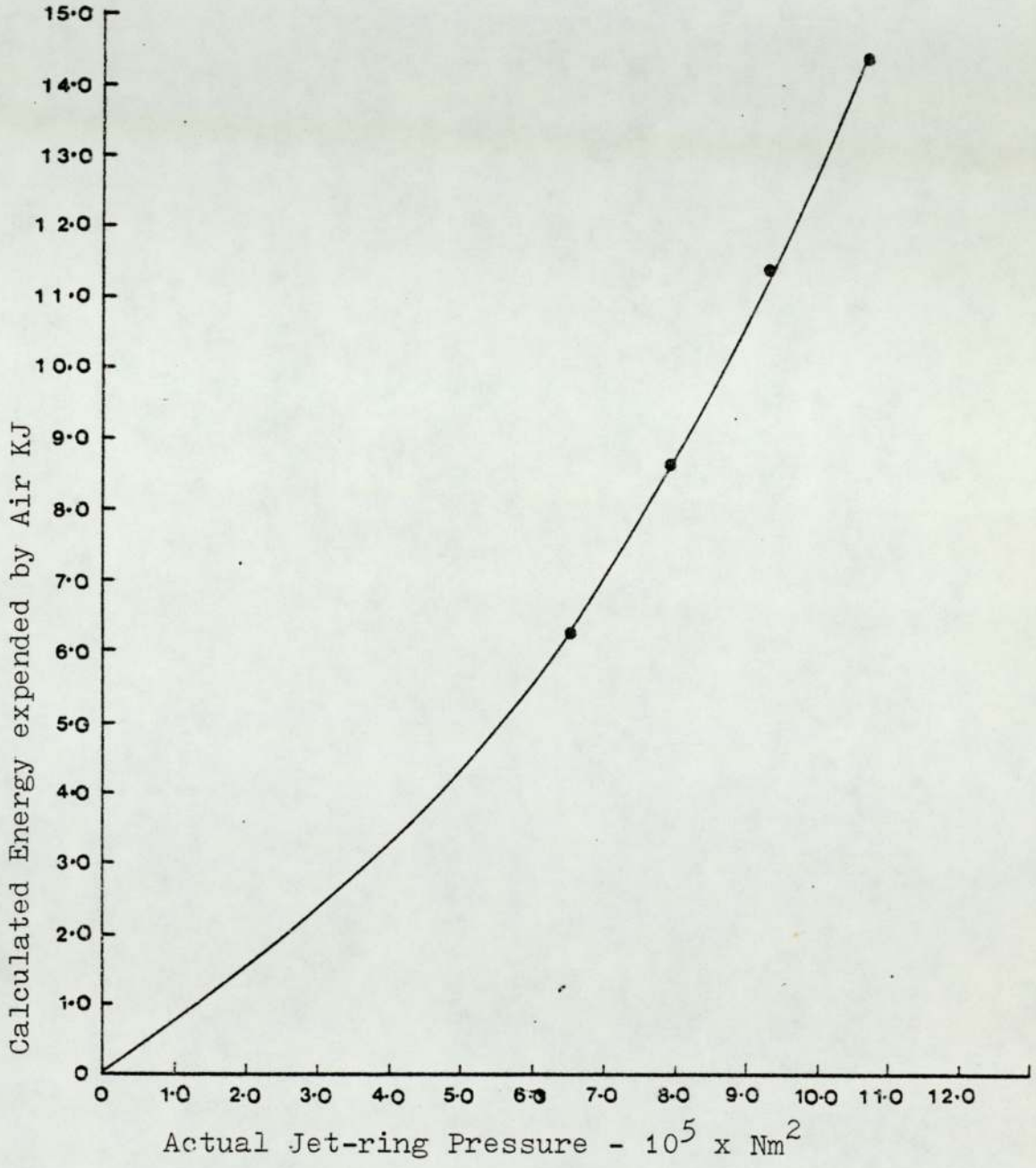

Figure 9.4: Calculated Energy Expended by Air Expansion for various jet ring pressures.

thus,

$$E_s = \frac{E}{C_m} \qquad \text{KJ/Kg} \qquad \text{Eq. 9.3}$$

9.3.1 Effect of Specific Energy Input on Size of the Product

Many of the energy models are of the form (Marshall Ref 48).

E = f (strength, efficiency criteria, mill efficiency, size reduction parameter)

For a given mill, under fixed operating conditions, and for a given material, the energy consumed would be of the form

E = f (size reduction parameter).

The calculated specific energy input versus increase in specific surface area is shown in Figure 9.5. These values were obtained from various feed sizes at $7.908 \times 10^5 N/m^2$ absolute pressure. A linear relationship is shown between specific energy input (in the region 1250 - 4500 KJ/Kg) and increase in specific surface area, the slope of the line being $0.0625\ m^2/KJ$. This linear relationship is analogous to "Rittinger's Law" which takes the following form:

$$E_R = C_R (S_F - S_p) \qquad \text{Eq. 9.4}$$

where C_R is a constant, and is characteristic of the material being comminuted.

This linear relationship, between energy input and surface produced was shown by experiments carried out by researchers on various materials comminuted to a superfine state; it was e.g. observed by Fairs (Ref 138) when experimenting with limestone and a variety of other materials. A break in the straight-line relationship is observed in Figure 9.5 at about 1250 KJ/Kg. Below this value a straight line relationship was also assumed, through the origin. The slope of this line was found to be 0.22 m^2/KJ and this change in slope indicates that comminution in the lower range of specific energy input is more efficient by order of 3 to 4 times than at high values of E_s. However, since the product obtained in this region is coarser in terms of particle size, the increase in energy utilization (efficiency) is due primarily to the fracturing of already faulty particles, which contain existing and weak cracks before undergoing any impacts. As E_s increases, particles are reduced to smaller size where the binding force approaches that of perfect crystals; hence energy requirements are greater.

Comparing specific energy input versus increase in specific surface area for various feed sizes A, B, C, D and E at pressure of 7.9×10^5 N/m^2 (Figure 9.5) linear relationships can be traced in this graph. Consider the specific surface energy in the region 0-2000 KJ/Kg in which a family of straight lines are obtained for the various fractions. The slopes of these lines are approximately equal, but the lines intercept the x-axis at varying distances from the origin. The point of intersection corresponds to an

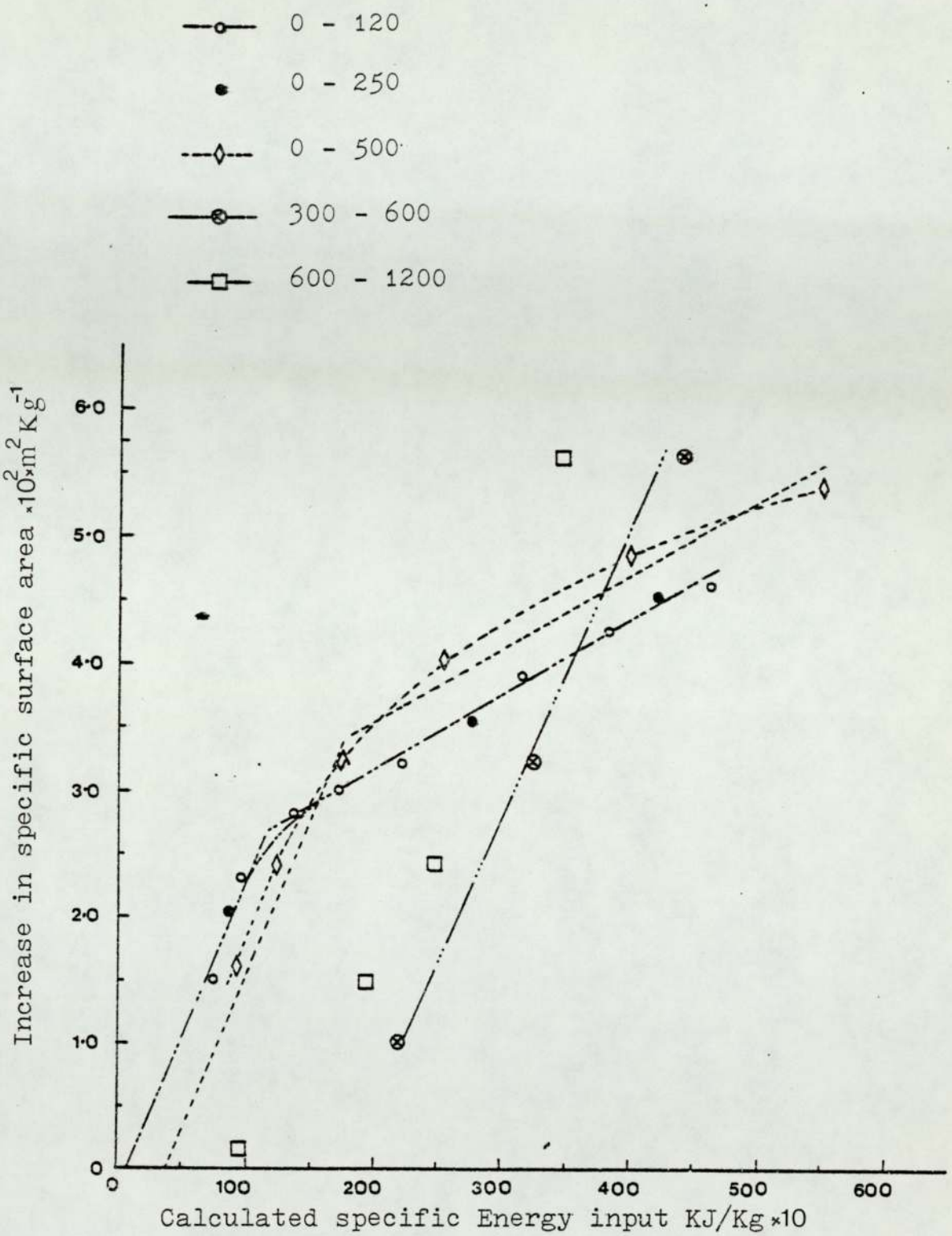

Figure 9.5: Increase in specific surface area versus Calculated Specific Energy input for various feed sizes.

apparent minimum specific energy input below which the energy is too low to produce any fracture. The approximate minimum E_s values were read from the graph, and together with the corresponding feed size are listed in Table 9.1.

Table 9.1 E_s (minimum)

Feed Size Microns	Es-min KJ/Kg
0 - 120	~>150
0 - 250	~ 150
0 - 500	~ 250
300 - 600	~1250
600 - 1200	~2000

The E_s-min values may be explained by considering the minimum fluid velocity (U_{min}) (or minimum pressure at the jet ring) required to keep a particle in suspension and cause a noticable change in surface area. As discussed in Chapter 4,

$$U_{min} = f \text{ (particle size, density)}.$$

For a given material U_{min} increases with particle diameter and E_s values given in Table 9.1 correspond to the minimum pressure or fluid requirement at the jet ring before any measured change in specific surface area may be observed. Above the initial region of E_s, the increase in the specific surface area is higher for the coarser feed.

9.3.2 Specific Energy Input and Limiting Product Particle Size

It is often asserted that all comminution machinery has a limiting minimum product size below which the material cannot be further reduced in size in that particular machine, and that particular technique of size reduction. Carry and Stairmand have shown that associated energy (KWh/Tonne) increases markedly with decreasing particle size, hence the energy requirement increases accordingly.

In Figure 9.6 particle size below which 95% of the product lies, is plotted against specific energy expended by the expanding air, (for the finest feed 'A', and at 7.908 x 10^5 N/m^2 abs - pressure). This indicates that the product size d_p appears to be approaching a limiting value of the order of 8 μm, and in that region of particle size the rate of change of size with energy expended decreases very sharply.

Figure 9.7a shows the same points plotted on a semi-log scale for the purpose of comparison with the "associated energy curve" obtained by Stairmand (Ref 48) for limestone, and shown in figure 9.7b.

9.4 Correlation of Results

In the search for a theoretical formula for energy consumed in the comminution process, the primary problem is to isolate and identify the various

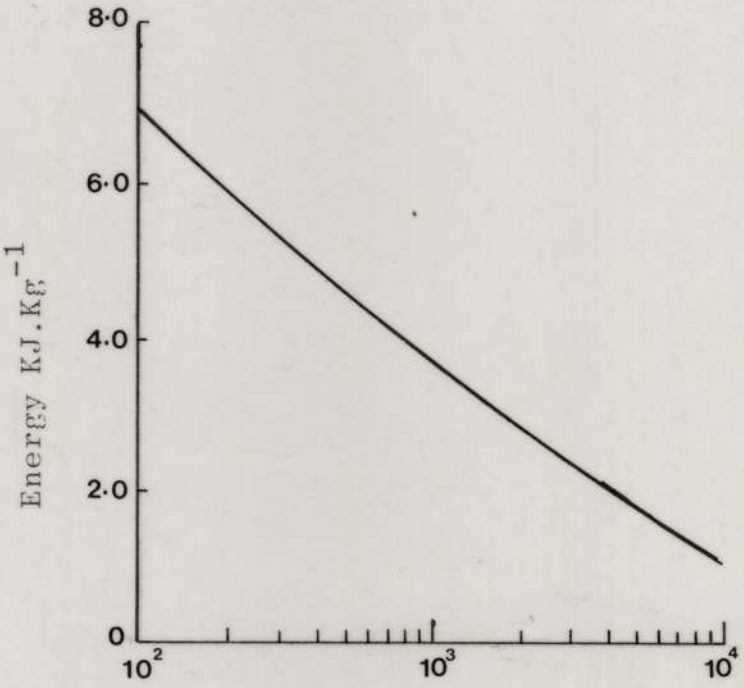

Figure 9.76 Associated Energy Curve for Limestone (stairmand

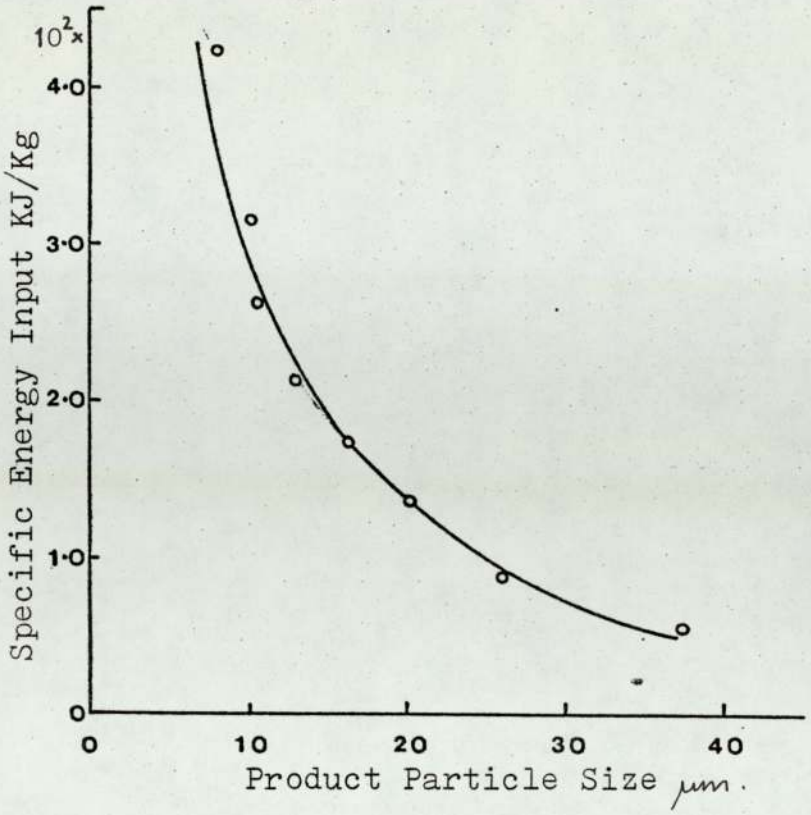

Figure 9.6: Limiting Product Particle Size

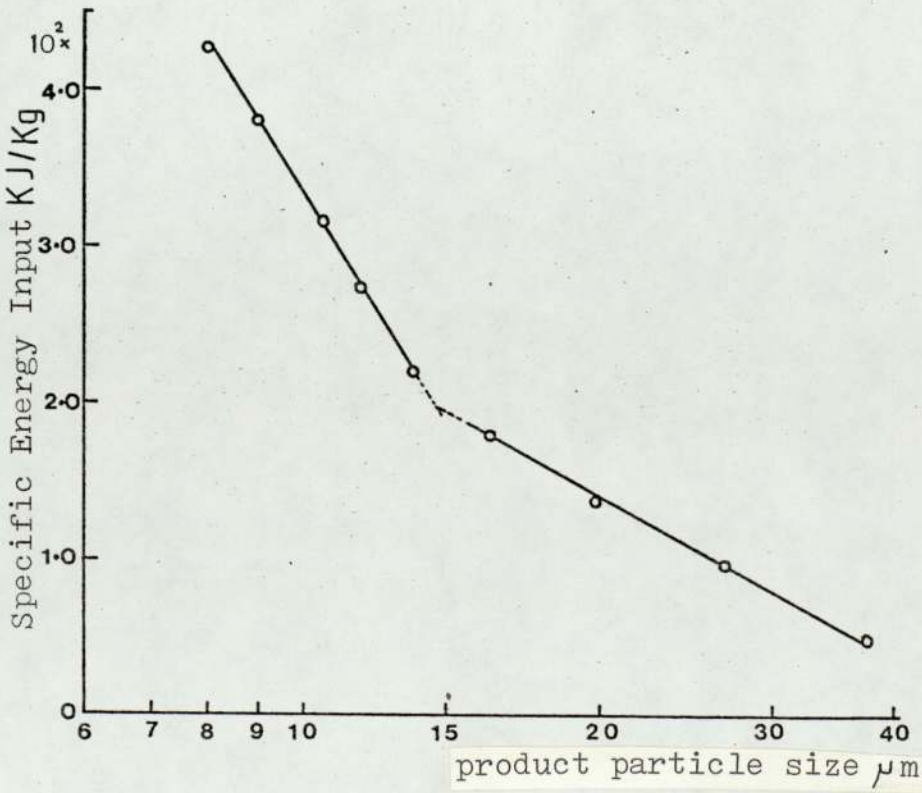

Figure 9.7: Semi-log Plot of Product Particle Size.

parameters involved and especially the energy required to break the material. The factors involved in the breaking process have been discussed in Chapter 2. There is also a second problem of assessing additional energy imparted to the material being comminuted. Hence the solution to this problem rests on assessing the efficiency of energy transfer to accelerate the material to sufficently high velocity and the energy utilized in the breakage process.

As discussed in Section 2.1, it is to be expected that there is a relationship between the energy required to fracture the material and the surface area created in the breaking process, but this relationship can only be established if the energy consumed in creating new surface can be separately measured.

In the micronizer operation the greater proportion of energy input (see 9.2) is only partly expended in the sole activity of comminution; energy is also directed towards suspending the solids and to the classification process. However the results discussed in Sections 9.2 - 9.7 were presented for the purpose of comparison and to indicate the magnitude of energy input and surface area produced.

In view of the difficulty experienced by previous workers in the field of comminution (and the special complexity of micronizer) to formulate purely theoretical equations for the breakage process, it was decided to carry out a dimensional analysis approach.

9.4.1 Parameters Considered

Considering the microniser operating at a constant temperature, the initial equation will be of the form -

$$\phi = f\ (Q_A,\ \mu_A,\ \rho_A,\ d_N,\ D_m,\ d_p,\ Q_m,\ \rho_m,\ E_m, v)$$

where ϕ is the size reduction parameter

Q_A	mass flow rate of fluid	
μ_A	fluid viscosity	fluid properties
ρ_A	fluid density	
d_N	nozzle diameter	
D_m	microniser diameter	microniser geometry
Q_m	material feed rate	
ρ_m	material density	Feed Material's
E_m	material strength	Properties.
v	fluid velocity.	
dp	feed particle size	

Various dimensionless groups were derived and the form by which the best fit was obtained in terms of ratio of product and feed specific surface area (S_P/S_F), thus:

$$(S_P/S_F) = f\ (N_{Re},\ N_m,\ N_d) \qquad \text{Eq. 9.5}$$

where N_{Re} is Reynolds number

$$N_{Re} = \frac{v\ d_N\ \rho_f}{\mu_A} = \frac{4\ Q_f}{\pi\ \mu_A d_N} \qquad \text{Eq. 9.6}$$

where v is the fluid velocity at the nozzle exit

d_N	nozzle diameter
ρ_f	fluid density
μ_A	fluid viscosity

Q_f is Fluid mass flow rate at each nozzle

N_m is the mixing ratio

$= \frac{Q_f'}{Q_m}$ where Q_f' is the total air throughput

N_d is the diameter ratio.

$= \frac{d_{p50}}{D_m}$

9.4.2 Mixing Ratio of N_m

N_m is the ratio of air mass flow rate to the solid material feed rate. It is the mass of fluid required to comminute the particles to a given size. However, this quantity alone does not determine the final size of the product, since the degree of comminution is primarily influenced by the jet velocity and thus the pressure at the jet (Section 9.6.4).

The air mass flow rate taken in this ratio is the total rate and includes the flow at the nozzle, and that at the venturi feeder. It determines the mass velocity of air within the micronizer chamber, and the radial velocity component of the fluid. The air velocity U_r directed outwards from the jet orifice towards the discharge section, flowing through the space near both upper and lower plates is given by

$$U_r = \frac{V_f}{2\pi r H_m} \qquad \text{Eq. 9.7}$$

where r is radius

H_m is chamber height

and V_f is fluid volume throughput.

Hence total fluid throughput largely determines fluid radial velocity, and thus the particle cut size leaving the microniser chamber.

For a given pressure at the nozzles, the change of specific surface area and particle size of product with material feed rate was presented in Chapter 8. It was shown experimentally that for given pressure and given feed size the specific surface area increases with increasing ratio Q_f/Q_M (= N_m) and that the size of product approaches that of the feed as this ratio is decreased. Typical plots of S_P/S_F versus mixing Ratio N_m, (and for the operating conditions indicated) are shown in Figures 9.8 and 9.9. A reasonable straight line relationship was obtained when using log coordinates. The range of experimental points about the line was ± 10% maximum, for the range of solid feed rates investigated.

9.4.3 Reynolds Number(N_{Re})

The Reynolds Number is the ratio of inertial force to viscous force of the flowing fluid. It is a measure of air velocity in the jet stream which determines the drag force exerted on the individual particles and thus determines their acceleration and their impact velocity (Section 5.5).

For compressible fluids such as air, the viscosity is

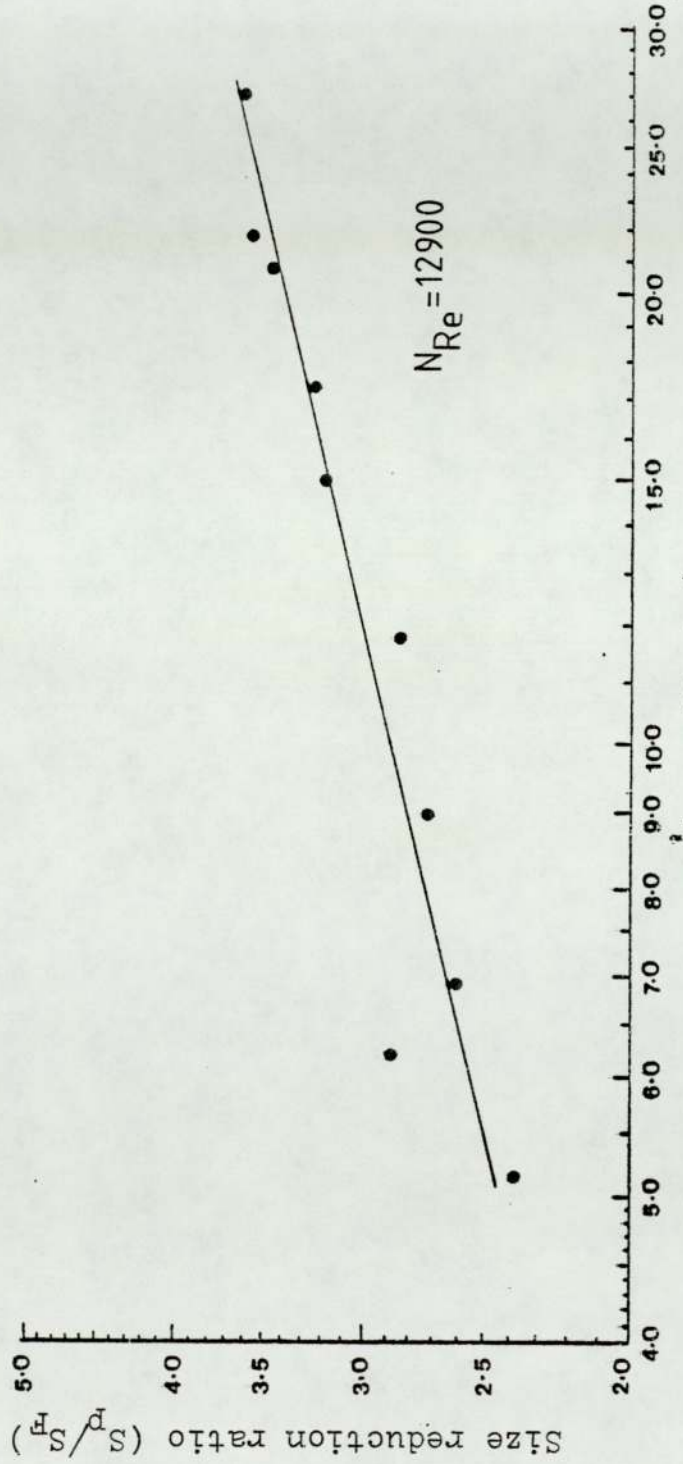

Figure 9.8: S_P/S_F) Vs (Q_f/Q_m) for feed 'A' (0 - 120μm)

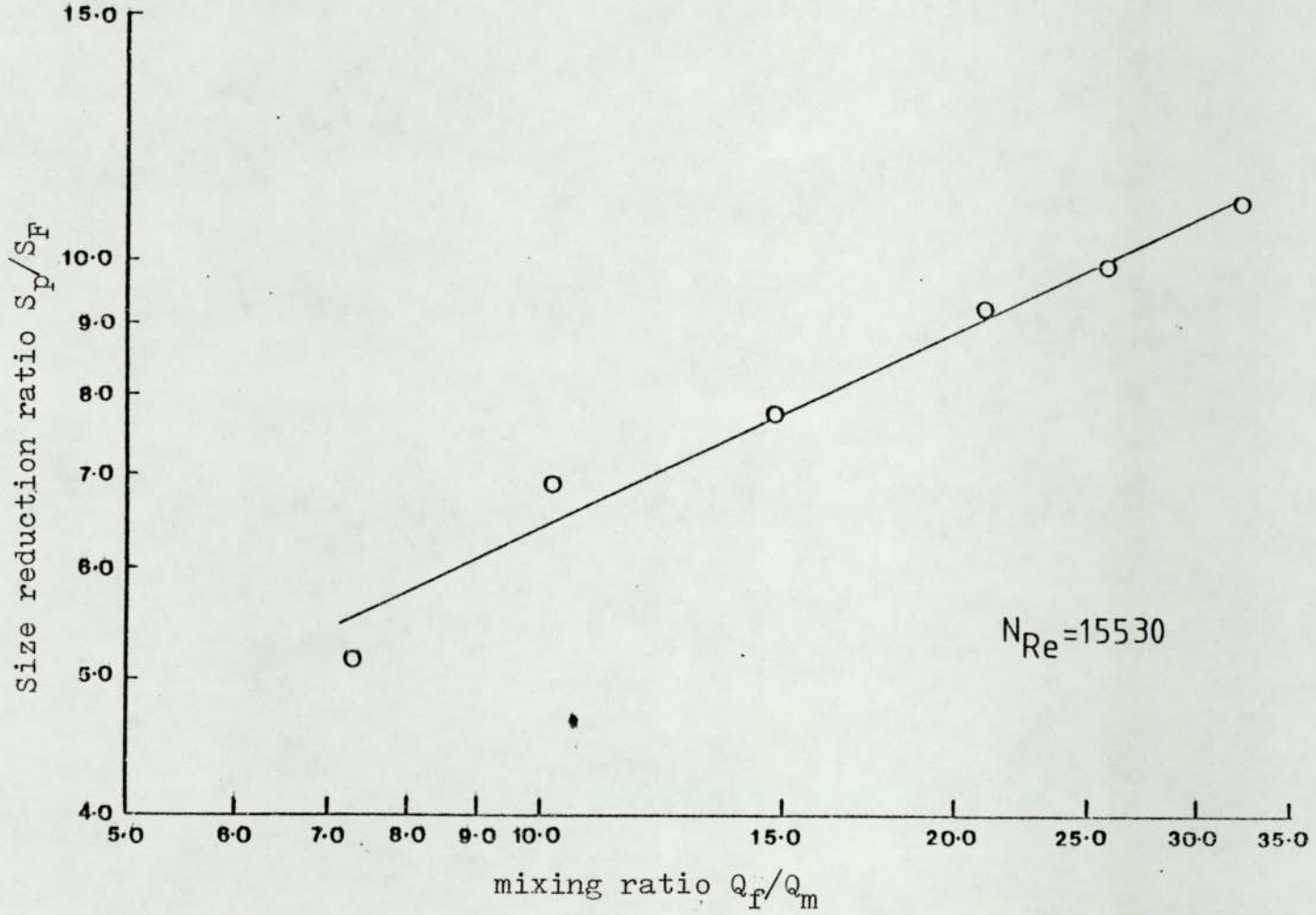

Figure 9.9: S_p/S_F) Vs (Q_f/Q_m) for feed 'C' (0 - 500μm)

not affected by pressure and it is a function of temperature. It was assumed in the computation of Reynolds Number that the drop in air temperature due to expansion was too small to cause any significant variation in the air viscosity. Reynolds Number was computed on the basis of air mass flow rate through a single nozzle (Q'_f) and on nozzle diameter (d_N) thus,

$$N_{Re} = \frac{4}{\pi} \frac{Q'_f}{d_N \mu} \qquad \text{Eq. 9.8}$$

and for a given microniser configuration, Reynolds Number and mixing ratio (Q_f/Q_m) are interrelated, and a variation in one will cause a corresponding change in the other.

Figure 8.4 shows the family of curves obtained for a range of pressures(where N_{Re} is 1 - 2 x 10^5). As Reynolds Number increases the size reduction ratio (S_P/S_F) increases. This would be expected since the jet and particle velocity increases with Reynolds Number. Figure 8.4 implies that the capacity of the microniser in terms of material throughput increases with increasing Reynolds Number for the same reduction ratio. Preliminary calculations show that the microniser capacity increases according to

$$Q_m \propto N_{Re}^2$$

This relationship agrees with the earlier findings by Mori (Ref 7) and Ramanujam (Ref 27), where the value of the exponent of N_{Re} was of the order of 2 - 3.3 (for jet-o-miser type)

9.4.4 Feed Particle Size and Microniser Diameter

The particle size of the product, thus degree of comminution in any mill is a function of the size of the feed (Chapter 2). The effect of the size of the feed on the size of the product was presented in Chapter 8. It was shown that at low solid feed rate, the product particle size is almost the same irrespective of the size of feed. At higher solid throughput the product size increases with feed size for the same throughput. The size reduction ratio (e.g. S_p/S_F) is found to increase with increased feed particle size. This observation agrees with the generally held conclusion suggesting that as particle size decreases, the specific energy requirement increases to produce same degree of comminution.

Interparticle collisions in the case of large sized feed particles and for relatively low impact velocities are more likely to result in fracture than in the case of small particles. This is because of already existing cracks and imperfections in the larger particle's structure (Section 2.3).

The microniser diameter (D_m) is also taken into consideration in this correlation, since D_m establishes the capacity of the microniser, volume of chamber and particles concentration. Also, D_m determines the tangential and radial velocities in the chamber.

For a feed in which particle size is distributed over a wide range, it is customary to express the size of the

particles by the median diameter d_{p50} and the geometric standard deviation σg. This median diameter of the feed was computed for the feed material used, and this value was used to compute the diameters ratio (d_{p50}/D_m)

9.5 Form of the Correlation

The degree of comminution in terms of size reduction ratio is found to be a function of Reynolds Number N_{Re}, mixing ratio N_m and feed size. It is desirable to obtain a functional relationship between these variables (Section 9.4) and product size in terms of specific surface area ratio.

The relationship assumed was

$$\left(\frac{S_p}{S_F}\right) = K\left[\frac{Q'_f \rho_f}{d_N \mu}\right]^X \left[\frac{Q_f}{Q_m}\right]^Y \left[\frac{d_p}{D_m}\right]^Z \qquad \text{Eq. 9.9}$$

where K,X,Y and Z are constants.
K is a dimensionless constant and it was assumed to include physical properties of the material and its breakage characteristics.

9.6 Optimisation of K.X.Y and Z Values

The values of the exponents X,Y and Z and constant K were found using Nelder and Mead (Ref 139) optimisation method which was developed for optimising a multivariable unconstrained nonlinear function of the form

$$F(x_1, x_2, \ldots\ldots\ldots\ldots x_n)$$

The procedure adopted by this method is an extension of the simplex method (Ref 140) which utilizes a regular geometric figure (called simplex) consisting of N + 1 vertices. Unimodality is assumed in this particular technique and thus several starting points should be considered. Thus arbitrary values of K, X, Y and Z are assumed at first to initiate the calculations until they converge to a minimum value each. This process was repeated with different starting values to check if they again converge to the same minimum.

These calculations were carried out with the aid of a Fortran computer. The algorithm, description and listing of the program is given in Appendix A7.

Each set of experiments was computed separately, and values of X, Y, Z and K were obtained in each case. Satisfactory conversion of X, Y, Z and K thus giving good agreement with the experimental values (within $\pm$ 15%) was achieved for data obtained at a given Reynolds Number in each set. For sets of data whose elements were obtained at varying conditions of N_{Re}, N_m and d_{p50} the values of X, Y, Z and K converged, but the deviation between computer values of S_p/S_F and those measured were within $\pm$ 20%.

The final form of correlation was

$$\ln \frac{S_p}{S_f} = K \; N_{Re}^{X} \; N_m^{Y} \; N_d^{Z} \qquad \text{Eq. 9.10}$$

Table 9.2 below sets out the optimum values of X, Y, Z and K. These values were obtained for each block of experiments carried out at the shown operating conditions (Table 9.2) in the 0.2m diameter microniser with 12 nozzles, a nozzle diameter of 1.5875mm and at an angle of 52^{o}.

Inspecting Table 9.2, the exponents of Reynolds Number (X), mixing ratio (Y) and diameter ratio (Z) are in close agreement with each other for feed fractions consisting of sizes 0 - 120μm and 0 - 500μm. These values were obtained for nozzles Reynold's Number ranging 1 - 2 x 10^5 and mixing ratio up to 30. Closely-sized fraction 300 - 600μm shows considerable deviation and particularly at higher solid feed rate. The exponent Z assumes value of 0.067, thus showing that the ratio S_p/S_F is independent of the feed size for coarse fractions and is only a function of mixing ratio and Reynolds number.

The experimental values of S_p/S_F plotted against values calculated using Equation 9.10 are shown in Figures 9.8 and 9.9 (above), also in Figures 9.10 and 9.11. The experimental points are within $\pm$ 20% deviation.

The values X, Y, Z and K obtained in this correlation are of the same order of magnitude of those determined by Ramanujam and Venkateswarlu (Ref 27) as shown in Table 9.3 for the jet-o-miser and using calcium carbonate as the

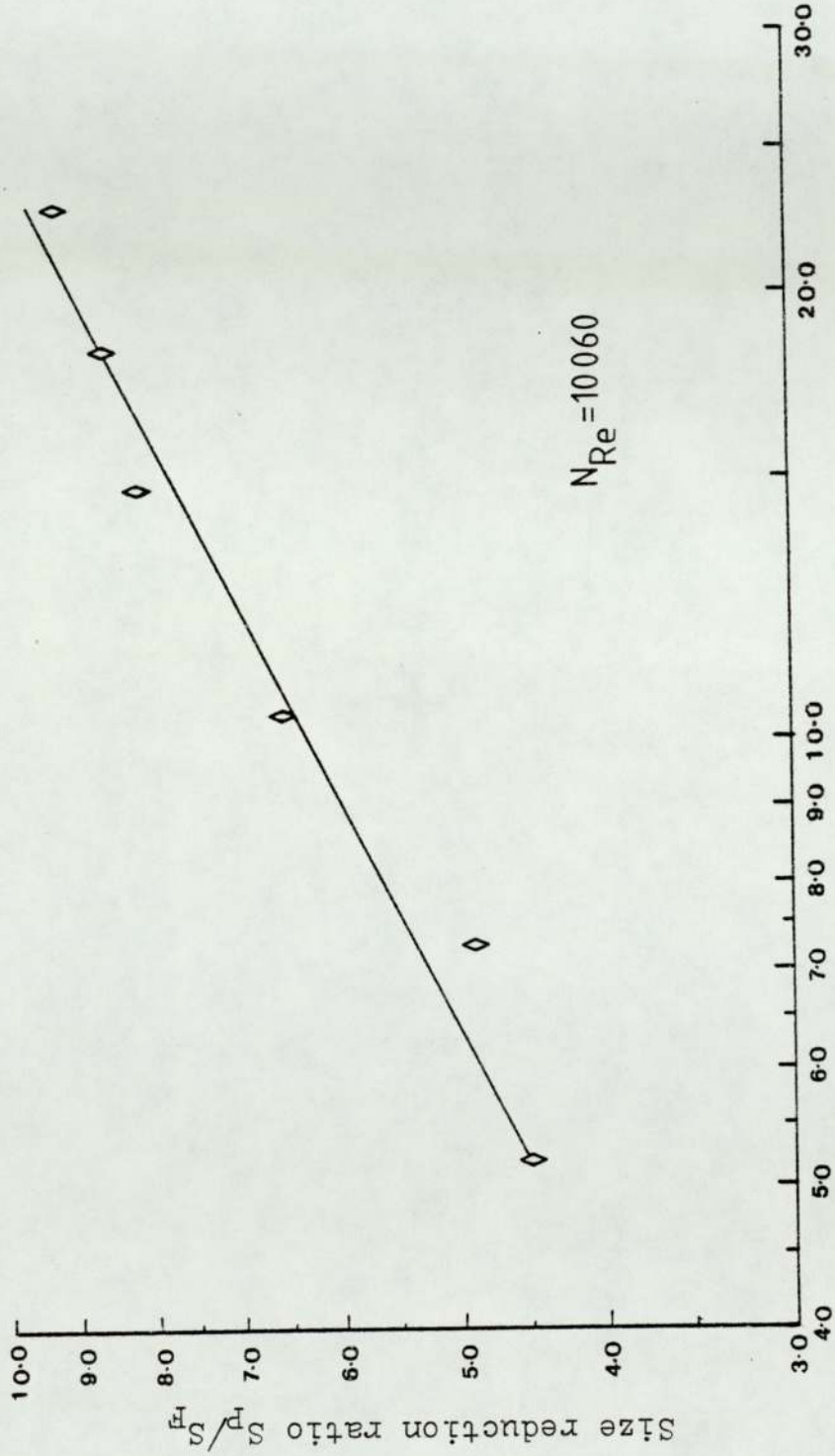

Figure 9.10: (S_p/S_F) Vs.(Q_f/Q_m) for feed 'C' (0 - 500μm)

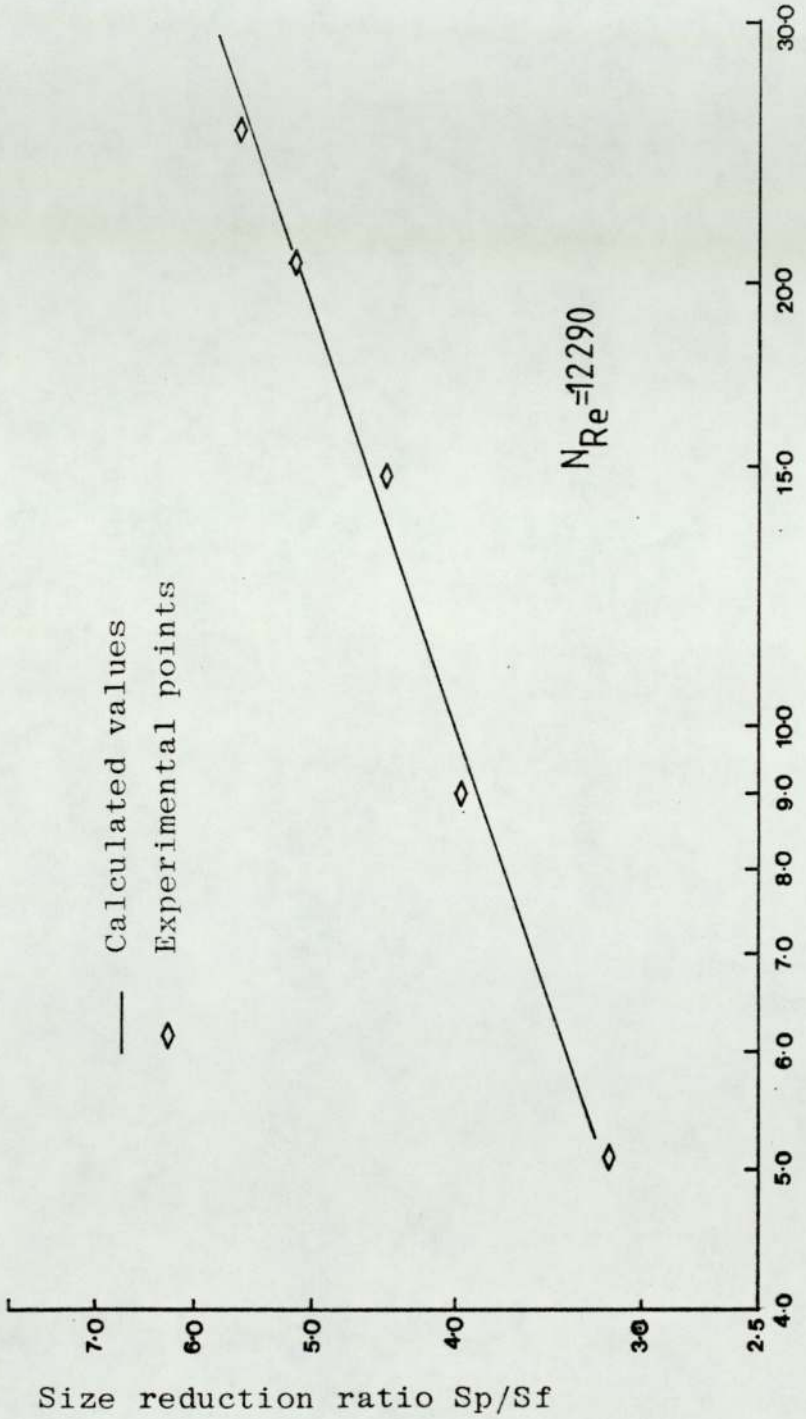

Figure 9.11 : Plot of (Sp/Sf) vs (Qf/Qn) for feed 0-250μm.
(Log-scale)

Table 9.2: Computed Optimum Values of X, Y, Z and K (Equation 9.10) For Various Operating Conditions

Particle Size of Feed μm	Operating Pressure 10^5 N/m^2	X	Y	Z	K
0 - 120	6.9	0.27	0.23	0.25	0.25
0 - 120	4 -9.7	0.28	0.22	0.26	0.28
0 - 250	6.9	0.32	0.23	0.31	0.29
0 - 250	5.1-9.7	0.28	0.20	0.27	0.35
0 - 500	5.1	0.30	0.26	0.31	0.32
0 - 500	6.9	0.30	0.22	0.26	0.27
0 - 500	8.4	0.30	0.22	0.33	0.42
0 - 500	9.7	0.31	0.20	0.27	0.25
300-600	6.9-9.7	0.09	0.227	-0.06	0.53

Table 9.3: Value of X, Y, Z, K

0.417	0.278	0.2	0.039

(Ref 27)

experimental material. Ramanujam and Venkateswarlu found that experimental data fall into two regions; one "Below Transition" and the other "Above Transition" (Table 9.3). The values obtained in this work are similar to those for "Below transition region" (Ref 27). However, in Ramanujam work the value of Z was pre-determined at 0.2.

The similarities between the values of the exponents obtained in this work and that of Ramanujam suggests that the size reduction ratio S_p/S_f is independent of the mill geometry and that grinding characteristics of the material could be expressed in terms of K.

Chapter 10: Conclusions

10. Conclusions

Using a 0.2m microniser experimental rig and a specially designed jet-ring in which number, diameter and angle of nozzles could be varied, the following effects of constructional and operational parameters were noted:

1 - A jet injection angle of 52 - 60° was found to be optimum in microniser construction. Settings in this range proved the most effective with regard to specific surface area produced and in crushing rate.

2 - Higher number of nozzles used in the microniser exhibited higher efficiency in terms of degree of comminution per unit mass/volume of air used. Also, it resulted in narrower product particle size range.

Using the optimum settings as indicated in 1) and 2) above, comminution in the microniser was investigated in terms of fluid velocity, fluid throughput, feed rate of solid and feed particle size.

3 - Hold-up within the microniser chamber was measured for various operational conditions. It was found that particles concentration in the chamber increases with solid feed rate and particle size and decreases with fluid feed rate (pressure) for a given solid feed rate.

4 - The product size, at low solid feed rate, is found independent of feed size. For higher solids feed rate the surface area produced was higher for finer feeds.

5 - The minimum possible particle size of micronised limestone

was 95% below 8μm (or 3.5μm - surface, volume mean diameter) for the widely varying conditions in these investigations.

6 - The micronised product particle size is found to increase with increased solids feed rate and decrease with increased fluid throughput.

7 - Considerable erosion of the chamber surfaces occured when feed size larger than 600μm was used. Below 600μm erosion was much less significant.

8 - Correlation of various operational parameters was found to be feasible. The correlation (Chapter 9) is in terms of nozzle Reynolds number, fluid to solid throughput ratio, particle size of feed to micronizer diameter ratio, and ratio of the specific surface area of product to that of the feed. Simple powers of these dimensionless groups were determined (Chapter 9).

Chapter 11: Recommendations for Further Work

Recommendations for Future Work

The research may be pursued in several area; these are:

1 - Further study of constructional features of the micronisers, in particular the chamber shape. Three possible configurations are detailed in Chapter 5. In addition to those, two other possible configurations are suggested and illustrated below; they have the advantage of ease of manufacturing, especially for large size micronisers.

Also, the nozzle diameter to chamber height ratio should be further investigated.

2 - Experimentation on other materials would be of great interest especially for those ofvarious hardnesses. In such experiments the correlations obtained in Chapter 9 may be further examined.

3 - Further work is required on the general behaviour of particles in a jet stream.

4 - Minimum velocities required to cause breakage of various particulate materials might be advantageously investigated. This would throw some light on relative minimum energy and jet velocities required for various materials.

5 - Other fluids, such as steam, may be used in the micronizer study. Comparison on an economic basis could then be made.

6 - Scaling up of the micronizer from laboratory scale to production scale should be investigated experimentally. The correlation given in Chapter 9 could then be tested against larger experimental mills and ultimately compared with industrial scale operation. The influence of geometrical and flow similarities in small and large scale micronisers should be shown up in such investigations.

Appendix A1 - Particle Size Distribution of the Feed.

Particle size Distribution of Feed Fraction 'A'

MATERIAL: LIMESTONE

SIZE RANGE: -120μm

Analysis Method: Sieving and coulter counter

SIZE RANGE μm	Mean Diameter μm	CUMULATIVE PERCENTAGE UNDER SIZE
+ 120		100.0
120-90	105	89.87
90-75	82.5	81.63
75-63	69	75.06
63-53	58	66.71
53-45	49	59.28
45-36	40.5	51.89
36-28	32	46.71
28-22	25	40.21
22-18	20	33.86
18-14	16	28.00
14-11	12.5	22.66
11-9	10.5	18.72
9-7	8	14.77
< 7		11.38

Particle Size Distribution of Feed 'B'

Size Range m	Average diameter m	Percentage in the range
250 - 212	231	7.06
212 - 150	181	15.02
150 - 75	112.5	16.39
75 - 45	60	13.43
> 45	22.5	48

Particle Size Distribution of Feed 'C'

Size Range m	Average diameter m	Percentage in the range
500 - 353	426.5	9.78
353 - 250	301.5	8.25
250 - 176	213	10.89
176 - 125	150.5	8.04
125 - 90	107.5	9.74
90 - 63	76.5	9.05
> 63		44.25

ARTICLE SIZE DISTRIBUTION OF FRACTION 'D'

aterial: Limestone

IZE RANGE: -600 + 300

nalysis Method: Sieving

ieve Aperture ange - μm	Average Diameter μm	Percentage in The Range
00 - 505	552.5	16.80
05 - 424	464.5	28.04
24 - 357	390.5	27.30
57 - 300	328.5	27.85

urface, volume mean diameter d_{32} = 443μm.

pecific surface area = 5.6 m^2/Kg.

Appendix A2 - Basic Computer Programme

For Processing the Coulter-Counter Data.

```
REM PROGRAM TO PROCESS COULTER COUNTER DATA OBTAINED BY
REM DUAL THRSHOLD TECHNIQUES
REM ------------------------------------------------------
REM COULTER COUNTER SETTINGS
READ A1, A2, A3, D1
DATA 40, 32, 3, 2.6
PRINT "ENTER K VALUE = ",
INPUT K
REM -------------------------
 REM CALCULATIONS OF CORRESPONDING RELATIVE VOLUME& DIAMETER
 DIM Y[ 13, 4]
 Y[ 1, 1]=A1*A2*A3
 FOR I=2 TO 13
 Y[I, 1]=Y[I-1, 1]*.5
 Y[I-1, 2]=Y[I, 1]
 Y[I-1, 3]=(Y[I-1, 1]+Y[I-1, 2])*.5
 Y[I-1, 4]=K*(Y[I-1, 3] ** .333333)
 NEXT I
 REMINPUT DATA FROM COULTER
 PRINT "NUMBER OF SETS OF DATA N = ",
 INPUT N
 DIM B[ 20], R[ 20], C[ 13, 3], V[ 13, 3], S[ 13, 3], W[ 13, 3], A[ 13, 4]
 DIM G[ 13, 3], L[ 13, 3]
 FOR Q=1 TO N
 PRINT "BLOCK NUMBER B(Q) & RUN NUMBER R(N) RESP>"
 INPUT B[Q], R[Q]
 PRINT " NUMBER OF SETTINGS USED H1"
 INPUT H1
 H=(16-H1)+1
 H2=16-H1
 FOR J=1 TO 2
 FOR I=1 TO H2
 C[I, J]=0
 V[I, J]=0
 S[I, J]=0
 L[I, J]=0
 W[I, J]=0
 A[I, J]=0
 A[I, J+2]=0
 G[I, J]=0
 NEXT I
 NEXT J
 PRINT "READ DATA IN ######"
 FOR I=H TO 16
 INPUT B1, B2, B3, B4, B5
 REM C(I,J) IS AVERAGE OF COUNTS &B1 IS NO. OF COUNTS
 C[I, 1]=(B2+B3+B4+B5)/B1
 D2=C[I, 1]
 REM L:LENGTH, S: SURFACE, V: VOLUME, A: AREA, G: GEOMETRIC
 V[I, 1]=D2*(Y[I, 4] ** 3)
 S[I, 1]=D2*(Y[I, 4] ** 2)
 L[I, 1]=D2*Y[I, 4]
 W[I, 1]=D2*(Y[I, 4] ** 4)
 A[I, 1]=D2*((Y[I, 4]/2) ** 2)
 A[I, 2]=D2*((Y[I, 4]/2) ** 3)
```

```
G[I, 1]=V[I, 1]*LOG(Y[I, 4])
NEXT I
I=H
C[I, 2]=C[I, 1]
V[I, 2]=V[I, 1]
S[I, 2]=S[I, 1]
L[I, 2]=L[I, 1]
W[I, 2]=W[I, 1]
A[I, 3]=A[I, 1]
A[I, 4]=A[I, 2]
G[I, 2]=G[I, 1]
F=H+1
FOR I=F TO 16
C[I, 2]=C[I-1, 2]+C[I, 1]
V[I, 2]=V[I-1, 2]+V[I, 1]
S[I, 2]=S[I-1, 2]+S[I, 1]
L[I, 2]=L[I-1, 2]+L[I, 1]
W[I, 2]=W[I-1, 2]+W[I, 1]
A[I, 3]=A[I-1, 3]+A[I, 1]
A[I, 4]=A[I-1, 4]+A[I, 2]
G[I, 2]=G[I-1, 2]+G[I, 1]
NEXT I
REM CALCULATE MEAN DIAMETERS
REM D(1, Q)=XNL, D(2, Q)=XNS, D(3, Q)=XNV, D(4, Q)=XLS, D(5, Q)=XLV
REM D(6, Q)=XSV, D(7, Q)=XVM
I=16
D[1, Q]=L[I, 2]/C[I, 2]
D[2, Q]=(S[I, 2]/C[I, 2]) ** .5
D[3, Q]=(V[I, 2]/C[I, 2]) ** .333333
D[4, Q]=S[I, 2]/L[I, 2]
D[5, Q]=(V[I, 2]/L[I, 2]) ** .5
D[6, Q]=V[I, 2]/S[I, 2]
D[7, Q]=W[I, 2]/V[I, 2]
D[8, Q]=(30000*(A[I, 3]/A[I, 4])/D1)
D[9, Q]=G[I, 2]/V[I, 2]
D[10, Q]=EXP(D[9, Q])
DIM P[13, 20], X[12, 20], Z[13, 20]
FOR I=1 TO 16
P[I, Q]=V[I, 1]/V[16, 2]
Z[I, Q]=V[I, 2]/V[16, 2]
NEXT I
REM CALCULATION OF STANDARD DEVIATION
FOR M=1 TO 7
T3=0
 FOR I=F TO 16
 T2=(Y[I, 4]-D[M, Q]) ** 2
 T3=T3+T2
 NEXT I
 X[M, Q]=(T3/(H-1)) ** .5
 NEXT M
 T9=0
 FOR I=F TO 16
 T4=((LOG(Y[I, 4]))-(LOG(D[9, Q])) ** 2)
 T9=T9+T4
 T5=T9
```

```
NEXT I
X[3, Q] = T5/(N1-1)
X[9, Q] = EXP(T5)
T6= T5
T7= 1/2.303
T8 = T6* T7
X[10, Q]=(EXP(4.5*T8)-3*(EXP(2.5*T8))+2*(EXP(1.5*T8)))
X[10, Q]=X[10, Q]/((EXP(2*T8)-EXP(T8)) ** 1.5)
REM X(10,Q) IS KURTOSIS<X(11,Q) IS SKEWNESS
X[11, Q]=(EXP(3*T8)-4*EXP(5*T8)+6*EXP(3*T8)-3*EXP(2*T8))
X[11, Q]=X[11, Q]/(EXP(4*T8)-2*EXP(3*T8)+EXP(2*T8))
X[11, Q]=X[11, Q]-3
PRINT
PRINT
PRINT "RESULTS COMPILED"
PRINT "NEXT SET OF DATA   ENTER "
NEXT Q
FOR Q=1 TO N
PRINT "BLOCK NUMBER", B[Q], "RUN NUMBER", R[Q]
PRINT
PRINT "CALIBRATION FACTOR ", K
PRINT
PRINT
PRINT "PARTICLE SIZE DISTRIBUTION (MASS)"
PRINT "-----------------------------------"
PRINT
PRINT "AVERAGE", "FRACTION", "FRACTION"
PRINT "DIAMETER", "CUMULATIVE", "IN RANGE"
PRINT " Y(I,4) ", "  Z(I,Q)  ", " P(I,Q) "
PRINT "--------", "----------", "--------"
FOR I=1 TO 16
PRINT Y[I, 4], Z[I, Q], P[I, Q]
PRINT
NEXT I
PRINT
PRINT
NEXT Q
PRINT " BLOCK     RUN     SUR. VOL.     ST. DEV    S. S. A.   KURTOSIS  SKEWNE
                          S
PRINT " NO        NO      MEAN D                   PER G1
PRINT "B(Q)       R(Q)    D(6,Q)       X(6,Q)     D(3,Q)     X(10,Q)    X(11
PRINT "------     ----    -------      ------     ------     --------  -----
                                  -
FOR Q=1 TO N
PRINT  USING 1540; B[Q], R[Q], D[6, Q], X[6, Q], D[3, Q], X[10, Q], X[11, Q]
IMAGE 2(4D4X), 2(3D.DD4X), 4D.D4X, 3D.D4X, 4D.D
PRINT
NEXT Q
PRINT
PRINT
PRINT " BLOCK     RUN      D(1,Q)     X(1,Q)     D(2,Q)     X(2,Q)     D(
X(3,Q)"
                          3
PRINT "   NO       NO   "
```

```
FOR Q=1 TO N
PRINT USING 1640; B(Q), P(Q), D(1,Q), X(1,Q), D(2,Q), X(2,Q), D(3,Q), X(3,
                                                  Q
IMAGE 2(4D4X), 6(3D.DD4X)
PRINT
NEXT Q
PRINT " BLOCK      FYN       D(4,Q)      X(4,Q)      D(5,Q)      X(5,Q)      D(7
X(7,Q)"
PRINT " NO          NO "
PRINT " -----      ----      ------      ------      ------      ------      ---
------"
FOR Q=1 TO N
PRINT USING 1720; B(Q), P(Q), D(4,Q), X(4,Q), D(5,Q), X(5,Q), D(7,Q), X(7,
                                                  Q
 IMAGE 2(4D4X), 6(3D.DD4X)
PRINT
NEXT Q
STOP
END
```

Appendix A3 - Experimental Conditions.

Symbols for Appendix A3

d_N - Nozzle diameter (mm)

α - Jet injection angle (deg.)

N - Number of nozzles

P_j - Pressure at the jet ring (N/m^2) Also P_N

Q_{fj} - Volumetric air flow rate at the jet ring (m^3/s)

Q_{fv} - Volumetric air flow rate at the venturi feeder (m^3/s)

Q_m - Solids throughput (Kg/s)

T_t - Starting-up time (s)

T_r - Run time (s)

h_c - Hold-up in the chamber (Kg)

P_{cm} - Static pressure at the chamber periphery (10^{-3}m Hg)

RUN	d_N	α	N	P_j 10^5 N/m^2 (A)	Q_{fj} 10^{-3} kg/s	Q_{fv} 10^{-3} kg/s	Q_m 10^{-3} kg/s	T_t s	T_r s	H_c	P_{cm} 10^{-3}m Hg	Feed Size
3/1	1.5875	51.3	12	6.53	29.4	3.7	5.87	120	300	0.129	*	A
3/2	"	"	"	7.22	32.0	4.1	2.78	-	600	0.108	*	"
3/3	"	"	"	"	"	"	-	-	-	-	*	"
3/4	"	"	"	"	"	"	3.87	-	600	0.088	*	"
3/5	"	"	"	"	"	"	12.19	150	270	0.0985	*	"
3/6	"	"	"	"	"	"	1.98	210	600	0.09	*	"
3/7	"	"	"	"	"	"	7.20	150	390	0.094	*	"
3/8	"	"	"	"	"	"	9.72	120	240	0.107	*	"
3/9	"	"	"	"	"	"	4.16	120	360	0.085	*	"
4/1	1.5875	51.3	12	7.22	32.0	4.1	1.98	240	600	*	*	A
4/2	"	"	"	"	"	"	-	-	-	-	*	"
4/3	"	"	"	6.65	"	"	5.93	120	390	*	*	"
4/4	2.36855	"	6	"	"	"	1.98	300	660	*	*	"
4/5	"	"	"	"	"	"	3.87	180	450	*	*	"
4/6	"	"	"	"	"	"	5.93	180	330	*	*	"
4/7	"	"	"	"	"	"	8.33	120	385	*	*	"

RUN	d_N		N	P_j 10^5 N/m^2 (A)	Q_{fj} 10^{-3} kg/s	Q_{fv} 10^{-3} kg/s	Q_m 10^{-3} kg/s	T_t s	T_r s	H_c	P_{cm} 10^{-3}m Hg	Feed Size
4/8	2.36855	51.3	6	6.65	32.0	4.1	2.8	150	390	*	*	A
4/9	3.175	"	3	-	"	"	1.98	-	-	-	*	"
4/10	"	"	"	-	"	"	5.93	-	-	-	*	"
4/11	"	"	"	-	"	"	3.87	-	-	-	*	"
5/1	1.5875	51.3	12	7.22	32.0	4.1	1.98	240	660	*	*	A
5/2	3.175	"	3	6.40	"	"	"	"	"	*	*	"
5/3	"	"	"	"	"	"	2.79	180	"	*	*	"
5/4	"	"	"	"	"	"	3.87	"	600	*	*	"
5/5	"	"	"	"	"	"	4.86	"	"	*	*	"
5/6	"	"	"	"	"	"	6.94	120	240	*	*	"
7/1	1.58	41.5	12	7.21	32.0	3.0	1.98	300	600	*	*	A
7/2	"	"	"	"	"	"	8.33	120	270	*	*	"
7/3	"	"	"	"	"	"	1.98	240	660	*	*	"
7/4	"	"	"	"	"	"	8.33	120	240	*	*	"

RUN	d_N		N	P_j 10^5 N/m^2 (A)	Q_{fj} 10^{-3} kg/s	Q_{fv} 10^{-3} kg/s	Q_m 10^{-3} kg/s	T_t s	T_r s	H_c	P_{cm} 10^{-3}m Hg	Feed Size
7/5	1.58	60	12	7.21	32.0	3.5	1.98	240	660	*		A
7/6	"	"	"	6.18	27.3	"	"	-	"	*		"
7/7	"	"	"	7.22	32.0	"	8.33	60	134	*		"
7/8	"	"	"	6.18	27.3	"	"	75	180	*		"
7/9	"	28.7	"	7.22	32.0	"	1.98	180	720	*		"
7/10	"	"	"	"	"	"	8.33	120	186	*		"
9/1	1.58	51.3	12	9.28	42.4		10.00	150	-	*		A
9/2	"	"	"	8.13	36.4		8.33	90	150	*		"
9/3	"	"	"	7.22	32.0		7.42	90	210	*		"
9/4	"	"	"	5.83			6.10	120	240	*		"
9/5	"	"	"	4.13			4.30	"	330	*		"
9/6	"	"	"	2.51			3.03	"	300	*		"
9/7	"	"	"	8.59	38.5		9.70	90	330	*		"
9/8	"	"	"	6.52	29.4		6.77	"	120	*		"
9/9	"	"	"	7.55	31.1		8.02	120	-	*		"

RUN	d_N		N	P_j 10^5 N/m^2 (A)	Q_{fj} 10^{-3} kg/s	Q_{fv} 10^{-3} kg/s	Q_m 10^{-3} kg/s	T_t s	T_r s	H_c	P_{cm} 10^{-3}m Hg	Feed Size
9/10	1.58	51.3	12	10.32	47.3		11.11	30	180	*		A
10/1	1.58	51.3	12	7.91	35.4	5.96	1.98	360	570	*	79	A
10/2	"	"	"	"	"	"	2.22	300	480	*	73	"
10/3	"	"	"	"	"	"	2.68	210	420	*	70	"
10/4	"	"	"	"	"	"	3.88	180	300	*	62	"
10/5	"	"	"	"	"	"	4.93	"	210	*	52	"
10/6	"	"	"	"	"	"	6.19	210	240	*	"	"
10/7	"	"	"	"	"	"	8.61	60	180	*	48	"
10/8	"	28.7	"	7.56	"	"	1.98	300	600	*	89	"
10/9	"	"	"	"	"	"	2.22	-	480	*	80	"
10/10	"	"	"	"	"	"	2.68	240	420	*	74	"
10/11	"	"	"	"	"	"	3.88	180	270	*	60	"
10/12	"	"	"	"	"	"	4.93	120	300	*	"	"
10/13	"	"	"	"	"	"	6.19	90	270	*	56	"

RUN	d_N		N	P_j 10^5 N/m^2 (A)	Q_{fj} 10^{-3} kg/s	Q_{fv} 10^{-3} kg/s	Q_m 10^{-3} kg/s	T_t s	T_r s	H_c	P_{cm} 10^{-3}m Hg	Feed Size
11/1	1.58	28.7	12	7.56	35.4	5.96	8.61	90	240	*	50	A
11/2	"	60	"	6.87	"	"	1.98	240	540	*	68	"
11/3	"	"	"	"	"	"	2.22	"	480	*	62	"
11/4	"	"	"	"	"	"	2.68	"	360	*	60	"
11/5	"	"	"	"	"	"	3.88	120	240	*	48	"
11/6	"	"	"	"	"	"	4.90	"	300	*	44	"
11/7	"	"	"	"	"	"	6.19	"	240	*	40	"
11/8	"	"	"	"	"	"	8.61	"	300	*	38	"
11/9	"	"	"	"	"	"	11.11	60	180	*		"
11/10					"	"						
11/11	"	41.5	"	8.0	"	"	1.98	780	540	0.158	78	"
11/12	"	"	"	"	"	"	2.22	540	420	0.175	74	"
12/1	1.58	41.5	12	8.0	35.4	5.96	3.33	240	300	0.220	57	A
12/2	"	"	"	"	"	"	6.00	180	"	0.290	46	"
12/3	"	"	"	"	"	"	2.79	480	420	0.202	60	"

RUN	d_N		N	P_j 10^5 N/m^2 (A)	Q_{fj} 10^{-3} kg/s	Q_{fv} 10^{-3} kg/s	Q_m 10^{-3} kg/s	T_t s	T_r s	H_c	P_{cm} 10^{-3}m Hg	Feed Size
12/4	1.58	41.5	12	8.03	35.4	5.96	8.33	180	180	0.343	40	A
12/5	"	"	"	"	"	"	11.11	"	"	0.332	38	"
12/6	"	"	"	"	"	"	9.72	"	210	0.327	42	"
12/7	"	51.3	"	7.91	"	"	1.81	540	540	0.156	44	"
12/8	"	"	"	"	"	"	6.01	180	180	0.290	54	"
13/1	1.58	51.3	12	10.66	49.3		6.41	180	300	0.252	*	A
13/2	"	"	"	3.78			2.06	420	420	0.234	16	"
13/3	"	"	"	6.52	29.4		3.74	240	360	0.222	36	"
13/4	"	"	"	9.28	42.2		5.61	"	300	0.183	68	"
13/5	"	"	"	5.15			2.77	"	"	0.214	*	"
13/6	"	"	"	10.66	49.3		9.72	120	180	0.261	*	"
13/7	"	"	"	9.28	42.2		8.33	-	-	0.117	*	"
13/8	"	"	"	7.91	35.4		6.94	180	240	0.218	*	"
13/9	"	"	"	6.52	29.4		4.17	240	-	0.272	*	"
13/10	"	"	"	5.15			"	180	-	0.296	*	"

RUN	d_N		N	P_j 10^5 N/m^2 (A)	Q_{fj} 10^{-3} kg/s	Q_{fv} 10^{-3} kg/s	Q_m 10^{-3} kg/s	T_t s	T_r s	H_c	P_{cm} 10^{-3}m Hg	Feed Size
13/11	1.58	51.3	12	3.77			3.05	240	240	0.228	*	A
14/1	1.58	51.3	12	7.91	35.4		1.98	360	300	0.131	74	A
14/2	"	"	"	"	"		11.11	90	150	0.258	50	"
14/3	"	"	"	"	"		1.98	300	300	0.113	72	"
14/4	"	"	"	"	"		9.72	120	180	0.245	48	"
14/5	"	"	"	"	"		1.98	360	300	0.100	90	"
14/6	"	"	"	"	"		9.72	120	-	0.268	64	"
14/7	"	"	"	"	"		1.98	360	300	0.071	88	"
14/8	"	"	"	"	"		9.72	150	180	0.282	50	"
15/1	1.58	51.3	12	7.91	35.4						*	B
15/2	"	"	"	"	"						*	"
15/3	"	"	"	"	"						*	"
15/4	"	"	"	"	"						*	"
15/5												

RUN	d_N		N	P_j 10^5 N/m^2 (A)	Q_{fj} 10^{-3} kg/s	Q_{fv} 10^{-3} kg/s	Q_m 10^{-3} kg/s	T_t s	T_r s	H_c	P_{cm} 10^{-3}m Hg	Feed Size
17/1+	1.5875	51.3	12	6.81	29.4		6.94	120	180	0.225	38	B
17/2+	"	"	"	7.91	35.4		"	"	-	0.243	44	"
17/3	"	"	"	6.88	30.2		5.44	"	90	0.255	28	D
17/4	"	"	"	7.91	35.4		8.33	180	120	0.074	50	A
17/5	"	"	"	"	"		"	210	150	0.262	38	"
17/6	"	"	"	"	"		"	180	150	0.313	*	"
17/7	"	"	"	"	"		"	"	"	0.285	47	"
17/8	"	"	"	"	"		"	120	"	0.073	50	"
17/9	"	"	"	"	"		"	180	180	0.330	44	"
17/10	"	"	"	"	"		"	150	210	0.320	40	"

RUN	d_N		N	P_j 10^5 N/m^2 (A)	Q_{fj} 10^{-3} kg/s	Q_{fv} 10^{-3} kg/s	Q_m 10^{-3} kg/s	T_t s	T_r s	H_c	P_{cm} 10^{-3}m Hg	Feed Size
19/1	1.5875	51.3	12	7.91	35.4	5.37	10.00	120	400	478	*	B
19/2	"	"	"	"	"	"	3.06	270	660	285	52	"
19/3	"	"	"	"	"	"	3.89	240	540	313	46	"
19/4	"	"	"	"	"	"	4.89	180	180	400	42	"
19/5	"	"	"	10.32	47.5	6.58	10.00	150	150	430	58	"
19/6	"	"	"	"	"	"	3.89	"	240	235	88	"
											*	
19/7	1.5875	51.3	12	7.91	35.4	5.37	2.50	180	180	374	72	D
19/8	"	"	"	"	"	"	4.44	"	-	447	82	"
19/9	"	"	"	10.32	47.5	6.32	"	150	150	483	74	
19/10	"	"	"	"	"	"	6.72	"	"	470	*	
19/11	"	"	"	9.29	42.4	6.00	1.72	240	*		130	
19/12	"	"	"	"	"	"	4.44			460	70	
19/13	"	"	"	6.53	29.4	4.00	"			470	*	
19/14	"	"	"	7.91	35.4	5.37	3.44				37	
19/15	"	"	"	"	"	"	2.00					

RUN	d_N		N	P_j 10^5 N/m^2 (A)	Q_{fj} 10^{-3} kg/s	Q_{fv} 10^{-3} kg/s	Q_m 10^{-3} kg/s	T_t s	T_r s	H_c	P_{cm} 10^{-3}m Hg	Feed Size.
20/1	1.5875	51.3	12	6.53	29.4	5.12	1.54	270	330	0.194	50	C
20/2	"	"	"	7.91	35.4	6.61	"	"	"	0.159	76	"
20/3	"	"	"	9.29	42.4	7.39	"	"	"	0.134	96	"
20/4	"	"	"	10.67	49.3	8.09	"	"	-	0.110	130	"
20/5	"	"	"	6.53	29.4	5.12	4.68	135	240	0.455	42	"
20/6	"	"	"	7.91	35.4	6.61	"	150	"	0.410	50	"
20/7	"	"	"	9.29	42.4	7.39	"	"	"	0.335	66	"
20/8	"	"	"	10.67	49.3	8.09	"	"	"	0.268	78	"
20/9	"	"	"	6.53	29.4	5.12	9.17	90	120	0.485	26	"
20/10	"	"	"	7.91	35.4	6.61	"	120	140	0.493	32	"
20/11	"	"	"	9.29	42.4	7.39	"	"	150	0.514	38	"
20/12	"	"	"	10.67	49.3	8.09	"	"	180	0.515	52	"
20/13	"	"	"	6.53	29.4	5.12	6.78	"	120	0.507	*	"
20/14	"	"	"	7.91	35.4	6.61	"	"	135	0.519	*	"
20/15	"	"	"	9.29	42.4	7.39	"	150	120	0.472	*	"
20/16	"	"	"	10.67	49.3	8.09	"	"	150	0.435	*	"

RUN	d_N		N	P_j 10^5 N/m^2 (A)	Q_{fj} 10^{-3} kg/s	Q_{fv} 10^{-3} kg/s	Q_m 10^{-3} kg/s	T_t s	T_r s	H_c	P_{cm} 10^{-3}m Hg	Feed Size
20/17	1.5875	51.3	12	6.53	29.4	5.12	3.33	180	120	342	40	C
20/18	"	"	"	7.91	35.4	6.61	"	"	180	287	54	"
20/19	"	"	"	9.29	42.4	7.39	"	"	"	236	70	"
20/20	"	"	"	10.67	49.3	8.09	"	"	-	203	90	"
20/21	"	"	"	6.53	29.4	5.12	2.36	210	390	357	42	"
20/22	"	"	"	7.91	35.4	6.61	"	"		249	*	"
20/23	"	"	"	9.29	42.4	7.39	"	240		201	80	"
20/24	"	"	"	10.67	49.3	8.09	"	300		170	*	"

Appendix A4 - Particle Size Distribution of Product.

Particle Size Analysis OF HOLD UP

FEED MATERIAL: Limestone

FEED SIZE RANGE: -120μm.

ANALYSIS METHOD: 45μm sieve.

RUN	FEED RATE 10^{3} Kg/s	Sample Mass 10^{-3} Kg	Mass Retained on sieve 10^{-3} Kg	Percentage Retained
311/12	2.194	21.0	5.54	26.4
312/3	2.81	21.0	6.45	30.7
312/1	3.25	21.13	7.00	33.1
312/2	6.00	20.0	8.70	43.5
312/4	8.25	22.00	11.72	51.5
312/6	9.72	21.22	11.40	53.7
312/5	11.38	21.45	12.49	58.2

ORIFICE TUBE SIZE: 140μm CALIBRATION FACTOR 3.71

RUN DIAMETER	B3/2	B3/2	B3/4	B3/5	B3/6	B3/7	B3/8	B4/1
73								
57.9								
46							4.17	
36.5				4.93		2.96	9.38	
29			2.75	10.68		5.92	13.56	
23	1.18	1.26	5.49	18.49		8.89	22.42	
18.3	2.36	5.65	9.96	27.12	1.50	11.48	30.50	1.89
14.5	5.60	6.59	13.13	38.01	2.63	17.31	42.23	5.05
11.5	8.11	8.63	22.49	49.87	5.31	30.92	54.61	7.81
9.1	14.89	14.20	37.55	60.19	11.37	47.77	65.69	10.5
7.2	29.12	28.36	54.12	70.14	25.56	63.09	74.99	18.35
5.7	43.24	41.68	65.53	77.59	43.03	73.33	81.53	30.68
4.6	60.11	59.71	76.92	84.64	62.42	82.11	87.51	52.33
3.6	75.70	75.30	86.72	91.17	79.27	89.76	92.94	72.62
2.9	88.20	88.24	94.58	96.50	91.85	95.91	97.24	89.00
+1.5 *	100.00	100	100	100	100	100	100	100

ORIFICE TUBE SIZE: 140μm CALIBRATION FACTOR 3.71

RUN DIAMETER	B4/3	B4/4	B4/5	B4/6	B4/7	B4/8	B5/1	B5/2
73.00								
57.9								
46					14.36			12.48
36.5				5.56	19.74			18.72
29				12.05	29.61			24.96
23	1.64		6.35	15.29	36.34	0.81		27.31
18.3	5.75	0.6	10.79	26.64	44.64	7.69	1.80	28.09
14.5	18.21	1.79	14.93	36.02	52.04	14.77	4.50	30.81
11.5	35.46	4.47	21.75	46.45	60.68	20.33	7.21	35.50
9.1	53.19	8.72	31.35	58.67	70.27	31.00	13.96	38.57
7.2	67.10	18.98	46.87	69.66	78.52	45.92	33.00	50.64
5.7	76.35	33.51	61.46	78.00	84.24	61.26	48.32	62.83
4.6	84.5	54.58	75.43	85.44	89.16	75.16	66.03	77.05
3.6	91.02	74.04	86.18	91.74	93.35	86.57	80.86	88.75
2.9	96.25	89.11	94.10	96.57	97.12	94.77	91.27	96.16
+1.5 *	100	100	100	100	100	100	100	100

ORIFICE TUBE SIZE: 140 CALIBRATION FACTOR 3.71

RUN DIAMETER	B5/3	B5/4	B5/5	B5/6
73.0				
57.9		9.21		14.07
46.0		18.42		28.14
36.5		27.634	4.23	35.18
29.0	9.69	31.08	8.46	45.73
23.0	16.16	35.69	16.91	54.96
18.3	23.43	42.03	23.0	62.33
14.5	27.87	49.37	31.84	70.47
11.5	35.95	55.56	43.67	78.71
9.1	47.10	64.26	56.35	85.75
7.2	62.20	74.01	69.30	91.45
5.7	75.17	81.83	78.78	94.58
4.6	85.12	89.01	87.17	96.78
3.6	92.29	94.30	93.14	98.29
2.9	97.00	97.87	97.34	99.28
+1.5 *	100	100	100	100

ORIFICE TUBE SIZE: 100 CALIBRATION FACTOR 2.61

RUN DIAMETER	B10/1	B10/1	B10/2	B10/3	B10/4	B10/5	B10/6	B10/7	B10/8
51.5									
40.5									
32.4								1.49	
25.7						0.38	0.85	4.47	0.94
20.4		0.48		0.19	0.23	1.61	4.46	9.20	3.30
16.2		0.85	0.25	0.46	1.87	4.74	8.70	16.28	4.56
12.9	0.19	1.45	0.76	1.25	6.09	14.98	19.26	29.80	6.06
10.2	1.34	2.93	3.57	6.53	19.81	33.23	33.29	42.28	7.85
8.1	8.48	11.28	16.05	23.02	39.04	49.88	48.24	55.54	12.37
6.4	28.66	32.88	36.95	44.45	54.38	63.67	61.87	67.04	27.33
5.1	50.66	54.73	55.4	61.57	68.45	74.94	73.53	77.04	45.45
4.1	65.88	69.24	68.45	73.09	78.26	82.93	81.75	84.40	59.93
3.2	78.74	80.70	80.38	83.01	86.99	89.74	89.15	90.63	73.89
2.6	89.08	89.8	90.06	90.93	93.54	94.92	94.62	95.27	86.28
2.0	96.10	96.16	96.50	96.58	97.86	98.14	98.09	98.30	95.21
+1.0 *	100.00	100	100	100	100	100	100	100	100

ORIFICE TUBE SIZE: 100 CALIBRATION FACTOR 2.61

RUN DIAMETER	B10/9	B10/10	B10/11	B10/12	B10/13	B11/1	B11/2	B11/3	B11/4
51.5						0			
40.5				0.55	1.17	1.5			
32.4			0.67	1.66	3.22	3.74			
25.7		1.43	1.52	4.14	7.40	7.86	0.79		
20.4	0.43	2.66	3.96	7.25	14.28	14.88	1.78	0.43	0.82
16.2	2.06	4.45	7.42	12.98	24.00	24.00	2.70	1.00	1.84
12.9	3.23	7.92	15.01	22.87	35.26	34.02	4.47	3.19	4.91
10.2	7.12	16.99	29.36	37.20	46.96	45.65	8.69	10.58	12.22
8.1	20.27	34.86	43.68	51.03	58.51	56.44	21.70	25.41	27.65
6.4	38.05	51.75	56.77	63.75	68.12	66.95	39.55	43.03	44.85
5.1	55.53	65.87	68.90	74.41	77.12	76.71	55.95	58.71	60.10
4.1	67.88	75.72	77.93	81.95	83.88	84.00	68.37	70.17	71.09
3.2	79.09	84.56	86.35	88.78	89.88	90.15	79.22	80.45	81.19
2.6	88.79	91.64	93.04	94.08	94.64	95.00	88.02	89.09	89.34
2.0	95.79	96.84	97.09	97.72	98.00	98.20	94.76	95.75	95.60
+1.0*	100	100	100	100	100	100	100	100	100

ORIFICE TUBE SIZE: 100 CALIBRATION FACTOR 2.61

RUN DIAMETER	B11/5	B11/6	B11/7	B11/8	B11/9	B11/10	B11/11	B11/12	B12/1
51.5				0	1.80	4.59			
40.5				1.38	5.86	10.56			
32.4		1.39	1.70	9.68	13.31	16.07			
25.7		2.55	4.46	17.46	23.63	25.54			
20.4	0.63	3.95	7.01	26.28	32.68	34.32			
16.2	2.07	6.30	12.18	36.39	43.25	42.93	0.34	0.43	4.62
12.9	7.75	12.22	20.79	47.30	51.16	50.53	0.91	1.41	9.38
10.2	18.17	21.82	31.92	56.87	60.19	57.89	1.83	4.89	24.81
8.1	35.10	35.59	44.75	65.96	68.47	65.71	7.77	19.44	42.99
6.4	49.41	48.79	56.61	73.82	75.48	73.27	24.95	39.60	57.96
5.1	63.58	62.80	68.13	80.86	82.15	80.80	45.23	56.95	70.44
4.1	73.81	73.53	77.28	86.36	87.37	86.59	60.60	69.37	79.63
3.2	83.07	83.84	85.46	91.50	92.11	91.77	74.44	80.26	87.23
2.6	90.68	92.23	92.26	95.53	95.83	95.69	86.05	89.46	93.20
2.0	96.26	98.11	97.00	98.36	98.41	98.39	94.65	96.07	97.43
+1.0*	100	100	100	100	100	100	100	100	100

ORIFICE TUBE SIZE: 140 CALIBRATION FACTOR 2.6

RUN DIAMETER	B12/2	B12/3	B12/4	B12/5	B12/6	B12/7	B12/8	B13/1	B13/2
51.5					2.20				
40.5	0.75		3.98	2.23	6.61				
32.4	3.01		5.84	9.47	10.20		4.45		
25.7	8.08		12.65	18.25	18.05	0.34	7.08		
20.4	15.04	0.15	22.36	30.09	25.35	2.06	10.93	0.57	0.85
16.2	25.38	0.68	34.14	41.51	37.00	3.57	16.95	1.42	3.19
12.9	39.34	3.46	49.41	53.25	49.12	5.18	29.19	3.93	6.59
10.2	51.93	15.22	59.88	62.89	59.85	7.33	43.89	13.27	14.36
8.1	63.27	37.14	69.13	71.88	69.68	12.66	57.18	29.22	26.03
6.4	71.82	54.32	76.68	78.60	77.61	28.23	68.13	46.34	39.13
5.1	79.88	67.86	83.06	84.96	84.67	51.64	77.57	62.34	54.83
4.1	85.71	77.21	88.06	89.67	89.63	67.40	84.55	73.97	67.43
3.2	91.09	85.61	92.61	93.71	93.73	79.78	90.46	84.57	79.73
2.6	95.36	92.40	96.13	96.74	96.76	89.08	95.04	92.89	89.70
2.0	98.30	97.16	98.54	98.75	98.76	95.71	98.14	97.80	96.33
+1.0*	100	100	100	100	100	100	100	100	100

ORIFICE TUBE SIZE: 100μm CALIBRATION FACTOR 2.6

RUN DIAMETER	B13/3	B13/4	B13/5	B13/6	B13/7	B13/8	B13/8	B13/9	B13/9
51.5									
40.5									
32.4						0.61			
25.7					1.93	1.23	0.66		1.42
20.4	0.68		0.36	1.67	3.37	2.46	1.99	1.24	3.56
16.2	2.03	1.46	1.72	2.62	5.42	4.84	3.87	5.44	8.53
12.9	4.50	3.65	5.99	5.13	8.19	11.30	10.25	9.89	14.88
10.2	12.98	7.52	15.46	10.86	13.91	23.25	21.73	16.56	21.99
8.1	24.04	14.84	28.15	19.60	23.27	37.30	36.15	26.55	29.71
6.4	37.25	26.25	42.81	31.36	36.15	51.51	50.62	38.63	41.09
5.1	52.09	41.79	57.73	47.36	51.73	64.89	65.02	53.32	54.34
4.1	64.63	55.27	69.69	60.87	64.75	75.35	75.95	65.61	66.31
3.2	77.46	70.28	81.04	74.83	77.53	84.81	85.24	77.64	78.47
2.6	88.22	83.83	90.48	86.58	88.33	92.23	92.33	87.86	88.67
2.0	95.76	93.92	96.80	95.09	95.74	97.25	97.12	95.34	95.82
+1.0*	100	100	100	100	100	100	100	100	100

ORIFICE TUBE SIZE: 100μm CALIBRATION FACTOR 2.61

RUN DIAMETER	B14/6	B14/7	B14/8
51.5			
40.5			
32.4			
25.7			1.17
20.4	1.09	1.00	2.49
16.2	4.91	1.80	7.32
12.9	12.65	3.55	14.06
10.2	22.95	6.63	24.39
8.1	36.78	16.51	36.74
6.4	51.96	33.83	49.85
5.1	65.77	52.98	63.68
4.1	76.05	66.46	74.87
3.2	85.35	78.88	84.51
2.6	92.67	88.95	91.95
2.0	97.50	96.00	97.00
+1.0*	100	100	100

ORIFICE TUBE SIZE: 100μm CALIBRATION FACTOR 2.63

RUN DIAMETER	B20/1	B20/2	B20/3	B20/4
51.3				
40.7				
32.3				
25.6				
20.4				
16.16				
12.8	0.05	0.12	0.07	
10.2	1.36	0.25	0.18	0.29
8.1	8.07	0.89	0.67	0.76
6.4	28.35	6.66	5.59	3.34
5.1	49.86	29.46	25.04	19.19
4.0	65.26	50.63	47.86	43.50
3.2	78.82	69.37	68.11	67.63
2.5	89.35	84.17	83.52	84.58
2.0	96.22	94.57	93.91	94.70
+1.0*	100	100	100	100

Appendix A5 - The Coulter Counter.

A5.1 Theory

The Coulter Counter determines the number and size of particles suspended in an electricity conductive liquid. This is done by causing the suspension to pass through a small orifice, on either side of the orifice two electrodes are immersed, to dectect changes in resistance of the electrolyte due to particles passing through; the change in resistance $\delta(\Delta R)$ is expressed by

$$\delta(\Delta R) = \frac{\rho_s \, a \, \delta l}{A^2} \left(1 - \frac{a}{A}\right) \text{ (Ref 74)} \qquad \text{Eq. A1.1}$$

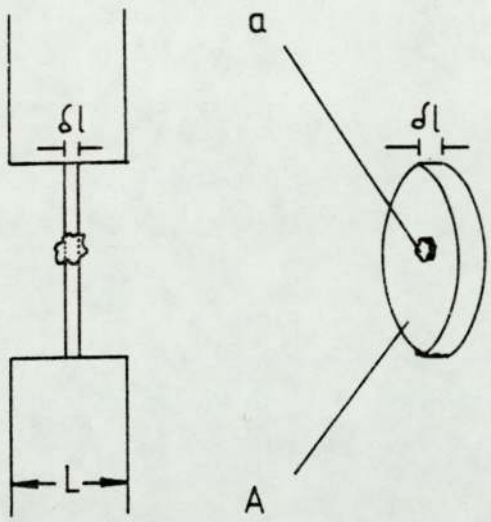

$\delta(\Delta R)$ produces a voltage pulse of short duration having a magnitude proportional to volume of particle term ($a\delta l$) in Equation A1.1; the pulses are then electronically amplified, scaled and counted. From the derived data size distribution of the suspended phase is determined.

When the stopcock (t) is opened, controlled vacuum

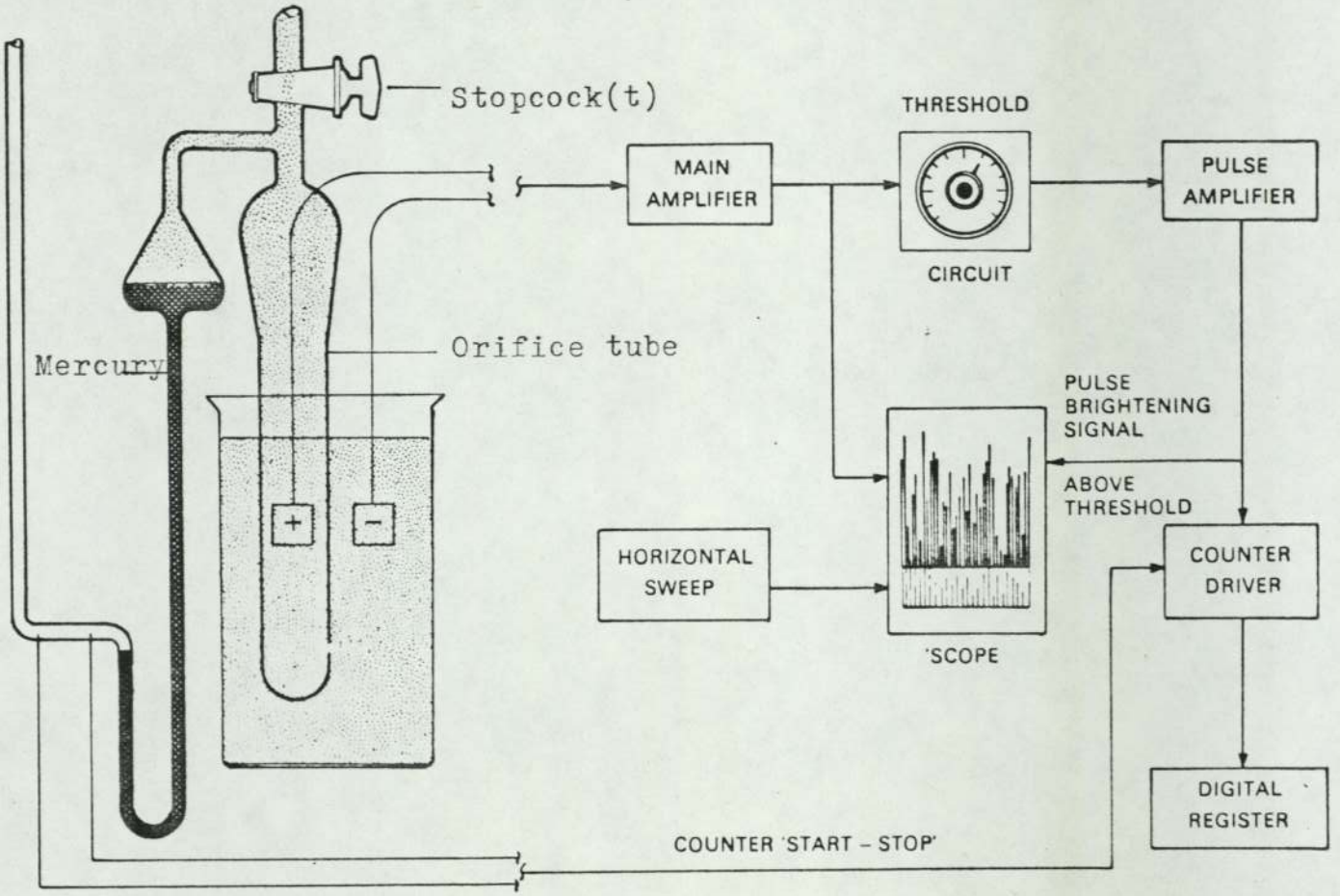

FigureA5.1: Schematic illustration of the coulter principle and operation

causes flow of suspension through the aperture and unbalance the mercury syphon (see figure A1.1), closing the stopcock; syphoning action of the mercury continues the sample flow. Advancing mercury column contacts start and stop probes which in turn initiate or stop the electronic counter. The probes are placed apart to give a precise and constant sample volume for all count. The sample volume is optional, 0.05, 0.5 or 2ml. Amplified voltage pulses are fed to an adjustable threshold circuit, which can be used with a lower limit only, or a lower and a higher limit (Dual Threshold). If the threshold level is reached or exceeded by the pulse, which can be observed on the oscilliscope screen, the pulse is counted.

A5.2 Electrolyte Preparation

A wide range of aqueous and non-aqueous electrolytes may be used, depending upon the nature of the material being analysed. For the particle size analysis of limestone, 1% Wt/Vol. aqueous sodium chloride solution was prepared in batches of 20 litres. The solution was saturated with limestone by adding about 0.01 Kg of the powder to each batch and continuously stirring for 4-5 hours. This was done to depress the dissolution of the sample being analysed in the electrolyte.

The suspension was allowed to settle and was filtered 2-3 times through 0.45 μm membrane filter paper. The solution was checked for blank count, if filtrate had a high

count the solution was filtered again until an acceptable level was reached.

A5.3 Orifice Tube Selection

The orifice size was selected on the basis of suspected largest particle present, so that the particle size range lies between 2 - 40% of the orifice tube aperture. For particle size analysis of the micronised product 100 μm and 140 μm orifice tubes were used. For some samples the largest particle size present was well below the 40% upper limit.

Orifice tubes of size 50 μm and 70 μm were found extremely sensitive to electrical and thermal noise, and were frequently blocked.

A5.4 Coulter Calibration

The Calibration was carried out using Half count-techniques; the Calibration particles, which are standardised and of known diameter and distribution, were selected for the given tube used, thus

Tube Dia(μm)	d_{32}	Material
140	17	Barley
50	4.88	Soot

(The recommended mean diameter of calibration material should lie between 5% and 20% of the aperture diameter), and are dispersed in 100ml of electrolyte (1% Nacl) using ultrasonic

probe for 30 seconds. The suspension is then transfered to a 250 ml beaker, and diluted further to 200ml. The Coulter Controls were set as follows;

Amplification Switch	A	1/8
Aperture Current Switch	I	1/8
Manometer Volume	V	0.5ml for 140μm tube.
		0.005ml for 50μm tube.
Lower Threshold	1	
Upper Threshold	off (110)	
Stirrer	on	
Matching switch	10K (140μm), 20K (50μm)	

tap (t) was opened until mercury column dropped, and pulses appeared on the screen, then tab (t) closed, the number obtained on the digital counter indicated the number of particles, per 0.5ml of suspension, and it was checked that it did not exceed the 10% conincidence recommended by manufacturers which is as follows.

tube size (μm)	manometer Volume (ml)	10% Max. (No.)
140	0.5	14,580
100	0.5	18,000
50	0.05	27,000

If the count was higher than the recommended no., further dilution was necessary, until count was within the limit.

Tap (t) was reopened, the attenuation and aperture

current switches were adjusted so that the majority of the pulses observed on the oscilliscope screen were 15 - 30 mm high. The lower threshold was increased until the base line almost coincided with the maximum height of the majority of the pulses. The threshold dial reading T was noted.

Lower Threshold was set to $\frac{T}{2}$, four counts were taken n_1, n_2, n_3, n_4, and averaged so that,

$$N_1 = (n_1 + n_2 + n_3 + n_4)/4$$

the dial was set to $\frac{3T}{2}$, and another four counted recorded, and averaged (N2). N_3 was calculated by

$$N_3 = \frac{N1 + N2}{2}$$

The dial was set to T; four counts taken and averaged to give N_T . N_T and N_3 are then compared, if they differ by 2 or 3 then T was taken as the calibration setting, otherwise the threshold dial was adjusted so that N_3 is obtained, and the new dial setting would be T_{New}. If T and T_{New} differ only by one division or one fraction off, then T was again taken as the calibration value, otherwise T is replaced by T_{New} and the procedure was repeated, until $T = T_{New}$.

Calibration factor K_d is calculated by

$$K_d = \frac{d32}{\sqrt[3]{t^1.I.A.}}$$

where d_{32} is the calibration material average diam. (μm)

t^1 = T

I The aperture current setting at calibration

A Attenuation Current Setting at calibration

typical values of K_d obtained

Tube size μm	K_d (exper)	Solutions	K_d (manu)
140	3.66 - 3.97		3.80 - 4.80
50	1.21 - 1.26		1.25 - 1.55

From above equation, error of 1 $\pm$ 2 in t^1 (usually t^1 $\approx$ 45), leads to very small error in K_d, since it is cubic vout.

The calibration was carried out every 3 days unless:-

(1) New batch of electrolyte was used

(2) Machine was serviced

(3) Any change in the analysis conditions was intorduced

A5.5 Analysis Procedure

Dual Threshold techniques were used to obtain particle size analysis, this allows a small size range step to be selected no. of particles (Δn) is obtained for each size step thus giving more information about the distribution, from which the surface area is calculated.

The technique makes use of the upper and lower threshold controllers, which are fixed at 2:1 ratio respectively. This would give a 2:1 volume ratio ($\sqrt[3]{2}$: 1 Diameter Ratio) over the size range that had been covered. A full range of 16 analysis points was taken for each of the samples under examination, see appendix

250 ml of cleaned electrolyte in 250 ml beaker is placed on the platform, and the controls are set as follows;

Table (5.5)

Attenuation (A)	1/8
Aperture Switch (I)	1/16 (140μm tube), 1/4 (50 μm tube)
Upper threshold (T_u)	110 (off)
Lower Threshold (T_L)	10
Manometer Volume	0.5 (140μm tube), 0.05 (50μm tube)
Matching Switch	10K (140μm tube), 20K (50μm tube)

a count (B) was taken by opening tab (t) until mercury column dropped then closing the tab. This count gives the number of particles (B) above diameter d*, thus

$$d^* = Kd \sqrt{t^1 \times A \times 1}$$

$$= Kd \sqrt{10 \times (1/8) \times (1/16)} \ \mu m$$

where Kd is the calibration factor (see equation). B is checked against acceptable level as shown below.

Table: Maximum Allowable Blank Count, Using Settings As Shown Above

Tube Size	B(Max.)
140 μm	150
50 μm	350

If B was above the allowable limit, the following procedure was carried out.

(1) Reclean and Rinse Glassware

(2) Refilter the electrolyte

(3) Check orifice for Blockage

(4) Check for external noise.

The previously prepared sample (see section 6.6.1), was then diluted to 200 - 250 ml of suspension in a 250ml beaker, and was then placed on the platform. The coulter controls are then readjusted as per table A1.5.5 and a count was taken and checked for coincidence level.

The analysis was then carried out.

Data obtained was then processed, and converted to standard particle size distribution presentation.

A.5.6 Data Conversion

A.5.6.1 Conversion of Coulter Counter Data to Cumulative Weight Percent Oversize

Each data point from the coulter counter was defined by Δni, tLi, tui, Ii and Ai, where the symbols are given in 5.

For each interval, the relative volume Vi was calculated as follows,

$$V_{ui} \text{ (Upper limit)} = t_{ui} \cdot A_i \cdot I_i$$

$$V_{Li} \text{ (Lower limit)} = t_{Li} \cdot A_i \cdot I_i$$

and the diameter di corresponding to the relative volume in the range calculated from

$$d_{ui} = K \sqrt[3]{V_{ui}} \qquad \text{(Upper diameter)}$$

$$d_{Li} = K \sqrt[3]{V_{Li}}$$

therefore average relative volume $\bar{V}i$ and average diameter $\bar{d}i$ in the interval are given by

$$\bar{d}_i = \frac{d_{ui} + d_{Li}}{2}$$

$$\bar{V}_i = \frac{V_{ui} + V_{Li}}{2}$$

hence the total volume (or mass) of particles in the range of average diameter $\bar{d}i$ will be,

$$V_i = M_i = \bar{V}_i \, \Delta n_i$$

and the total volume of the sample

$$V_{TOT} = \sum_{N}^{i=1} \bar{V}_i \, \Delta n_i$$

where N is the number of points of observation and percentage mass of volume of an average diameter.

$\bar{d}_i$ is given by $\bar{d}_i = \dfrac{\bar{V}_i \, \Delta n_i}{\sum_{N}^{i=1} \bar{V}_i \, \Delta n_i} = fi\%$

The cumulative volume oversize $= F_1 + F_2 \quad + F_i$

The calculations were done using a basic computer programme which is listed in Appendix A2.

A.5.6.2 Specific Surface Area Calculations

The specific surface area of the feed and micronised product was estimated from the particle size distribution obtained from the coulter counter, and using the following equation.

$$\text{sp.s Area} = \frac{\Sigma_0^{100} \Delta n \, \frac{\bar{d}_i^{\,2}}{2}}{\Sigma_0^{100} \Delta n \, \frac{\bar{d}_i^{\,3}}{2}} \quad x3x10^4 + \frac{1}{} \; cm^2/gm$$

where is the materials density.

For samples whose distribution was obtained by sieve analysis the equation was

$$\text{sp.s Area} = \frac{\Sigma_0^{100} \frac{W_i}{\bar{d}_i}}{\Sigma_0^{100} W_i} \quad cm^2/gm$$

where wi is the mass fraction.

and for powder whose distribution was log-normal the expression used

$$\text{s.p.s. Area} = \frac{1}{6}$$

It was found that the s.p. surface area calculated using the above three equations, for log-normally distributed powder agreed within 3%.

A.5.6.3. Calculation of the Mean Diameter

The surface volume mean diameter d_{32}, (Sauter mean diameter) was calculated using

$$d_{32} = \frac{\Sigma^{i=1} \bar{d}i^3 \, dn}{\Sigma \bar{d}i^2 \, dn} \qquad \text{ref(74)}$$

The particle size distribution, specific surface area and mean diameter were calculated in an integrated basic digital computer program; this is listed in appendix

Appendix A6 - Hopper Calibration.

A6. Calibration of the Feeder System

The hopper and trough were switched on to check that solid material is flowing freely from the hopper.

The feeder was calibrated by collecting the discharged solid for a period of 7 minutes at a given trough setting. This was repeated three times. Also repeated for different trough settings. So, obtained calibrations are shown in Figure A6.1

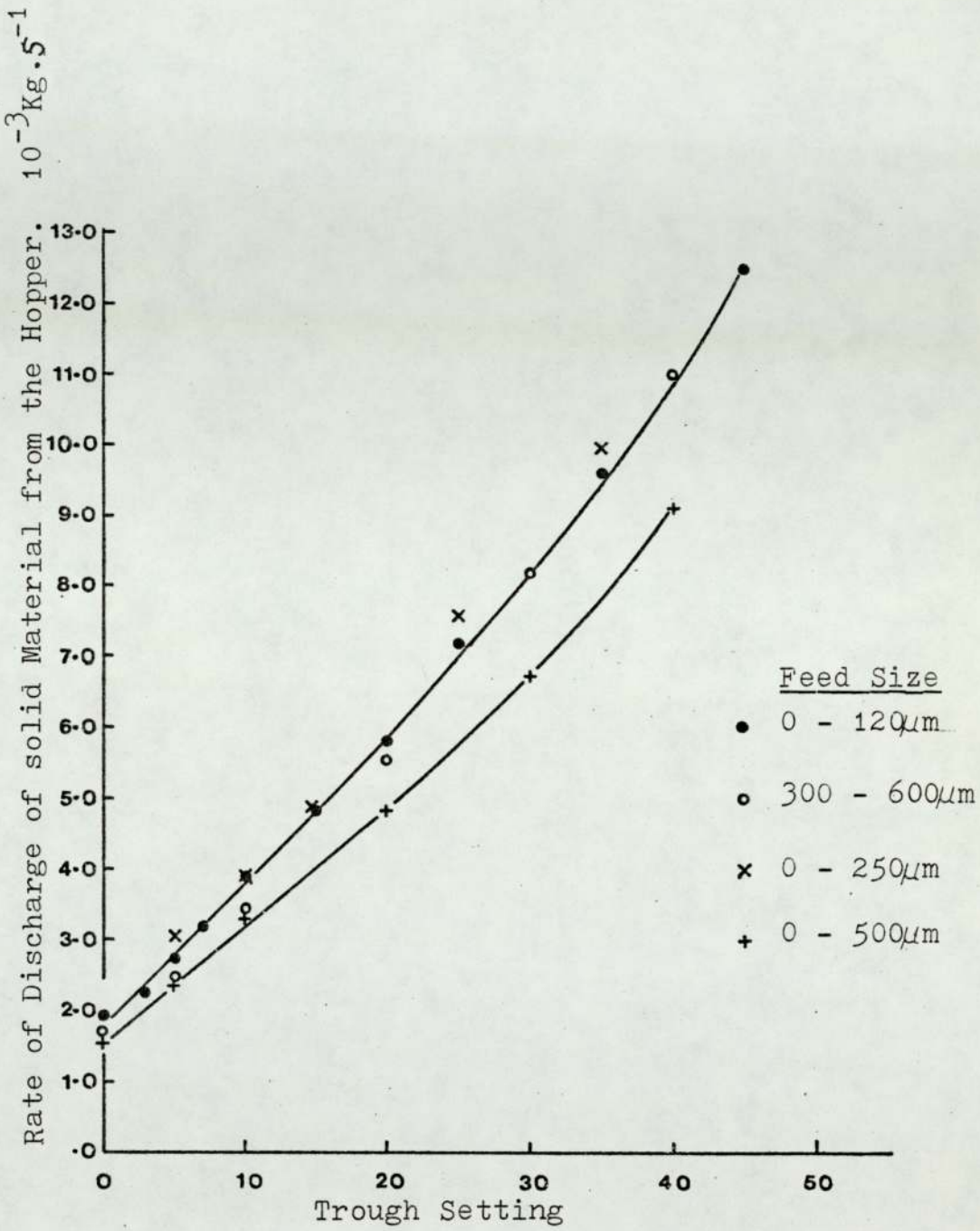

Figure A6.1: Calibration Curves of Feeder system (for limestone)

Appendix A7 - Optimisation-Fortran Computer Programme for Nedder-Mead Method.

```
      TRACE 2
      SUBROUTINE PRINEL(IC,N,V,SC,Y,YF,CAK,IO)
      DIMENSION X(11,10),SC(10),Y(10),YF(10),V(11,10)
      DIMENSION XJ1(50),YJ(50)
      COMMON XJ1,YJ,NDJ
      DO 18 I=1,N+1
      DO 18 J=1,N
   18 X(I,J)=V(I,J)*SC(J)
      GO TO(1,2,3),IO
    1 WRITE(2,100)IC
  100 FORMAT(///49X,16HITERATION NUMBER,I6,/)
      IF(N-6)14,15,15
   15 WRITE(2,123)
  123 FORMAT(2X,5HPOINT,12X,55HVALUES FOR THE INDEPENDENT VARIABLES  X(1
     1),X(2),...X(N),13X,9HY(CARROL),7X,11HOBJ. FUNCT.,)
   14 GO TO(4,5,6,7,8,9,10,11,12,13),N
    4 WRITE(2,110)
  110 FORMAT(20X,39HTHIS IS NOT A PROGRAM FOR LINEAR SEARCH,//,20X,48HTH
     1E MINIMUN NUMBER OF INDEPENDENT VARIABLES IS 2,)
      RETURN
    5 WRITE(2,115)
  115 FORMAT(25X,4HX(1),18X,4HX(2),16X,9HY(CARROL),12X,11HOBJ. FUNCT.,)
      WRITE(2,116)((X(I,J),J=1,N),Y(I),YF(I),I=1,N+1)
  116 FORMAT(21X,1PE12.5,3E22.5)
      RETURN
    6 WRITE(2,117)
  117 FORMAT(14X,4HX(1),18X,4HX(2),18X,4HX(3),16X,9HY(CARROL),12X,11HOBJ
     1. FUNCT.,)
      WRITE(2,118)((X(I,J),J=1,N),Y(I),YF(I),I=1,N+1)
  118 FORMAT(10X,1PE12.5,4E22.5)
      RETURN
    7 WRITE(2,119)
  119 FORMAT(15X,4HX(1),13X,4HX(2),13X,4HX(3),13X,4HX(4),11X,9HY(CARROL)
     1,7X,11HOBJ. FUNCT.,)
      WRITE(2,120)((X(I,J),J=1,N),Y(I),YF(I),I=1,N+1)
  120 FORMAT(11X,1PE12.5,5E17.5)
      RETURN
```

```
  8 WRITE(2,121)
121 FORMAT(8X,4HX(1),11X,4HX(2),11X,4HX(3),11X,4HX(4),11X,4HX(5),9X,9H
   1Y(CARROL),5X,11HOBJ. FUNCT.,)
    WRITE(2,122)((X(I,J),J=1,N),Y(I),YF(I),I=1,N+1)
122 FORMAT(4X,1PE12.5,6E15.5)
    RETURN
  9 WRITE(2,124)(I,(X(I,J),J=1,N),Y(I),YF(I),I=1,N+1)
124 FORMAT(I5,4X,1P5E15.5,/9X,E15.5,60X,2E15.5)
    RETURN
 10 WRITE(2,125)(I,(X(I,J),J=1,N),Y(I),YF(I),I=1,N+1)
125 FORMAT(I5,4X,1P5E15.5,/9X,2E15.5,45X,2E15.5)
    RETURN
 11 WRITE(2,126)(I,(X(I,J),J=1,N),Y(I),YF(I),I=1,N+1)
126 FORMAT(I5,4X,1P5E15.5,/9X,3E15.5,30X,2E15.5)
    RETURN
 12 WRITE(2,127)(I,(X(I,J),J=1,N),Y(I),YF(I),I=1,N+1)
127 FORMAT(I5,4X,1P5E15.5,/9X,4E15.5,15X,2E15.5)
    RETURN
 13 WRITE(2,128)(I,(X(I,J),J=1,N),Y(I),YF(I),I=1,N+1)
128 FORMAT(I5,4X,1P5E15.5,/9X,7E15.5)
    RETURN
  2 WRITE(2,129)CAK
129 FORMAT(///40X,29HSOLUTION FOR CARROL CONSTANT=,1PE14.5,//)
    DO 19 J=1,N
 19 WRITE(2,130)J,X(N+1,J)
130 FORMAT(51X,2HX(,I2,2H)=,1PE14.5)
    WRITE(2,132)Y(N+1),YF(N+1)
132 FORMAT(46X,10HY(CARROL)=,1PE14.5/37X,19HOBJECTIVE FUNCTION=,E12.5)
    RETURN
  3 WRITE(2,133)
133 FORMAT(1H1,6(/),36X,47HEND OF THE DIRECT SEARCH OPTIMIZATION PROCE
   1DURE,/36X,47H*** ** *** ****** ****** ********** *********,///,
   229X,61HTHE FOLLOWING VALUES WERE FOUND FOR THE INDEPENDENT VARIABL
   3ES,//,41X,37HWHICH OPTIMIZE THE OBJECTIVE FUNCTION,5(/),)
    DO 16 J=1,N
 16 WRITE(2,130) J,X(N+1,J)
```

```
      WRITE(2,134)IC,YF(N+1)
  134 FORMAT(3(/),34X,45HTHE TOTAL NUMBER OF FUNCTION EVALUATIONS WERE,
     1I8,//,29X,47HTHE OPTIMUM VALUE FOR THE OBJECTIVE FUNCTION IS,
     2 1PE15.6)
      RETURN
      END
      SUBROUTINE PRIMEAD(N,EL,A,GAM,B,VI,SC,MSO,ITRAC,NIBP,ICARR,CAK,
     1KFCAR,FCAR,EF)
      DIMENSION VI(10),SC(10)
      DIMENSION XJ1(50),YJ(50)
      COMMON XJ1,YJ,NDJ,XJ2,XJ3
      IF(MSO)1,1,2
    1 WRITE(2,100)
  100 FORMAT(//43X,34HTHE METHOD WILL LOOK FOR A MINIMUM,)
      GO TO 3
    2 WRITE(2,101)
  101 FORMAT(//43X,34HTHE METHOD WILL LOOK FOR A MAXIMUM,)
    3 IF(ICARR)4,4,5
    4 WRITE(2,112)
  112 FORMAT(//43X,33HTHE OPTIMIZATION IS UNCONSTRAINED,)
      GO TO 6
    5 WRITE(2,102)
  102 FORMAT(//44X,31HTHE OPTIMIZATION IS CONSTRAINED,/20X,80HTHE CREATE
     1D RESPONSE SURFACE TECHNIQUE WILL BE USED TO DEAL WITH THE CONSTRA
     2INTS,)
      WRITE(2,103)CAK,KFCAR,FCAR
  103 FORMAT(/16X,74HTHE OPTIMIZATION WILL BE FIRST CARRIED OUT FOR A VA
     1LUE OF CARROL CONSTANT=,1PE15.6//19X,39HTHE OPTIMIZATION WILL THEN
     2 PROCEED WITH,  I3,1X,36HOTHER VALUES FOR THE CARROL CONSTANT,//,
     328X,34HWHICH WILL BE REDUCED BY A FACTOR=,E15.6,1X,15HEVERY ITERAT
     4ION,/)
    6 WRITE(2,104)EL,EF,A,GAM,B
  104 FORMAT(//,30X,60HTHE SELECTED PARAMETERS FOR THE VARIATION OF THE
     1SIMPLEX ARE,//,45X,14HINITIAL LENGTH,1PE15.6/43X,19HSTOPPING DIFFE
     2RENCE,E15.6,/,41X,22HREFLEXION COEFFICIENT=,E15.6,/,41X,22HEXPANSI
     3ON COEFFICIENT=,E15.6,/,40X,24HCONTRACTION COEFFICIENT=,E15.6,/)
```

```
      WRITE(2,105)
  105 FORMAT(//,50X,20HTHE INITIAL GUESS IS,//)
      DO 7 I=1,N
    7 WRITE(2,106)I,VI(I)
  106 FORMAT(50X,2HX(,I2,2H)=,1PE15.6)
      WRITE(2,107)
  107 FORMAT(//,48X,23HTHE SCALING FACTORS ARE,//)
      DO 8 I=1,N
    8 WRITE(2,108)I,SC(I)
  108 FORMAT(50X,2HS(,I2,2H)=,1PE15.6)
      WRITE(2,109)NIBP
  109 FORMAT(///,32X,31HTHERE WILL BE A PRINT OUT EVERY,I5,1X,15HITERATI
     1ONS. AND,)
      IF(ITRAC)9,9,10
    9 WRITE(2,110)
  110 FORMAT(/,44X,32HNO TRACE INCLUDED IN THE RESULTS.)
      GO TO 11
   10 WRITE(2,111)
  111 FORMAT(/,43X,34HA TRACE IS INCLUDED IN THE RESULTS.)
   11 WRITE(2,113)
  113 FORMAT(1H1)
      RETURN
      END
      SUBROUTINE OBF(V,Y)
      DIMENSION V(10)
      DIMENSION XJ1(50),YJ(50),XJ2(50),XJ3(50)
      COMMON XJ1,YJ,NDJ,NXJ,XJ3
      Y=0.
      DO 1 I=1,NDJ
    1 Y=Y+(YJ(I)-YVAL(XJ1(I),XJ3(I),V))**2
      RETURN
      END
      SUBROUTINE CARROL (AK,X,Y,YM,NSO,NOC)
      DIMENSION X(10),F(10),FF(10)
      DIMENSION XJ1(50),YJ(50),XJ3(50)
      COMMON XJ1,YJ,NDJ,XJ2,XJ3
```

```
      F(1)=X(1)*X(1)+X(2)*X(2)
      F(2)=(X(3)-3.)*(X(3)-3.)+(X(4)-3.)*(X(4)-3.)-20.
      DO 1 I=1,NOC
    1 FF(I)=ABS(F(I))
      DO 2 I=1,NOC
      IF(FF(I)-.1E-30)3,3,2
    2 CONTINUE
      IMP=0
      S=0.
      S1=0.
      DO 4 I=1,NOC
      IF(F(I))23,13,13
   23 IMP=2
   13 S=S+FF(I)
      S1=S1+1./FF(I)
    4 CONTINUE
      IF(IMP-1)5,5,6
    5 YM=Y-MSO*AK*S1
      RETURN
    6 YM=-MSO*(.1E05+AK*S)
      RETURN
    3 YM=-MSO*.1E05
      RETURN
      END
      MASTER NELDER
     0DIMENSION X(11,10),VI(10),Y(11),XO(11,10),YO(11),GX(11,10),C(10),
     1XS(10),XSS(10),GORV(11),YFF(11),YFFO(11),GYFF(11),SC(10)
      DIMENSION XJ1(50),YJ(50),XJ2(50),XJ3(50)
      COMMON XJ1,YJ,NDJ,XJ3
      READ (1,3177,END=999)NDJ
3177  FORMAT(I0)
      READ(1,3178)(XJ1(I),XJ2(I),XJ3(I),YJ(I),I=1,NDJ)
3178  FORMAT(4F0.0)
      READ(1,1605)IJIJ
1605  FORMAT(I0)
      READ(1,250)N,MSO,ITRAC,NIBP,ICARR
```

```
250 FORMAT(5I0)
    DO 305 IJJJ=1,IJIJ
    WRITE(2,1173)
    WRITE(2,317)N
317 FORMAT(///38X,32HTHIS PROGRAM IS GOING TO SOLVE A,I2,12H DIMENSION
   1AL,//39X,43HOPTIMIZATION PROBLEM USING THE ALGORITHM OF,//53X,15HN
   2ELDER AND MEAD,///)
    READ(1,300)EL,EF,A,GAM,B
300 FORMAT(5F0.0)
    READ(1,350)(VI(J),J=1,N)
    READ(1,350)(SC(J),J=1,N)
350 FORMAT(10F0.0)
    IF(ICARR)301,301,302
301 DO 303 J=1,N+1
303 YFF(J)=0.
    GO TO 304
302 READ(1,365)CAK,FCAR,KFCAR,NOC
365 FORMAT(2F10.0,2I5)
    KCAR=1
304 PN=((N+1.)**(.5)-1.+N)/(N*2.**(.5))*EL
    CALL PRIMEAD(N,EL,A,GAM,B,VI,SC,MSO,ITRAC,NIBP,ICARR,CAK,KFCAR,FCA
   1R,EF)
    QN=((N+1.)**(.5)-1.)/(N*2.**(.5))*EL
    IBP=0
    ICONT=0
    DO 5 J=1,N
  5 X(1,J)=VI(J)/SC(J)
    DO 15 I=2,N+1
    DO 10 J=1,N
 10 X(I,J)=X(1,J)+QN
 15 X(I,I-1)=X(1,I-1)+PN
 45 DO 16 I=1,N+1
    ICONT=ICONT+1
    IBP=IBP+1
    DO 116 J=1,N
116 VI(J)=X(I,J)*SC(J)
```

```
      CALL OBF(VI,YRF)
      IF(ICARR)71,71,72
   72 CALL CARROL(CAK,VI,YRF,YZZ,MSO,NOC)
      GO TO 73
   71 YZZ=YRF
   73 YFF(I)=YRF
   16 Y(I)=YZZ
  329 YO(1)=Y(1)
      YFFO(1)=YFF(1)
      DO 11 J=1,N
   11 XO(1,J)=X(1,J)
      I=1
  114 IF((Y(I+1)-YO(I))*MSO)1,2,2
    2 YO(I+1)=Y(I+1)
      YFFO(I+1)=YFF(I+1)
      DO 13 J=1,N
   13 XO(I+1,J)=X(I+1,J)
      GO TO 12
    1 DO 3 J=1,I
      IF((Y(I+1)-YO(J))*MSO)4,3,3
    3 CONTINUE
    4 DO 14 K=J,I
      GORV(K)=YO(K)
      GYFF(K)=YFFO(K)
      DO 14 KJ=1,N
   14 GX(K,KJ)=XO(K,KJ)
      YO(J)=Y(I+1)
      YFFO(J)=YFF(I+1)
      DO 216 KJ=1,N
  216 XO(J,KJ)=X(I+1,KJ)
      DO 6 K=J,I
      YO(K+1)=GORV(K)
      YFFO(K+1)=GYFF(K)
      DO 6 KJ=1,N
    6 XO(K+1,KJ)=GX(K,KJ)
   12 IF(I-N)112,113,113
```

```
112 I=I+1
    GO TO 114
113 DO 17 I=1,N+1
    Y(I)=YO(I)
    YFF(I)=YFFO(I)
    DO 17 J=1,N
 17 X(I,J)=XO(I,J)
 46 IF(IBP-NIBP)52,53,53
 53 CALL PRINEL(ICONT,N,X,SC,Y,YFF,CAK,1)
    IBP=0
 52 IF(ABS(Y(1)-Y(N+1))-EF      )48,47,47
 47 DO 18 J=1,N
    SUM=0.
    DO 19 I=2,N+1
 19 SUM=SUM+X(I,J)
    C(J)=SUM/N
 18 VI(J)=C(J)*SC(J)
    IF(ITRAC)54,54,55
 55 WRITE(2,1004)(VI(J),J=1,N)
1004 FORMAT(1H0,6X,8HCENTROID,/1X,1P5E16.5,/1X,5E16.5//)
 54 DO 20 J=1,N
    XS(J)=(1.+A)*C(J)-A*X(1,J)
 20 VI(J)=XS(J)*SC(J)
    ICONT=ICONT+1
    IBP=IBP+1
    CALL OBF(VI,YRFS)
    IF(ICARR)74,74,75
 75 CALL CARROL(CAK,VI,YRFS,YS,MSO,NOC)
    GO TO 76
 74 YS=YRFS
 76 IF(ITRAC)56,56,57
 57 WRITE(2,1005)(VI(J),J=1,N),YS,YRFS
1005 FORMAT(1H0,6X,10HREFLECTION,/1X,1P6E16.5,/1X,6E16.5//)
 56 IF((Y(N+1)-YS)*MSO)22,22,21
 21 IF((YS-Y(2))*MSO)23,23,24
 22 DO 25 J=1,N
```

```
      XSS(J)=GAM*XS(J)+(1.-GAM)*C(J)
   25 VI(J)=XSS(J)*SC(J)
      ICONT=ICONT+1
      IBP=IBP+1
      CALL OBF(VI ,YRFSS)
      IF(ICARR)77,77,78
   78 CALL CARROL(CAK,VI ,YRFSS,YSS,MSO,NOC)
      GO TO 81
   77 YSS=YRFSS
   81 IF(ITRAC)58,58,59
   59 WRITE(2,1006)(VI (J),J=1,N),YSS,YRFSS
 1006 FORMAT(1H0,5X,9HEXPANSION,/1X,1P6E16.5,/1X,6E16.5,//)
   58 DO 29 I=1,N
      Y(I)=Y(I+1)
      YFF(I)=YFF(I+1)
      DO 29 J=1,N
   29 X(I,J)=X(I+1,J)
      IF((YSS-YS)*MSO)26,26,27
   27 Y(N+1)=YSS
      YFF(N+1)=YRFSS
      DO 30 J=1,N
   30 X(N+1,J)=XSS(J)
      GO TO 46
   26 Y(N+1)=YS
      YFF(N+1)=YRFS
      DO 31 J=1,N
   31 X(N+1,J)=XS(J)
      GO TO 46
   24 DO 34 I=1,N
      IF((YS-Y(I+1))*MSO)32,32,33
   33 Y(I)=Y(I+1)
      YFF(I)=YFF(I+1)
      DO 34 J=1,N
   34 X(I,J)=X(I+1,J)
      Y(N+1)=YS
      YFF(N+1)=YRFS
```

```
      DO 51 J=1,N
   51 X(N+1,J)=XS(J)
      GO TO 46
   32 Y(I)=YS
      YFF(I)=YRFS
      DO 35 J=1,N
   35 X(I,J)=XS(J)
      GO TO 46
   23 IF((YS-Y(1))*MSO)36,36,37
   36 DO 38 J=1,N
      XS(J)=B*X(1,J)+(1.-B)*C(J)
   38 VI(J)=XS(J)*SC(J)
      GO TO 39
   37 DO 40 J=1,N
      XS(J)=B*XS(J)+(1.-B)*C(J)
   40 VI(J)=XS(J)*SC(J)
   39 CALL OBF(VI,YRFS)
      IF(ICARR)79,79,80
   80 CALL CARROL(CAK,VI,YRFS,YS,MSO,NOC)
      GO TO 82
   79 YS=YRFS
   82 IF(ITRAC)60,60,61
   61 WRITE(2,1007)(VI(J),J=1,N),YS,YRFS
 1007 FORMAT(1HO,5X,11HCONTRACTION,/1X,1P6E16.5,/1X,6E16.5//)
   60 ICONT=ICONT+1
      IBP=IBP+1
      IF((YS-Y(2))*MSO)41,41,24
   41 DO 43 I=1,N
      DO 43 J=1,N
   43 X(I,J)=(X(I,J)+X(N+1,J))*.5
      GO TO 45
   48 IF(ICARR)1305,1305,306
  306 CALL PRINEL(ICONT,N,X,SC,Y,YFF,CAK,2)
      WRITE(2,1173)
 1173 FORMAT(1H1)
      IF(KCAR-KFCAR)307,381,1305
```

```
  381 CAK=0.
  307 CAK=CAK*.1
      KCAR=KCAR+1
      DO 327 I=1,N+1
      DO 328 J=1,N
      XS(J)=X(I,J)
  328 VI(J)=XS(J)*SC(J)
  327 CALL CARROL(CAK,VI,YFF(I),Y(I),MSO,NOC)
      GO TO 329
 1305 CALL PRINEL(ICONT,N,X,SC,Y,YFF,CAK,3)
      DO 399 J=1,N
  399 VI(J)=X(N+1,J)*SC(J)
      WRITE(2,3473) (VI(J),J=1,N)
C
C    CHANGE THIS FORMAT TO DESCRIBE FORMULA FITTED
C
3473  FORMAT (1H1////30X,1P5E12.5///)
      DO 4173 I=1,NDJ
      YV=YVAL(XJ1(I),XJ2(I),XJ3(I),VI)
      WRITE(2,4174)XJ1(I),XJ2(I),XJ3(I),YJ(I),YV
 4174 FORMAT(1H0,15X,5F20.5)
 4173 CONTINUE
  305 CONTINUE
999   STOP
      END
      FUNCTION YVAL(RE,RW,RD,V)
C
C        EVALUATE CORELATION
C
      DIMENSION V(10)
      X=V(1)
      Y=V(2)
       W=V(4)
      Z=V(3)
```

```
      YVAL=EXP(X*((RE**Y))*(RU**Z)*(RD**W))
      RETURN
      END
      FINISH
****
```

References

1. E Muschelknautz and N Rink. Chemie-Ing Techn 1971, 42 (1), 6

2. E Muschelknautz and N Rink. Verfahrenstechnik 1971, 5 (6), 225

3. L A Behie, M A Bergougnou, C G Baker and W Bulani. Cand. J Chem Engng 1970, 48 (April), 158

4. H Rumpf and H Kurten. Chem Ing Techn 1966, 38 (11), 1187

5. H Rumpf, N Rink and H Kurten. Powd Techn. 1970/71, 4, 221

6. F Kaiser. Chemie Ing Techn 1973, 45 (10a), 676

7. Y Mori. Proc 1st European symp. on size reduction Duchema monograph 1962, 515

8. S Okuda. Proc 6th Symposium on industrial crystallisation Sep 1975, (Ed. J W Mullin), 67

9. H Rumpf. Chemie Ing Techn 1960, 32 (5), 335

10. H Rumpf. Ibid 1960, 32 (3), 129

11. U Haese. Silikat J 1970, 9 (5), 101

12. A Brandt and L L Perini. J Space craft 1970, 7 (7), 880

13. R Hogland. AR1S J 1962, May, 662

14. N Rink, G Giersiepen and Leverkusen. Aufberreitungs Technik 1971, Nr.9, 562

15. K Dubik. Przemysl chemicsny 1966, 45 (12), 665

16. K Rietema and H J Krajenbrink. App Sci Rcs Section A, 8, 177

17. L A Behie, M A Bergaugnou C G Baker and T E Base. Can J Chem Engng 1972, 19 (Oct), 557

18. K Schonert and K Steier. Chemie Ing Techn 1971, 43 (13), 773

19. J Prochazka. Bergakademie 1969, 21 (12), 732

20. T Tanka. Ind Engng Chem Proc Des Develop 1973, 12 (2), 213

21. T Tanka. Ind Engng Chem Pros Des Develop 1972 11 (2), 238

22. C J Stairmand. 1963, 14th Congress "Chemistry Days", Societa Chimica Italiana, Milan, 7 - 16 June, 181

23. R Hendry. Proc 2nd Europ Symp on size reduction, Amsterdam, Dechema Monagraph 1966, 695-727

24. R G Baines. Bull Powd Advisory Centre 1970, 1, 33

25. H W Fowler. Manufacturing Chemists and Aerosol News 1970, January, 51

26. M F Dufour and J B Chatelain. Mining Engng 1952, (Mar, 262

27. M Ramanujam and D Venkates. Warlu Powd Tech 1969/70, 3 92

28. H E Kingston. Brit Chem Engng 1956 (May), 30

29. J A Holmes. Trans. I.Ch E. 1957, 35, 125

30. T Tanaka and M Hayashi. J Chem Eng Japan 1972, 5 (3), 94

31. J L Speirs. Ceramic age 1942, 40, 37

32. J M Dotson. Ind Engng Chem 1962, 54 (2), 62

33. Chemical Processing 1962 (June), 90

34. F. Bond, Chem Eng Progress 1959, 55 (1), 108

35. N P Chopey. Chem Engng 1973, Sept 3, 54

36. W P Gillingham. Compressed Air Magz. 1950, Feb, 32

37. N H Andrews. US Patent 2,032,827

38. H N V Temperley and G E K Blythe. Nature 1968, 219 (Sep 21), 1218

39. Process Engng 1976, Mar, 55

40. B Dobson and E Rothwell. Powder Tech 1969/70, 3, 213

41. C E Berry. Ind Engng Chem, 1946, 38 (7), 672

42. G C Lowrison. Crushing and Grinding Butterworths 1974

43. Y Mori and G Jimbo. Kagaku Kogaku 1962, 25 (6), 477-486

44. G Jimbo. J Res Assoc Powder Techn (Japan) 1969, 6, 438

45. Y Mori and G Jimbo. Chem Engng (Japan) 1958, 6, 363-371

46. W H Bickle. Bibliography of Crushing and Grinding, HM50 1958

47. D E Creasy. "Private communication".

48. V C Marshall (Ed.). Comminution, 1975 Inst. Chem. Engng

49. M Clement and E Huwald. Inst. Chem Engng (Publications on Comminution)

50. N Rink and G Giersiepen. Inst. Chem Engng (Publications on Comminution

51. R H Snow. Powd Technology 1971/2, 5, 351

52. R H Snow. ibid 1972/3, 7, 63

53. R H Snow. ibid 1974, 10, 129

54. R H Snow. ibid 1976, 13, 33

55. S Okuda. Kagaku Kogaku 1971, 35, 294, (C.A. 74, 128030e)

56. W A Beveloo, H A Leniger and J A C Weldring. Brit Chem Engng 1963 (Oct), 678

57. A M Godridge, S Badzioch and P G Hawksley. J Sci Instrument 1962, 39, p 611

58. R E Payne. Mining Engng 1957 (Oct), 1113

59. A Goetz. Public Works 1959 (Feb), 91

60. A R Lukens. Mining Engng 1957 (Oct), 1120

61. E Yigit. Int J Min process 1973, 3, 365

62. L Gregor and E Rumpf. Powd Technol 1976, 15, 43

63. C C Harris. Powd Technol 1973, 8, 123

64. R P Gardner and R S Rogers. Powd Technol 1975, 12, 247

65. S R Broadbent and T G Callcott. J Inst Fuel 1956 (Dec), 524

66. T H Hughes. Proc 1st Europe Symp on size Reduction Duchema Mono 1962, 667

67. Mining J 1967 (Jun)

68. C J Stairmand. 1963, 14th Congress "Chemistry days" Societa Chemical Italiana, Milan, 181

69. L G Austin, R R Klimpel. Ind Engng Chem. 1964, 56, (11), 19

70. A D Randolph and A R Durando. AIME Soc Mining Engrs Preprint 71-8-78

71. R G Boothroyd. Flowing Gas Solids Suspensions, Chapman and Hall 1971

72. Shih - I - Pai. Fluid Dynamics of Jets 1954, Van Nostrand 1954

73. H P Greenspan. Theory of Rotating Fluids, Cambridge University Press 1968

74. T Allen. Particle Size Measurements, 2nd ed, Chapman and Hall 1975

75. J M Kay and R M Nedderman. An Introduction into Fluid Mechanics and Heat Transfer, 3rd ed, Cambridge University Press, 1974

76. P M Gy. Inter J Minrl Process, 1976, 3, 289-312

77. J W Mulling and H M Powd Thechnel 1974, 10, 153-156

78. R H Perry and C H Chilton. Chemical Engineering Handbook, 5th ed, McGraw-Hill 1977. (section 5-45)

79. R D Cadle. Particle Size: Theory and Industrial Application, 1st ed, Reinhold 1965.

80. L Silverman, C E Billings and M W First. Particle Size Analysis In Industrial Hygiene, Academic Press 1971

81. R R Irani and C F Callis. Particle Size - measurement Interpretation and Application, Wiley 1963

82. G. Herdan. Small Particle Statistics, Academic Press 1960

83. R H Perry and C H Chilton. Chemical Engineering Handbook, 5th ed, McGraw-Hill 1977, (section 8-1D)

84. Eldor. Heating Piping Air Conditioning 1954, 26 (3), 149-155

85. M.B.Donald and H.Sing. Trans Inst Chem Engrs 1959, 37, 255-267

86. Heating Piping Air Conditioning 1953, 25 (1), 181-191

87. M L Albertson, Y. B. Dai and N Rouse. Tran A soc civil Engrs , 115, 639-664

88. Keagy and Weller. A SME Proc Heat Transfer Fluid Mech 1949, (June 22-24), 89-98

L.M.K
89. V.Cleeves and Boelter. Chem Engng Prog 1947, 43, 123-134

90. H.Schlichting. Boundary Layer Theory, 4th ed, McGraw-Hill 1960, 170-174 and 218-222

91. G.Abramovich. The Theory of Turbulent Jets, MIT Press 1963

92. J M Coulson and J F Richardson. Chemical Engineering Vol 1, Pergamon, 1977

93. M A Fisher and E F Davis. Mech Engng 1949, 71, 481

94. R L Stoker. Ind Engng Chem 1949, 41, 1196

95. P J Morris. AIAA J 1976, 14 (10), 1468-1475

96. H B Nottage. Heating Piping Air Cond, 1952 (Jan), 165-176

97. A Putnane. ARS J 1961 (Oct), 31, 1467-1468

98. A E Knoll. Chem Engng Prog. 1947, 1 (2), 21-24

99. W S Bailey, E N Nilson and R A Serra. ARS J 1961 (June), 31, 793-798

100. G L Tuve and C Ohio. Heating Piping Air Cond. 1953 (Jan), 181-190

101. S L Soo. AIChE J, 7, (3), 384-391

102. L D Smoot. AIAA J 1976, 14, (12), 1699-1705

103. L D Smoot and L A Fort. AIAA J 1975, 13

104. F K Owen. AIAA J 1976, 14 (11), 1556-1562

105. J W Ramsey and R J Goldstein. J Heat Tranf. 1971 (Nov)

365-372

106. R A Kahawita. AIAA J 1975, 13, (11), 1517-1518

107. J D McLean, E H Dowell. AIAA J 1975, 13, (11), 1435-1440

108. L Fekete. Banyasz Kut Intez Kozlem 1973, 106, (4), 239, C A 80, 5219q

109. L Fekete. Chem Tech (Liepzig) 1973, 25 (11), 673, CA 80 97917s

110. F E Marble. Phys Fluids 1964, 7, 1270

111. _____

112. Pugh. Brit J Appl Physics 1967, 18 (2), 129

113. A A Griffith. Phil Trans R Soc 1921, 221, 163

114. R J Wasely. "Stress Wave Propagation", Marcal-Dekker 1973

115. J Greenwood and F J Hirons. "A comparison of Two conditions of Particle Breakage" Dechema Monograph, Band 57, 993

116. C J Stairmand and W F Carry Recent. Advances in Mineral Dressing, 1953, Inst Min and Met

117. M Mehyhart and L Muskiewicz. Powd Technlgy 1976, 15, 261-266

118. A D Randolph and M A Larson. Theory of particulate Processes analysis and Techniques of continuous Crystallisation Acadamic press 1971

119. B Bleke. Principles of Comminution 19 , Hungarian Academy of Sciences

120. A Jaffe. The Physics of solids McGraw-Hill, 1928

121. H E Rose and R M E Sullivan. Vibration Mills and Vibrating milling, Constable, 1961

122. W C Peck. Ind Engng Chem May 1962

123. Engels. Farbeu Lack 1965, 71, 375

124. S L Soo. Fluid Dynamics of Multiphase Systems Waltham, 1967

125. F A Zenz and D F Othmer. Fluidisation and Fluid Particle System, 1960, Reinhold

126. W E Ranz, G R Talandis and B Gutterman. AIChE J 1960, 6, 124

127. G Segre and A Silberg. Nature 1961, 189, 219

128. B B Morgan. BCURA (monthly Bull.) 191, 25 (4).

129. M Corn. J Air Poll control Assn 1961, 11, 566

130. R G Boothroyd. Trans ASME, J Eng Ind 1969, 91B, 303

131. C Lapple and C Shepherd. Ind Eng Chem 1940, 32, 605

132. H Heywood. Proc Symp on the Interaction Between Fluid and Particles, I. Chem Eng (1962), 1

133. R L Peskin and C H Rin. ASME paper 67-EE-17

134. R G Boothroyd. Trans Instr Chem Engrs 1967, 45, 297

135. G I Taylor. Proc Roy Soc (1935), A151, 421

136. J O Hinze. App Sci Res 1962, A11, 33.

137. P P Owen. J Fluid Mech 1969, 407

138. G L Fairs. Trans IMM 1953, 63, 41

139. G L Kuester and J H Miz. "Optimization Techniques with Fortran", McGrew-Hill, 197

140. V G Jenson and G V Jeffreys. "Mathematical Methods in Chemical Engineering", Acadmic Press 1963, p 485.